THE UNIVERSITY OF CHICAGO

THE DIVERSITY AND FUNCTIONAL ROLE OF MICROBIAL COMMUNITIES ASSOCIATED WITH THE BULL KELP, *NEREOCYSTIS LUETKEANA*

A DISSERTATION SUBMITTED TO

THE FACULTY OF THE DIVISION OF THE BIOLOGICAL SCIENCES

AND THE PRITZKER SCHOOL OF MEDICINE

IN CANDIDACY FOR THE DEGREE OF

DOCTOR OF PHILOSOPHY

COMMITTEE ON EVOLUTIONARY BIOLOGY

BY

BROOKE LAUREEN WEIGEL

CHICAGO, ILLINOIS

AUGUST 2021

TABLE OF CONTENTS

LIST OF TABLES iii

LIST OF FIGURES v

ACKNOWLEDGEMENTS vii

ABSTRACT x

INTRODUCTION xii

LIST OF PUBLICATIONS xvii

CHAPTER 1: SUCCESSIONAL DYNAMICS AND SEASCAPE-LEVEL PATTERNS OF MICROBIAL COMMUNITIES ON THE CANOPY-FORMING KELPS NEREOCYSTIS LUETKEANA AND MACROCYSTIS PYRIFERA 1

- ABSTRACT 1
- INTRODUCTION 2
- METHODS 7
- RESULTS 12
- DISCUSSION 31
- APPENDIX 1.1 SUPPLEMENTAL INFORMATION FOR CHAPTER 1 39

CHAPTER 2: OXYGEN METABOLISM SHAPES MICROBIAL SETTLEMENT ON PHOTOSYNTHETIC KELP BLADES COMPARED TO ARTIFICIAL KELP SUBSTRATES 51

- ABSTRACT 51
- INTRODUCTION 52
- METHODS 56
- RESULTS AND DISCUSSION 61
- APPENDIX 2.1 SUPPLEMENTAL INFORMATION FOR CHAPTER 2 72

CHAPTER 3: THE DYNAMICS AND STOICHIOMETRY OF DISSOLVED ORGANIC CARBON RELEASE BY KELP 76

- ABSTRACT 76
- INTRODUCTION 77
- METHODS 80
- RESULTS 89
- DISCUSSION 100
- APPENDIX 3.1 SUPPLEMENTAL EQUATIONS FOR CHAPTER 3 109
- APPENDIX 3.2: SUPPLEMENTAL TABLES AND FIGURES FOR CHAPTER 3 113

CHAPTER 4: FUNCTIONAL INSIGHTS INTO THE KELP MICROBIOME FROM METAGENOME ASSEMBLED GENOMES 119

- INTRODUCTION 119
- METHODS 122
- RESULTS 127
- DISCUSSION 140
- APPENDIX 4.1: SUPPLEMENTAL TABLES AND FIGURES FOR CHAPTER 4 151

REFERENCES 156

LIST OF TABLES

Table 1.1. Results of statistical tests comparing beta diversity among (A) kelp species and geographic locations, and (B) kelp meristem and tip vs. date 14

Table 1.2. Mean relative abundances of top bacterial classes and mean relative abundances of orders on *M. pyrifera* and *N. luetkeana*, across all locations 17

Table 1.3. Mean relative abundances and taxonomic information for the 10 most abundant ASVs on *M. pyrifera* and *N. luetkeana*, from all sampling locations 21

Table S1.1. Additional results of beta diversity tests comparing microbial communities among a) the two kelp species only at geographic locations where they co-occur 43

Table S1.2. PERMANOVA pairwise comparisons of kelp microbial communities at each site for the overall tests of N. luetkeana vs. location and M. pyrifera vs. location 44

Table S1.3. Differentially abundant ASVs detected with ANCOM on N. luetkeana and M. pyrifera across all sites 46

Table S1.4. PERMANOVA pairwise comparisons of seawater microbial communities at each location 48

Table S1.5. Mean number of total 16S sequences, mean bacterial sequences and mean chloroplast sequences for all N. luetkeana, M. pyrifera, and seawater samples 49

Table 2.1. PERMANOVA pairwise comparisons of microbial community structure among substrate types 63

Table S2.1. List of samples analyzed in this study 72

Table S2.2. PERMANOVA pairwise comparisons of microbial community structure among substrate types with the dataset rarefied to the lowest bacterial read count 73

Table 3.1. Summary of carbon fixation and DOC release rates 83

Table 3.2. Summary of total DOC release and ^{13}DOC release 86

Table S3.1. Summary of linear mixed-effects models using pooled data from all daytime measurements with *N. luetkeana* blades 113

Table S3.2. Summary of mean nutrient uptake rates across all experiments 114

Table S3.3. Comparison of Tatoosh Island and Squaxin Island blade tissue characteristics and carbon dynamics 115

Table 4.1. Functional categories and metabolisms in the *Granulosicoccus* pangenome 136

Table S4.1. List of metagenome samples, co-assembled samples, and sequence reads 151

Table S4.2. List of all 79 metagenome assembled genomes (MAGs), length, completion, redundancy, and taxonomy. 151

Table S4.3. Detection of all MAGs across kelp blade samples. 151

Table S4.4. Abundance of the top 20 MAGs across kelp blade samples. The top 5 MAGs most abundant MAGs across all samples are bolded. 151

Table S4.5. List of DOM transporter genes, COG numbers, and descriptions..... 151

Table S4.6. List of core gene clusters and functions in the *Granulosicoccus* pangenome..... 151

Table S4.7. Detailed list of functional genes in the *Granulosicoccus* pangenome and presence or absence across all 10 *Granulosicoccus* genomes..... 151

LIST OF FIGURES

Figure 1.1. Map of kelp forests sampled in Washington 6

Figure 1.2. Alpha diversity indices for *N. luetkeana*, *M. pyrifera*, and seawater microbial communities 15

Figure 1.3. Non-metric multidimensional scaling plot of *M. pyrifera*, *N. luetkeana*, and seawater microbial communities across 12 sites in Washington 15

Figure 1.4. Size of *N. luetkeana* on Tatoosh Island, WA. 18

Figure 1.5. Relative abundance barplots of kelp blade microbial communities from *N. luetkeana* and *M. pyrifera* across 11 and 5 sites, respectively 19

Figure 1.6. Mean length of sampled blades and linear blade growth rates 22

Figure 1.7. Heatmap showing the relative abundances of the 100 most abundant bacterial ASVs from *N. luetkeana* blade meristem, blade tip, and seawater microbial communities 23

Figure 1.8. Alpha diversity indices for *N. luetkeana* blade meristem and tip microbial communities throughout the growing season 25

Figure 1.9. Principal coordinate analysis plot of all *N. luetkeana* microbial communities across 12 sites in Washington 25

Figure 1.10. Mean abundances of ASVs from *N. luetkeana* blade tip microbial communities that displayed significantly different abundances across time with ANCOM 27

Figure 1.11. Mean nearest taxon index and net relatedness index of microbial communities on *N. luetkeana* blade meristem, *N. luetkeana* blade tip and seawater samples 29

Figure S1.1. Barplots showing variation in the relative abundances of bacterial orders in kelp blade microbial communities from *N. luetkeana* and *M. pyrifera* 39

Figure S1.2. Mean temperature and salinity at sites across the geographic gradient 40

Figure S1.3. Ordination analysis of sequence data across the geographic gradient 41

Figure S1.4. Barplots showing variation in the relative abundances of the bacterial families Hyphomonadaceae and Saprospiraceae across sites 42

Figure 2.1. Artificial kelp substrates 56

Figure 2.2. Non-metric multidimensional scaling plot of samples by treatment 61

Figure 2.3. Barplots depicting the relative abundances of bacterial families across substrate types, colored by the oxygen metabolism of each bacterial family 64

Figure 2.4. Heatmap showing the $\log_{10}$ transformed relative abundance of the 50 most common amplicon sequence variants across all samples 66

Figure S2.1. Barplots depicting the diversity and detection of different *Granulosicoccus* sp. amplicon sequence variants (ASVs) across all samples 74

Figure S2.2. Amplicon sequence variants that were significantly enriched or depleted on kelp agar compared to control agar substrates 75

Figure 3.1. Conceptual diagram depicting two mechanisms of DOC release by kelps 80

Figure 3.2. Chamber design for measuring DOC production and nutrient fluxes by kelp blades and isotopic signatures ($\delta^{13}C$) of *N. luetkeana* blade tissues 84

Figure 3.3. Carbon fixation and DOC production by *N. luetkeana* 92

Figure 3.4. Relationships depicting carbon fixation vs. DOC production over a natural gradient of light levels 94

Figure 3.5. DOC production vs. blade tissue nitrogen content and dissolved inorganic nitrogen (DIN) uptake 96

Figure 3.6. Biogeochemical responses of *N. luetkeana* blades from Squaxin Island to nitrate addition 97

Figure 3.7. Comparisons of biogeochemical rates between *N. luetkeana* and *Macrocystis pyrifera* blades during the day and at night 99

Figure S3.1. Nitrate uptake by Nereocystis blades incubated in chambers 116

Figure S3.2. Biogeochemical responses in chamber experiments with N. luetkeana blades during the day and at night 117

Figure S3.3. Relationships between *N. luetkeana* blade dry mass and blade tissue percent nitrogen and DOC production. 118

Figure 4.1. Detection of MAGs across different kelp metagenome samples 129

Figure 4.2. Presence and absence of genes involved in dissolved organic matter (DOM) transport across all MAGs. 131

Figure 4.3. Presence and absence of genes involved in nitrogen cycling 133

Figure 4.4. Conceptual model of the functions and metabolisms of *Granulosicoccus* sp. that are important to its role as a macroalgal symbiont 137

Figure 4.5. *Granulosicoccus* sp. *pufLM* sequences in relation to photosystem II reaction center *pufLM* sequences from other known lineages of aerobic anoxygenic phototrophic bacteria 139

Figure S4.1. Maximum-likelihood phylogenetic tree showing the 66 non-redundant bacterial MAGs assembled from kelp blades 152

Figure S4.2. Abundance of MAGs across different kelp metagenome samples 153

Figure S4.3. Tree of *Granulosicoccus* genomes, including 8 kelp-associated MAGs and two reference genomes, *Granulosicoccus antarcticus* and *Granulosicoccus* sp. 002746645 154

Figure S4.4. Pangenome representing 10 *Granulosicoccus* genomes 155

ACKNOWLEDGEMENTS

My dissertation research would not have been possible without the help of many people, organizations, and funding sources. To begin, I would like to acknowledge my advisor, Cathy Pfister, for all of her enthusiastic support, assistance, time, expertise and mentorship. Thanks to Cathy Pfister and Tim Wootton for facilitating field research expeditions to Tatoosh Island, Washington, and for welcoming me into their home. I was constantly inspired and motivated by their passion for ecology, and my scientific worldview was expanded and enriched by being a part of their lab. Thank you to my committee members, Joy Bergelson, Tim Wootton and Maureen Coleman for helpful feedback throughout my graduate school experience, and for valuable comments during the preparation and writing of this dissertation. Thanks to my friends and fellow grad students in the CEB community and Darwinian Cluster for making my graduate program experience wonderful. A huge thank you to Mike Coates, Carolyn Johnson, Audrey Aronowsky, Marcy Hochberg, Bonnie Brown, Mary Johnson, and Jeff Wisniewski for being constantly helpful as I navigated the financial and administrative path of this PhD program.

I am extremely grateful to the Makah Tribe for permitting me to conduct research on their land. Tatoosh Island is an overwhelmingly beautiful and special place, and it was such a privilege to be able to conduct research there. Thanks to the Squaxin Island Tribe and Helen Berry for facilitating research at Squaxin Island, and thanks to the NOAA Olympic Coast National Marine Sanctuary for providing boat access to outer coast sites. I was lucky to have a team of incredible field assistants each summer, including Khashiff Miranda, Olivia Cattau, and Ty Bowyer. Thanks to Alisha Friel, Helen Berry, Max Calloway, Lauren Johnson, Ruby An, and Anna Wootton for additional fieldwork assistance. Thanks to Sativa Volbrecht and Connor Sauceda for assistance with lab research in Chicago. Thank you to the Erickson family for

generous field season internet, and thanks to the entire Sekiu Vista neighborhood community for being so welcoming during my summer field seasons.

Next-generation sequencing was made possible by Sarah Owens, Jason Koval and Stephanie Greenwald at Argonne National Lab. I could not have completed the metagenomic data analysis and bacterial genome assembly without help from Emily Fogarty, Andrea Watson, Khashiff Miranda, Justin Podowski, and the Meren lab anvi'o slack channel. Thanks to Kathy Krogsland and Aaron Morello at the UW Marine Chemistry Lab for seawater chemistry expertise. Stable isotope tracer experiments were greatly facilitated by advice from Mark Altabet, and technical expertise in isotope-ratio mass spectrometry from Gerry Olack, Andrew Masterson, Paul Middlestead, and others at the Ján Veizer Stable Isotope Laboratory. Special thanks to my amazing collaborators and role model women in science: Jessica Mark Welch, Tabita Ramirez-Puebla, and Sophie McCoy. Jessica and Tabita, thank you for opening my eyes to the micron-scale bacterial world, and I am ever so grateful for your expertise in microscopy.

This research was funded by a National Geographic Society Early Career Grant, a Climate Change Initiative Grant funded by the Rebecca Susan Buffett Foundation, the University of Chicago Hinds Fund, and the Phycological Society of America Grants-in-Aid of Research. Travel to from Chicago to Washington was supported by the Committee on Evolutionary Biology. Research funding also included a NOAA-COCA program research grant (#1556874) awarded to Cathy Pfister, and a NSF-DEB grant (#1556874) awarded to Tim Wootton. I am grateful that my graduate studies were supported by a Graduate Assistance in Areas of National Need Fellowship from the U.S. Department of Education, funding from the Washington State Department of Natural Resources, and the University of Chicago Harper Fellowship.

Finally, thanks to my family for being so loving and supportive of my desire to become a marine ecologist. I am grateful to have been raised by a family who values time spent outdoors and privileged to have been able to spend my childhood summers at Auburn Lake. Thanks for encouraging me to follow my dreams and passions, even when they involved scuba diving under frozen Wisconsin lakes during the winter. Special thanks to my parents, Bill and Laureen Weigel, for allowing me to live and work at the cabin for much of 2020 during the coronavirus pandemic. My graduate school experience would not have been as joyful without the company of my 15 housemates in the Gamma Alpha Cooperative House; thanks for making my time in Hyde Park much more interesting and fun! Finally, I am ever so grateful to my partner, fellow graduate student and pandemic companion, Arvind Pillai, for all of the support, love, inspiration, delicious dinners, and company during long field season road trips.

ABSTRACT

Most eukaryotic organisms live in intimate association with diverse communities of Bacteria, and sometimes Archaea, which can have a profound influence on the ecology and evolution of their eukaryotic hosts. Microbial symbionts can expand the metabolic capabilities and functional traits associated with their host, with cascading impacts to nutrient cycles in the surrounding ecosystem. Kelp, brown macroalgae in the order *Laminariales*, play an important role in the global carbon cycle by creating highly productive underwater forests in temperate coastal marine ecosystems. Photosynthetic kelp blades harbor abundant microbial communities, providing a large surface area that is rich in organic carbon resources, yet we know little about the diversity, community structure, and functional role of the kelp microbiome. In four chapters, this dissertation research 1) characterized the microbiome of the bull kelp, *Nereocystis luetkeana*, and the giant kelp, *Macrocystis pyrifera*, through field surveys across spatial and temporal scales, 2) examined microbial community assembly on *N. luetkeana* blade surfaces through *in situ* experiments, 3) quantified carbon fixation and dissolved organic carbon (DOC) release by the canopy-forming kelps *N. luetkeana* and *M. pyrifera*, and 4) determined the functional role of Bacteria associated with *N. luetkeana* by reconstructing bacterial genomes from metagenomes. The kelp microbiome was specific to each host kelp species, distinct from microbial communities in the surrounding seawater, and displayed significantly geographic and temporal variation. Quantifying carbon cycling by canopy-forming kelps demonstrated that kelps release ~16% of their total fixed carbon into the surrounding seawater, providing a consistent metabolic resource to heterotrophic bacteria. The most abundant bacterial genus on kelp blades, *Granulosicoccus*, was ubiquitous across spatial and temporal scales and became abundant on new meristematic kelp blade tissues within days. Genomes of *Granulosicoccus* sp. revealed that

these bacteria have the ability to assimilate dissolved organic carbon resources, synthesize cobalamin (vitamin B12), and reduce oxidized nitrogen sources to ammonium, which may provide the host kelp with reduced nitrogen and vitamins. Overall, this dissertation research expanded our knowledge of the factors structuring the kelp microbiome, examined microbial settlement on kelp tissues, quantified carbon cycling in kelp forests, and provided insight into the metabolic functions of key bacterial taxa in the kelp microbiome that persisted across spatial and temporal scales.

INTRODUCTION

Recent advances in next-generation DNA sequencing have revealed the exceptional diversity of microbial communities across environments, which contain, on average, hundreds to thousands of distinct taxa per sample (Thompson et al. 2017). In addition to existing as free-living microbes in the environment, many Bacteria and some Archaea associate with eukaryotic hosts by living on their surface or within host tissues. Microbial symbionts (used throughout this dissertation in the board sense, without implying mutualism) can have profound impacts on the ecology and evolution of their eukaryotic hosts by affecting their development, reproduction, disease susceptibility, or by introducing novel traits not encoded in the host genome (Goecke et al. 2010; Egan et al. 2013, Wilkins et al. 2019). In addition to influencing the biology of their host, the metabolisms of host-associated microbiomes can directly impact biogeochemical cycles and fluxes in the surrounding ecosystem (Pfister and Altabet 2019, Beinart 2019). Despite the potential to significantly influence host traits and functions as well as ecosystem-level nutrient cycles, basic knowledge about microbiome composition, assembly and function is still lacking for many marine organisms (Wilkins et al. 2019).

It is particularly important to determine the functional role and metabolisms of microbes associated with large, habitat-forming foundational species, as high total microbial symbiont abundances could make host-associated microbes important players in biogeochemical cycles (Beinart 2019). Kelp, brown macroalgae in the order *Laminariales*, are distributed globally in temperate and arctic coastal marine ecosystems (Krumhansl et al. 2016). Canopy-forming kelp that extend to the surface of the ocean are foundational species, forming vast and highly productive underwater forests that provide structural habitat for a diversity of marine organisms, including marine mammals, fish and invertebrates (Steneck et al. 2002). Canopy-forming kelp

are among the fastest growing and most productive marine algae, with photosynthetic blade growth rates of up to 5-10 cm per day (Wheeler and Druehl 1986, Graham et al. 2007) and adult sporophyte thalli that can extend 10 to 30 m in height (Steneck et al. 2002). Despite their enormous size and importance as primary producers, we know little about the diversity and functional role of microbial communities associated with these photosynthetic giants.

Microbial communities associated with macroalgae are distinct from those in seawater (Bengtsson et al. 2010, Michelou et al. 2013, Mancuso et al., 2016) and their composition tends to be unique to each host species (Lachnit et al. 2009, Bondoso et al. 2014, Aires et al. 2016), but microbial taxa are often shared between different macroalgal hosts (Florez et al. 2017, Lemay et al. 2018), suggesting some common properties of the macroalgal microbiome. Macroalgae host dense microbial biofilms that cover their photosynthetic surfaces, with roughly 10^6-10^8 microbial cells per cm^2 of algal tissue (Mazure and Field 1980, Stratil et al. 2013, Bengtsson et al. 2010). In addition to providing a large surface area for bacterial settlement, kelp provide heterotrophic microbes with metabolic resources, including surface polysaccharides (Bengtsson et al. 2011, Lin et al. 2018). Additionally, all aquatic algae release some proportion of their fixed carbon into the surrounding water as dissolved organic carbon, or DOC (Tolbert and Zill 1956, Fogg 1963, Baines and Pace 1991), which includes carbohydrate sugars and other intracellular metabolites (Newell et al. 1980, Wada et al. 2007). On average, kelps release between 14 and 43% of their total fixed carbon as DOC (Sieburth 1969, Abdullah and Fredriksen 2004, Wada et al. 2007, Reed et al. 2015), potentially providing an abundant metabolic resource for kelp-associated microbes. While there is a clear benefit to host-association for heterotrophic microbes, we know little about how microbial symbionts influence the biology of the host kelp or nutrient cycling in

kelp forests, as the metabolic functions of the uncultured majority of kelp-associated microbes are still relatively unexplored.

On the Pacific Coast of North America, two canopy-forming kelps with different life histories co-occur: the annual bull kelp *Nereocystis luetkeana* and the perennial giant kelp *Macrocystis pyrifera*. The giant kelp *M. pyrifera* is distributed along the Pacific coast of North and South America and regions in the Southern hemisphere, while *N. luetkeana* has a smaller geographic range, from central California to the Aleutian Islands in Alaska. My dissertation research examines the genetic diversity, community structure and functional role of microbial symbionts associated with these canopy-forming kelp species. While my research focuses on the bull kelp, *N. luetkeana*, due to its dominance in Washington and the paucity of literature on this species, Chapters 1 and 3 characterize the microbiome and carbon cycling functions of *M. pyrifera*, respectively, for comparison with those of *N. luetkeana*.

The factors that shape the composition, diversity and structure of microbial communities associated with canopy-forming kelps are poorly understood. In Chapter 1 of this dissertation, I examined variation in the kelp microbiome across geographic and temporal scales to identify the factors contributing to variation in microbial community structure. Using 16S rRNA gene sequencing, I characterized microbial communities living on photosynthetic blades of the canopy forming kelps *N. luetkeana* and *M. pyrifera* across geographic locations ranging from the outer Pacific Ocean to southern Puget Sound, revealing that the kelp microbiome is specific to each kelp species, distinct from seawater microbial communities, and varies significantly with geographic location. In addition, microbial communities on *N. luetkeana* blades sampled throughout the spring and summer growing season displayed significant temporal variation, and

mature tissues from the tip of the kelp blade had significantly greater bacterial sequence abundances and diversity compared to new, meristematic blade tissues.

In Chapter 2, I conducted an *in situ* experiment in the kelp forest to test patterns of microbial community settlement on artificial kelp substrates vs. real kelp blades relative to the pool of microbes in the surrounding seawater. Microbial community assembly on kelp surfaces demonstrated strong host filtering from the pool of microbes in the surrounding environment, with host-associated taxa such as *Granulosicoccus* sp. becoming abundant on new meristematic kelp blade tissues within days, while common seawater bacteria settled on artificial kelp substrates. Kelp blade tissues were colonized by markedly distinct microbial taxa relative to artificial kelp substrates during the same time interval, and the dominant bacterial groups on living kelp blades had primarily aerobic metabolisms, suggesting that oxygen production by kelp blade may shape microbial membership. Finally, microbial communities on artificial kelp substrates infused with dried *N. luetkeana* blades displayed significantly lower bacterial diversity relative to control agar substrates, suggesting that non-living components of the kelp blade also impact microbial community assembly.

Kelps release a large proportion of their fixed carbon as dissolved organic carbon (DOC), which likely provides an abundant organic carbon resource to heterotrophic microbes living on the surfaces of kelp. In addition to potentially fueling microbial metabolisms, export of DOC to the deep sea is hypothesized to be the main pathway for carbon sequestration by macroalgae (Krause-Jensen and Duarte 2016). Despite growing efforts to use kelp as a potential "blue carbon" sink (Hill et al. 2015, Krause-Jensen and Duarte 2016), we know little about the factors that control DOC release by kelps. In Chapter 3, I quantified carbon fixation and DOC release by *N. luetkeana* in the field, demonstrating that ~16% of the total fixed carbon is released as DOC.

Further, I examined the physiology of DOC release by by testing the effects of light levels and nitrogen availability on DOC release rates, and I used a stable isotope approach to quantify the proportion of DOC released that was derived from recently fixed carbon.

Bacteria associated with the kelp surface likely metabolize DOC and nutrients in a variety of forms, yet there is a significant knowledge gap concerning the range of metabolisms present in the kelp microbiome. In Chapter 4, I reconstructed 79 bacterial genomes from *N. luetkeana* blades to identify the functional roles and metabolisms of kelp-associated microbes. Using a genome-resolved metagenomics approach allowed me to match functional genes and metabolic capabilities with the taxonomy each bacterial species, revealing the functionally important members of the kelp microbiome. Genes related to DOC metabolism and assimilation, nitrate reduction and urea hydrolysis, and vitamin B12 (cobalamin) biosynthesis were present in diverse bacterial groups. In addition, we reconstructed 8 genomes of the common and abundant macroalgal symbiont *Granulosicoccus* sp., demonstrating that they are aerobic anoxygenic phototrophic bacteria, making them the first photoheterotrophic representatives of this genus.

LIST OF PUBLICATIONS

CHAPTER 1

- Weigel, B.L. and Pfister, C.A. 2019. Successional dynamics and seascape-level patterns of microbial communities on the canopy-forming kelps *Nereocystis luetkeana* and *Macrocystis pyrifera*. Frontiers in Microbiology 10(346): doi: 10.3389/fmicb.2019.00346

CHAPTER 2

- Weigel, B.L. and Pfister, C.A. 2021. Oxygen metabolism shapes microbial settlement on photosynthetic kelp blades compared to artificial kelp substrates. Environmental Microbiology Reports 13(2): 176-184. doi:10.1111/1758-2229.12923

CHAPTER 3

- Weigel, B.L. and Pfister, C.A. 2021. The dynamics and stoichiometry of dissolved organic carbon release by kelp. Ecology 102(2): e03221. doi:10.1002/ecy.3221

CHAPTER 4

- Weigel, B.L., et al. *In preparation*. Functional insights into the kelp microbiome from metagenome assembled genomes.

CHAPTER 1: SUCCESSIONAL DYNAMICS AND SEASCAPE-LEVEL PATTERNS OF MICROBIAL COMMUNITIES ON THE CANOPY-FORMING KELPS NEREOCYSTIS LUETKEANA AND MACROCYSTIS PYRIFERA

Citation: Weigel BL and Pfister CA. 2019. Successional dynamics and seascape-level patterns of microbial communities on the canopy-forming kelps *Nereocystis luetkeana* and *Macrocystis pyrifera*. Frontiers in Microbiology 10(346): doi: 10.3389/fmicb.2019.00346

Abstract

Canopy-forming kelps create underwater forests that are among the most productive marine ecosystems. On the Pacific coast of North America, two canopy-forming kelps with contrasting life histories co-occur; *Macrocystis pyrifera*, a perennial species, and *Nereocystis luetkeana*, an annual species. Kelp blade-associated microbes were sampled from 12 locations across a spatial gradient in Washington, United States, from the outer Pacific Coast to Puget Sound. Microbial communities were characterized using next-generation Illumina sequencing of 16S rRNA genes. At higher taxonomic levels (bacterial phylum and class), canopy-forming kelps hosted remarkably similar microbial communities, but at the amplicon sequence variant level, microbial communities on *M. pyrifera* and *N. luetkeana* were host-specific and distinct from free-living bacteria in the surrounding seawater. Microbial communities associated with blades of each kelp species displayed significant geographic variation. The microbiome of *N. luetkeana* changed along the spatial gradient and was significantly correlated to salinity, with outer Pacific coast sites enriched in *Bacteroidetes* (family *Saprospiraceae*) and *Gammaproteobacteria* (*Granulosicoccus* sp.), and southern Puget Sound sites enriched in *Alphaproteobacteria* (family *Hyphomonadaceae*). We also examined microbial community development and succession on meristematic and apical *N. luetkeana* blade tissues throughout the summer growing season on Tatoosh Island, WA. Across all dates, microbial communities were less diverse on younger, meristematic blade tissue compared to the older, apical tissues. In addition, phylogenetic

relatedness among microbial taxa increased from meristematic to apical blade tissues, suggesting that the addition of microbial taxa to the community was a non-random process that selected for certain phylogenetic groups of microbes. Microbial communities on older, apical tissues displayed significant temporal variation throughout the summer and microbial taxa that were differentially abundant over time displayed clear patterns of community succession. Overall, we report that host species identity, geographic location, and blade tissue age shape the microbial communities on canopy-forming kelps.

Introduction

Kelps (brown algae in the order *Laminariales*) are important habitat-forming foundational species in temperate coastal marine ecosystems worldwide (Krumhansl et al., 2016). Canopy-forming kelps create vast and highly productive underwater forests, fixing up to 1.3 kg C per m2 each year (Wheeler and Druehl, 1986). Macroalgae present an abundant surface for bacterial settlement, and they provide heterotrophic microbes with potential metabolic resources, including algal polysaccharides (Martin et al., 2015; Lin et al., 2018) and dissolved organic carbon (Abdullah and Fredriksen, 2004; Reed et al., 2015). As a result, kelps host an abundant epiphytic microbial community in their surface mucus layer (Bengtsson and Øvreås, 2010; Michelou et al., 2013; Lemay et al., 2018). Epiphytic microbial communities on macroalgae tend to be host species-specific (Lachnit et al., 2009; Bondoso et al., 2014; Aires et al., 2016), and they have a distinct composition from free-living microbial communities in the surrounding seawater (Staufenberger et al., 2008; Bengtsson et al., 2010; Michelou et al., 2013; Mancuso et al., 2016). The kelp microbiome can be an indicator of overall host health (Marzinelli et al., 2015) and exposure to environmental stressors (Minich et al., 2018). Microbial

symbionts in coral reefs and the plant rhizosphere can contribute substantially to host health and may add adaptive capacity in changing environments (Correa and Baker, 2011; Philippot et al., 2013; Cunning et al., 2015). Recent research has shown that the microbiome of the canopy kelp *M. pyrifera* is susceptible to disruption by elevated temperatures (Minich et al., 2018), and there has been increasing concern about kelp forests declining in abundance in some regions of the world (Krumhansl et al., 2016; Pfister et al., 2018). Despite these concerns, we know little about the ecological and evolutionary processes that shape the microbiome of canopy-forming kelps.

Two species of canopy-forming kelps co-occur along the Pacific Coast of North America but have contrasting life histories: *Macrocystis pyrifera* is a perennial species that can persist for several years and *Nereocystis luetkeana* is an annual species. These two canopy-forming kelp species often coexist together in Washington kelp forests (Pfister et al., 2018), yet no studies have directly compared their microbial communities. One study found that epiphytic microbial communities among eight sympatric kelp species were structured by life history strategy (annual vs. perennial) rather than by host phylogeny (Lemay et al., 2018), indicating that the longevity of the thallus may affect microbial community assembly on kelps. Lemay et al. (2018) reported that the microbiome of *N. luetkeana* was similar to the microbial communities of other co-occurring annual kelps. However, all *N. luetkeana* samples in Lemay et al. (2018) were from the relatively young meristematic region at the base of the blade, which might have lower bacterial abundance and diversity than other regions of the kelp thallus (Staufenberger et al., 2008). The microbiome of *M. pyrifera* was first characterized in central California, with dominant bacterial phyla consisting of Proteobacteria, *Bacteroidetes*, and Verrucomicrobia (Michelou et al., 2013). In our study, we characterize the microbial communities of co-occurring *N. luetkeana* and *M. pyrifera*,

using both spatial and temporal sampling to understand how host species identity, geographic location, and time shape the microbiome of these giant, ecologically important kelps.

First, we ask whether these kelps display geographic variation in blade-associated microbial communities. Examining the degree of similarity in microbial communities from one host species across a geographic scale can provide an understanding of how strongly the host, environmental variables, or geographic distance (i.e., dispersal limitation) structures the microbiome (Hanson et al., 2012; Pita et al., 2013). If microbial symbionts are environmentally acquired, which is likely on annual kelps, they may reflect the microbial composition of the surrounding seawater. The assembly of a host-specific microbiome may also relate to the strength of functional interactions between the host and its microbial associates (Burke et al., 2011; Fahimipour et al., 2017). For example, the leaf microbiome of eelgrass (Zostera marina) was spatially variable and similar to local seawater microbial communities, while the root microbiome contained a set of core taxa and remained distinct from sediment microbial communities across a global spatial scale (Fahimipour et al., 2017). Determining whether kelp-associated microbial communities change as the species pool in the surrounding seawater changes across large geographic distances is a first step toward understanding the stability and specificity of the interactions between canopy-forming kelps and their microbial associates. This study characterized the spatial dynamics of microbial communities associated with *N. luetkeana*, *M. pyrifera*, and seawater across a broad spatial gradient in Washington, encompassing significant environmental variation in temperature, salinity, and seawater nutrient concentrations.

In addition to the effects of host kelp species identity, environmental variables, and geographic distance, time may also be an important factor structuring kelp-associated microbial communities. For example, epiphytic biofilms on the kelp *Laminaria hyperborea* displayed

temporal changes in cell density and bacterial community composition over 1 year. Bacterial cell densities were lowest (10^2 cells cm^2) at the start of the kelp growing season, reaching a peak (10^7 cells cm^2) after the end of the growing season (Bengtsson et al., 2010). The epiphytic microbiome of the brown algae *Cystoseira compressa* displayed a successional pattern, with a gradual increase in the number of bacterial taxa throughout the growing season (Mancuso et al., 2016). Another study examined the microbiome of *M. pyrifera*, finding temporal variation in the relative abundances of dominant bacterial phyla (*Proteobacteria*, *Bacteroidetes*, *Verrucomicrobia*) between kelp sampled in March and May (Michelou et al., 2013). While it is clear that microbial communities on kelp undergo temporal or seasonal changes, studies with high-resolution sequencing and greater replication are necessary to characterize the temporal dynamics of the kelp microbiome.

Canopy kelp blades grow outward from the float at extraordinarily high rates, expanding linearly 1–2 cm each day (Brown et al., 1997). This creates tissues of varying age along the length of the blade, which can be used to examine how kelp thallus age affects microbial community development. The first studies to recognize this cultured and counted colonies of bacteria from basal meristem, middle, and tip regions of *Laminaria* spp. fronds, finding that bacterial densities were highest at the tip and lowest at the basal meristem (Laycock, 1974; Mazure and Field, 1980). Another study found that epiphytic bacterial communities on the kelp *Saccharina latissima* were more similar on older tissues from different individuals than between old and new (meristematic) tissues from the same individual (Staufenberger et al., 2008). The rapid growth of kelp blades provides new surface area for microbial colonization from the surrounding seawater, or other microbial reservoirs. There is some evidence that microbial symbionts on algae may be recruited from motile marine bacteria in the surrounding seawater.

For example, motile marine bacteria exhibit chemotaxis toward phytoplankton cells and their extracellular products (Seymour et al., 2010, 2017). Extracted compounds from the brown algae *Fucus vesiculosus* mediated epiphytic microbial settlement and community composition onto artificial surfaces (Lachnit et al., 2013), and a recent kelp metagenome revealed a two-to threefold enrichment in flagellum, motility, and chemotaxis genes on the kelp surface relative to the surrounding seawater (Minich et al., 2018). Tracking microbial communities on meristemic vs. apical blade tissues over time can thus be used to examine how microbial communities assemble onto new kelp tissues and continue to develop on older tissues. To test whether tissue age affects microbial community assembly on the annual kelp *N. luetkeana*, we tracked microbial communities on new (meristematic) and old (apical) *N. luetkeana* blade tissues and the free-living microbial community in the surrounding seawater at one site throughout the spring and summer growing season.

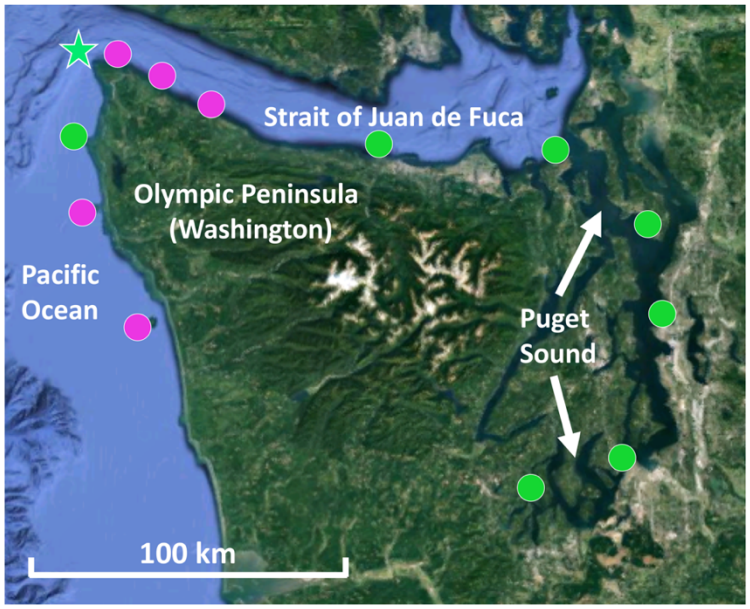

Figure 1.1. Map of kelp forests sampled in Washington, including co-occurring *N. luetkeana* and *M. pyrifera* kelp forests (pink circles) and locations where only *N. luetkeana* was sampled (green circles). The filled circles indicate kelp forests that were sampled for geographic comparisons (n = 12), while the green star indicates the location of Tatoosh Island.

Methods

Sample collection

Kelp blade tissue samples (n = 6 individuals) and seawater microbial samples (n = 2 or 3) were collected from 12 sites in Washington, including five sites on the outer Olympic Coast, three along the Strait of Juan de Fuca, and four within Puget Sound (Fig. 1.1). For mixed kelp forests, both *N. luetkeana* and *M. pyrifera* tissues were collected. Kelp tissue samples were collected by boat from the floating kelp canopy by removing 2 x 1 cm^2 of tissue from the middle of the kelp blade with sterile scissors. Individual samples were placed into 1.5 ml microcentrifuge tubes. Seawater samples were collected near the surface from within the kelp forest using sterile 1.0 L plastic bottles. After transporting seawater to the lab in a cooler with ice packs, microbial samples were collected by filtering seawater through 0.22 μm Millipore SterivexTM filters with a peristaltic pump. All kelp tissue and seawater samples were immediately frozen at 20°C until they were transferred to 80°C for storage until processing. Temperature and salinity were measured at each site using a Hydrolab MS5 water quality sonde (Bullman, Tatoosh, Koitlah) or a CastAway-CTDQR (all other sites).

Temporal sampling was conducted by monitoring one *N. luetkeana* population at the north-facing Main Beach site on Tatoosh Island (48.39°N, 124.74°W) at six time points from 12 May to 22 August 2017. Kelp tissue samples were collected at low spring tides. At each time point, two tissue samples were collected from a single blade – one at the basal meristem, roughly 2 cm from where the blade connects to the stipe, to capture recently produced tissue (24–48 h old) and another near the apical end of the blade tip to sample older tissue (weeks to months old). Samples were collected from different kelp individuals (n = 6) at each time point. In contrast, samples from the 11 other sites across the geographic range were collected from the middle of

the kelp blade (see above). *N. luetkeana* blade linear growth rates were measured during the time interval between each sampling date by putting a small 2 mm hole punch near the basal meristem of all censused kelp. Using this method to visually track growth rates near the base of the blade, we verified that meristem tissue collected at each census date was recently produced. In addition, the total length of each sampled blade was measured to determine the approximate age of apical (hereafter "blade tip") samples. The large thallus size of *N. luetkeana* is demonstrated in Fig. 1.4.

Molecular methods

DNA was extracted from whole kelp tissues and seawater SterivexTM filters using the DNeasy Power Soil Kit (Qiagen). For seawater samples, Sterivex casings were cut with PVC cutters and half of the filter paper was removed and extracted as a solid sample (Jackrel et al., 2017). After DNA extraction, extracts were sent to Argonne National Laboratory for amplification of the V4 region of the 16S rRNA gene using the Earth Microbiome Project universal primers 515f–806r (Caporaso et al., 2011), with the modified forward primer (Parada et al., 2016) to reduce bias against *Crenarchaeota*, *Thaumarchaeota*, and the SAR11 clade (Walters et al., 2016). DNA amplicons were sequenced on an Illumina MiSeq paired-end run at Argonne National Laboratory following the procedures of Caporaso et al. (2012). Raw 16S rRNA sequences were deposited as FASTQ files to the Qiita platform1 (study ID #12016), through which all sequences and metadata were uploaded to the European Bioinformatics Institute (accession # PRJEB29319).

16S rRNA sequence data processing and statistical analyses

Raw sequences were processed with QIIME2. After raw sequence reads were demultiplexed, sequence quality control was performed, paired-end reads were merged, and amplicon sequence variants (ASVs) were generated using the Divisive Amplicon Denoising Algorithm (DADA2) (Callahan et al., 2016). With this algorithm, quality control included chimera detection and removal, sequence error elimination, singleton exclusion, and sequence trimming based on per-base-pair sequence quality graphs (both forward and reverse sequences were trimmed between 13 and 150 base pairs). The resulting sequences were classified with the Greengenes reference database (gg_13_8_99), trimmed to the V4 region. Note that the final bacterial order-level barplots were constructed using Silva taxonomy, because Green Genes taxonomy classifications did not go past the class level for many abundant ASVs (Fig. S1.1). After classification, chloroplast and mitochondria reads were removed. We used the "qiime diversity core-metrics-phylogenetic" function to analyze alpha and beta diversity among sample types, which requires rarefaction to a user-specified sampling depth prior to computing diversity metrics. For the geographic dataset (n = 115 total samples), we rarefied each sample to a depth of 1,000 sequences. For the temporal study of microbial community assembly on kelp blades, we found consistently low bacterial sequence abundances in kelp blade meristem samples; thus, we did not exclude low bacterial abundance meristem samples. Instead, for the temporal dataset (n = 80 total samples) we rarefied each sample to a depth of 200 sequences. To allow comparison between the geographic and temporal datasets, we used a sampling depth of 200 sequences per sample.

Alpha diversity indices (ASV richness, Shannon diversity, Faith's phylogenetic diversity, and Pielou's evenness) were calculated in QIIME2 with q2-diversity following the sequence depth normalizations listed above, and one-way non-parametric Kruskal–Wallis analyses of

variance (ANOVA) were used to statistically compare the diversity indices for each sample type (*M. pyrifera* vs. *N. luetkeana* vs. seawater for geographic dataset, meristem vs. tip vs. seawater for temporal dataset). To compare overall microbial community structures between different sample types, one-way (fixed factor) non-parametric permutational multivariate ANOVA (PERMANOVA) were conducted based on unweighted unifrac distance matrices using q2-diversity beta group significance. Pairwise comparisons were conducted for significant PERMANOVA results with the Benjamini and Hochberg correction (q-value) to account for multiple pairwise comparisons. To ensure that differences in microbial community structure are not due to unequal dispersion of variability among groups, permutational multivariate analyses of dispersion (PERMDISP) were conducted for all significant PERMANOVA outcomes in PRIMER (version 6.1.11). Additional PERMANOVA tests were conducted in PRIMER test for (1) possible effects of geography on the distinction between microbial communities from each kelp species (two-way PERMANOVA with "species" as a fixed factor and "location" as a random factor, using only samples from locations where the two kelps co-occur) and (2) random effects of "kelp individual," because meristem and tip communities were sampled from the same plant (two-way PERMANOVA with "meristem vs. tip" as a fixed factor and "kelp individual" as a random factor).

To search for differentially abundant microbial taxa across sample types or locations, analysis of composition of microbiomes (ANCOM) tests were implemented in QIIME2 (Mandal et al., 2015). To examine the variation in microbial communities that could be explained by environmental variables measured at each site (temperature and salinity), we performed a Constrained Analysis of Principal Coordinates (CAP) analysis (Anderson and Willis, 2003) based on Bray–Curtis dissimilarities in the R package Vegan (version 2.5-1; Oksanen et al.,

2014). Statistical significance for CAP was determined with an ANOVA permutation test (anova.cca) using 1,000 permutations in Vegan. This constrained ordination was visually compared to an unconstrained ordination (PCoA) based on the same Bray–Curtis dissimilarity matrix. All statistical tests were examined with a post-correction experiment-wide error rate of 0.05. Differences in microbial communities were visualized in R (version 3.4.4) with the phyloseq package (McMurdie and Holmes, 2013) by creating (1) non-metric multidimensional scaling (NMDS) and principal coordinate analysis (PCoA) ordinations based on Bray–Curtis dissimilarities and (2) barplots and heatmaps based on relative abundances of microbial taxa across sample types.

Phylogenetic signal methods

All phylogenetic structure analyses were implemented in R with the package "picante" (Kembel et al., 2010). Briefly, we created a phylogenetic distance matrix based on a maximum-likelihood 16S rRNA tree generated in QIIME2 with FastTree2 (Price et al., 2010). The net relatedness index (NRI) was calculated from the phylogenetic distance matrix using the "standardized effect size of pairwise distances in communities" function (ses.mpd) and the nearest taxa index (NTI) was calculated using the "standardized effect size of mean nearest taxon distances" function (ses.mntd). NRI is a measure of the mean relatedness between members of microbial communities, and the NTI is a measure of the smallest mean phylogenetic distance between all pairs of n taxa in a community sample. For both NRI and NTI analyses, the null model was randomized 999 times and set to "phylogeny.pool," which randomly draws species from the phylogeny for its null distribution. NRI and NTI were calculated for microbial communities from each individual kelp tissue or seawater sample. Final graphs include only

microbial community samples where $P < 0.05$. Positive NRI/NTI values describe a microbial community where members are on average more closely related to one another than they are to members of the randomized, regional (null model) microbial species pool. One-way ANOVA were run in R to statistically compare the NRI and NTI for each sample type (kelp meristem, kelp tip, seawater).

Results

Environmental variables

Mean temperature increased with decreasing ocean influence, from a mean of 8.8°C at Destruction Island to 13.6°C at Squaxin Island, the location of the southernmost kelp bed in Puget Sound (Fig. 1.1 and Fig. S1.2). Salinity showed the opposite pattern, as expected, decreasing with decreasing ocean influence from a mean of 33.45 at Destruction Island to 27.60 at Squaxin Island (Fig. S1.2). Note that Tatoosh Island displays the most variability (Fig. S1.2), because while most locations were only sampled once on the day that microbial samples were collected, temperature and salinity data were collected at Tatoosh Island multiple times throughout the summer, from June until August. Despite this variability, there is a strong pattern of increasing temperature and decreasing salinity as you move across the 13 locations, from the Pacific Ocean to the inner Puget Sound.

Comparative analysis of *M. pyrifera* and *N. luetkeana* microbial communities

After removing samples with less than 1,000 sequences, the spatial dataset contained n = 28 *M. pyrifera* samples from 5 sites, n = 59 *N. luetkeana* samples from 11 sites, and n = 28 seawater samples from 9 sites. *N. luetkeana* samples from one location (Bullman Beach) had

consistently low sequence abundances and were excluded from all analyses. Across all sites, alpha diversity metrics including mean ASV species richness, Shannon diversity, Faith's phylogenetic diversity, and Pielou's Evenness were significantly higher on *M. pyrifera* than *N. luetkeana*, and all alpha diversity metrics were significantly higher in seawater compared to both kelp species (Kruskal–Wallis ANOVA, df = 2; $H = 82.98$ and $P < 0.001$ for ASV richness, $H = 75.81$ and $P < 0.001$ for Shannon diversity, $H = 74.64$ and $P < 0.001$ for Faith's PD, $H = 61.32$ and $P < 0.001$ for Pielou's Evenness; corrected P-values < 0.001 for all Kruskal–Wallis pairwise tests; Fig. 1.2). Mean ASV richness per sample was 36 for *N. luetkeana* blades, 102 for *M. pyrifera* blades, and 147 for seawater microbial communities.

Epiphytic microbial communities hosted by the canopy-forming kelps *N. luetkeana* and *M. pyrifera* were distinct from each other and from the surrounding seawater, despite co-occurrence of these two species in mixed kelp forests (Table 1.1a; all PERMANOVA pairwise comparisons q-value = 0.001; Fig. 1.3). Because *N. luetkeana* were sampled at sites where *M. pyrifera* did not occur, we eliminated the potential that geography confounded differences between the species by testing for the effect of species only at the four sites where they do co-occur (Table S1.1). This restricted PERMANOVA demonstrated that *N. luetkeana* and *M. pyrifera* still hosted significantly different microbial communities at these sites (Table S1.1). Although the PERMDISP test was significant (Table 1.1a), indicating unequal dispersion of variability among groups, the significance resulted from a difference in dispersion between each kelp species and seawater (pairwise test for *N. luetkeana* and seawater: $t = 6.67$, $P = 0.001$; pairwise test for *M. pyrifera* and seawater: $t = 3.40$, $P = 0.004$), while *N. luetkeana* and *M. pyrifera* microbial communities did not display significant differences in dispersion (PERMDISP pairwise: $t = 1.78$, $P = 0.112$). *N. luetkeana* and *M. pyrifera* hosted significantly different

microbial communities (PERMANOVA pairwise, df = 1, pseudo-F = 9.84, q-value = 0.001), yet the relative abundances of the top bacterial phyla, classes, and orders on *N. luetkeana* and *M. pyrifera* were quite similar (Table 1.2). The top bacterial phyla on each kelp were *Proteobacteria* (74.9% for *N. luetkeana*; 76.5% for *M. pyrifera*), followed by *Bacteroidetes* (11.8% for *N. luetkeana*; 16% for *M. pyrifera*), *Verrucomicrobia* (10.5% for *N. luetkeana*; 1.3% for *M. pyrifera*), and Planctomycetes (2.1% for *N. luetkeana*; 3.9% for *M. pyrifera*). These four phyla accounted for 98–99% of all microbial taxa on each kelp species. The top classes on *N. luetkeana* and *M. pyrifera* included *Gammaproteobacteria* (49 and 47%, respectively), *Alphaproteobacteria* (25 and 28%), *Verrucomicrobiae* (11 and 1%), *Saprospirae* (9 and 10%), *Flavobacteriia* (3 and 6%), and *Planctomycetia* (2 and 3%; Table 1.2). While bacteria made up most of the microbial communities on kelp, we detected one archeal phylum hosted by *M. pyrifera* (*Crenarchaeota*, <0.001% mean relative abundance) and one by *N. luetkeana* (*Euryarchaeota*, <0.001% mean relative abundance).

Table 1.1. Results of statistical tests comparing beta diversity (variation in microbial community structure) among (A) kelp species and geographic locations, and (B) kelp meristem and tip vs. date. For all significant PERMANOVA results, PERDISP tests were conducted to ensure that significant results were not due to unequal dispersion of variability among groups.

	PERMANOVA			PERMDISP		
a) Geographic groups compared	**df**	**pseudo-F**	**P**	**df**	**F**	**P**
Macrocystis, Nereocystis, seawater	2	18.78	0.001*	2	23.57	0.001*
Macrocystis by 5 Locations	4	1.98	0.001*	4	3.34	0.141
Nereocystis by 11 Locations	10	2.40	0.001*	10	1.63	0.429
Seawater by 9 Locations	8	2.16	0.001*	8	10.96	0.012*
b) Temporal groups compared						
Meristem, tip, seawater	2	4.00	0.001*	2	3.89	0.043*
Meristem by Date	5	1.44	0.002*	5	1.58	0.479
Tip by Date	5	3.57	0.001*	5	3.69	0.102
Seawater by Date	4	2.09	0.001*	4	6.78	0.226

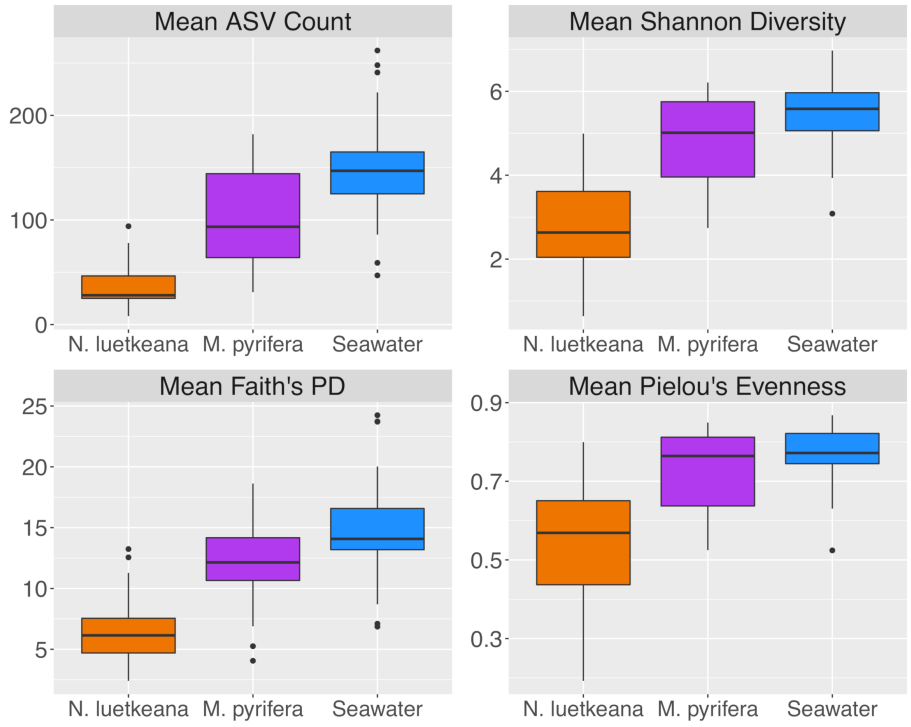

Figure 1.2. Alpha diversity indices including (A) mean ASV count, (B) mean Shannon diversity, (C) mean Faith's Phylogenetic diversity, and (D) mean Pielou's evenness for *N. luetkeana*, *M. pyrifera*, and seawater microbial communities.

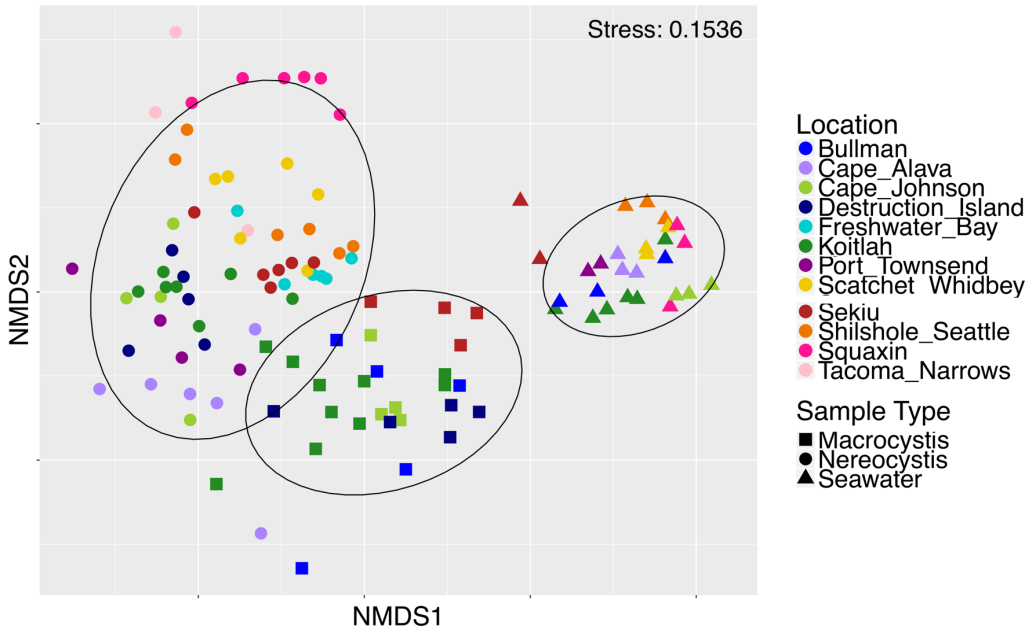

Figure 1.3. Non-metric multidimensional scaling plot of *M. pyrifera*, *N. luetkeana*, and seawater microbial communities across 12 sites in Washington.

At the ASV level, *N. luetkeana* and *M. pyrifera* microbial communities were more distinct. Across all sites, *N. luetkeana* hosted 1,046 unique ASVs from 21 bacterial and 1 archaeal phyla and *M. pyrifera* hosted 1,643 ASVs from 23 bacterial and 1 archaeal phyla. *N. luetkeana* and *M. pyrifera* shared 33 and 21% of unique microbial ASVs, respectively. Interestingly, only 32% of kelp ASVs on each species were also found in the surrounding seawater (334 out of 1,046 ASVs for *N. luetkeana* and 527 out of 1,643 for *M. pyrifera*). Of the top 10 most abundant ASVs on *N. luetkeana* and *M. pyrifera*, many were shared and four had high relative abundances on both kelps (Table 1.3). The single most abundant ASV on *M. pyrifera*, *Granulosicoccus* sp. (*Gammaproteobacteria*), was the third most abundant ASV on *N. luetkeana*, making up about 17% of the total microbial communities on both kelps (Table 1.3). The top two ASVs on *N. luetkeana*, another *Granulosicoccus* sp. (22% of total community) and an *Alphaproteobacteria* from the family *Hyphomonadaceae* (19%), were present at very low abundance on *M. pyrifera* (<1%; Table 1.3).

Geographic variation in kelp blade microbial communities

Both *N. luetkeana* and *M. pyrifera* microbial communities displayed significant spatial variation across 11 (*N. luetkeana*) and 5 (*M. pyrifera*) geographically separated kelp forests (Table 1.1a and Fig. 1.5). Further, PERMANOVA tests were significant for each species vs. location while PERMDISP tests were not, indicating that significant differences in beta diversity are not due to differences in dispersion (Table 1.1a). *M. pyrifera* displayed significantly different microbial communities at Sekiu compared to the other four sites, and Koitlah was different from three out of four other sites (Table S1.2). Differential abundance analysis with ANCOM revealed four ASVs with significantly different relative abundances on *M. pyrifera* across sites (Table

S1.3). Three ASVs had a higher relative abundance on *M. pyrifera* from Sekiu compared to the other four sites, and they were classified as: (1) family *Francisellaceae* (*Gammaproteobacteria*), (2) *Granulosicoccus* sp. (*Gammaproteobacteria*), and (3) family *Saprospiraceae* (*Bacteroidetes*). The fourth differentially abundant ASV, also classified as *Granulosicoccus* sp., was absent at Sekiu but present at the other four sites.

Table 1.2. Mean relative abundances (proportion out of 1.0 ± SE) of top bacterial classes and mean relative abundances of orders on *M. pyrifera* (n = 28) and *N. luetkeana* (n = 59), across all locations. Table includes all bacterial classes and orders that have a mean abundance >0.01 for each species.

Phylum	Class	*M. pyrifera* mean abundance *(± SE)*	*N. luetkeana* mean abundance *(± SE)*	*M. pyrifera* orders (mean abundance)	*N. luetkeana* orders (mean abundance)
Proteobacteria	*Gammaproteobacteria*	0.47 (± 0.03)	0.49 (± 0.03)	Chromatiales (0.05), Thiohalorhabdales (0.04), Alteromonadales (0.03), Thiotrichales (0.03), Legionellales (0.01)	Chromatiales (0.06), Thiohalorhabdales (< 0.01), Alteromonadales (0.02), Thiotrichales (< 0.01), Legionellales (< 0.01)
Proteobacteria	*Alphaproteobacteria*	0.28 (± 0.02)	0.25 (± 0.03)	Rhodobacterales (0.24), Rhizobiales (0.01), Sphingomonadales (0.01), BD7-3 (0.01), Rickettsiales (0.01)	Rhodobacterales (0.24), Rhizobiales (> 0.01), Sphingomonadales (> 0.01), BD7-3 (> 0.01), Rickettsiales (> 0.01)
Verrucomicrobia	*Verrucomicrobiae*	0.01 (± 0.01)	0.11 (± 0.01)	Verrucomicrobiales (0.01)	Verrucomicrobiales (0.11)
Bacteroidetes	*Saprospirae*	0.10 (± 0.02)	0.09 (± 0.02)	Saprospirales (0.10)	Saprospirales (0.09)
Bacteroidetes	*Flavobacteriia*	0.06 (± 0.01)	0.03 (± 0.01)	Flavobacteriales (0.06)	Flavobacteriales (0.03)
Planctomycetes	*Planctomycetia*	0.03 (± 0.01)	0.02 (± 0.00)	Pirellulales (0.03)	Pirellulales (0.02)
Proteobacteria	*Deltaproteobacteria*	0.01 (± 0.00)	0.01 (± 0.00)	Bdellovibrionales (0.01)	Bdellovibrionales (0.01)
Actinobacteria	*Acidimicrobiia*	0.01 (± 0.00)	< 0.01 (± 0.00)	Acidimicrobiales (0.01)	Acidimicrobiales (< 0.01)
	Unknown	0.02 (± 0.00)	< 0.01 (± 0.00)	Unknown (0.33)	Unknown (0.41)

Across 11 sites, *N. luetkeana* displayed significant spatial variation in microbial community composition (Table S1.2 and Fig. 1.5). Notably, the sites at either end of the geographic sampling, Cape Alava and Squaxin, had significantly different microbial communities from all other sites (PERMANOVA pairwise comparisons, q-value < 0.05, Table S1.2). Sites closer in proximity tended to have more similar microbial communities, and a

Figure 1.4. Size of *N. luetkeana* on Tatoosh Island, WA, which were often as tall as 4x Brookes, or 6.8 m from the holdfast to the end of the blades. No kelp were harmed in the making of this measurement; this is an example of how this annual kelp species dislodges and washes ashore.

gradient of microbial community composition spans the 11 sites sampled (Fig. 1.5). CAP analysis revealed that while salinity was significantly correlated with microbial community composition in the CAP model ($F = 1.90$, $df = 1$, $P = 0.035$), temperature was not ($F = 1.22$, $df = 1$, $P = 0.284$). However, temperature and salinity together only accounted for 5% of the variation in microbial communities across the geographic gradient (Fig. S1.3). In the unconstrained (PCoA) ordination, the first two axes explained 44.4% of the variation in microbial community structure (Fig. S1.3), while the first two axes of the CAP ordination constrained by temperature and salinity only explained 0.053% of the variation in the same dataset (Fig. S1.3), further indicating that measured environmental variables were not important predictors of microbial community structure.

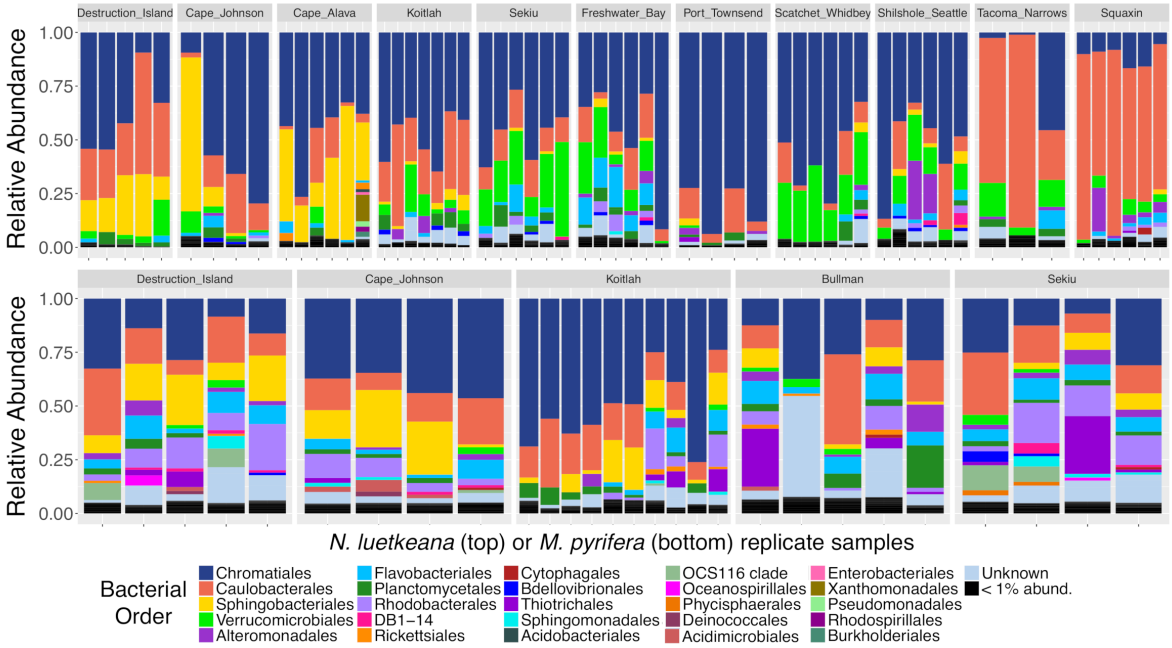

Figure 1.5. Relative abundance barplots of kelp blade microbial communities from *N. luetkeana* (top row) and *M. pyrifera* (bottom row) across 11 and 5 sites, respectively. Colors represent bacterial orders classified by Silva taxonomy. Sites are listed from left to right in order of decreasing ocean influence, from the outer coast (Destruction Island, Cape Johnson, Cape Alava and Koitlah) to the Strait of Juan de Fuca (Sekiu, Freshwater Bay, and Port Townsend) and Puget Sound (Scatchet Whidbey, Shilshole Seattle, Tacoma Narrows, and Squaxin Island).

Analysis of composition of microbiomes detected that 31 ASVs contributed to the spatial variation in *N. luetkeana* microbial communities across the 11 sites (Table S1.3). Of these, ASVs from the family *Saprospiraceae* (*Bacteroidetes*) had a much higher abundance on *N. luetkeana* from the outer coast of Washington compared to sites in the Strait of Juan de Fuca and Puget Sound (yellow bars corresponding to order *Sphingobacteriales* in Fig. 1.5 and Table S1.3). The third most abundant bacterium on *N. luetkeana*, classified as *Granulosicoccus* sp. (*Gammaproteobacteria*), was significantly less abundant at the Southern Puget Sound sites (Tacoma Narrows and Squaxin) than on the outer coast and in the Strait of Juan de Fuca (navy blue bars corresponding to order *Chromatiales* in Fig. 1.5 and Table S1.3). While it was not detected as significantly different with ANCOM, one *Alphaproteobacteria* (*Robiginitomaculum* sp. family *Hyphomonadaceae*) had a much greater relative abundance in the Southern Puget Sound sites. This ASV had a mean abundance of 10–37% of all sequences at outer coast sites, 1–9% in the Strait of Juan de Fuca, and it increased to 50–77% of all sequences at Tacoma Narrows and Squaxin Island, the two Southern Puget Sound sites (pink bars in Fig. 1.5). This was also the second most abundant ASV on *N. luetkeana* across all sites, with a mean relative abundance of 18.6% (Table 1.3). Microbes that had altered abundances across the geographic gradient were not differentially abundant in the surrounding seawater at these sites (Fig. S1.4). Other notable differentially abundant bacteria included ASVs belonging to the families *Flavobacteriaceae* (*Bacteroidetes*) and *Verrucomicrobiaceae* (*Verrucomicrobia*), which were both more abundant on *N. luetkeana* from the Strait of Juan de Fuca and the upper Puget Sound than on the outer coast or in Southern Puget Sound (Table S1.3).

Table 1.3. Mean relative abundances (proportion out of 1.0 ± SE) and taxonomic information for the 10 most abundant ASVs on *M. pyrifera* and *N. luetkeana*, from all sampling locations. Mean abundances of each ASV in surrounding seawater samples are included. The four bolded ASVs have a high mean abundance on both kelp species.

M. pyrifera mean abundance	*N. luetkeana* mean abundance	Seawater mean abundance	Phylum	Class	Order	Family
0.178 (± 0.02)	**0.173 (± 0.03)**	**< 0.001**	***Proteobacteria***	***Gammaproteobacteria***	***Chromatiales***	***Granulosicoccaceae***
0.075 (± 0.01)	**0.015 (± 0.00)**	**< 0.001**	***Proteobacteria***	***Alphaproteobacteria***	***Rhodobacterales***	***Hyphomonadaceae***
0.059 (± 0.02)	< 0.001	< 0.001	*Proteobacteria*	*Gammaproteobacteria*	*Chromatiales*	*Granulosicoccaceae*
0.039 (± 0.01)	**0.057 (± 0.01)**	**< 0.001**	***Proteobacteria***	***Gammaproteobacteria***	***Chromatiales***	***Granulosicoccaceae***
0.033 (± 0.00)	0.011 (± 0.00)	< 0.001	*Proteobacteria*	*Alpha-proteobacteria*	*Rhodobacterales*	*Hyphomonadaceae*
0.029 (± 0.01)	< 0.001	< 0.001	*Proteobacteria*	*Gamma-proteobacteria*	*Chromatiales*	*Granulosicoccaceae*
0.018 (± 0.02)	0.002 (± 0.00)	< 0.001	*Proteobacteria*	*Gamma-proteobacteria*	*Thiohalorhabdales*	*Unknown*
0.016 (± 0.00)	< 0.001	< 0.001	*Proteobacteria*	*Alpha-proteobacteria*	*Rhodobacterales*	*Hyphomonadaceae*
0.015 (± 0.00)	**0.016 (± 0.00)**	**< 0.001**	***Planctomycetes***	***Planctomycetia***	***Pirellulales***	***Pirellulaceae***
0.015 (± 0.00)	0.003 (± 0.00)	0.003	*Proteobacteria*	*Alpha-proteobacteria*	*Rhodobacterales*	*Hyphomonadaceae*
0.009 (± 0.00)	0.186 (± 0.03)	< 0.001	*Proteobacteria*	*Alpha-proteobacteria*	*Rhodobacterales*	*Hyphomonadaceae*
0.009 (± 0.00)	0.220 (± 0.03)	< 0.001	*Proteobacteria*	*Gamma-proteobacteria*	*Chromatiales*	*Granulosicoccaceae*
0.003 (± 0.00)	0.014 (± 0.00)	< 0.001	*Bacteroidetes*	*Saprospirae*	*Saprospirales*	*Saprospiraceae*
0.001 (± 0.00)	0.030 (± 0.01)	0	*Bacteroidetes*	*Saprospirae*	*Saprospirales*	*Saprospiraceae*
< 0.001	0.027 (± 0.01)	< 0.001	*Bacteroidetes*	*Saprospirae*	*Saprospirales*	*Saprospiraceae*
< 0.001	0.050 (± 0.01)	0.001	*Verrucomicrobia*	*Verrucomicrobiae*	*Verrucomicrobiales*	*Verrucomicrobiaceae*

Comparative analysis of kelp and seawater microbial communities

Microbial communities in the surrounding seawater contained 3,725 unique ASVs from 42 bacterial and 3 archaeal phyla. Seawater microbial communities were dominated by the phyla *Bacteroidetes* (50%), *Proteobacteria* (42%), *Verrucomicrobia* (4%), and *Actinobacteria* (2%). Archeal phyla in the seawater included *Crenarchaeota* (0.12% mean relative abundance), *Euryarchaeota* (0.01%), *and Parvarchaeota* (<0.001%). At the class level, seawater contained a high abundance of *Flavobacteriia* (48%), followed by *Alphaproteobacteria* (25%), *Gammaproteobacteria* (15%), *Verrucomicrobiae* (4%), and *Betaproteobacteria* (1%). Of the 3,725 unique seawater ASVs, 334 of them were also found on *N. luetkeana* and 527 were found on *M. pyrifera*. All but one of the top 10 most abundant ASVs found on each kelp species were

also found in the surrounding seawater, but at extremely low abundances of <0.03% (Table 1.3). Kelp forest seawater microbial communities displayed significant spatial variation (Table 1.1a and Table S1.4), but significant PERMDISP tests also indicated differences in dispersion (Table 1.1a). A greater percentage of pairwise site comparisons were significantly different for *N. luetkeana* and *M. pyrifera* blade microbial communities (69 and 60%, respectively) than for seawater microbial communities (29%; Tables S1.1, S1.3), suggesting that the kelp microbiome has greater spatial variation than surrounding seawater microbial communities. This difference in kelp vs. seawater spatial variation is also visible on the NMDS plot (Fig. 1.3).

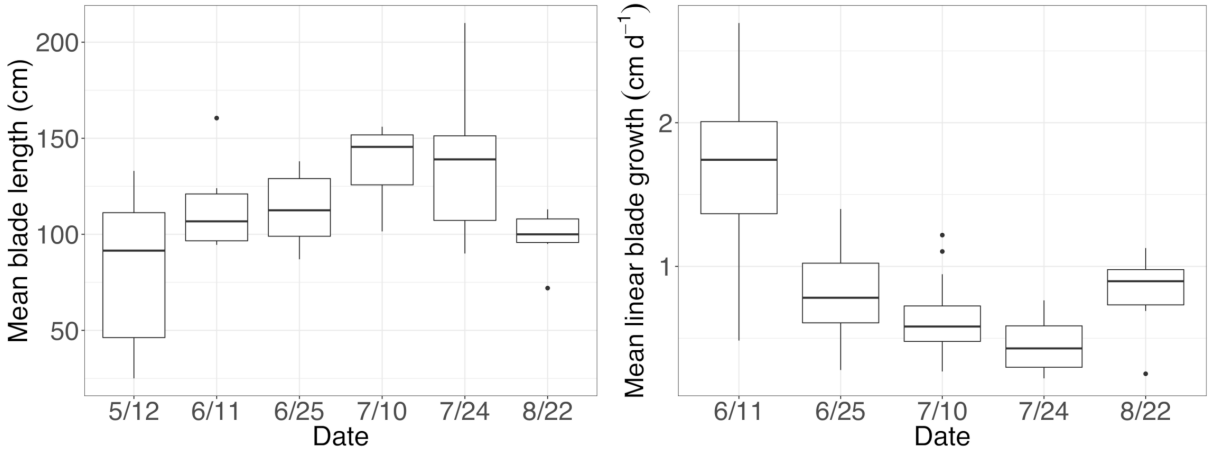

Figure 1.6. (A) Mean (± standard error) length of sampled blades, and (B) Mean (± standard error) linear blade growth rates throughout the growing season.

Microbial abundance and diversity on new and old *N. luetkeana* blade tissues

On Tatoosh Island, *N. luetkeana* linear blade growth rates were measured in intervals from mid-May to late August, averaging 0.84 cm per day. Blade growth rates were highest in early June (1.7 cm per day) and lowest in late July (0.45 cm per day, Fig. 1.6). These growth rates demonstrate that basal blade meristem tissues were at most a few days old. In contrast, kelp blades increased in length throughout the growing season (Fig. 1.6) and blade tip tissues were

likely a few months old. After removing six meristem samples with <200 bacterial sequences, our dataset contained n = 30 *N. luetkeana* meristem samples (new tissue), n = 36 *N. luetkeana* blade tip samples (old tissue), and n = 14 seawater samples from six time points that spanned the growing season, from 12 May to 22 August. Across all dates, younger *N. luetkeana* meristem tissues hosted fewer bacterial sequences than samples from the older blade tips (paired t-test, df = 35, t = 16.16, P < 0.01), with an average of 961 bacterial sequences from the meristem and 39,661 bacterial sequences from the tip of the kelp blades (Table S1.5). *N. luetkeana* meristem samples had a significantly higher abundance of chloroplast sequences than blade tips (paired t-test, df = 35, t = 6.36, P < 0.01), with an average of 24,212 chloroplast sequences from the meristem and 8,614 chloroplast sequences from the tip of the kelp blades (Table S1.5). The meristem samples had very low percentage of bacterial sequences (1.4–7.4%) compared to chloroplast sequences (92.6– 98.6%), while the older blade tip communities had a much higher percentage of bacterial sequences (67.4–90%) compared to chloroplast sequences (9.98–32.6%, Table S1.5).

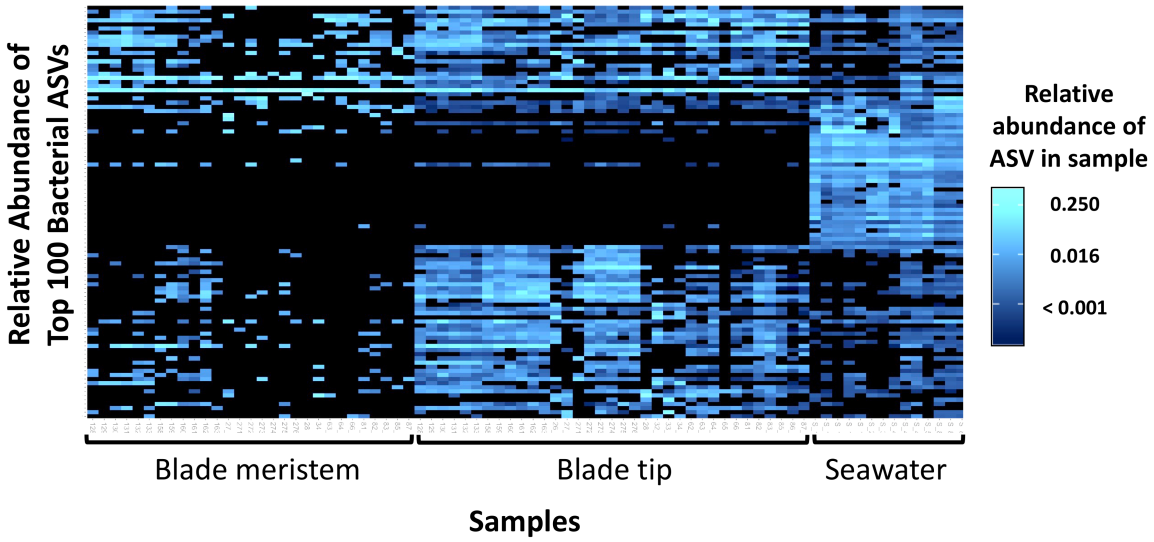

Figure 1.7. Heatmap showing the relative abundances of the 100 most abundant bacterial ASVs from *N. luetkeana* blade meristem, blade tip, and surrounding seawater microbial communities.

Across all dates, alpha diversity metrics including mean ASV species richness, Shannon diversity, Faith's phylogenetic diversity, and Pielou's Evenness were significantly higher on blade tip than meristem microbial communities, but seawater communities had higher alpha diversity compared to kelp blades (Kruskal– Wallis ANOVA; $H = 55.29$ and $P < 0.001$ for ASV richness, $H = 47.6$ and $P < 0.001$ for Shannon diversity, $H = 39.7$ and $P < 0.001$ for Faith's Phylogenetic Diversity, $H = 30.98$ and $P < 0.001$ for Pielou's Evenness; corrected P-values < 0.03 for all Kruskal–Wallis pairwise tests). Mean ASV richness per sample was 49 for tip samples, 24 for meristem samples, and 81 for seawater microbial communities. Across all samples, the total observed diversity for meristem samples was 459 ASVs, while blade tip samples contained 1,408 ASVs. Of these microbial taxa, 201 ASVs were shared between *N. luetkeana* meristem and tip communities. Microbial communities in the surrounding seawater were the most diverse, with 3,115 total ASVs. The meristem communities shared 42% of ASVs with the surrounding seawater microbial community (191 total shared ASVs), while only 14% (201 ASVs) of blade tip ASVs were found in the seawater. Most of the ASVs with the highest relative abundance on *N. luetkeana* blades were also found in the surrounding seawater microbial communities, but many of the most abundant seawater ASVs were absent from the *N. luetkeana* blade microbial community (Fig. 1.7). Throughout the summer, alpha diversity indices generally increased in blade tip microbial communities, reaching a peak in July and August, while ASV count and Shannon Diversity in meristem communities remained low (Fig. 1.8). Interestingly, the gradual increase and end of July maximum in blade tip ASV count, Shannon Diversity, and Faith's Phylogenetic Diversity matched the trend observed in the length of the sampled blades, where mean blade length increased throughout the summer and peaked in July, decreasing slightly in August (Fig. 1.6).

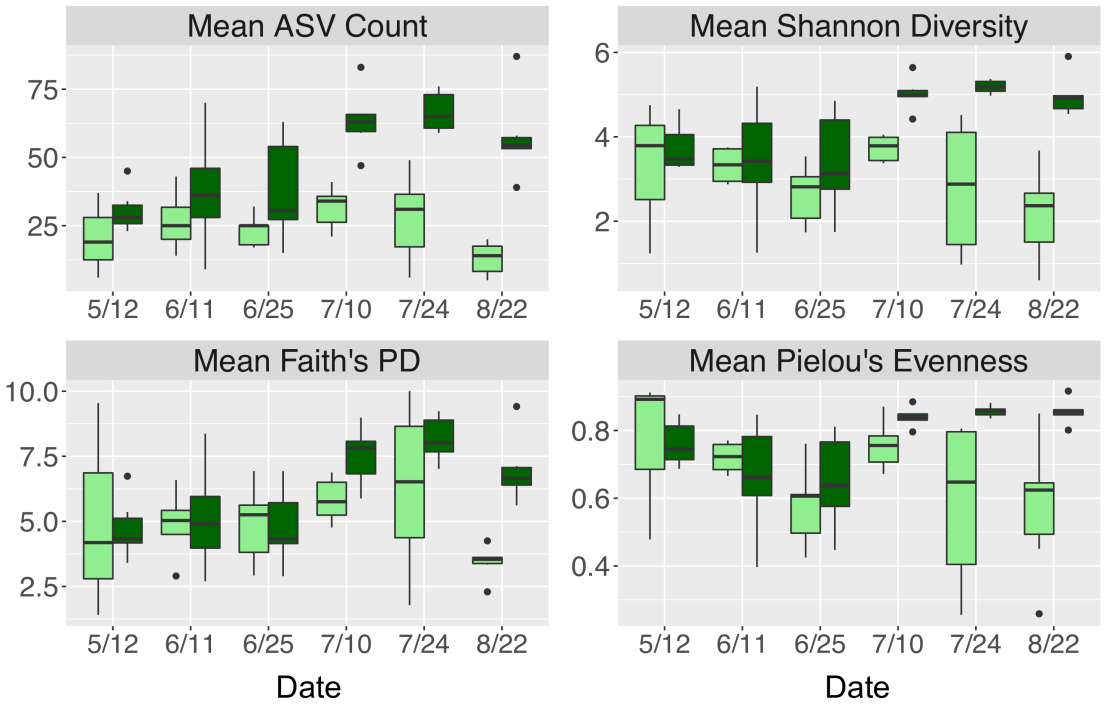

Figure 1.8. Alpha diversity indices including (A) mean (± standard error) ASV count, (B) mean (± standard error) Shannon diversity, (C) mean (± standard error) Faith's Phylogenetic diversity, and (D) mean (± standard error) Pielou's evenness for *N. luetkeana* blade meristem (light green) and blade tip (dark green) microbial communities throughout the growing season.

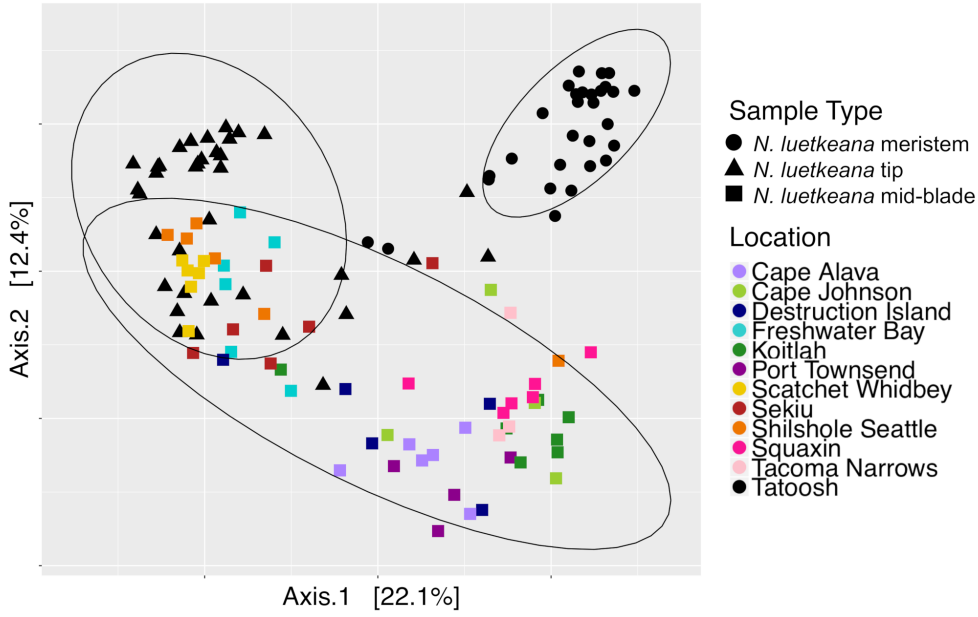

Figure 1.9. Principal coordinate analysis (PCoA) plot of all *N. luetkeana* microbial communities across 12 sites in Washington, combining the *N. luetkeana* mid-blade samples from the geographic sampling (squares) with the temporal dataset from Tatoosh Island, WA (black circles = *N. luetkeana* blade meristem, black triangles = *N. luetkeana* blade tip).

Microbial community composition and successional dynamics on new and old *N. luetkeana* blade tissues

Across all time points, microbial communities on *N. luetkeana* tissue from the meristem (new tissue) and tip of the blade (old tissue) were significantly different from one another and from the surrounding seawater (Table 1.1b; meristem–tip pairwise, df = 1, pseudo-F = 6.29, q-value = 0.004; Fig. 1.9). There was no effect of kelp individual, as a random factor, on this difference between meristem and tip microbial communities (Table S1.1). While the PERMDISP test was significant (Table 1.1b), the significance resulted from a difference in dispersion between the kelp and seawater (pairwise test for tip vs. seawater: t = 2.32, P = 0.063; pairwise test for meristem vs. seawater: t = 2.95, P = 0.012), while *N. luetkeana* meristem and tip microbial communities did not display significant differences in dispersion (PERMDISP pairwise: t = 0.703, P = 0.516). Many of the most abundant bacterial ASVs on the *N. luetkeana* blade tip tissues were present on the blade meristem, but at much lower relative abundances (Fig. 1.7). *N. luetkeana* blade tip microbial communities displayed significant temporal variation (Table 1.1b). Each date was distinct (PERMANOVA pairwise comparisons, q-value < 0.05), except for 11 June and 25 June (PERMANOVA pairwise, df = 1, pseudo-F = 1.46, q-value = 0.163). *N. luetkeana* meristem communities also displayed significant temporal variation (Table 1.1b). However, of the six dates, the only significant difference was between meristem microbial communities from 10 July and 22 August (PERMANOVA pairwise comparison, df = 1, pseudo-F = 2.57, q-value = 0.045). While the overall test for seawater microbial communities indicated temporal variation (Table 1.1b), none of the dates were significantly different from one another after correction for multiple pairwise tests (PERMANOVA pairwise comparisons, q-value > 0.133).

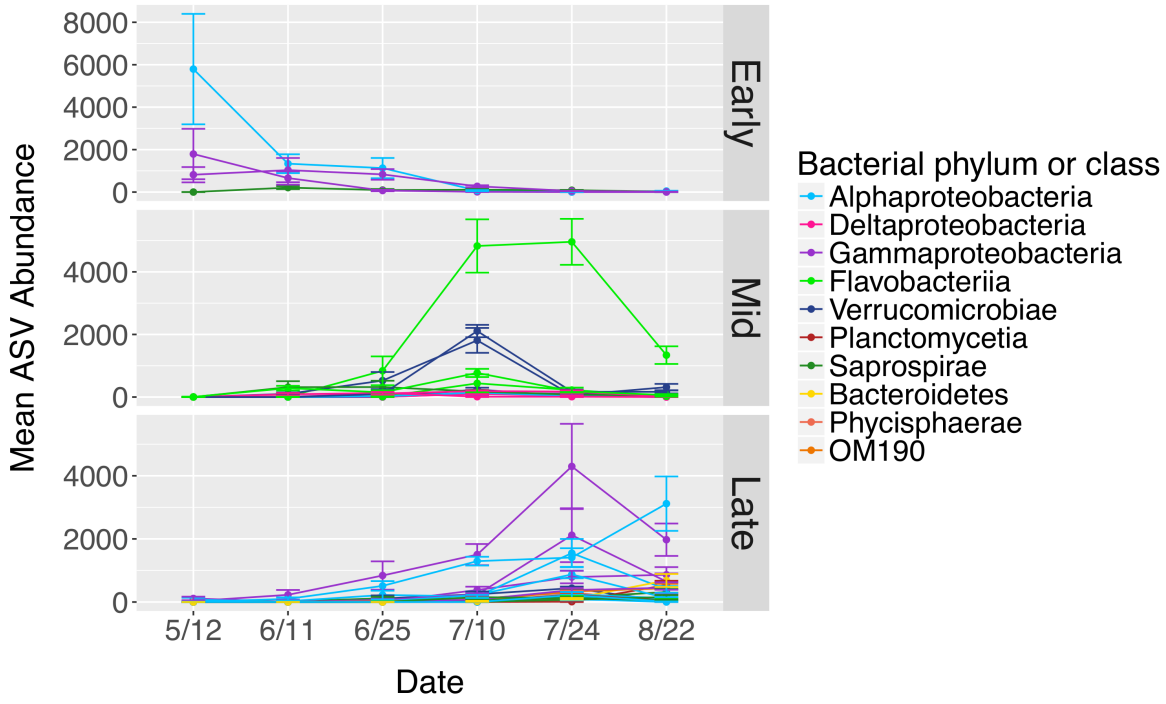

Figure 1.10. Mean abundances of ASVs (n = 40) from *N. luetkeana* blade tip microbial communities that displayed significantly different abundances across time with ANCOM. The ASVs that displayed significant temporal patterns were classified as early, mid and late successional taxa based on when they were most abundant in blade tip communities. Each ASV is plotted individually and colored by bacterial class.

The total number of bacterial sequences was invariant across time on blade tip samples (ANOVA, df = 5, F = 1.87, P = 0.131), allowing us to identify differentially abundant taxa over time. *N. luetkeana* blade tip samples contained 40 microbial ASVs that significantly differed in relative abundance through time (ANCOM, W-scores range from 1249 to 1385). The ASVs that displayed significant temporal patterns using ANCOM were classified as early, mid, and late successional taxa based on when they were most abundant in blade tip communities. Early successional microbes included bacteria from the classes *Alphaproteobacteria*, *Gammaproteobacteria* (*Granulosicoccus* sp.), and *Saprospirae* (Fig. 1.10). In particular, one *Alphaproteobacteria* (family *Hyphomonadaceae*) ASV decreased from a mean abundance of 5,794 sequences per samples in May down to six sequences per sample in late July (Fig. 1.10).

Mid-successional ASVs included *Flavobacteriia* (family *Flavobacteriaceae*, *Olleya* sp., and *Tenacibaculum* sp.), *Verrucomicrobiae*, *Alphaproteobacteria*, *Gammaproteobacteria* (Vibrio sp.), *Deltaproteobacteria* (order *Bdellovibrionales*), and *Saprospirae* (Fig. 1.10). Of the mid-successional ASVs, one *Flavobacteriia* (family *Flavobacteriaceae*) increased from a mean abundance of 0 in May up to 4,827 and 4,960 in early and late July, decreasing back to 1,339 in late August. Two *Verrucomicrobiae* (*Roseibacillus* sp.) ASVs increased from a mean abundance of 0 in May up to 1,811 and 2,109 in early July, decreasing back to abundances of 315 and 166 in late August (Fig. 1.10). Late-successional ASVs were the most numerous and included members of the class *Gammaproteobacteria* (*Granulosicoccus* sp. and the order *Thiohalorhabdales*), *Alphaproteobacteria* (*Octadecabacter antarcticus* and families *Rickettsiaceae*, *Hyphomonadaceae*, and *Erythrobacteraceae*), *Phycisphaerae*, *Planctomycetia*, *Saprospirae*, *Verrucomicrobiae*, *Flavobacteriia*, and OM190 (Fig. 1.10). Late-successional ASVs that were particularly abundant included one *Gammaproteobacteria* (*Granulosicoccus* sp.) ASV that increased from a mean abundance of 28 in May up to 4,296 in late July, and one *Alphaproteobacteria* (family *Hyphomonadaceae*) ASV that increased from a mean abundance of 7 in May up to 3,117 in late August (Fig. 1.10).

The total number of bacterial sequences on meristem samples was significantly different over time (ANOVA, df = 5, F = 4.77, P = 0.003; Table S1.5). In contrast to tip communities, ANCOM only revealed five ASVs in *N. luetkeana* meristem communities that differed in relative abundance through time (ANCOM, W-scores range from 485 to 538). These included one

Gammaproteobacteria (family HTCC2089), one *Bacteroidetes* (*Aquimarina* sp.), and three ASVs from the class *Verrucomicrobiae* (*Rubritalea* sp.).

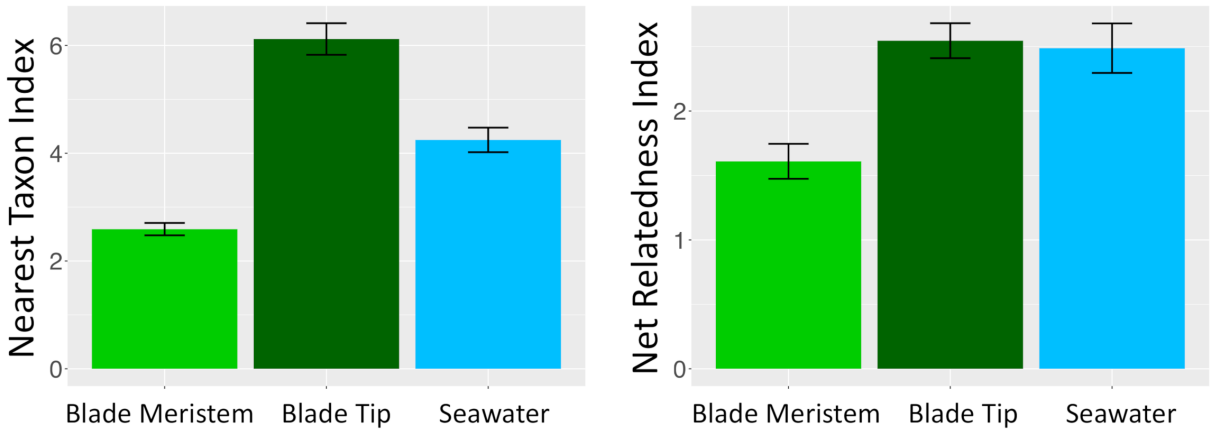

Figure 1.11. Mean (± standard error) (A) Nearest Taxon Index and (B) Net Relatedness Index of microbial communities on *N. luetkeana* blade meristem (n = 30), *N. luetkeana* blade tip (n = 36) and surrounding seawater samples (n = 22) from Tatoosh Island, WA.

Phylogenetic signal in microbial community assembly

Microbial taxa from kelp and seawater communities displayed significant phylogenetic clustering (Fig. 1.11). Members of kelp and surrounding seawater communities were more closely related to one another than would be expected by chance if microbial communities were randomly assembled from a regional species pool of all detected kelp and seawater microbial taxa. For the NTI, all n = 36 *N. luetkeana* blade tip samples, all n = 22 seawater samples, and n = 18 out of 30 *N. luetkeana* meristem samples displayed significant phylogenetic clustering ($P < 0.05$; Fig. 1.11). For the NRI, n = 26 out of 36 *N. luetkeana* blade tip samples, n = 13 out of 22 seawater samples, and n = 9 out of 30 *N. luetkeana* meristem samples displayed significant phylogenetic clustering ($P < 0.05$; Fig. 1.11). The NTI was positive for all samples that displayed significant phylogenetic signal, but differed significantly among kelp meristem, kelp tip, and seawater samples (ANOVA, df = 2, $F = 42.9$, $P < 0.001$). For NTI, all three groups were

significantly different from one another – kelp meristem communities displayed the lowest NTI, followed by seawater, and kelp tip microbial communities had the highest NTI values (Tukey HSD post hoc pairwise tests, $P < 0.001$; Fig. 1.11). The NRI also differed significantly among kelp meristem, kelp tip, and seawater samples (ANOVA, $df = 2$, $F = 7.29$, $P < 0.01$), with a significantly lower NRI from kelp meristem microbial communities than kelp tip or seawater communities (Tukey HSD post hoc pairwise tests, $P < 0.01$; Fig. 1.11). The NRI of kelp tip and seawater microbial communities did not differ (Tukey HSD post hoc pairwise tests, $P = 0.96$).

Comparing geographic and temporal variation in *N. luetkeana* microbial communities

Across all samples from both spatial and temporal datasets, the *N. luetkeana* meristem ($n = 30$), blade tip ($n = 36$), and mid-blade microbial communities from the geographic dataset ($n = 59$) were significantly different (PERMANOVA, $df = 2$, pseudo-$F = 7.55$, $P = 0.001$; all pairwise comparisons q-value = 0.001). This is visible on the PCoA plot of combined spatial and temporal datasets, where microbial communities from the three sample types form distinct clusters (Fig. 1.9). The total number of ASVs found on *N. luetkeana* increased from blade meristem (459 ASVs) to mid-blade samples (1,046 ASVs) and was highest in blade tip communities (1,408 ASVs), despite a higher number of samples from mid-blade microbial communities. Kelp tissues from Tatoosh Island (*N. luetkeana* meristem and tip samples from all dates) were significantly different from *N. luetkeana* mid-blade microbial communities collected at the 11 other sites (PERMANOVA, $df = 11$, pseudo-$F = 2.53$, $P = 0.001$; all pairwise comparisons against Tatoosh Island, q-value < 0.04). While we only tracked temporal variation at Tatoosh, the temporal variation there only overlapped partially with the large amount of spatial variation that we

observed across the other 11 sites (Fig. 1.9), suggesting that geographic differences in kelp blade microbial communities and local successional dynamics are distinct.

Discussion

Microbial community structure and composition on canopy-forming kelps

The two canopy forming kelp in the northeast Pacific host distinct microbial communities on their blades, consistent with previous studies reporting host-specific microbial communities associated with macroalgae (Lachnit et al., 2009; Aires et al., 2016; Lemay et al., 2018). *N. luetkeana* and *M. pyrifera* shared only 33 and 21% of unique microbial ASVs, respectively. Similarly, Lemay et al. (2018) found that 37% of bacterial taxa were shared among eight kelp species. However, a recent meta-analysis of macroalgal microbial communities found that many families of epiphytic bacteria are generalists commonly found on red, green, and brown algal hosts (Florez et al., 2017), suggesting that common properties of the macroalgae microbiome may promote the growth of similar microbial taxa. Many of the abundant kelp-associated bacterial families that we detected (Rhodobacteraceae, Flavobacteriaceae, Alteromonadaceae, *Saprospiraceae*) were found to be generalist macroalgal associates by Florez et al. (2017). We found that relative abundances of the top bacterial phyla, classes, and orders on *N. luetkeana* and *M. pyrifera* were remarkably similar. Microbial communities on each species were dominated by Proteobacteria (75% of all sequences), followed by *Bacteroidetes*, Verrucomicrobia, and Planctomycetes. The only large phylum-level difference in microbial communities between the two kelps was Verrucomicrobia; this phylum made up 10% of microbial sequences on *N. luetkeana*, and only 1% on *M. pyrifera*. Despite similar compositions at higher microbial

taxonomic levels, blades of *N. luetkeana* and *M. pyrifera* each host a unique microbiome at the ASV level.

Relatively few extremely abundant ASVs dominated the microbial symbiont community of *N. luetkeana*, while *M. pyrifera* hosted a more diverse community with fewer dominant symbionts. Supporting this observation, Pielou's evenness was significantly greater for *M. pyrifera* than *N. luetkeana* microbial communities. The three most abundant ASVs on *N. luetkeana* averaged 58% of the total microbial symbiont community, while the combined abundances of the top 20 symbionts made up the same proportion of the *M. pyrifera* microbial community. The most abundant ASV on *N. luetkeana* (mean abundance 22%) was *Granulosicoccus* sp. (*Gammaproteobacteria*). Bacteria from the genus *Granulosicoccus* have been isolated from seagrass (Kurilenko et al., 2010) and brown algae (Park et al., 2014), and they have been characterized as aerobic, chemoheterotrophic bacteria that are capable of nitrate reduction to nitrite (Baek et al., 2014; Park et al., 2014). Three of the four most abundant ASVs on *N. luetkeana* were classified as *Granulosicoccus* sp., indicating that there are multiple, closely related sequence variants that dominate the microbiome of *N. luetkeana*. The second most abundant ASV on *N. luetkeana*, an *Alphaproteobacteria* from the family *Hyphomonadaceae* (mean abundance 19%), displayed a large amount of spatial variation across sites. It was highly abundant on the outer coast (10–37%), had a very low abundance in the Strait of Juan de Fuca (1–9%), and became very dominant in Puget Sound, making up 50–77% of all sequences from kelp at the two Southern Puget Sound sites. This ASV was further classified as *Robiginitomaculum* sp. A bacterium in this genus, isolated from Antarctic seawater, was characterized as obligately aerobic, chemoheterotrophic, and capable of nitrate reduction (Lee et al., 2007). While these two *N. luetkeana* symbionts were present at <1% relative abundance on

M. pyrifera, the single most abundant ASV on *M. pyrifera*, *Granulosicoccus* sp., was the third most abundant ASV on *N. luetkeana* and made up 17% of microbial communities on both kelps. The second most abundant ASV on *M. pyrifera* (mean abundance 8%), an *Alphaproteobacteria* from the family *Hyphomonadaceae*, was present at lower abundances (1.5%) on *N. luetkeana*.

We found that across all sites, the perennial kelp *M. pyrifera* hosted a more diverse microbiome than the annual kelp *N. luetkeana*. *M. pyrifera* had a mean ASV richness per sample of 102 and hosted a total of 1,643 unique ASVs, while *N. luetkeana* had a mean richness of 36 ASVs per sample and hosted 1,046 unique ASVs. Faith's phylogenetic diversity was significantly greater on *M. pyrifera* compared to *N. luetkeana*, suggesting that the increase in the number of microbial taxa found on *M. pyrifera* is due to associations with many microbial lineages, rather than association with taxa from one or a few particular taxonomic groups. Our data support the hypothesis that thallus longevity allows perennial kelps to accumulate more mature and highly colonized microbial communities compared with annuals (Lemay et al., 2018). Further, it has been hypothesized that perennial tissue could provide a reservoir of kelp-associated microbes for the colonization of new tissues (Bengtsson et al., 2010; Lemay et al., 2018). We found that *N. luetkeana* shared a similar proportion (33%) of its microbial community with the perennial *M. pyrifera* as with the surrounding seawater (32%), suggesting that both the surrounding seawater and perennial kelps may contribute to microbial community assembly on annual kelp blades. While the microbiome of each kelp species was clearly distinct from the seawater microbial community, both canopy-forming kelps shared a remarkably similar proportion of microbes with the seawater (32%). The fraction of kelp-associated microbial taxa detected in the surrounding seawater is reported to be highly variable across studies, from as low as 2% (Michelou et al., 2013) to as high as 86% (Lemay et al., 2018), and may reflect a broad

array of differences among studies, including differences in sequencing depth or differences in retention time of seawater in proximity to the kelp.

Geographic variation in kelp blade microbial communities

Blades of *N. luetkeana* and *M. pyrifera* exhibited significant variation in microbial communities across 11 (*N. luetkeana*) and 5 (*M. pyrifera*) geographically distinct kelp forests. Other studies have reported regional differences in microbial symbiont composition associated with eight kelp species located <100 km apart (Lemay et al., 2018), as well as the kelp Ecklonia radiata from different habitat types located <10 km apart (Marzinelli et al., 2018) and >1,000 km apart (Marzinelli et al., 2015). In our study, *N. luetkeana* forests were located 10–400 km apart, but experience very different environmental conditions (Fig. S1.2). Kelp forests in Puget Sound are exposed to warmer temperatures and lower nutrient concentrations, while outer coast kelp experience cooler temperatures and higher nutrient concentrations due to coastal upwelling. Additionally, Southern Puget Sound kelp forests experience greater anthropogenic stressors than outer coast kelp forests (Pfister et al., 2018). Elevated temperatures led to a disruption in the blade surface microbiome of *M. pyrifera* (Minich et al., 2018). Despite a range of 9–14◦C, we found that salinity but not temperature was significantly correlated with microbial community composition on *N. luetkeana* blades. However, both environmental variables together only accounted for 5% of the variation in *N. luetkeana* microbial communities across the spatial gradient, suggesting that these environmental variables are not an important determinant of microbial community composition in our study. However, we note that the temperature and salinity values only represent a snapshot in time and a subset of the many abiotic factors influencing these sites.

Our analysis revealed regional differences in the relative abundance of certain microbial taxa across the spatial gradient. In particular, ASVs from the family *Saprospiraceae* (*Bacteroidetes*) had higher abundances on the outer coast, while Southern Puget Sound sites displayed a relative increase in the family *Hyphomonadaceae* (*Alphaproteobacteria*) and a decrease in the relative abundance of *Granulosicoccus* sp. (*Gammaproteobacteria*). *Saprospiraceae* are among the core microbial symbionts associated with the red algae Porphyra umbilicalis (Miranda et al., 2013) and they were found on *N. luetkeana* meristem communities in Vancouver, Canada (Chen and Parfrey, 2018). This group of microbes may play a role in metabolizing complex carbon resources (McIlroy and Nielsen, 2014). Microbes that had altered abundances across the geographic gradient were not differentially abundant in the surrounding seawater at these sites, suggesting that the kelp blades surfaces may be highly selective environments that promote the growth of certain microbial taxa under different conditions.

Temporal variation, microbial community succession, and phylogenetic signal

Our temporal study demonstrated that microbial communities on the meristem of *N. luetkeana* blades have much lower species diversity, evenness, and likely lower total microbial abundances than the older and more developed microbial communities on the tip of the kelp blade. Another study found that Laminaria saccharina meristem tissue hosted less diverse microbial communities than older thallus tissue (Staufenberger et al., 2008). Because *N. luetkeana* blades grew linearly 1 cm per day (Fig. 1.6), meristem tissues hosted microbial communities that were at most a few days old. Kelp blades gradually increased in length throughout our study, thus blade tip microbial communities were likely a few months old (Fig. 1.6). Many water column bacteria are motile (Fenchel, 2001), and microbial metagenomes on

kelp contained a high abundance of motility genes (Minich et al., 2018), suggesting that microbes may be recruited from the surrounding seawater onto the kelp surface. Meristem microbial communities were more similar to the surrounding seawater (42% ASVs shared with seawater) than the kelp blade tip communities (14% shared ASVs), suggesting possible recruitment of seawater microbes onto new kelp tissues. However, it is also possible that meristem communities contained a larger proportion of seawater microbes due to the small number of bacterial sequences on kelp meristems (Table S1.5), and possible contamination from seawater.

While kelp meristem microbial communities were almost temporally stable, with a difference between only two of the six dates, we found significant temporal variation in blade tip microbial communities across all dates. On the kelp blade tip, we found evidence for microbial community succession, including increasing ASV richness and evenness through time and thus kelp age. Interestingly, ASV richness, Shannon diversity, and Pielou's Evenness on blade tip communities reached a maximum by early July, remaining high but not increasing further through the end of August (Fig. 1.8). Other studies have reported similar patterns of temporal variation, including an increase in microbial species richness on the brown algae C. compressa over its annual growth cycle (Mancuso et al., 2016) and an increase in microbial richness and evenness with tissue age on the kelp L. hyperborea (Bengtsson et al., 2012). The 40 ASVs that showed significantly different relative abundances on blade tip microbial communities across time also displayed clear patterns of early, mid, and late successional taxa (Fig. 1.10). Interestingly, one of the abundant mid-successional taxa, *Olleya sp*. (*Flavobacteriaceae*), may produce exopolysaccharides (Nichols, 2005). Given these patterns of microbial community succession, we hypothesize that the addition of microbial taxa to the kelp

surface biofilm facilitates the recruitment of additional microbial taxa by providing potentially novel metabolic substrates and increasing microbial niche space (Rivett et al., 2016).

Interestingly, we found that phylogenetic similarity among taxa in the microbiome was higher in blade tip communities than in meristem communities. Microbial communities in both kelp and seawater samples were more phylogenetically clustered than expected by chance, a pattern that has been reported for seawater microbial communities (Pontarp et al., 2012). Both the number and phylogenetic relatedness (NTI and NRI indices) of microbial taxa increased with kelp tissue age, suggesting that microbes were added to the kelp surface microbial community deterministically. Phylogenetic clustering may be consistent with kelp acting as selective filters, promoting the growth of specific microbial taxa that might fill similar niche space in the kelp surface microbiome. It may also indicate that interactions among microbes are repeatedly important in the colonization process that occurs throughout the kelp growing season.

Conclusion

Canopy-forming kelps create vast and highly productive underwater forests in temperate marine ecosystems (Wheeler and Druehl, 1986), yet we are just beginning to gain perspective on the importance of the microbial symbiont communities to these foundational species. Here, we found evidence for host-specificity and geographic variation in microbial communities on the blades of *M. pyrifera* and *N. luetkeana*, two canopy-forming kelps with different life histories. We demonstrated temporal variation in microbial communities over the summer growing season on blades of the annual kelp *N. luetkeana*. By tracking both geographic and temporal variation in kelp microbial communities, we confirm previous studies showing that one or the other factor is important (Staufenberger et al., 2008; Bengtsson et al., 2010; Marzinelli et al., 2015; Mancuso et

al., 2016), revealing that both processes simultaneously shape microbial symbiont communities on kelps. Our temporal study demonstrated that microbial communities on younger, meristematic blade tissue were less developed, displaying significantly lower ASV diversity and evenness than communities at the tip of the blade. Further, we found that relatedness among microbial taxa increased from basal to apical blade tissues, suggesting that the process of microbial community assembly on kelp blades may be deterministic. To understand why certain groups of closely related microbes are abundant on kelp blades, future research should focus on identifying the functions of the dominant symbionts to determine their importance to the host kelp.

Appendix 1.1 Supplemental Information for Chapter 1

Figure S1.1. Barplots showing variation in the relative abundances of bacterial orders in kelp blade microbial communities from *N. luetkeana* (top row) and *M. pyrifera* (bottom row) across 11 and 5 sites, respectively. Colors represent bacterial orders classified by Green Genes taxonomy. Sites are in order of decreasing ocean influence, from the outer coast (Destruction Island, Cape Johnson, Cape Alava and Koitlah) to the Strait of Juan de Fuca (Sekiu, Freshwater Bay, and Port Townsend) and Puget Sound (Scatchet Whidbey, Shilshole Seattle, Tacoma Narrows, and Squaxin Island).

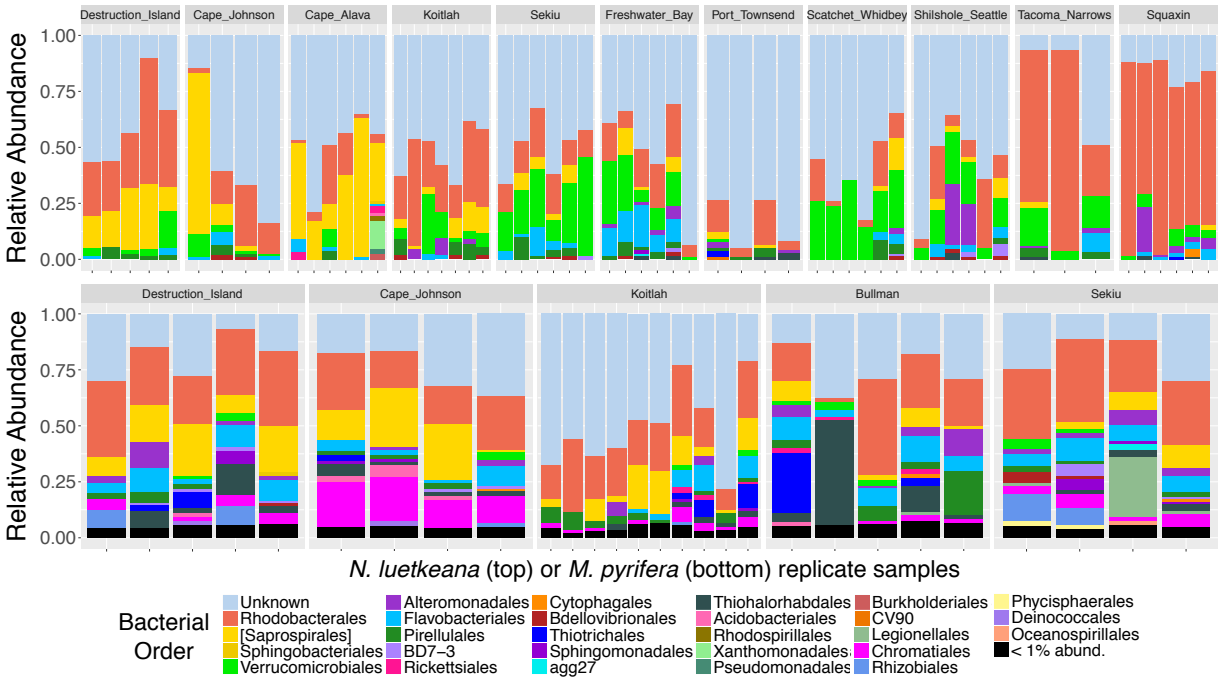

Figure S1.2. Mean (± standard error) temperature and salinity at sites across the geographic gradient. Sites are in order of increasing ocean influence, from Squaxin (inner Puget Sound) to Destruction Island (outer coast Washington on the Pacific Ocean).

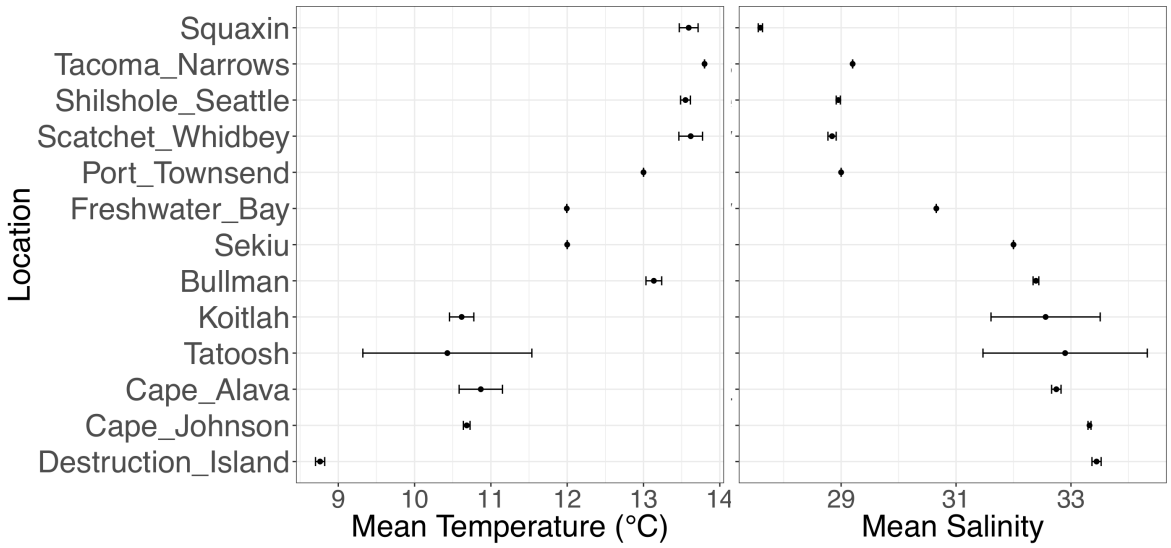

Figure S1.3. Ordination analysis of sequence data using A) Constrained Analysis of Principal Coordinates (CAP) and B) unconstrained Principal Coordinates Analysis (PCoA) based on Bray-Curtis distances for N. luetkeana microbial communities from different sites across the geographic gradient (colored circles, same for both plots). For the constrained (CAP) plot, microbial communities are shown in relation to temperature and salinity.

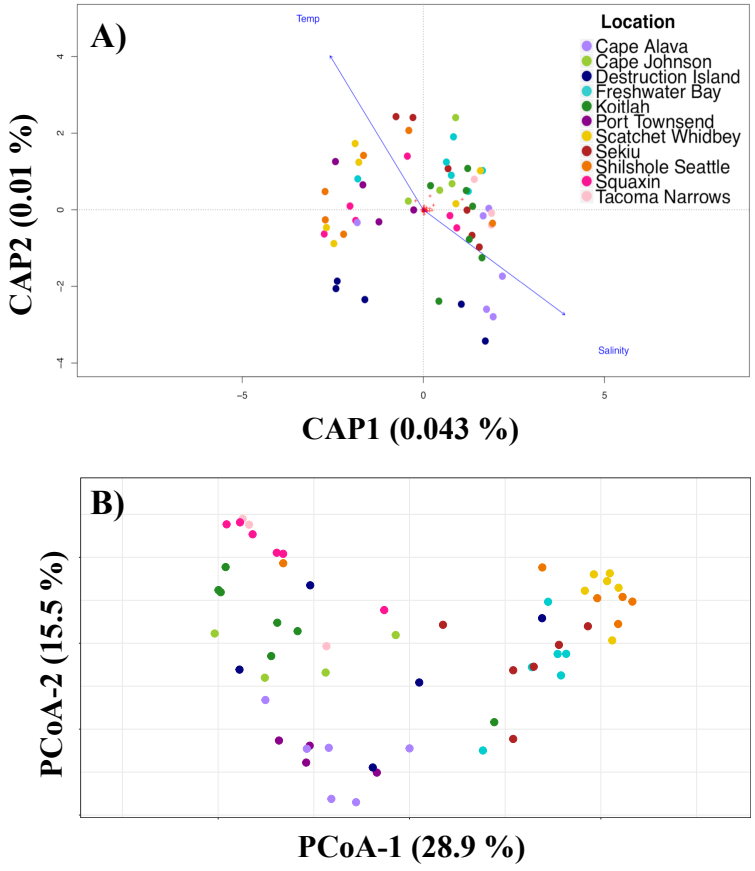

Figure S1.4. Barplots showing variation in the relative abundances of the bacterial families Hyphomonadaceae (class Alphaproteobacteria; top row) and Saprospiraceae (phylum Bacteroidetes; bottom row) in N. luetkeana blade microbial communities (left side) and seawater microbial communities (right side) across sites. Sites are in order of decreasing ocean influence, from the outer coast (Destruction Island, Cape Johnson, Cape Alava and Koitlah) to the Strait of Juan de Fuca (Sekiu, Freshwater Bay, and Port Townsend) and Puget Sound (Scatchet Whidbey, Shilshole Seattle, Tacoma Narrows, and Squaxin Island).

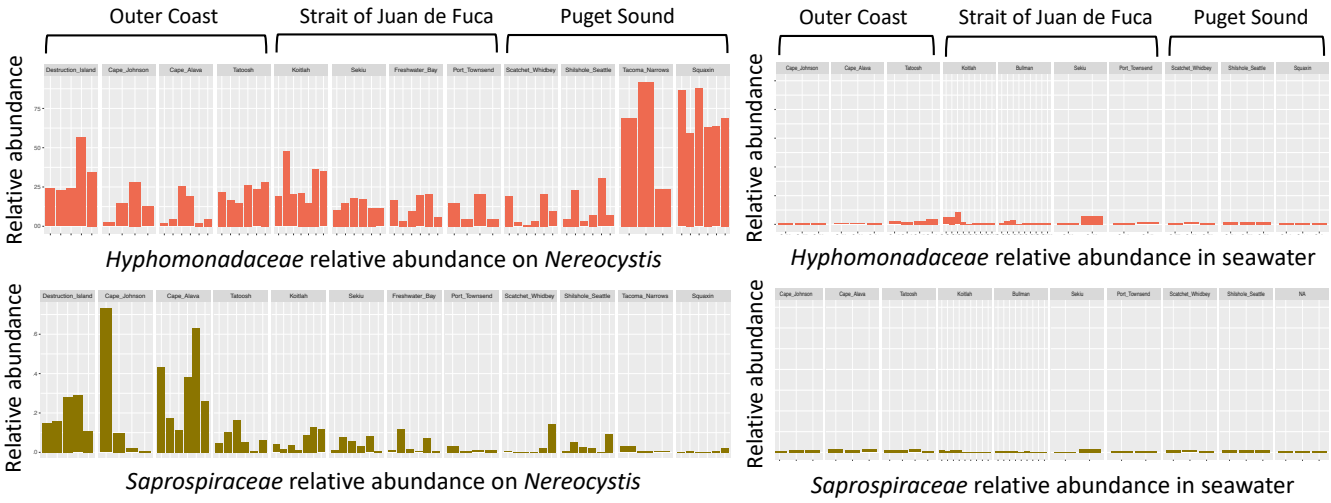

Table S1.1. Additional results of beta diversity tests comparing microbial communities among a) the two kelp species only at geographic locations where they co-occur (two-way PERMANOVA with "species" as a fixed and "location" as a random factor), and b) kelp meristem vs. tip, while controlling for kelp individual (two-way PERMANOVA with "meristem vs. tip" as a fixed factor and "kelp individual" as a random factor).

		PERMANOVA	
a) Effect of kelp species only at co-occurring locations	**df**	**pseudo-F (or *t*)**	**P**
Location (random, 4 levels)	3	F = 3.03	0.001*
Species (fixed, 2 levels)	1	F = 4.74	0.015*
N. luetkeana – M. pyrifera pairwise		*t* = 2.17	0.012*
Species*Location	3	F = 2.58	0.001*
N. luetkeana – M. pyrifera pairwise @ Sekiu		*t* = 2.27	0.007*
N. luetkeana – M. pyrifera pairwise @ Koitlah		*t* = 2.66	0.001*
N. luetkeana – M. pyrifera pairwise @ Cape Johnson		*t* = 2.26	0.028*
N. luetkeana – M. pyrifera pairwise @ Destruction Is.		*t* = 1.85	0.005*
b) Meristem – tip analysis			
Meristem vs. tip (fixed, 2 levels)	1	F = 25.49	0.001*
Effect of "kelp individual" (random, 36 levels)	35	F = 1.12	0.182

Table S1.2. PERMANOVA pairwise comparisons of kelp microbial communities at each site for the overall tests of N. luetkeana vs. location (11 sites) and M. pyrifera vs. location (5 sites).

Location 1	Location 2	Species	pseudo-F	p-value	q-value
Destruction_Island	Cape_Johnson	*N. luetkeana*	1.72	0.06	0.08
Destruction_Island	Cape_Alava	*N. luetkeana*	2.72	0.00	**0.01**
Destruction_Island	Koitlah	*N. luetkeana*	1.34	0.19	0.20
Destruction_Island	Sekiu	*N. luetkeana*	3.15	0.00	**0.01**
Destruction_Island	Freshwater_Bay	*N. luetkeana*	5.09	0.01	**0.02**
Destruction_Island	Port_Townsend	*N. luetkeana*	1.25	0.22	0.23
Destruction_Island	Scatchet_Whidbey	*N. luetkeana*	2.72	0.00	**0.01**
Destruction_Island	Shilshole_Seattle	*N. luetkeana*	3.21	0.01	**0.03**
Destruction_Island	Tacoma_Narrows	*N. luetkeana*	2.99	0.02	**0.03**
Destruction_Island	Squaxin	*N. luetkeana*	4.36	0.01	**0.02**
Cape_Johnson	Cape_Alava	*N. luetkeana*	1.88	0.01	**0.02**
Cape_Johnson	Koitlah	*N. luetkeana*	1.01	0.43	0.43
Cape_Johnson	Sekiu	*N. luetkeana*	1.34	0.11	0.13
Cape_Johnson	Freshwater_Bay	*N. luetkeana*	2.21	0.03	**0.04**
Cape_Johnson	Port_Townsend	*N. luetkeana*	1.39	0.09	0.11
Cape_Johnson	Scatchet_Whidbey	*N. luetkeana*	1.21	0.14	0.15
Cape_Johnson	Shilshole_Seattle	*N. luetkeana*	1.52	0.07	0.09
Cape_Johnson	Tacoma_Narrows	*N. luetkeana*	1.42	0.06	0.08
Cape_Johnson	Squaxin	*N. luetkeana*	1.99	0.01	**0.02**
Cape_Alava	Koitlah	*N. luetkeana*	2.75	0.00	**0.01**
Cape_Alava	Sekiu	*N. luetkeana*	3.72	0.00	**0.02**
Cape_Alava	Freshwater_Bay	*N. luetkeana*	4.71	0.01	**0.02**
Cape_Alava	Port_Townsend	*N. luetkeana*	2.09	0.02	**0.03**
Cape_Alava	Scatchet_Whidbey	*N. luetkeana*	2.81	0.00	**0.01**
Cape_Alava	Shilshole_Seattle	*N. luetkeana*	3.22	0.00	**0.01**
Cape_Alava	Tacoma_Narrows	*N. luetkeana*	2.69	0.01	**0.02**
Cape_Alava	Squaxin	*N. luetkeana*	3.53	0.00	**0.01**
Koitlah	Sekiu	*N. luetkeana*	1.70	0.04	**0.05**
Koitlah	Freshwater_Bay	*N. luetkeana*	3.37	0.01	**0.02**
Koitlah	Port_Townsend	*N. luetkeana*	1.56	0.10	0.12
Koitlah	Scatchet_Whidbey	*N. luetkeana*	1.79	0.01	**0.02**
Koitlah	Shilshole_Seattle	*N. luetkeana*	2.35	0.01	**0.02**
Koitlah	Tacoma_Narrows	*N. luetkeana*	2.12	0.01	**0.02**
Koitlah	Squaxin	*N. luetkeana*	3.77	0.00	**0.01**
Sekiu	Freshwater_Bay	*N. luetkeana*	1.44	0.12	0.13
Sekiu	Port_Townsend	*N. luetkeana*	3.20	0.01	**0.02**

Table S1.2. Continued.

Sekiu	Scatchet_Whidbey	*N. luetkeana*	1.63	0.02	**0.03**
Sekiu	Shilshole_Seattle	*N. luetkeana*	1.52	0.05	0.07
Sekiu	Tacoma_Narrows	*N. luetkeana*	1.87	0.01	**0.02**
Sekiu	Squaxin	*N. luetkeana*	3.49	0.00	**0.02**
Freshwater_Bay	Port_Townsend	*N. luetkeana*	4.10	0.01	**0.02**
Freshwater_Bay	Scatchet_Whidbey	*N. luetkeana*	2.41	0.02	**0.03**
Freshwater_Bay	Shilshole_Seattle	*N. luetkeana*	1.48	0.12	0.13
Freshwater_Bay	Tacoma_Narrows	*N. luetkeana*	2.06	0.02	**0.03**
Freshwater_Bay	Squaxin	*N. luetkeana*	3.08	0.01	**0.02**
Port_Townsend	Scatchet_Whidbey	*N. luetkeana*	2.13	0.01	**0.02**
Port_Townsend	Shilshole_Seattle	*N. luetkeana*	2.74	0.01	**0.02**
Port_Townsend	Tacoma_Narrows	*N. luetkeana*	2.23	0.06	0.08
Port_Townsend	Squaxin	*N. luetkeana*	3.08	0.00	**0.01**
Scatchet_Whidbey	Shilshole_Seattle	*N. luetkeana*	1.49	0.05	**0.07**
Scatchet_Whidbey	Tacoma_Narrows	*N. luetkeana*	1.28	0.12	0.13
Scatchet_Whidbey	Squaxin	*N. luetkeana*	2.23	0.00	**0.01**
Shilshole_Seattle	Tacoma_Narrows	*N. luetkeana*	1.41	0.11	0.13
Shilshole_Seattle	Squaxin	*N. luetkeana*	1.96	0.02	**0.03**
Tacoma_Narrows	Squaxin	*N. luetkeana*	1.69	0.02	**0.04**
Destruction_Island	Cape_Johnson	*M. pyrifera*	1.33	0.16	0.16
Destruction_Island	Koitlah	*M. pyrifera*	1.66	0.05	0.06
Destruction_Island	Bullman	*M. pyrifera*	1.50	0.04	0.06
Destruction_Island	Sekiu	*M. pyrifera*	2.46	0.01	**0.03**
Cape_Johnson	Koitlah	*M. pyrifera*	1.80	0.03	**0.05**
Cape_Johnson	Bullman	*M. pyrifera*	1.66	0.06	0.06
Cape_Johnson	Sekiu	*M. pyrifera*	2.98	0.03	**0.05**
Koitlah	Bullman	*M. pyrifera*	1.74	0.02	**0.05**
Koitlah	Sekiu	*M. pyrifera*	3.19	0.00	**0.02**
Sekiu	Bullman	*M. pyrifera*	1.87	0.03	**0.05**

Table S1.3. Differentially abundant ASVs detected with ANCOM on N. luetkeana (n = 31) and M. pyrifera (n = 4) across all sites. Each ASV is listed by taxonomic class, with lowest taxonomic classification indicated in parenthesis, along with the ANCOM W score. Mean relative abundances of ASVs across all sites are listed. Sites are listed left to right in order of decreasing ocean influence, from the outer coast (DSI = Destruction Island, CJO = Cape Johnson, CPA = Cape Alava and KOI = Koitlah) to the Strait of Juan de Fuca (BUL = Bullman, SEK = Sekiu, FWB = Freshwater Bay, and PTW = Port Townsend) and Puget Sound (SCW = Scatchet Whidbey, SHS = Shilshole Seattle, TAC = Tacoma Narrows, and SQX = Squaxin).

ASV	W score	Lowest Taxonomic Classification	DSI	CJO	CPA	KOI	SEK	FWB	PTW	SCW	SHS	TAC	SQX
Nereo_1	1045	Gammaproteobacteria (Granulosicoccus sp.)	29 52	76 1	48 39	87 7	16 26	18 98	44 65	44 7	9	11 1	0
Nereo_2	1045	Bacteroidetes (Saprospiraceae)	93 0	15 2	17 37	19	0	0	3	0	0	0	0
Nereo_3	1045	Bacteroidetes (Saprospiraceae)	19 72	27 8	12 40	11	0	0	21	1	0	0	0
Nereo_4	1018	Verrucomicrobia (Rubritalea sp.)	12 57	25	22 7	13 7	25 49	56 3	25	54 59	38 7	35	60
Nereo_5	1007	Bacteroidetes (Flavobacteriaceae)	0	0	13 9	0	0	0	0	0	0	0	0
Nereo_6	1044	Bacteroidetes (Saprospiraceae)	47 6	0	96	4	0	0	18	5	0	0	0
Nereo_7	1044	Bacteroidetes (Saprospiraceae)	91 6	0	76	2	0	0	27	0	0	0	0
Nereo_8	1026	Bacteria (unclassified)	0	0	47	0	0	0	0	0	0	0	0
Nereo_9	1012	Alphaproteobacteria (Rickettsiales)	0	3	29	0	0	0	0	0	0	0	0
Nereo_10	998	Bacteroidetes (unclassified)	0	1	29	0	0	0	0	0	0	0	0
Nereo_11	996	Deltaproteobacteria (Bacteriovoracaceae)	15	11	15	0	0	0	0	0	0	0	0
Nereo_12	1027	Gammaproteobacteria (Pseudoalteromonas sp.)	0	5	5	0	0	5	1	46	35	1	1
Nereo_13	1033	Verrucomicrobia (Verrucomicrobiaceae)	15	7	1	17 0	36 4	13 1	0	36 6	11 42	6	0
Nereo_14	966	Bacteroidetes (Flavobacteriaceae)	0	0	1	1	15	56	0	0	2	2	0
Nereo_15	1018	Verrucomicrobia (Verrucomicrobiaceae)	0	3	1	22 7	12 8	32 5	0	12 8	53 7	23	0
Nereo_16	1026	Alphaproteobacteria (Hyphomonadaceae)	0	6	0	0	16 1	17 6	0	20 9	23 3	0	0
Nereo_17	994	Alphaproteobacteria (Hyphomonadaceae)	0	0	0	10 0	15 7	17 2	0	0	72	4	0
Nereo_18	991	Alphaproteobacteria (Rickettsiales)	0	3	0	0	21	24	0	0	72	0	0
Nereo_19	1034	Bacteroidetes (Flavobacteriaceae)	17	0	0	2	23 6	55 4	0	22 4	37 0	2	0
Nereo_20	987	Bacteroidetes (Flavobacteriaceae)	0	0	0	0	0	14 7	0	21	11	0	0
Nereo_21	1029	Bacteroidetes (Saprospiraceae)	0	7	0	10 1	96 6	57 6	6	79 4	26 7	14	0

Table S1.3. Continued

Nereo_22	992	Bacteroidetes (Saprospiraceae)	0	0	0	0	38	178	0	0	0	2	0
Nereo_23	1042	Gammaproteobacteria (unclassified)	0	0	0	113	18	0	0	0	0	0	0
Nereo_24	974	Gammaproteobacteria (Vibrio sp.)	0	0	0	0	0	0	0	34	14	0	0
Nereo_25	974	Planctomycetes (Class OM190)	0	0	0	31	14	79	0	0	0	0	0
Nereo_26	990	Planctomycetes (family Pirellulaceae)	0	0	0	0	94	379	0	17	11	16	0
Nereo_27	964	Verrucomicrobia (Persicirhabdus sp.)	11	11	0	65	248	1301	0	50	705	8	0
Nereo_28	1045	Gammaproteobacteria (Granulosicoccus sp.)	0	0	0	330	3474	3622	32	21	5976	58	10
Nereo_29	993	Alphaproteobacteria (Hyphomonadaceae)	75	27	0	0	193	218	0	12	982	3	12
Nereo_30	1034	Gammaproteobacteria (Granulosicoccus sp.)	0	0	0	0	75	185	0	6	41	0	12
Nereo_31	1030	Gammaproteobacteria (Thalassomonas sp.)	0	0	0	0	0	18	0	0	14	0	88

ASV	**W score**	**Lowest Taxonomic Classification**	**DSI**	**CJO**	**BUL**	**KOI**	**SEK**
Macro_1	1640	Gammaproteobacteria (Granulosicoccus sp.)	7	26	2	459	0
Macro_2	1555	Gammaproteobacteria (family Francisellaceae)	1	0	0	0	2377
Macro_3	1498	Gammaproteobacteria (Granulosicoccus sp.)	0	0	0	11	375
Macro_4	1543	Bacteroidetes (Saprospiraceae)	0	0	0	0	363

Table S1.4. PERMANOVA pairwise comparisons of seawater microbial communities at each location (9 sites).

Group 1	Group 2	pseudo-F	p-value	q-value
Cape_Johnson	Cape_Alava	2.53	0.11	0.12
Cape_Johnson	Koitlah	3.13	0.00	**0.04**
Cape_Johnson	Bullman	2.73	0.00	**0.04**
Cape_Johnson	Sekiu	2.00	0.10	0.12
Cape_Johnson	Port_Townsend	2.28	0.09	0.12
Cape_Johnson	Scatchet_Whidbey	2.79	0.10	0.12
Cape_Johnson	Shilshole_Seattle	3.51	0.11	0.12
Cape_Johnson	Squaxin	3.15	0.10	0.12
Cape_Alava	Koitlah	2.86	0.01	**0.04**
Cape_Alava	Bullman	2.68	0.01	**0.04**
Cape_Alava	Sekiu	2.01	0.11	0.12
Cape_Alava	Port_Townsend	2.27	0.11	0.12
Cape_Alava	Scatchet_Whidbey	2.54	0.11	0.12
Cape_Alava	Shilshole_Seattle	2.86	0.12	0.13
Cape_Alava	Squaxin	3.05	0.10	0.12
Koitlah	Bullman	1.32	0.06	0.12
Koitlah	Sekiu	1.88	0.02	0.07
Koitlah	Port_Townsend	1.47	0.02	0.06
Koitlah	Scatchet_Whidbey	1.56	0.01	**0.04**
Koitlah	Shilshole_Seattle	2.69	0.01	**0.04**
Koitlah	Squaxin	2.84	0.01	**0.04**
Bullman	Sekiu	1.58	0.06	0.12
Bullman	Port_Townsend	1.23	0.14	0.15
Bullman	Scatchet_Whidbey	1.62	0.01	**0.05**
Bullman	Shilshole_Seattle	2.60	0.00	**0.04**
Bullman	Squaxin	1.94	0.01	**0.04**
Sekiu	Port_Townsend	1.12	0.34	0.34
Sekiu	Scatchet_Whidbey	1.74	0.11	0.12
Sekiu	Shilshole_Seattle	1.69	0.10	0.12
Sekiu	Squaxin	1.94	0.09	0.12
Port_Townsend	Scatchet_Whidbey	1.89	0.09	0.12
Port_Townsend	Shilshole_Seattle	1.99	0.09	0.12
Port_Townsend	Squaxin	1.80	0.10	0.12
Scatchet_Whidbey	Shilshole_Seattle	1.79	0.10	0.12
Scatchet_Whidbey	Squaxin	2.57	0.10	0.12
Shilshole_Seattle	Squaxin	2.86	0.12	0.13

Table S1.5. Mean number of total 16S sequences, mean bacterial sequences and mean chloroplast sequences (as well as mean % chloroplast and bacterial sequences) for all N. luetkeana, M. pyrifera, and seawater samples.

Sample Type	Date	*n*	Total Sequences	Bacterial Sequences	Chloroplast Sequences	% Chloroplast	% Bacterial
Nereocystis meristem (Tatoosh)	5/12/17	3	26,161	369	25,792	98.6	1.4
Nereocystis meristem (Tatoosh)	6/11/17	4	26,178	419	25,759	98.4	1.6
Nereocystis meristem (Tatoosh)	6/25/17	5	31,313	1,135	30,177	96.5	3.5
Nereocystis meristem (Tatoosh)	7/10/17	6	31,811	1,392	30,420	95.8	4.2
Nereocystis meristem (Tatoosh)	7/24/17	6	33,278	2,550	30,728	92.6	7.4
Nereocystis meristem (Tatoosh)	8/22/17	6	22,057	320	21,738	98.6	1.4
Nereocystis tip (Tatoosh)	5/12/17	6	42,967	30,132	12,834	32.6	67.4
Nereocystis tip (Tatoosh)	6/11/17	6	45,636	35,547	10,090	25.7	74.3
Nereocystis tip (Tatoosh)	6/25/17	6	46,808	39,140	7,667	17.7	82.3
Nereocystis tip (Tatoosh)	7/10/17	6	54,983	49,532	5,451	10.0	90.0
Nereocystis tip (Tatoosh)	7/24/17	6	52,888	47,500	5,388	11.1	88.9
Nereocystis tip (Tatoosh)	8/22/17	6	45,667	35,014	10,653	27.3	72.7
Seawater (Tatoosh)	5/12/17	3	45,752	40,080	5,672	12	88
Seawater (Tatoosh)	6/11/17	2	42,812	35,431	7,382	18	82
Seawater (Tatoosh)	6/25/17	4	44,915	35,242	9,673	24	76
Seawater (Tatoosh)	7/24/17	2	49,269	44,231	5,038	10	90
Seawater (Tatoosh)	8/22/17	3	50,531	45,853	4,679	10	90
Macrocystis (Bullman)	7/5/17	5	40,246	10,859	29,387	73.0	27.0
Macrocystis (Cape Johnson)	7/31/17	4	38,907	27,549	11,358	26.5	73.5
Macrocystis (Destruction Island)	8/1/17	5	40,726	29,344	11,382	32.1	67.9

Table S1.5. Continued

Macrocystis (Koitlah)	8/11/17	10	37,679	20,460	17,219	47.9	52.1
Macrocystis (Sekiu)	7/2/17	4	45,463	30,834	14,629	32.5	67.5
Nereocystis (Cape Alava)	8/2/17	6	35,700	13,643	22,057	62.0	38.0
Nereocystis (Cape Johnson)	7/31/17	4	29,486	3,574	25,912	85.9	14.1
Nereocystis (Destruction Island)	8/1/17	5	33,083	21,081	12,002	33.8	66.2
Nereocystis (Freshwater Bay)	7/19/17	6	38,562	23,078	15,484	40.4	59.6
Nereocystis (Koitlah)	8/11/17	7	40,969	6,402	34,567	85.8	14.2
Nereocystis (Port Townsend)	7/19/17	4	29,185	9,642	19,543	67.9	32.1
Nereocystis (Scatchet Whidbey)	8/10/17	6	47,728	30,977	16,751	35.4	64.6
Nereocystis (Sekiu)	7/2/17	6	36,338	18,954	17,384	50.5	49.5
Nereocystis (Shilshole Seattle)	8/10/17	6	46,159	21,258	24,901	56.1	43.9
Nereocystis (Squaxin)	6/21/17	6	39,660	4,776	34,884	88.1	11.9
Nereocystis (Tacoma Narrows)	8/19/17	3	29,472	2,150	27,323	92.4	7.6
Seawater (Bullman)	7/5/17	3	45,386	39,526	5,861	13.0	87.0
Seawater (Cape Alava)	8/2/17	3	53,451	49,665	3,786	7.4	92.6
Seawater (Cape Johnson)	7/31/17	3	39,032	22,628	16,404	43.4	56.6
Seawater (Koitlah)	8/11/17	6	40,398	27,924	12,474	31.6	68.4
Seawater (P.Townsend)	7/19/17	2	41,495	32,434	9,061	22.1	77.9
Seawater (Scatchet Whidbey)	8/10/17	3	71,919	67,661	4,258	8.5	91.5
Seawater (Sekiu)	7/2/17	2	41,297	29,226	12,072	30.9	69.1
Seawater (Shilshole Seattle)	8/10/17	3	96,088	93,957	2,131	2.2	97.8
Seawater (Squaxin)	6/21/17	3	50,251	45,674	4,578	9.3	90.7

CHAPTER 2: OXYGEN METABOLISM SHAPES MICROBIAL SETTLEMENT ON PHOTOSYNTHETIC KELP BLADES COMPARED TO ARTIFICIAL KELP SUBSTRATES

Citation: Weigel, B.L. and Pfister, C.A. 2021. Oxygen metabolism shapes microbial settlement on photosynthetic kelp blades compared to artificial kelp substrates. Environmental Microbiology Reports 13(2): 176-184. doi:10.1111/1758-2229.12923

Abstract

Marine macroalgae host dense microbial biofilms on their photosynthetic blade surfaces. Here, we examined factors shaping community assembly of the bull kelp (*Nereocystis luetkeana*) microbiome by comparing biofilm formation on photosynthetic kelp blade tissues and artificial kelp substrates ("agar substrates") deployed into a kelp forest. New kelp blade tissues were colonized by markedly distinct microbial taxa relative to agar substrates during the same time interval, even when agar substrates were infused with *N. luetkeana* blades, suggesting that microbial settlement onto kelp surfaces is more than just attraction to a polysaccharide-rich surface. Further, common seawater taxa such as *Colwellia sp*. and *Psychromonas sp*. became abundant on agar substrates but avoided new kelp blade tissues, indicating that host-specific factors may deter certain surface-associated marine microbial taxa. Over two-thirds of taxa in the kelp microbiome were associated with strictly aerobic metabolisms; thus, photosynthetic production of O_2 may favor aerobic microbial metabolisms. While living kelp blades primarily recruited aerobic microbes, including the obligate aerobe *Granulosicoccus sp.*, microbes that colonized agar substrates were predominantly facultative anaerobes. We also found that infusion of kelp tissues into agar substrates altered microbial community composition and lowered taxonomic diversity relative to control agar substrates, suggesting that non-living components of the kelp blade also impact microbial community assembly.

Introduction

The importance of microbial communities to the health and functioning of multicellular organisms is becoming increasingly recognized across the tree of life, from the human gut to the plant rhizosphere. Association with eukaryotic hosts plays a large role in structuring microbial communities globally; host-associated microbiomes are generally less speciose than free-living microbial communities (Thompson *et al.*, 2017). In the ocean, host-associated microbiomes can impact marine ecosystem functioning by altering the way that hosts reproduce and develop, metabolize nutrients, or respond to environmental stressors (Wilkins *et al.*, 2019). Marine host-associated microbiomes may be useful for microbial-based management and conservation, yet knowledge about the basic rules of microbiome assembly and persistence is still lacking for most marine organisms (Wilkins *et al.*, 2019). Marine macroalgae host dense microbial biofilms on their photosynthetic surfaces, with roughly 10^6-10^8 microbial cells per cm^2 of algal tissue (Mazure and Field, 1980; Stratil *et al.*, 2013). Microorganisms that live in biofilms on the macroalgal surface may greatly affect the biology of their host by influencing development, disease susceptibility, biofouling, or nutrient acquisition (Goecke *et al.*, 2010; Egan *et al.*, 2013). Despite strong differentiation of macroalgal microbiomes from free-living microbial communities in the surrounding seawater (Bengtsson *et al.*, 2010; Mancuso *et al.*, 2016; Weigel and Pfister, 2019), little is known about the factors that structure microbial biofilm assembly on macroalgal hosts compared to the surrounding environment.

In the ocean, bacteria can rapidly colonize available substrates, forming dense biofilms with more than 10^5 cells/cm^2 on artificial surfaces in just 20 hours (Fischer *et al.*, 2014). Algal tissues may be colonized partially by microbes from the seawater, as algal hosts share 32% (Weigel and Pfister, 2019) to 86% (Lemay *et al.*, 2018) of their microbial taxa with the

surrounding seawater. It is possible that motile microbes from the seawater are especially likely to settle onto kelp surfaces, as microbial motility and chemotaxis genes were enriched in the kelp blade surface biofilm relative to the seawater microbial community (Minich *et al.*, 2018). Common properties of the macroalgal surface may attract generalist microbial taxa that can colonize many algal host species (Florez *et al.*, 2017). For example, new blade tissues on nine sympatric macroalgal species shared a large number (36%) of overlapping microbial taxa (Lemay *et al.*, 2018). Given the proclivity of seawater microbes to adhere to surfaces and rapidly generate biofilms (Fischer *et al.*, 2014), it is possible that the macroalgae are "just a surface" for microbial settlement from the seawater. However, microbial settlement onto macroalgal surfaces is likely shaped by a variety of host-associated factors.

The macroalgal surface environment may select for a subset of potential colonizing microbes from the seawater using certain biological, morphological, or chemical cues. Macroalgal blade surfaces are rich in organic nutrients and carbohydrates, provision microbes with a source of dissolved organic matter (Reed *et al.*, 2015, Weigel and Pfister, 2020), and produce oxygen, which may provide a preferred habitat for certain microbes. In addition, surface-associated metabolites from macroalgal hosts may shape microbial membership by attracting or deterring certain microbial groups (Lachnit *et al.*, 2013, Saha and Weinberger, 2019). For example, Lachnit *et al.* (2010, 2013) discovered that certain algal-produced compounds had a "profouling effect" on the artificial algal surfaces, while others such as fucoxanthin deterred bacterial colonization in a nondiscriminatory manner. Macroalgae shape not only organic matter availability but also local oxygen concentrations (Irwin and Davenport, 2002; Noisette and Hurd, 2018; Pfister *et al.*, 2019), which can be a critical determinant of microbial community structure due to differing microbial respiratory metabolisms and defenses

against reactive oxygen species (Morris and Schmidt, 2013). Finally, morphology alone can be a determinant of microbial community structure. For example, a recent study using artificial seaweed cut to mimic different thallus morphologies found that morphology and structural complexity shaped surface microbial communities in the absence of biological or chemical interactions (Lemay et al. *in review*). Despite all of these factors, we are still just beginning to understand the processes shaping microbial community assembly on macroalgal surfaces.

Macroalgae known as kelp (order Laminariales) play a vital role in coastal ecosystems, creating kelp forest habitat and fixing tremendous amounts of carbon, yet we know little about microbial community assembly on kelps. Photosynthetic blade tissues of the canopy-forming kelp *Nereocystis luetkeana* host an abundant and spatially structured microbiome of 10^7-10^8 cells/cm^2 (Ramirez-Puebla *et al.*, 2020). Despite high cell density, the biofilm community is dominated by a few highly abundant bacterial taxa that displayed repeatable spatial structure over multiple months (Ramirez-Puebla *et al.*, 2020) and persisted over large geographical distances (Weigel and Pfister, 2019). As an annual species, *N. luetkeana* rapidly grows from a microscopic gametophyte to a massive sporophyte during the spring and summer, becoming one of the largest primary producers in the ocean by mid-summer. The photosynthetic blades of *N. luetkeana* elongate rapidly and produce 1 to 5 cm of new blade tissue per day (Maxell and Miller, 1996; Weigel and Pfister, 2019), constantly providing new tissues for microbial colonization. By comparing microbial biofilm formation on new kelp blade tissues with artificial kelp substrates, this study examined the processes shaping recruitment of microbiota from the seawater onto living and non-living kelp substrates.

Here, we deployed artificial kelp substrates consisting of agar gel plates with and without infusion of crushed *N. luetkeana* blades into a kelp forest in Washington, USA (Fig. 2.1).

Artificial kelp substrates were deployed at the north-facing Main Beach site on Tatoosh Island, Washington, USA (48.39°N, 124.74°W), where *N. luetkeana* forests are abundant and have persisted over decades (Fig. 2.1A, Pfister *et al.*, 2018). Agar is a polysaccharide extracted from red algal cell walls, composed of agarose (a polymer of galactose and galactopyranose) and agaropectin, and thus is an excellent mimic for the macroalgal surface. Given that motile marine bacteria exhibit chemotaxis towards phytoplankton cells and their extracellular compounds (Seymour *et al.*, 2010), we hypothesized that infusing crushed kelp blades into the "kelp agar" treatment will alter microbial recruitment. After 4 days of deployment in the kelp forest, we sampled control and kelp agar artificial substrates, nearby *N. luetkeana* blade tissues, and surrounding seawater. We characterized microbial communities with 16S rRNA gene sequencing to answer the following questions: 1) Do artificial kelp substrates and new *N. luetkeana* blade tissues develop similar microbial communities after 4 days in a kelp forest? 2) Does infusion of agar with crushed *N. luetkeana* blades ("kelp agar") alter microbial settlement or increase microbiome similarity between artificial substrates and real *N. luetkeana* blades? 3) Do any of the common microbial taxa associated with *N. luetkeana* settle onto artificial kelp substrates?

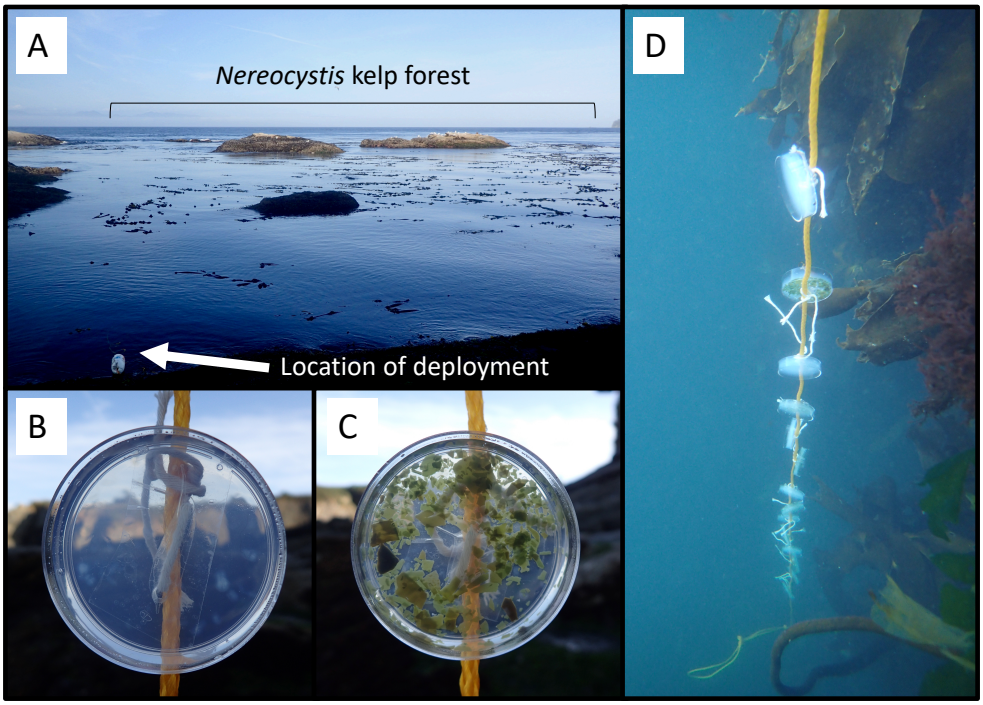

Figure 2.1. A. Artificial kelp substrates were deployed at the north-facing Main Beach site on Tatoosh Island, WA, USA in close proximity to a *N. luetkeana* forest. The substrates consisted of B. control agar plates and C. kelp agar plates, infused with dried *N. luetkeana* blades. Agar substrates were deployed for 4 days by suspending them from a rope D. connected to a surface buoy and an anchor, so that they remained underwater at all times.

Methods

Artificial kelp substrate deployment and sample collection

Artificial kelp agar substrates were made by dissolving 1.5 g of agar (Fisher Scientific, molecular genetics grade, product # BP1423) into 150 mL of nanopure water, boiling for ~10 mins, and pouring 20 mL into 60 x 15 mm petri dishes ("control agar" treatment, Fig. 2.1B). For the "kelp agar" treatment (Fig. 2.1C), an additional 1.5 g of dried and ground blade tissue from *N. luetkeana* was added before boiling. *N. luetkeana* blade tissues were collected ~2 weeks prior from the same location where the artificial kelp substrates were deployed, and they were dried for 48 hours at 50 °C and crushed with a mortar and pestle. Petri dishes contained pre-drilled

holes, allowing attachment to a larger rope for deployment with a simple knotted string (Fig. 2.1D). Artificial kelp substrates were deployed into the field in an area adjacent to a dense *N. luetkeana* forest (Fig. 2.1A). The rope contained alternating control and kelp agar treatments (n = 5 replicates of each treatment), spaced roughly 20 cm apart on the rope, which was connected to an anchor at the bottom and a float at the top, further secured to a rocky outcrop on land with a rope from the buoy leading to an eyelet screw drilled into the rock. With this deployment design, the agar substrates remained suspended ~2 to 4 m under the surface at all times, while still moving freely up and down with the tides, mimicking the water column movement of *N. luetkeana*.

Artificial kelp substrates were deployed at the north-facing Main Beach site on Tatoosh Island, Washington, USA (48.39°N, 124.74°W), where *N. luetkeana* forests are abundant and have persisted over decades (Fig. 2.1A, Pfister *et al.*, 2018). Sporophytes of *N. luetkeana* were < 5 m from the deployed substrates. The substrates were deployed on 19 Aug 2017 and sampled on 23 Aug, which allowed for microbial colonization over a total of 88 hours (~3.7 days). Sampling consisted of collecting the substrates from the seawater, letting them drip-dry, and swabbing the surface of each agar plate with a sterile cotton swab for 5 seconds. Cotton swab tips were snapped off into a 2 mL sterile collection tube. On the same day that agar surfaces were sampled, nearby *N. luetkeana* blades from the Main Beach site were sampled to compare artificial kelp substrates to real blade surfaces (22 Aug 2017). Two tissue samples (2 x 1 cm^2) were collected from a single blade – one at the basal meristem, roughly 2 cm from where the blade connects to the stipe, to capture recently produced tissue (~2 to 4 days old) and another near the apical end of the blade tip to sample older tissue (weeks to months old). Samples were collected from n = 6 different kelp individuals. Additionally, two individuals were sampled at the blade base and tip;

tissues were swabbed for 5 seconds with a sterile cotton swab to compare microbial communities from swabs vs. whole blade tissues. Finally, seawater samples were collected near the surface from within the kelp forest in sterile 1.0 L Nalgene™ bottles. After transporting seawater to the lab on ice, microbial samples were collected by filtering seawater through 0.22 μm Millipore Sterivex™ filters with a peristaltic pump. Total replication for this study included 5 control agar, 5 kelp agar, 6 *N. luetkeana* blade base tissues, 6 *N. luetkeana* blade tip tissues, 2 blade base swabs, 2 blade tip swabs and 3 seawater samples. All samples were temporarily frozen at -20°C, shipped to -80°C and stored until DNA extraction.

16S rRNA sequence data processing and statistical analyses

Complete details of DNA extraction and 16S rRNA gene sequencing are contained in Weigel and Pfister (2019), as these samples were sequenced alongside the *N. luetkeana* samples analyzed therein. Briefly, DNA was extracted using the DNeasy Power Soil Kit (Qiagen), amplification of the V4 region of the 16S rRNA gene was completed using the Earth Microbiome Project universal primers 515f–806r (Caporaso *et al.*, 2011) with the modified forward primer (Parada *et al.*, 2016), and 250 bp amplicons were sequenced on an Illumina MiSeq 2 x 150 bp paired-end run. Sequence data were processed in QIIME2 (Bolyen *et al.*, 2019) and amplicon sequence variants (ASVs) were generated using the Divisive Amplicon Denoising Algorithm (DADA2) (Callahan *et al.*, 2016). Using DADA2, quality control included chimera detection and removal, sequence error elimination, singleton exclusion, and sequence trimming based on per-base-pair sequence quality graphs (both forward and reverse sequences were trimmed between 13 and 150 base pairs). Sequences were classified with the Silva 119 database, trimmed to the V4 region, and chloroplast and mitochondrial reads were subsequently

removed. Raw 16S rRNA sequences are available as FASTQ files on the NCBI Sequence Read Archive and the European Bioinformatics Institute (accession # PRJEB29319; Table S2.1). After removing chloroplast sequences, the average number of bacterial sequences in kelp blade base samples was two orders of magnitude lower (320 ± 56 reads, mean ± SE) than the kelp blade tip (35,014 ± 7,381), agar substrates (48,699 ± 4,161) and seawater samples (45,811 ± 4,849); see Appendix 2: Table S2.1 for all sample read depths. The significantly and consistently lower bacterial sequence count on kelp blade base tissues likely reflects the low bacterial cell counts on these newly formed kelp tissues (Weigel and Pfister 2019; see Fig. 3 in Ramirez-Puebla et al. 2020 for images showing extremely low microbial cell density on kelp blade base compared to tip tissues). Thus, we did not exclude these low bacterial abundance blade base samples from our analyses because the low bacterial sequence read count is likely representative of the true microbial cell densities on these new tissues.

Amplicon sequence variant and taxonomy tables were imported into R (version 3.4.4) for analysis and visualization using the phyloseq (version 1.22.3; McMurdie and Holmes, 2013), ggplot2 (version 2.2.1; Wickham, 2016) and vegan (version 2.5-1; Oksanen *et al.*, 2014) packages. Differences in microbial communities were visualized using taxonomic barplots as well as non-metric multidimensional scaling (NMDS) plots and heatmaps, based on Bray-Curtis dissimilarity matrices of microbial relative abundances across sample types. We tested for differences in community structure (beta diversity) as a function of sample type using a permutational multivariate analysis of variance (PERMANOVA) test with the function “adonis” in vegan. To verify that significant PERMANOVA outcomes were not a result of unequal dispersion of variance among sample types, permutation tests for homogeneity of multivariate dispersions were conducted with the function “betadisper” in vegan. Alpha diversity (ASV

richness) was calculated using phyloseq, and differences in ASV richness among sample types were assessed with ANOVA. We used DESeq2 (Love *et al.*, 2014, McMurdie and Holmes, 2014) to test for differentially abundant ASVs between control and kelp agar substrates, with a minimum abundance of 20 sequences per sample. All analyses were conducted with unrarefied data due to low microbial abundance samples from the base of *N. luetkeana* blades (Table S2.1). However, for NMDS visualization, we rarefied the data to the lowest bacterial read count (213) to account for the low blade base read counts. To ensure that significant differences among treatments were not due to sequence depth, we verified that PERMANOVA tests were still significant with the rarefied dataset (Table S2.2).

To assess potential oxygen metabolisms, we grouped bacterial families into 5 categories based on metabolic oxygen requirements (Morris and Schmidt, 2013): 1) obligately aerobic bacteria that require O_2 for respiration under atmospheric (~20%) O_2 concentrations, 2) microaerobic bacteria that grow best at sub-atmospheric (< 20%) O_2 concentrations, 3) facultatively anaerobic bacteria capable of metabolizing O_2 or alternative terminal electron acceptors and fermentation when O_2 is not available, 4) aerobic or facultatively anaerobic bacteria from families that contain both strict aerobes as well as facultative anaerobes, and 5) obligately anaerobic bacteria unable to grow in the presence of O_2. Classification of the oxygen requirements of bacterial families found in this study were based on descriptions of each bacterial family found in Rosenberg *et al.* (2014). We used a chi-squared test in R (chisq.test) to test whether obligately aerobic vs. facultatively anaerobic microbial metabolisms were distributed identically among substrate types (kelp blades vs. agar substrates).

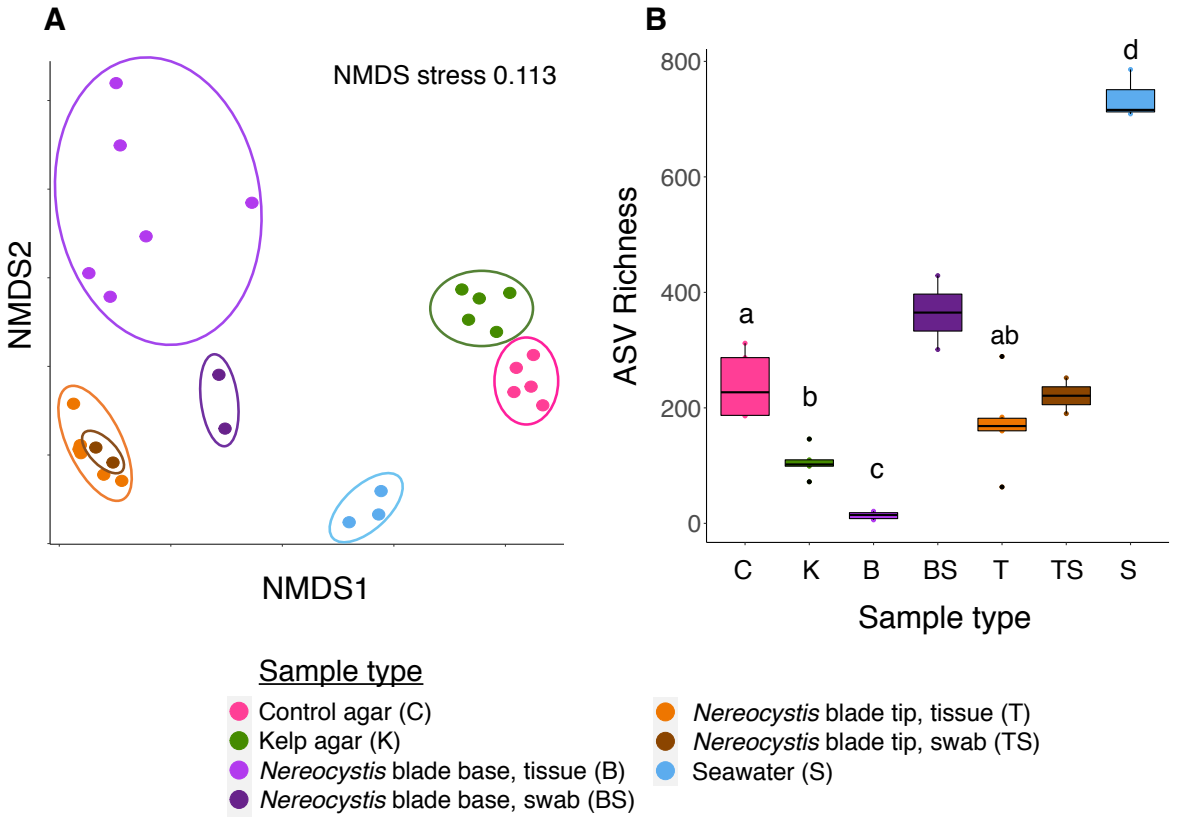

Figure 2.2. A. Microbial community structure of each sample type visualized with a non-metric multidimensional scaling (NMDS) plot. Each point represents one microbial community sample, and points clustered more closely together have more similar microbial communities. Color and ellipses around data points help to visually group samples by treatment. B. Mean amplicon sequence variant (ASV) richness in each sample type. Different letters indicate significant differences in ASV richness among sample types (ANOVA pairwise comparisons, $P < 0.05$), but swabs of base and tip tissues were not included due to low replication ($n = 2$) per sample type.

Results and Discussion

Artificial kelp substrates recruit a distinct microbiome compared to real kelp blades

We found that artificial kelp substrates deployed in a *N. luetkeana* forest for 4 days recruited a distinct microbial biofilm compared to microbial taxa associated with *N. luetkeana* blade surfaces and the surrounding seawater (Fig. 2.2A). Microbial community structure varied significantly with substrate type between control agar, kelp agar, *N. luetkeana* blade base, *N.*

luetkeana blade tip and seawater samples (PERMANOVA, df = 4, total df = 24, F = 13.87, R^2 = 0.74, P = 0.001; Fig. 2.2A; Table 2.1), and these differences were not due to unequal dispersion of variance among sample types (PERMDISP, df = 4, total df = 24, F = 0.95, P = 0.46). Further, after samples were rarefied to the lowest sample read count, the differences between sample types were still significant (PERMANOVA, df = 4, total df = 24, F = 11.29, R^2 = 0.69, P = 0.001; Appendix 2: Table S2.2), and there were still no differences in dispersion (PERMDISP, df = 4, total df = 24, F = 0.38, P = 0.82). After 3.7 days in the *N. luetkeana* kelp forest, both agar substrates had significantly different microbial communities from those living on blades of *N. luetkeana* (PERMANOVA pairwise comparisons, $p < 0.01$; Table 2.1; Fig. 2.2A). There were also significant differences in ASV richness among sample types (ANOVA, df = 4, total df = 24, F = 123, $P < 0.001$), where seawater samples had the highest ASV richness, the base of the kelp blade had the lowest ASV richness, and both kelp agar and control agar had similar ASV richness to the blade tip samples (Fig. 2.2B). Microbial community composition on *N. luetkeana* blades was significantly different from that of the agar substrates (Fig. 2.3A). Across all *N. luetkeana* samples, the most abundant taxon was *Granulosicoccus sp.*, a *Gammaproteobacteria* from the family *Granulosicoccaceae*, with a mean relative abundance of 38.7% (± 6.25, std. error; Fig 3A). While 25 ASVs were detected on *N. luetkeana* blades, 3 *Granulosicoccus* ASVs comprised an average of 38.1% (± 6.34% std. error) of the *N. luetkeana* blade microbiome, while the others had mean abundances of less than 1% of the community (Appendix 2: Fig. S2.1). In contrast, *Granulosicoccus* were hardly detected on agar substrates (Fig. 2.3A, Fig S1B), making up negligible proportions of the total microbial community (0.34% ± 0.50). Despite extremely low abundances, 11 *Granulosicoccus sp.* ASVs were detected on control agar substrates, many of which differed from the ASVs that recruited to kelp blades (Appendix 2: Fig. S2.1). The

microbiome of *N. luetkeana* blades was also enriched in *Alphaproteobacteria* from the *Hyphomonadaceae* family, *Bacteroidetes* from the *Flavobacteriaceae* and *Saprospiraceae* families, *Verrucomicrobia* from the *Rubritaleaceae*, and *Planctomycetes* from the *Planctomycetaceae* compared to agar substrates (Fig. 2.3A).

Table 2.1. PERMANOVA pairwise comparisons of microbial community structure among substrate types (control agar, kelp agar, *N. luetkeana* blade base and tip, seawater), based on a Bray Curtis distance matrix of microbial community similarity among samples. Swabs of base and tip tissues were not included due to low replication (n = 2) per sample type.

PERMANOVA Pairwise Tests	**df**	**Sum Squares**	***F* statistic**	***p*-value**
Control agar vs. Kelp agar	1	0.80	8.38	0.017
Control agar vs. *N. luetkeana* blade base	1	2.23	20.6	0.017
Kelp agar vs. *N. luetkeana* blade base	1	2.15	16.8	0.008
Control agar vs. *N. luetkeana* blade tip	1	1.98	14.8	0.002
Kelp agar vs. *N. luetkeana* blade tip	1	1.96	12.8	0.002
Control agar vs. Seawater	1	1.25	20.5	0.015
Kelp agar vs. Seawater	1	0.93	10.3	0.017
N. luetkeana blade base vs. tip	1	2.03	12.8	0.001
N. luetkeana blade base vs. Seawater	1	1.68	15.7	0.013
N. luetkeana blade tip vs. Seawater	1	1.30	9.28	0.017

Examining the distribution of the 50 most abundant ASVs across sample types revealed that the abundant microbial symbionts from *N. luetkeana* blade tip communities colonized at a lower abundance onto artificial agar surfaces, while many of the ASVs abundant on agar substrates were not found on *N. luetkeana* blades (Fig. 2.4). In contrast to the kelp blade surface, agar substrate biofilm communities were comprised mainly of *Gammaproteobacteria* from the families *Colwelliaceae* (mostly *Colwellia sp*.), *Pseudoalteromonadaceae* and *Psychromonadaceae*, *Alphaproteobacteria* from the *Rhodobacteraceae* family, as well as *Arcobacter sp.* from the *Epsilonproteobacteria* family *Campylobacteraceae* (Fig. 2.3A). A few of the most abundant ASVs found in seawater were highly abundant on agar substrates (Fig. 2.4), including ASVs classified as *Colwellia sp*., *Pseudoalteromonas sp.*, and *Psychromonas sp.*,

demonstrating settlement of these taxa from the seawater onto agar substrates. Both agar substrates and seawater samples are enriched in these three families, while they are nearly absent or found in low abundance on *N. luetkeana* blades (Fig. 2.3A). These results are well-matched with those of Lachnit *et al.* (2013), where artificial hydrogel surfaces hosted significantly different microbial communities from those of *Fucus vesiculosus* after 3 days in the field, with abundant *Epsilonproteobacteria* and *Gammaproteobacteria* on artificial substrates.

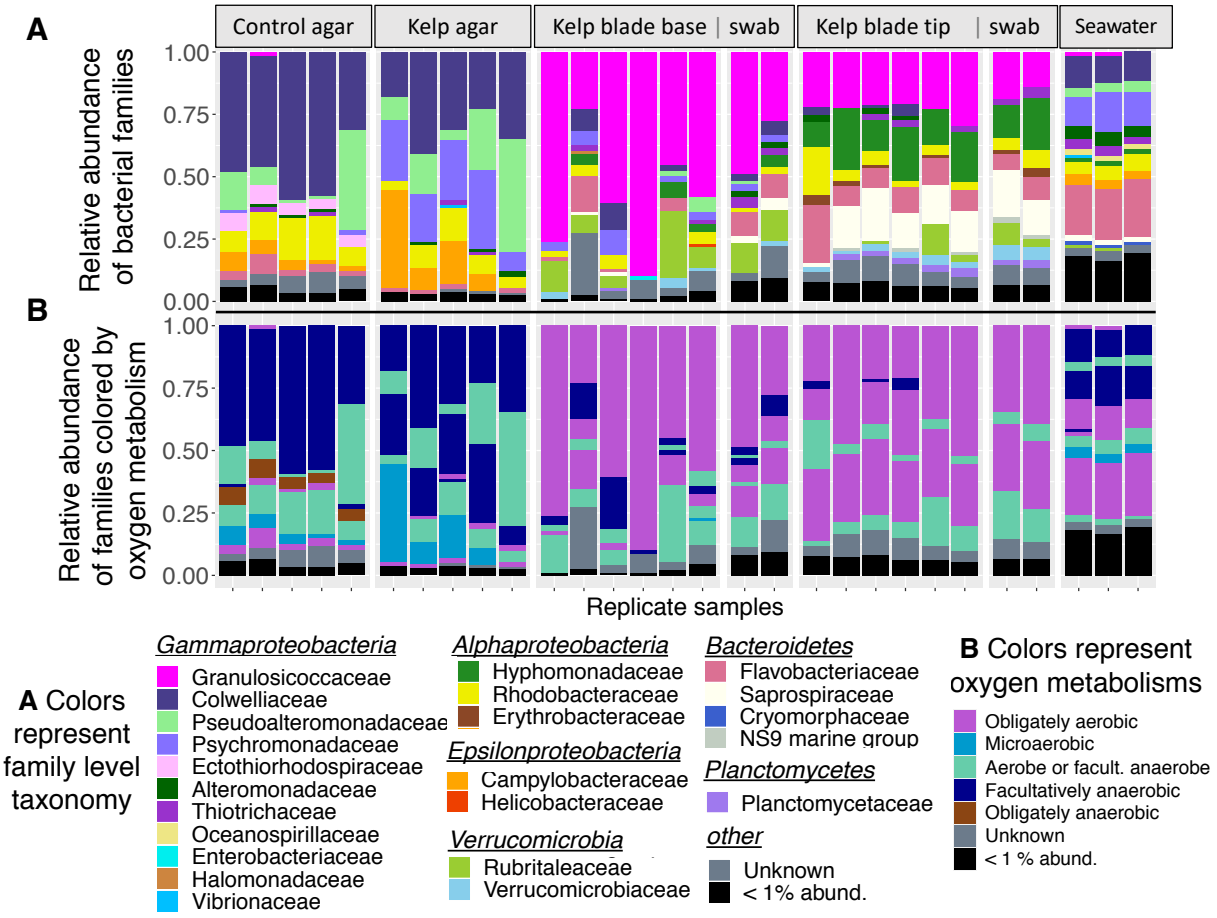

Figure 2.3. Barplots depicting A. the relative abundances of bacterial families across substrate types, and B. the relative abundances of bacterial families across substrate types, colored by the oxygen metabolism of each bacterial family. Each bar represents one microbial community sample. For *N. luetkeana* blade base and tip samples, two swabbed samples demonstrated compositional similarity between whole tissue and swabbed microbial communities. In the legend of A, families are grouped by phylum, or class for *Proteobacteria*, to add taxonomic information. For B, families are colored by oxygen metabolisms, as indicated in the legend.

The same families of *Gammaproteobacteria* reported here, including *Colwelliaceae* and *Pseudoalteromonadaceae*, were enriched in seawater amended with alginate and agarose in the Arctic Ocean (Jain *et al.*, 2020), suggesting that polysaccharides such as agarose may select for common microbial taxa in the seawater, even in different ocean basins.

While short-term artificial surfaces might not resemble the microbiome of a mature macroalgal host given the differences in biofilm age or succession, examining microbial settlement on artificial surfaces compared to new algal tissues can reveal how the macroalgal microbiome is structured differently than inert substrates exposed to the same field conditions and pool of potential colonizing microbes. Sampling the extremely rapid new blade growth of the annual kelp *N. luetkeana* (~2 to 4 days old) revealed that kelp blade biofilms recruited a distinct community from those that developed on agar substrates (3.7 days old) during the same time interval, even when agar substrates were infused with *N. luetkeana* blades (Table 2.1; Fig. 2.2A). We found that *Granulosicoccus sp.* made up an average of 59% (± 24%) of the microbiome of *N. luetkeana* blade base samples but were nearly absent from agar substrates (Fig. 2.3A, Appendix 2: Fig. S2.1), indicating selective recruitment of this taxon to new kelp tissues rather than nearby artificial kelp substrates. *Granulosicoccus sp*. reaches high densities on the tip of *N. luetkeana* blades, with up to $9x10^6$ cells/cm^2, but only sparse cells are visible on new tissue at the base of the blade (Ramirez-Puebla *et al.*, 2020). While we cannot differentiate between colonization of these taxa and performance differences post-settlement (cell growth, differential survival), the presence of *Granulosicoccus sp.* on new kelp blade tissues suggests possible colonization from the seawater or from older, mature portions of the *N. luetkeana* blade.

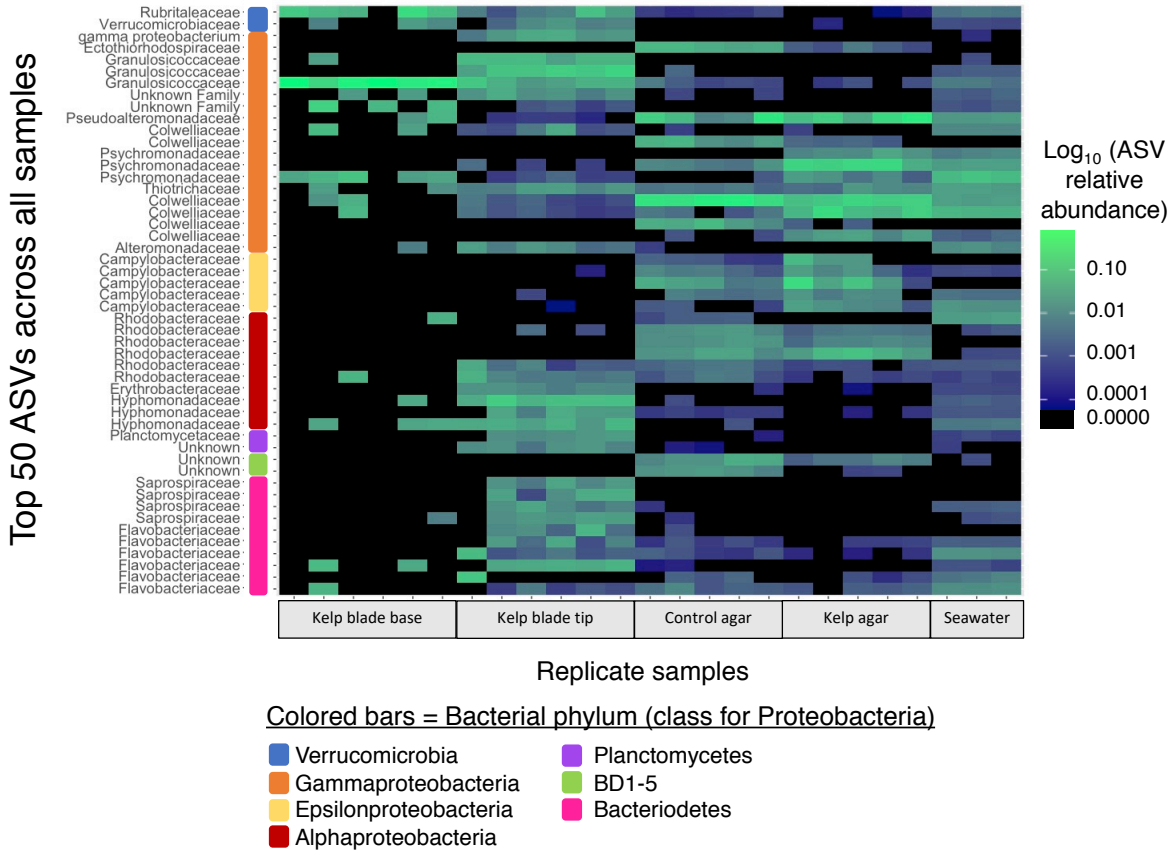

Figure 2.4. Heatmap showing the $\log_{10}$ transformed relative abundance of the 50 most common amplicon sequence variants (rows) across all samples (columns), grouped by sample type. ASVs are labelled by bacterial family on the y-axis, colored by phylum (legend at the bottom of the graph). Within the heatmap, each cell indicates the log-transformed relative abundance of ASVs, where lighter green indicates greater relative abundance, dark blue indicates extremely low abundance, and black indicates absence.

As demonstrated previously (Weigel and Pfister 2019, Ramirez-Puebla *et al.*, 2020), *N. luetkeana* blade base and tip microbial biofilms had significantly different microbial community structure (Table 2.1; Fig. 2.2A). Newer tissues from the base of the kelp blade had a lower number of bacterial sequences, lower overall diversity, and many of the abundant ASVs on the tips of the blade were absent from the base of the blade (Fig. 2.4). Further, the diversity of the most abundant bacterium on kelp blades, *Granulosicoccus sp.*, increased from new to mature kelp tissues; while one *Granulosicoccus* ASV was most abundant on new kelp tissues at the base

of the blade, 3 *Granulosicoccus* ASVs reached high abundances on mature blade tip tissues (Appendix 2: Fig. S2.1). We found similar microbiome composition when sequencing DNA from whole kelp blade tissue extracts and surface swabs (Fig. 2.2A, Fig. 2.3A), suggesting that surface swabs are a useful proxy for whole tissue extracts, while minimizing host chloroplast contamination. However, we caution that the surface swabs more closely resembled the microbial communities from whole tissue extracts of the kelp blade tip (Fig. 2.2A), while the kelp blade base swabs had much higher ASV richness than the kelp blade base whole tissue extracts (Fig. 2.2B). While our low replication of kelp surface swabs (n = 2 per base and tip) prohibits strong inference, we suspect that whole tissue extracts from the base of the blade more accurately the reflect low microbial abundance environment of new kelp tissues (Ramirez-Puebla *et al.*, 2020), while the swabs gathered a higher number of microbial taxa by covering a larger surface area. Finally, we note that this study has limitations including a low sample size (5-6 replicates per treatment) and geographic restriction to one field site, when we know that the *N. luetkeana* blade microbiome displays geographic variation across the Salish Sea in Washington (Weigel and Pfister 2019). A recent study found that plastic seagrass mimics deployed in a *Zostera marina* bed for 6 days developed different microbiomes than real seagrass blades, despite showing similar biogeographic trends to real seagrass microbial communities (Adamczyk et al., in review), suggesting that geographic factors may affect both host-associated and nonliving substrates.

Oxygen metabolisms shape microbial composition on kelp blades vs. agar substrates

We found that aerobic and facultatively anaerobic metabolisms were not distributed evenly across kelp blades; rather, living kelp blades recruited ASVs belonging to families with

primarily aerobic metabolisms, while ASVs that colonized agar substrates were predominantly facultative anaerobes (Fig. 2.3B, chi-squared = 57.10, df = 1, $P = < 0.001$). Grouping the 23 most abundant microbial families by metabolic oxygen requirements revealed that 67% of kelp blade-associated bacterial ASVs belonged to families with strictly aerobic metabolisms, 17% of ASVs were aerobic or facultatively anaerobic, 5% were facultatively anaerobic and only 0.002% were microaerobic or strictly anaerobic (Fig. 2.3B). In contrast, only 6% of ASVs associated with agar substrates belonged to strictly aerobic families, while 51% were facultative anaerobes, 27% were aerobic or facultatively anerobic, 9% were microaerobic, and 3% were strictly anaerobic (Fig. 2.3B). This trend is largely driven by the high relative abundance of *Granulosicoccus sp.* on kelp blades, which are known to be obligately aerobic (Baek *et al.*, 2014), and *Colwellia sp*. (family Colwelliaceae) on agar substrates, which are facultative anaerobes (Bowman, 2014). We note that these results are based on assignments of oxygen metabolisms to bacterial families (Rosenberg *et al.*, 2014), which may not always be consistent at the family level as some microbes are metabolically diverse, thus they should be taken as putative oxygen metabolisms until these findings are confirmed with physical measurements and culture-based assays.

Kelp forests produce oxygenated seawater through photosynthesis during the daytime (Pfister *et al.*, 2019), and kelp blades produce highly oxygenated microenvironments at the diffusive boundary surface layer (0.1 to 1 mm from the kelp blade) relative to the surrounding seawater (Irwin and Davenport, 2002; Noisette and Hurd, 2018). Further, there is evidence that motile bacterial cells are capable of chemotactic behavior to orient themselves towards optimum oxygen concentrations (Thar and Fenchel, 2001). Kelp forests also create strong diel cycles in oxygen concentrations (Pfister *et al.*, 2019), producing highly oxygenated conditions during the day but relatively oxygen-depleted conditions at night through respiration (Noisette and Hurd,

2018). We found that ~67% of microbial ASVs from highly oxygenated kelp blade surface biofilms were associated with strictly aerobic metabolisms, suggesting that photosynthetic production of O_2 may be an important factor structuring the composition of the macroalgal microbiome. In contrast to kelp blade-associated microbes, colonists of agar substrates had a much greater proportion of facultatively anaerobic (51%), microaerobic (9%), and obligately anaerobic (5%) metabolisms (Fig. 2.3B). The strictly anaerobic purple sulfur bacterium *Thiorhodospira sp*. (Bryantseva *et al.*, 1999) from the family *Ectothiorhodospiraceae* was abundant on agar substrates but absent was from kelp blade surfaces (Fig. 2.3B). In aquatic microbial biofilms, oxygen concentrations decay over time as oxygen is consumed through aerobic respiration, creating low-O_2 microoxic and anoxic zones within the biofilm (Rubol *et al.*, 2018). It is possible that agar substrates, without a photosynthetic host, developed oxygen-depleted or anoxic microsites that supported anaerobic microbial metabolisms. Finally, we note that the morphological disparity between real *N. luetkeana* blades and artificial kelp substrates, with the latter lacking the undulating movements that kelp blades experience in fluid environments (Koehl *et al.*, 2008), may have contributed further to the differences in microbial biofilm development and oxygen metabolisms.

Infusion of kelp tissues altered microbial community assembly on agar substrates

We found that infusing dried and crushed *N. luetkeana* blades into agar substrates significantly altered microbial biofilm communities (PERMANOVA pairwise comparison, P = 0.017; Table 2.1). This difference in community structure is visible on the NMDS plot, where each agar type formed a distinct cluster of samples (Fig. 2.2A). We also found that kelp agar substrates had significantly lower ASV richness than the control agar substrates (Fig. 2.2B),

providing evidence that some component of the *N. luetkeana* blade likely inhibits the settlement or growth of some bacterial taxa. While the kelp blade metabolite composition was not characterized here, dried *N. luetkeana* blades likely contributed additional carbohydrates, nutrients and cell wall components to the kelp agar treatment. Despite infusion of dried *N. luetkeana* tissues into the kelp agar treatment, microbial communities on the kelp agar did not become more similar to the kelp blade surface (Table 2.1). To test whether common kelp-associated microbes were more abundant on the kelp agar compared to the control agar, we used differential abundance testing with DESeq2 and detected 14 ASVs that were significantly enriched on kelp agar and 17 ASVs that were depleted on kelp agar compared to control agar substrates (Benjamini–Hochberg adjusted p-values < 0.01; Appendix 2: Fig. S2.2). However, none of the ASVs that were significantly enriched on the kelp agar, including *Psychromonas sp*., *Arcobacter sp.*, *Colwellia sp*., and *Alteromonas sp*. (Appendix 2: Fig. S2.2) were common on real kelp blades; rather, these taxa were more abundant in the seawater samples (Fig. 2.3A).

In addition to the oxygen environment and the chemical composition of the kelp surface, compounds actively exuded by macroalgae can attract or deter settlement or growth of certain microbes (see review in Goecke *et al.*, 2010). Kelps in particular release large quantities of dissolved organic carbon (DOC) into the surrounding seawater, and *N. luetkeana* blades release ~16% of the carbon that they fix as DOC (Weigel and Pfister, 2020). DOC exuded by primary producers can contribute to microbial growth in surface biofilms (Espeland *et al.*, 2001), and it likely provides an important carbon resource to heterotrophic microbes such as *Granulosicoccus sp*. that reside in the photosynthetic blade biofilm. In contrast to provisioning microbes with carbon, organic compounds such as fucoxanthin can deter bacterial colonization (Lachnit *et al.*, 2013). Surface-associated metabolites from the red algae *Agarophyton vermiculophyllum*

reduced the settlement of pathogens and recruited beneficial bacterial strains, while microbe-microbe interactions provided additional protection against invading pathogens (Saha and Weinberger, 2019), possibly through the production of antibiotics (Florez *et al.*, 2017). We found that common seawater microbes settled and became abundant on agar substrates, while at the same time, new tissues at the base of the kelp blade largely avoided colonization by the same seawater microbes (Fig. 2.4). Thus, it is possible that chemical defenses or physical cues by *N. luetkeana* or its associated microbiome limited colonization of these common seawater microbial taxa. Future experiments using artificial macroalgal substrates with different combinations of factors such surface metabolites, dissolved organic carbon or oxygen will continue to elucidate the factors affecting microbial biofilm formation on macroalgae.

Appendix 2.1 Supplemental Information for Chapter 2

Table S2.1. List of samples analyzed in this study. Sequence files associated with these samples are available at the NCBI Sequence Read Archive as well as at the European Bioinformatics Institute (accession # PRJEB29319). Total bacterial reads refer to the number of bacterial sequences in each sample after sequence data processing & removal of chloroplast reads.

Sample_name	16S Barcode	Description	Sample type	Total bacterial reads
12016.282	GTGTGTGCCATA	Control_Agar	Agar swab	36,476
12016.284	GGAGGCCATAAG	Control_Agar	Agar swab	50,581
12016.286	CTTACGAGTAGA	Control_Agar	Agar swab	49,342
12016.288	AGTACAACTGAA	Control_Agar	Agar swab	53,904
12016.290	ATTGAGTGAGTC	Control_Agar	Agar swab	69,308
12016.281	TGAGAGTCCCTC	Kelp_Agar	Agar swab	40,283
12016.283	TGCTGCTCAACG	Kelp_Agar	Agar swab	21,670
12016.285	GTTAGATCTATT	Kelp_Agar	Agar swab	59,130
12016.289	GTCCAAAGCGTT	Kelp_Agar	Agar swab	51,929
12016.291	TCGGTCCATAGC	Kelp_Agar	Agar swab	54,365
12016.271B	ATTAACTCCTAC	Nereocystis_base	Nereocystis tissue	213
12016.272B	TCTAAGAAAGAA	Nereocystis_base	Nereocystis tissue	254
12016.273B	TTGCAAGTACCG	Nereocystis_base	Nereocystis tissue	251
12016.274B	TGGGCCGGAATG	Nereocystis_base	Nereocystis tissue	321
12016.275B	CAGCGTTTAGCC	Nereocystis_base	Nereocystis tissue	591
12016.276B	TACATATCTACA	Nereocystis_base	Nereocystis tissue	288
12016.271BS	TTACTAGTTAAC	Nereocystis_base_swab	Nereocystis swab	39,187
12016.272BS	ACAGAACCGGCG	Nereocystis_base_swab	Nereocystis swab	31,831
12016.271A	CCTGGAATTAAG	Nereocystis_tip	Nereocystis tissue	3,635
12016.272A	TGTCCTATCAAT	Nereocystis_tip	Nereocystis tissue	44,927
12016.273A	GGCATGTTATCG	Nereocystis_tip	Nereocystis tissue	43,807
12016.274A	ATTATCGTCCCT	Nereocystis_tip	Nereocystis tissue	38,628
12016.275A	ATATATAGTATC	Nereocystis_tip	Nereocystis tissue	54,038
12016.276A	GCGCGAATGGTG	Nereocystis_tip	Nereocystis tissue	25,051
12016.271AS	TAGCTCACAGCA	Nereocystis_tip_swab	Nereocystis swab	44,523
12016.272AS	AGTTCATACGGC	Nereocystis_tip_swab	Nereocystis swab	60,646
12016.S80	GCTGTCGTCAAC	Seawater	Filtered seawater	39,372
12016.S81	GAATGGATGGGC	Seawater	Filtered seawater	55,311
12016.S82	GGTAGACCGGGT	Seawater	Filtered seawater	42,750

Table S2.2. To ensure that significant differences among treatments were not due to sequence depth, we verified that PERMANOVA pairwise comparisons of microbial community structure among substrate types were still significant with the dataset rarefied to the lowest bacterial read count (213) from the low microbial abundance blade base samples. Swabs of base and tip tissues were not included due to low replication (n = 2) per sample type.

PERMANOVA Pairwise Tests	**df**	**Sum Squares**	***F* statistic**	***p*-value**
Control agar vs. Kelp agar	1	0.72	6.56	0.024
Control agar vs. *N. luetkeana* blade base	1	2.08	17.5	0.014
Kelp agar vs. *N. luetkeana* blade base	1	2.00	16.8	0.016
Control agar vs. *N. luetkeana* blade tip	1	2.02	13.8	0.017
Kelp agar vs. *N. luetkeana* blade tip	1	2.03	13.8	0.014
Control agar vs. Seawater	1	1.20	9.39	0.050
Kelp agar vs. Seawater	1	0.87	6.71	0.050
N. luetkeana blade base vs. tip	1	1.57	10.4	0.014
N. luetkeana blade base vs. Seawater	1	1.25	9.09	0.024
N. luetkeana blade tip vs. Seawater	1	1.22	7.05	0.026

Figure S2.1. Barplots depicting the diversity and detection of different *Granulosicoccus* sp. amplicon sequence variants (ASVs) across all samples as A. the relative proportions of each unique *Granulosicoccus* sequence variant detected in every sample, and B. the absolute abundance of each unique *Granulosicoccus* ASV across samples. Each bar represents one microbial community sample, with substrate types listed in grey boxes at the top of the graph.

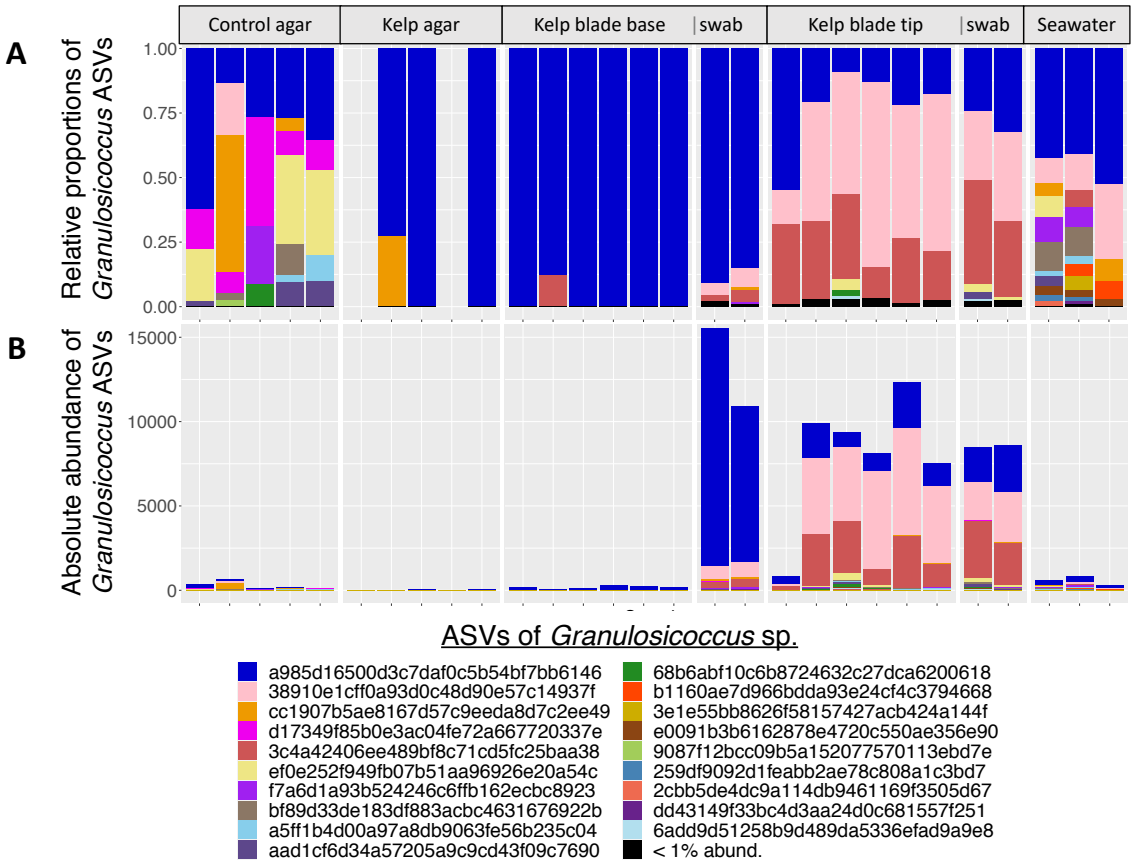

Figure S2.2. Differential abundance testing with DESeq2 revealed amplicon sequence variants (ASVs) that were significantly enriched (above the dashed line) or depleted (below the dashed line) on kelp agar compared to control agar substrates. Each dot indicates one ASV, grouped by lowest taxonomy (usually genus) on the x-axis and colored by bacterial family (or class for the uncultured *Epsilonproteobacteria*).

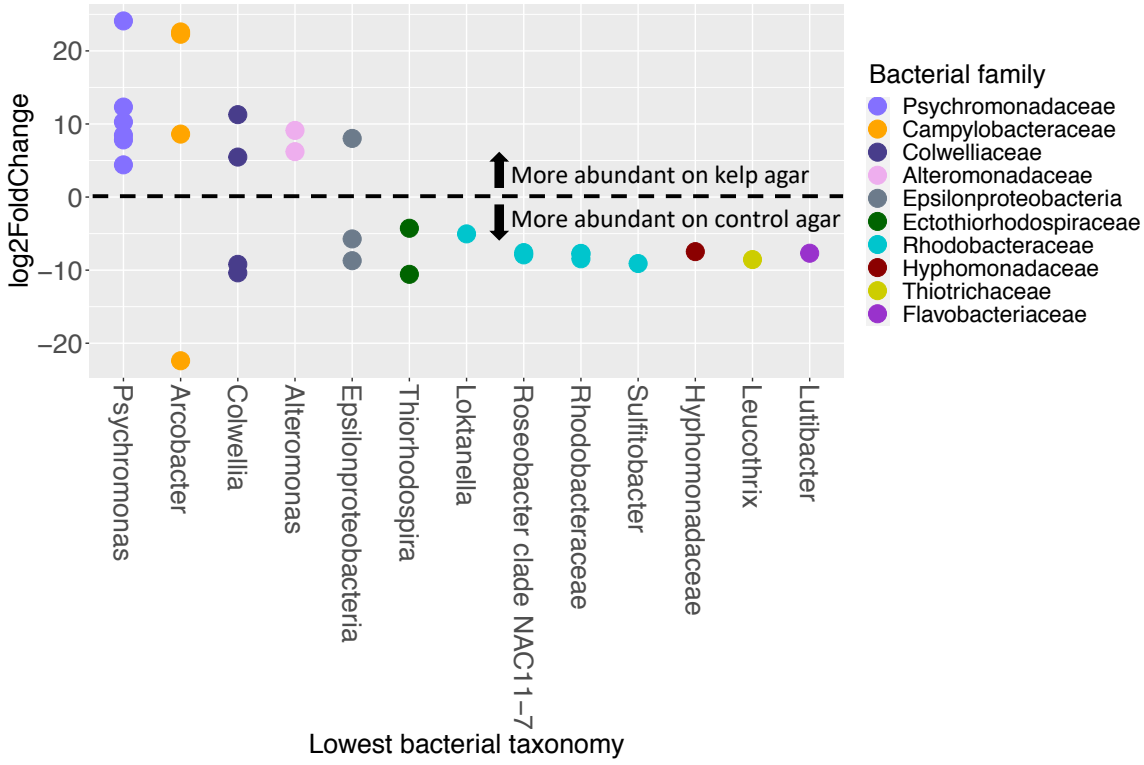

CHAPTER 3: THE DYNAMICS AND STOICHIOMETRY OF DISSOLVED ORGANIC CARBON RELEASE BY KELP

Citation: Weigel, B. L., and C. A. Pfister. 2021. The dynamics and stoichiometry of dissolved organic carbon release by kelp. Ecology 102(2): e03221. doi:10.1002/ecy.3221

Abstract

Canopy-forming kelps are foundational species in coastal ecosystems, fixing tremendous amounts of carbon, yet we know little about the ecological and physiological determinants of dissolved organic carbon (DOC) release by kelps. We examined DOC release by the bull kelp, *Nereocystis luetkeana*, in relation to carbon fixation, nutrient uptake, tissue nitrogen content, and light availability. DOC release was approximately 3.5 times greater during the day than at night. During the day, *N. luetkeana* blades released an average of 16.2% of fixed carbon as DOC. Carbon fixation increased with light availability but DOC release did not, leading to a lower proportion of fixed carbon released as DOC at high light levels. We found no relationship between carbon fixation and DOC release rates measured concurrently. Rather, DOC release by *N. luetkeana* blades declined with marginal significance as blade tissue nitrogen content increased and with experimental nitrate addition, supporting the role of stoichiometric relationships in DOC release. Using a stable isotope (^{13}C) tracer method, we demonstrated that inorganic carbon is rapidly fixed and released by *N. luetkeana* blades as ^{13}DOC, within hours. However, recently fixed carbon (^{13}DOC) comprised less than 20% of the total DOC released, indicating that isotope studies that rely on tracer production alone may underestimate total DOC release, as it is decoupled from recent kelp productivity. Comparing carbon and nitrogen assimilation dynamics of the annual kelp *N. luetkeana* with the perennial kelp *Macrocystis pyrifera* revealed that *N. luetkeana* had significantly higher carbon fixation, DOC production and nitrogen uptake rates per unit dry mass. Both kelp species were able to perform light-

independent carbon fixation at night. Carbon fixation by the annual kelp *N. luetkeana* is as high as 2.35 kg C m^2 yr^{-1}, but an average of 16% of this carbon (376 g C m^{-2} yr^{-1}) is released as DOC. As kelp forests are increasingly viewed as vehicles for carbon sequestration, it is important to consider the fate of this substantial quantity of DOC released by canopy-forming kelps.

Introduction

While it has been more than 60 years since the discovery that algae release some proportion of their photosynthetic products as dissolved organic compounds (Tolbert and Zill 1956, Fogg 1963, Fogg et al. 1965), we still know little about the ecological importance of dissolved organic carbon (DOC) release by macroalgae. In freshwater and marine systems, both macroalgae and phytoplankton release photosynthates as DOC (Baines and Pace 1991), but the largest organisms known to produce DOC are the giant canopy-forming kelps that comprise kelp forests (Reed et al. 2015). Canopy-forming kelps are extraordinarily productive, fixing teragram quantities of carbon each year in the North Pacific alone (Wilmers et al. 2012). Kelp also release substantial quantities of DOC, elevating seawater DOC concentrations by almost 50% inside kelp forests (Pfister et al. 2019). The production of DOC by aquatic phototrophs alters surface seawater carbon dynamics on a global scale (Aluwihare et al. 1997), driving nearshore microbial processes (Carlson and Ducklow 1996). Kelp forests are undergoing declines in many locations globally (Krumhansl et al. 2016). Carbon assimilation by temperate kelp forests will likely decline with future warming (Pessarrodona et al. 2018), although the combined impact of ocean acidification and warming on kelp forest productivity is unclear. Despite the growing need to quantify carbon fluxes in the ocean, we lack important baseline data on the carbon dynamics of several ecologically important kelp species.

The relationship between carbon fixation and DOC release is particularly important to understand for kelps, as recent efforts to mitigate our global CO2 surplus have focused on using kelp as a potential "blue carbon" sink (Hill et al. 2015, Krause-Jensen and Duarte 2016). The export of DOC is hypothesized to be the main pathway for carbon sequestration by macroalgae (Krause-Jensen and Duarte 2016), yet many blue carbon sequestration calculations do not consider the release of fixed carbon as DOC (Hill et al. 2015). Studies that have quantified carbon release by kelps demonstrate that, on average, 14–43% of fixed carbon is released as DOC (Sieburth 1969, Hatcher et al. 1977, Abdullah and Fredriksen 2004, Wada et al. 2007, Reed et al. 2015). For instance, the annual net productivity of the canopy-forming kelp Macrocystis is as high as 1.3 kg of carbon per m^2 of benthos per year (Wheeler and Druehl 1986), potentially releasing between 180–560 g C per m^2 as DOC. To better predict the magnitude of DOC release by kelp forests and evaluate their contribution to nearshore carbon cycling, we must first determine the factors that control DOC release by kelps.

While DOC release may be tightly coupled to nutrient availability or kelp productivity, little is known about the physiological mechanisms controlling DOC release by kelps. The release of DOC may be attributed to the passive leakage of low molecular weight compounds that occurs during cell growth and lysis (Bjørnsen 1988, Nagata 2000), or to active exudation of photosynthates (Moran and Estrada 2002). Studies with freshwater and marine phytoplankton support the photosynthate diffusion hypothesis (Fig. 3.1a), where DOC release was proportional to the amount of carbon fixed (Fogg et al. 1965, Berman 1976, Zlotnik and Dubinsky 1989, Maranon et al. 2004). The stoichiometric overflow hypothesis (Fogg 1983) posits that DOC release results from an excess of fixed carbon relative to the availability of other essential nutrients, such as nitrogen (Nagata 2000; Fig. 3.1b). Thus, DOC release should increase with

decreasing nutrient availability. Studies with phytoplankton also support this hypothesis; DOC release is higher when nutrients are depleted (Nagata 2000, Myklestad 1995) and lower in nutrient-rich regions, including upwelling zones (Thornton 2014). While support for both of these hypotheses has been demonstrated using phytoplankton, it is uncertain whether either hypothesis applies to large, more structurally complex macroalgae.

Here, we investigated the mechanisms of DOC release in one of the largest macroalgae, the canopy-forming bull kelp, *Nereocystis luetkeana*, by quantifying carbon fixation, DOC release and nutrient uptake using chamber incubations of *N. luetkeana* blades. Further, we used a ^{13}C stable isotope tracer method to determine the proportion of total exuded DOC that comes from recently fixed carbon. We tested aspects of the passive cell leakage hypothesis (Bjørnsen 1988) by comparing carbon fixation and DOC release by *N. luetkeana* blades during the day and at night, by testing the relationship between carbon fixation and DOC release over a large range of natural variation in kelp productivity, and by quantifying the proportion of released DOC attributable to recently fixed carbon (Fig. 3.1a). We tested the stoichiometric overflow hypothesis (Fogg 1983) by examining the relationships between DOC production and both tissue nitrogen content and dissolved inorganic nitrogen uptake, and by directly manipulating inorganic nitrogen availability to *N. luetkeana* from nitrogen-poor Southern Puget Sound (Fig. 3.1b). Finally, we compared daytime and nighttime carbon fixation, DOC production and nutrient uptake rates by *N. luetkeana* with those of the giant kelp, *Macrocystis pyrifera*, from a mixed kelp forest.

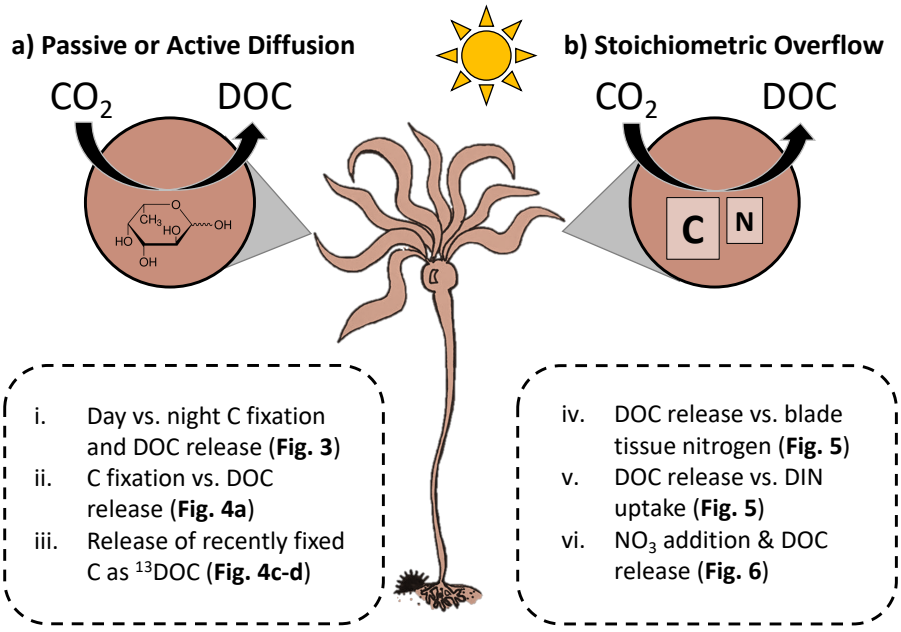

Figure 3.1. Conceptual diagram depicting two mechanisms of dissolved organic carbon (DOC) release by kelps: (a) passive or active diffusion of intracellular photosynthates. This process may be dependent on the concentration of intracellular photosynthates, and thus on the rate of carbon fixation, or it may be the result of carbohydrate leakage that occurs during cell lysis. (b) Stoichiometric overflow, where DOC release results from an excess of fixed carbon relative to the availability of other essential nutrients, such as nitrogen, thus DOC release should increase when nitrogen is less available. Note that the two mechanisms are not mutually exclusive. Below each panel is a figure roadmap that outlines specific tests for each mechanism, indicated by sections i–vi.

Methods

Kelp blade collection and chamber incubation experiments

We simultaneously quantified carbon fixation, DOC production and nutrient uptake using short-term (3–8 h) chamber incubations with kelp blades. In total, seven experiments were conducted between 2016 and 2019, including a total of n = 51 replicate *N. luetkeana* blades, during peak biomass for the annual kelp from June to September (Table 3.1). Biological replicates for each experiment consisted of kelp blades collected from distinct individuals incubated in separate chambers (Table 3.1). Kelp blades were collected from Tatoosh Island,

Washington, USA (48.39° N, 124.74° W) at the north-facing Main Beach, where abundant *N. luetkeana* forests persist annually (Pfister et al. 2019), or the southwest-facing Strawberry Draw, where there is a mixed canopy of *N. luetkeana* and *M. pyrifera*. At both sites, the substrate is rocky, water depth ranges from 3 to 12 m, and wave heights average 1–3 m during the summer (see NOAA National Data Buoy Center Station 46087). Experiments were conducted using detached blades of *N. luetkeana* (with the exception of one experiment using *M. pyrifera*). *N. luetkeana* blades were detached by clipping the small tissue junction where the base of the blade connects to the float, and *M. pyrifera* blades were collected by separating the blade at the junction between the pneumatocyst and stipe. Blades of *M. pyrifera* were collected near the surface of the canopy by snorkeling, while blades of *N. luetkeana* were collected by snorkeling or by sampling from the intertidal on low spring tides. Kelp blades were collected haphazardly from adult sporophyte populations, but blades with abundant reproductive sori patches or severe fragmentation were avoided. For daytime experiments conducted in September 2018 and June 2019, *N. luetkeana* blades were collected across a range of light levels at the Main Beach site. *N. luetkeana* blades used in chamber experiments averaged 4.13 ± 0.27 g dry mass and 142 ± 8.50 cm in length; *M. pyrifera* blades averaged 5.28 ± 0.22 g dry mass and 49.2 ± 4.10 cm in length (mean SE).

To test for DOC leakage as a result of blade agitation and separation from the thallus, we compared DOC release rates of blades and whole *N. luetkeana* individuals gently removed from the substrate at the holdfast. Whole thallus experiments were conducted for 3 h in August, both during the day (n = 4) and at night (n = 4), by incubating the individual kelp in 5-gallon buckets (1 gallon = 3.79 L) filled with seawater and buried partially into wet sand to remain cool. Whole individual measurements were compared to those from *N. luetkeana* blade chamber experiments

conducted on consecutive days during the day (n = 8) and at night (n = 8) in July and August (Table 3.1). Whole kelp had similar sized blades to the detached blades used for comparison; the average maximum length of blades attached to whole *N. luetkeana* individuals was 175 6.37 cm, while the average length of the detached blades used for comparison was 147 8.35 cm.

All other experiments were conducted using single detached kelp blades placed into clear polycarbonate tube chambers (2.6 L). Chambers were designed to be watertight, yet readily opened for sampling, by capping each end of the chamber with a wing nut expansion plug containing a rubber seal (Fig. 3.2a). Chambers were filled with fresh local seawater, collected during the incoming tide. Kelp blades were added individually to each chamber (usually n = 4 chambers per treatment; Table 3.1), while control chambers (n = 1–3) were filled entirely with seawater to quantify nutrient uptake and DOC production by water column phytoplankton. Chambers were suspended horizontally in a recreational float that was partially deflated to ensure that they remained immersed, thereby keeping the chambers close to ambient seawater temperature and permitting wave motion. Seawater inside the chambers was sampled periodically at 0, 1, 3, or 8 h for inorganic nutrients, while DOC concentrations were measured at the start and end of each incubation (see Appendix 3.1: Sections S3, S4). At each time point, the dissolved oxygen, temperature and pH of seawater inside the chambers was also measured with a hand-held probe (Hach HQ40D, Loveland, Colorado, USA). Light measured as PAR (photosynthetically active radiation) was quantified at 1-h intervals in proximity to the chambers with a LICOR LI-1000 equipped with a LI-190 quantum sensor (LICOR, Lincoln Nebraska, USA). Daytime experiments always began between 09:00 and 10:30 and lasted for 3 or 8 h, while nighttime experiments, conducted the following day using new kelp blades, were initiated after sunset (~21:00) and lasted for 3 or 8 h. The experiment with *M. pyrifera* was run

concurrently with *N. luetkeana*, during the day and at night, to allow a direct comparison of the two kelp species under the same conditions. Additional daytime experiments were conducted without corresponding nighttime experiments (Table 3.1). For all chamber experiments, carbon fixation, nutrient uptake and DOC production were quantified using the methods outlined below.

Table 3.1. Summary of carbon fixation and DOC release rates (mean with SE in parentheses), including the percentage of fixed carbon released as DOC, across all experiments. The percentage of carbon released as dissolved organic carbon (DOC) is expressed relative to the corresponding daytime carbon fixation rate. Replication refers to the number of biological replicates per experiment or treatment.

Experiment	Site	Date	Hrs	Treatment	Replication	Carbon fixation (µmol C/g*hr)	DOC release (µmol C/g*hr)	% fixed C released as DOC
1) *Nereocystis* whole plant	Tatoosh	Aug 2016	3	Day	n = 4	not measured	10.19 (0.88)	not measured
1) *Nereocystis* whole plant	Tatoosh	Aug 2016	3	Night	n = 4	not measured	1.77 (0.78)	not measured
2) *Nereocystis* blade	Tatoosh	July 2017	8	Day	n = 4	47.74 (4.19)	8.34 (1.29)	17.69 (2.58)
2) *Nereocystis* blade	Tatoosh	July 2017	8	Night	n = 4	not measured	0.74 (1.31)	not measured
3) *Nereocystis* blade	Tatoosh	Aug 2018	3	Day	n = 4	60.15 (4.45)	14.32 (0.72)	24.16 (1.95)
3) *Nereocystis* blade	Tatoosh	Aug 2018	3	Night	n = 4	3.75 (0.42)	6.55 (1.16)	10.89 (1.93)
3) *Macrocystis* blade	Tatoosh	Aug 2018	3	Day	n = 4	48.36 (1.42)	8.42 (2.15)	17.27 (3.94)
3) *Macrocystis* blade	Tatoosh	Aug 2018	3	Night	n = 4	0.83 (0.00)	1.79 (0.68)	3.71 (1.40)
4) *Nereocystis* blade	Tatoosh	Sept 2018	8	Day	n = 8	61.89 (3.77)	13.85 (1.78)	23.09 (3.49)
5) *Nereocystis* blade	Tatoosh	June 2019	8	Day	n = 8	120.78 (10.01)	9.47 (1.01)	8.22 (1.06)
6) *Nereocystis* blade	Tatoosh	July 2018	8	Day	n = 3	75.49 (10.75)	4.79 (0.94)	6.74 (1.81)
7) *Nereocystis* NO_3 addition	Squaxin	June 2018	8	Low NO3	n = 4	55.58 (6.64)	3.90 (3.03)	6.33 (5.58)
7) *Nereocystis* NO_3 addition	Squaxin	June 2018	8	High NO3	n = 4	50.58 (0.71)	0.76 (2.76)	1.68 (5.48)

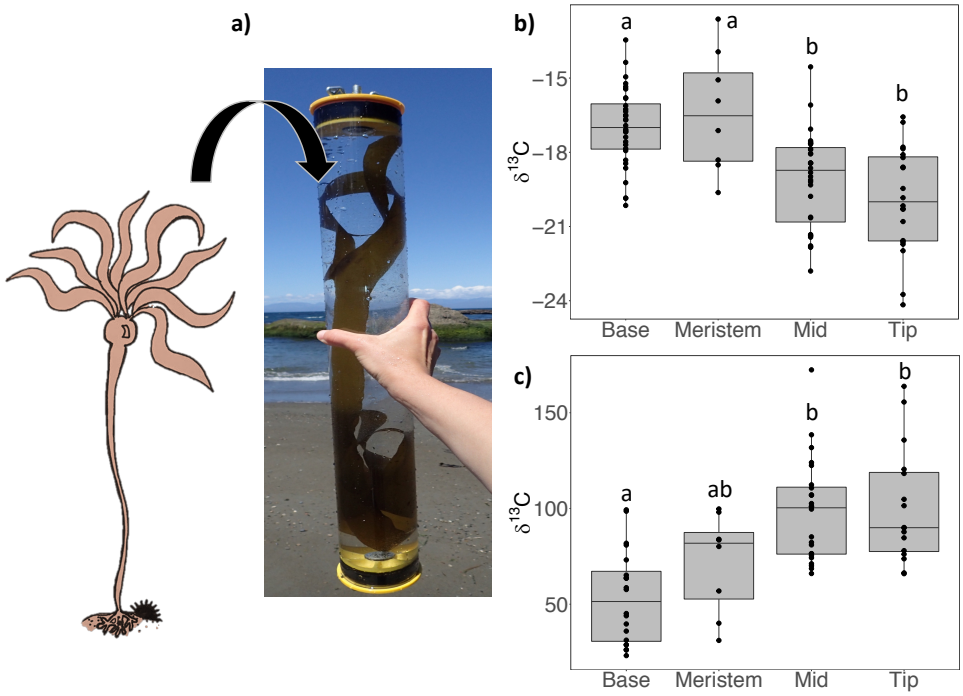

Figure 3.2. (a) Chamber design for measuring DOC production and nutrient fluxes by kelp blades (*Nereocystis luetkeana* depicted). Replicate chambers were then incubated horizontally at the seawater surface in a floating raft. (b) Pre-enrichment isotopic signatures ($\delta^{13}C$) of *N. luetkeana* blade tissues sampled from the base, meristem, mid-blade and tip, and (c) post-enrichment $\delta^{13}C$ of *N. luetkeana* blade tissues, indicating differences in carbon fixation rates along the length of the blade. For box plots, the median and interquartile range (the 25th and 75th percentiles) are indicated in gray, and the whiskers indicate the maximum and minimum values that are within 1.5 times the interquartile range. Letters indicate statistically significant ($P < 0.05$) differences after ANOVA and Tukey HSD pairwise comparisons.

^{13}C tracer method for carbon fixation and ^{13}DOC release

Carbon fixation was quantified using the ^{13}C assimilation method, where the amount of inorganic carbon fixed through photosynthesis is measured using a ^{13}C stable isotope tracer (Miller and Dunton 2007). The methods in this section correspond to Fig. 3.1a (sections i–iii). Upon collection, adjacent blades from the same individual (dichotomous blade pairs for *N. luetkeana*) were taken so that one blade could be destructively sampled for initial (natural abundance $\delta^{13}C$) stable isotope measurements, while the other was immediately prepared for the

chamber incubation experiment. To each chamber, 286 µL of enriched ^{13}C -sodium bicarbonate (1.0 mol/L of 99% $NaH^{13}C$ O3, Cambridge Isotope Lab CLM-441-PK) was added to achieve a dissolved inorganic carbon enrichment level of approximately 4,718 per mil (or 6.04 at%), assuming a dissolved inorganic carbon concentration of 2.11 mmol/L (Wootton and Pfister 2012). Kelp blades were exposed to this enriched inorganic carbon source for 3 or 8 h using the chamber method described above. At the end of each experiment, kelp blades were sampled for $\delta^{13}C$ to determine final tissue enrichment. For both initial and final sampling, *N. luetkeana* blades were sampled at multiple positions: at the base, where the blade attaches to the float, at the meristem ~ 10 cm from the base of the blade, in the middle of the blade, and near the tip (Fig. 3.2b and c). Blades of *M. pyrifera* were sampled at the base, where the blade attaches to the float, and at the mid-blade (halfway from the base to the tip). To standardize across experiments and avoid underestimation of carbon fixation (Fig. 3.2c), $\delta^{13}C$ values from the middle of the blade were used. Dried kelp blade tissues were pulverized with a GenoGrinder, Spex (Metuchen, NJ), weighed, and analyzed on an elemental-analyzer–isotope-ratio mass spectrometer at the University of Chicago or at Northwestern University. The equation used to calculate carbon fixation via ^{13}C-bicarbonate assimilation can be found in Appendix 3.1: Section S1. We note that this represents gross carbon fixation, or carbon that is fixed and retained in the kelp blade, as it does not account for carbon respired or lost as DOC. Recently assimilated ^{13}C is not available for respiration by macroalgae (Søndergaard 1988, Miller and Dunton 2007).

From three experiments where carbon fixation was quantified through ^{13}C assimilation, we also measured ^{13}DOC release (Table 3.2), allowing us to quantify the release of recently assimilated carbon as isotopically enriched ^{13}DOC (Fig. 3.1a, section iii). Seawater samples were collected at the beginning of each experiment and after 3 or 8 h of kelp blades incubating in

enriched ^{13}C-sodium bicarbonate. Seawater samples were filtered with a 0.7-lm filter (Whatman GF/F), frozen, and shipped to the Jan Veizer Stable Isotope Laboratory at the University of Ottawa (Ottawa, Ontario, Canada) for analysis of DOC concentrations and δ^{13}C of DOC. Briefly, samples were acidified to remove all inorganic carbon, and remaining organic carbon was combusted and analyzed as CO2 gas following methods in Lalonde et al. (2014). Analysis was performed using an OI Analytical Aurora TOC Analyzer (Model 1030W, with a model 1088 autosampler; College Station, TX, USA) with a combustion unit interfaced to a Finnigan Mat DeltaPlusXP isotope ratio mass spectrometer Thermo Electron, Bremen, Germany; interface designed by P. Middlestead). Data were normalized using two different internal organic standards. The equation used to calculate ^{13}DOC release is listed in Appendix 3.1: Section S2.

Table 3.2. Summary of total DOC release and ^{13}DOC release (mean and SE) by kelp blades, including the percentage of DOC that was recently fixed and released, across all experiments. Replication refers to the number of biological replicates per experiment or treatment. For the NO_3^- addition experiment, the same replicate chambers were sampled at 3 and 8 h, as indicated by the length (h) column; n = 2 chambers from each treatment were conducted on both a sunny and cloudy day. DOC consumption indicates that the net DOC flux was negative.

Experiment	Site	Date	Treatment	Replication	Hrs	DOC release (µmol C/g*hr)	^{13}DOC release (µmol C/g*hr)	% recently fixed (labeled) DOC
1) *Nereocystis* blade	Tatoosh	July 2017	Day	n = 4	8	8.34 (1.29)	1.60 (0.42)	20.39 (5.96)
2) *Nereocystis* blade	Tatoosh	July 2018	Day	n = 3	8	4.79 (0.94)	0.35 (0.07)	8.71 (3.87)
3) *Nereocystis* NO_3 addition	Squaxin	June 2018	Low NO3, high light	n = 2	3	18.42 (2.31)	2.17 (0.56)	11.58 (1.58)
3) *Nereocystis* NO_3 addition	Squaxin	June 2018	Low NO3, low light	n = 2	3	1.81 (0.78)	1.22 (0.70)	62.02 (12.15)
3) *Nereocystis* NO_3 addition	Squaxin	June 2018	High NO3, high light	n = 2	3	11.98 (1.06)	1.11 (0.05)	9.30 (0.43)
3) *Nereocystis* NO_3 addition	Squaxin	June 2018	High NO3, low light	n = 2	3	-1.47 (2.79)	1.44 (0.80)	DOC consumption
3) *Nereocystis* NO_3 addition	Squaxin	June 2018	Low NO3, high light	n = 2	8	8.82 (2.52)	1.95 (0.22)	23.31 (4.23)
3) *Nereocystis* NO_3 addition	Squaxin	June 2018	Low NO3, low light	n = 2	8	-1.03 (0.05)	0.57 (0.25)	DOC consumption
3) *Nereocystis* NO_3 addition	Squaxin	June 2018	High NO3, high light	n = 2	8	5.47 (0.10)	1.13 (0.18)	20.59 (2.82)
3) *Nereocystis* NO_3 addition	Squaxin	June 2018	High NO3, low light	n = 2	8	-3.95 (1.12)	0.63 (0.36)	DOC consumption

Nutrient uptake and unlabeled DOC production

During the same short-term (3–8 h) chamber incubation experiments described above, we also quantified nutrient uptake and unlabeled, total DOC production, based on changes in DOC concentration alone rather than ^{13}DOC. The methods in this section correspond to DOC release from Fig. 3.1a (sections i–ii) and Fig. 3.1b (sections iv–vi), and nutrient uptake from Fig. 3.1b (sections v– vi). Seawater inside the chambers was sampled periodically at 0, 1, 3, or 8 h and filtered with a 0.7-lm filter (Whatman GF/F). DOC concentrations were determined at the University of Washington Marine Chemistry Lab from seawater filtered into 40-mL glass, carbon-free vials and frozen at 20°C until analysis. Seawater inorganic nutrient concentrations of NO_3^-, NO_2^-, NH_4^+, PO4, and $Si(OH)_4$ were measured in the same lab using standard methods (Intergovernmental Oceanography Commission 1994). Total dissolved inorganic nitrogen (DIN) represents summed concentrations of NO_3^-, NO_2^-, and NH_4^+. Nutrient uptake followed an exponential decay function (Fig. S3.1a), thus nutrient uptake rates were calculated from the slope of log-transformed nutrient concentrations (Fig. S3.1b). DOC production was calculated from the difference between DOC concentrations measured at the beginning and end of chamber incubations. Nutrient and DOC fluxes from seawater control chambers were subtracted in both calculations to account for phytoplankton activity. Detailed equations used to calculate DOC release and nutrient uptake by kelp blades are listed in Appendix 3.1: Sections S3 and S4. Data with all values for replicate measurements of carbon fixation, DOC release, ^{13}DOC release, and nutrient uptake rates by *Nereocystis luetkeana* and *Macrocystis pyrifera* kelp blades are available in the Dryad Digital Repository: https://doi.org/10.5061/ dryad.djh9w0vxp.

Scaling up to seasonal productivity per area of kelp forest

To scale up kelp blade carbon fixation rates to units of kg Cm^2yr^1, we multiplied the mean carbon fixation rate for all daytime experiments conducted on Tatoosh Island by areal biomass measurements of *N. luetkeana* surveyed at the same location. We converted hourly to seasonal rates by multiplying by the number of daylight hours in the annual growing season (April–September). We converted gross carbon fixation measurements to net primary production by accounting for estimated carbon lost as respiration. Finally, we quantified the range in seasonal productivity by using the minimum and maximum values for all parameters (blade mass, number of blades, kelp density, and carbon fixation rate); see Appendix 3.1: Section S5 for further details.

Nitrate addition experiment

To determine the effect of nitrogen availability on DOC exudation, a short-term (sampled after 3 and 8 h) nitrate addition experiment was conducted in June 2018 with *N. luetkeana* blades from Squaxin Island, in Southern Puget Sound (47.18° N, 122.91° W). This site was chosen for the DIN addition experiment, as seawater nitrate concentrations at Squaxin remain low (<10 µmol/L) during the summer months that coincide with the annual sporophyte growth of *N. luetkeana*. This experiment was not conducted at Tatoosh Island on the outer coast, as nitrate availability is generally high during the summer (~15–20 µmol/L) due to upwelling (Pfister et al. 2007, Wootton and Pfister 2012). Sodium nitrate ($Na\ NO_3$) was added to the experimental chambers (n = 4) containing *N. luetkeana* blades at a concentration of 30 µmol/L, increasing the nitrate concentration to 35.9 0.8 µmol/L, while control chambers (n = 4) remained at low, ambient nitrate concentrations (6.8 0.2 µmol/L). The experiment was conducted with replicates split over two days (see Table 3.2); however, one of the days was sunny while the other was

cloudy (mean PAR = 1438 and 875 µmol m-2 s-1, respectively). To account for PAR differences between days, this experiment was analyzed using both treatment (NO_3^- addition) and day (sunny vs. cloudy) as factors. This methods section pertains to Fig. 3.1b (section vi).

Statistical analysis

One-way and two-way analyses of variance (ANOVA) were used to examine the effects of treatment (low vs. high NO_3^-), time of day (day vs. night), or species (*M. pyrifera* vs. *N. luetkeana*) on rates of carbon fixation, DOC production, and nutrient uptake. For significant ANOVA outcomes, Tukey HSD pairwise tests were conducted with a post-correction experiment-wide error rate of 0.05. To test for broad trends in DOC release, we pooled data from all daytime DOC release measurements with *N. luetkeana* blades (n = 35), all ^{13}DOC production measurements (n = 23 and n = 15 with corresponding carbon fixation measurements), or all *N. luetkeana* measurements conducted on Tatoosh Island (n = 27). With pooled data, we used linear mixed-effects models (R package nlme) with the factors of carbon fixation, DOC production, ^{13}DOC production, tissue N content, DIN uptake rate, or PAR light levels as fixed effects, while experiment was treated as a random factor in all models (see Table S3.1 for a summary of all linear mixed-effects models). All statistical tests were performed in R studio (R version 3.4.4).

Results

Carbon δ^{13}C enrichment changes with position along kelp blades

Pre-enrichment isotopic signatures of natural *N. luetkeana* blade tissues demonstrated that δ^{13}C differed along the length of the blade (ANOVA, df = 3, error df = 88, F = 14.4, P<0.001). Blade base and meristem tissues were significantly more enriched in ^{13}C than middle

and tip tissues (Tukey HSD pairwise tests, P<0.01; Fig. 3.2b). Mean $\delta^{13}C$ values decreased from 17.0± 0.28 (mean ± SE) and 16.39 ± 0.86 in base and meristem samples to 19.12 ± 0.34 and 19.91 ± 0.48 in middle and tip samples, respectively. C:N ratios and $\delta^{15}N$ of natural tissues did not differ with blade position (ANOVA, df = 3, error df = 88, F = 2.32 for C:N, F = 2.04 for d15N, P > 0.05). The mean C:N ratio for *N. luetkeana* blade tissues was 10.90 (± 0.25), and the mean $\delta^{15}N$ was 7.13 (± 0.21).

Carbon fixation quantified using the ^{13}C-bicarbonate assimilation method revealed that more distal *N. luetkeana* blade tissues had higher ^{13}C enrichment (ANOVA, df = 3, error df = 64, F = 13.42, P < 0.001; Fig. 3.2c). Carbon fixation was significantly higher at the middle and tip of the blade than at the base (Tukey HSD pairwise tests, P < 0.001; Fig. 3.2c), while the meristem did not differ from the base (P = 0.38) and was marginally different from the middle and tip (P = 0.08 and P = 0.06, respectively Mean $\delta^{13}C$ values of enriched *N. luetkeana* blades increased from 53.6 (± 5.4) and 71.7 (± 9.2) in base and meristem tissues to 98.2 (± 5.4) and 100.8 (± 7.6) in middle and tip tissues. For *M. pyrifera*, sampled in only two positions, the mid-blade fixed more carbon than the base (ANOVA, df = 1, error df = 6, F = 132.2, P < 0.001). After ^{13}C assimilation, *M. pyrifera* base and mid-blade tissues had mean $\delta^{13}C$ values of 14.71 ± 2.13 and 55.18 ± 2.80, respectively. We found no statistical evidence that carbon assimilation at night differed with blade position in either kelp species (ANOVA, df = 2, error df = 9, F = 0.314, P = 0.74 for *N. luetkeana*; ANOVA, df = 2, error df = 9, F = 0.341, P = 0.72 for *M. pyrifera*).

Diurnal differences in carbon fixation and DOC production

As expected, carbon fixation by *N. luetkeana* blades was significantly higher during the day than at night (ANOVA, df = 1, error df = 10, F = 88.55, P < 0.001; Fig. 3.3a). Blades and

whole individuals of *N. luetkeana* released dissolved organic carbon (DOC) at a rate approximately 3.5 times greater during the day than at night (Fig. 3.3b). DOC release did not differ between detached blades and whole *N. luetkeana* individuals, and significantly more DOC was released during the day than at night by blades and whole kelp (two-way ANOVA, df = 1, error df = 21, $F = 36.17$, $P < 0.001$ for day vs. night, df = 1, error df = 21, $F = 1.16$, $P = 0.29$ for blades vs. whole kelp). Single blades were thus a useful proxy for estimating DOC release (Fig. 3.3b).

Daytime carbon fixation rates by *N. luetkeana* blades from all experiments conducted on Tatoosh Island ($n = 27$ replicate daytime blade incubations) averaged 78.50 (± 6.45) µmol C g^{-1} h^{-1}, while daytime DOC release averaged 10.80 (± 0.87) µmol g^{-1} h^{-1}. Scaling up and assuming growth between April and September, our daytime carbon fixation rates translate into a mean seasonal net productivity for *N. luetkeana* of 2.35 kg C m^{-2} yr^{-1}, with a range of 1.15 – 4.28 kg C m^{-2} yr^{-1}. Across daytime experiments, the percent of fixed carbon released as DOC by *N. luetkeana* blades (or PER, percent extracellular release) averaged 16.23% (± 1.81). Blades of the perennial kelp *M. pyrifera* fixed an average of 48.36 (± 1.42) µmol C g^{-1} h^{-1} during the day, with a corresponding DOC release of 8.42 (± 2.15) µmol g^{-1} h^{-1} and a mean PER of 17.27% (± 3.94).

At night, light-independent carbon fixation was measured for both *N. luetkeana* and *M. pyrifera* blades. Mean nighttime dark carbon fixation rates were 3.75 (± 0.42) µmol g^{-1} h^{-1} for *N. luetkeana* ($n = 8$ replicate blades, Table 3.1) and 0.83 (± 0.00) µmol g^{-1} h^{-1} for *M. pyrifera* ($n = 4$ replicate blades, Table 3.1). Interestingly, nighttime DOC release by *N. luetkeana* blades (3.65 ± 1.36 µmol g^{-1} h^{-1}) was approximately equal to the amount of carbon fixed at night, while *M.*

pyrifera blades released a greater amount of carbon as DOC (1.79 ± 0.68 µmol g^{-1} h^{-1}) than was fixed at night, indicating net carbon release at night.

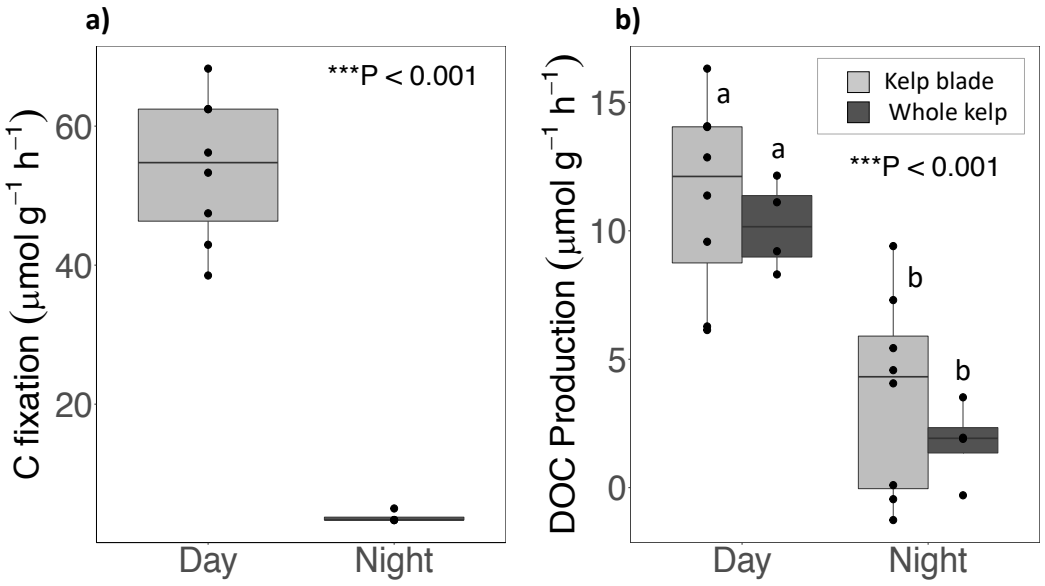

Figure 3.3. (a) Carbon fixation and (b) DOC production by *N. luetkeana* from three comparative experiments conducted during the day (light gray) and at night (dark gray), where both daytime and nighttime measurements were conducted within a 24-h period. DOC production by *N. luetkeana* blades was compared to that of the whole kelp thallus. All rates are normalized by kelp dry mass. Letters indicate statistically significant ($P < 0.05$) differences after ANOVA tests, and P values indicate results of ANOVA tests comparing daytime vs. nighttime rates.

Nutrient uptake by *N. luetkeana* blades

Diurnal differences in carbon metabolism corresponded with nitrogen uptake activity by kelp blades and pH changes in the seawater. On Tatoosh Island, nutrient uptake rates determined at ambient seawater nutrient concentrations demonstrated that *N. luetkeana* blades removed NO_3^- at the highest rate (Fig. S3.2a), with a daytime mean uptake rate of 3.51 (± 0.32) µmol g^{-1} h^{-1} and a nighttime mean of 1.37 (± 0.27) µmol g^{-1} h^{-1} (n = 27 replicate daytime measurements, n = 8 at night, Table S3.2). NO_3^- uptake was significantly higher during the day than at night during

experiments directly comparing diurnal differences (ANOVA, df = 1, error df = 14, F = 21.57, P < 0.001; Fig. S3.2a), while uptake rates for all other nutrients were constant during the day and at night (ANOVA, df = 1, error df = 14, P < 0.50; Table S3.2). Uptake rates of NH_4^+ and PO_4^- averaged 0.30 (± 0.07) and 0.06 (± 0.01) μmol g^{-1} h^{-1}, respectively (Fig. S3.2a). Both NO_2^- and inorganic silica ($Si(OH)_4$) displayed net production during the day and at night, with production rates of 0.28 (± 0.06) and 0.15 (± 0.04) μmol g^{-1} h^{-1}, respectively (Fig. S3.2a). During daytime chamber incubations, kelp blades increased seawater pH by approximately 0.38 ± 0.02 units per hour, while at night, kelp blades decreased seawater pH by 0.04 ± 0.02 units per hour (Fig. S3.2b).

Relationships between carbon fixation, light availability, and DOC release

We tested the hypothesis that DOC production is directly related to the rate of carbon fixation with data pooled across all daytime experiments conducted with *N. luetkeana* blades, from both Squaxin and Tatoosh Island (Table 3.1, n = 35). There was no relationship between carbon fixation and DOC production by *N. luetkeana* blades (linear mixed-effects model, df = 28, t = 0.50, P = 0.62; Fig. 3.4a). While carbon fixation by *N. luetkeana* blades increased with irradiance (Fig. 3.4a), DOC production was higher at low light levels (Fig. 3.4a), leading to a significant and negative relationship between light availability and the percent of fixed carbon released as DOC (linear mixed-effects model, df = 28, t = 3.52, P = 0.002; Fig. 3.4b). Thus, while carbon fixation and DOC production were not directly related (Fig. 3.4a), the increase in carbon fixation but not DOC production with increasing light availability led to a lower proportion of fixed carbon released as DOC at high light levels (Fig. 3.4b).

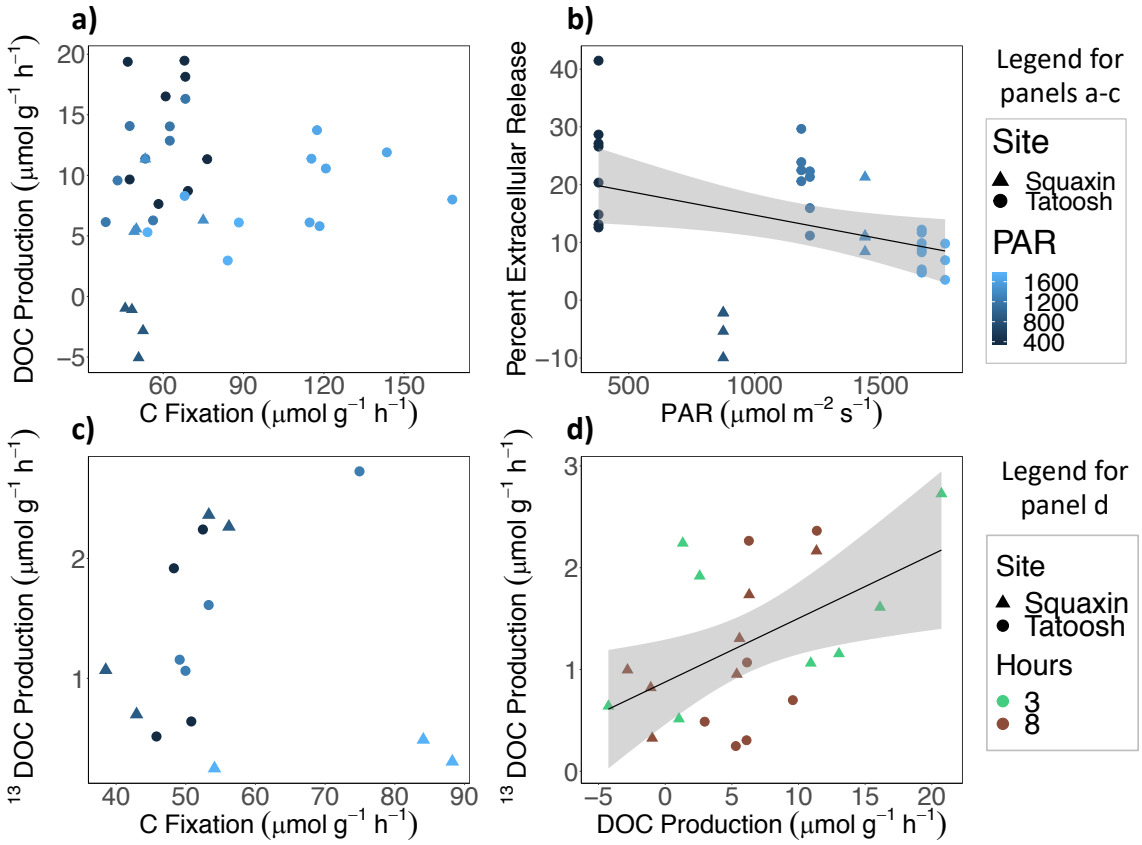

Figure 3.4. Relationships depicting (a) carbon fixation vs. DOC production and (b) the percentage of fixed carbon released as DOC over a natural gradient of light levels (PAR, photosynthetically active radiation), pooled over all experiments conducted with *N. luetkeana* blades (n = 35), (c) carbon fixation vs. ^{13}DOC production (recently fixed and released DOC) by *N. luetkeana* blades (n = 15), and (d) ^{13}DOC production vs. unlabeled DOC production by *N. luetkeana* blades (n = 23) over 3 and 8 h. Statically significant relationships ($P \leq 0.05$; with 95% confidence intervals) from linear mixed-effects models are shown.

Testing mechanisms of DOC release: release of recently fixed carbon as ^{13}DOC

Stable isotope (^{13}C-bicarbonate) tracer experiments revealed that carbon was fixed and rapidly released as ^{13}DOC after 3 and 8 hours by *N. luetkeana* blades (Table 3.2, Fig. 3.4c-d). Across all experiments, ^{13}DOC production by *N. luetkeana* blades ranged from 0.25 – 2.73 µmol g^{-1} h^{-1} (Fig. 3.4d), with a mean of 1.21 µmol g^{-1} h^{-1} (± 0.16). The release of labeled ^{13}DOC made up 10 to 20% of the total DOC produced (Table 3.2), with a mean of 15.94% (± 9.35) across all measurements, indicating that more than 80% of the DOC released during these experiments was

unlabeled carbon, or carbon fixed prior to the start of the experiment. The release of recently fixed ^{13}DOC displayed a positive and marginally significant relationship with carbon fixation rates measured concurrently (linear mixed-effects model, df = 11, t = 2.13, P = 0.057; Fig. 3.4c). The exudation of ^{13}DOC increased significantly with total DOC release, regardless of measurement at 3 or 8 hours (Fig. 3.4d), indicating that recently fixed carbon was a relatively constant proportion of total DOC released (linear mixed effects model, df = 19, t = 3.25, P = 0.004). Overall, ^{13}DOC production did not vary by site (Tatoosh vs. Squaxin) or whether it was measured after 3 or 8 hours (two-way ANOVA; df = 1, error df = 20, F = 1.13, P = 0.30 for time; F = 0.37, P = 0.55 for site; Fig. 3.4d), further indicating that *N. luetkeana* blades released a relatively constant but low proportion of recently fixed carbon as DOC.

Testing mechanisms of DOC release: stoichiometric overflow

Consistent with the stoichiometric overflow hypothesis, the relationship between DOC production and blade tissue nitrogen content was negative using pooled data across all daytime experiments with *N. luetkeana* blades from Tatoosh Island (linear mixed-effects model, df = 21, t = 2.03, P = 0.0548; Fig. 3.5). While this relationship was marginally significant with experiment included as a random factor (P = 0.0548), there was a fourfold difference in DOC production, ranging from 5 to nearly 20 μmol DOC g-1 h-1 across the range of blade tissue nitrogen (Fig. 3.5). The stoichiometric overflow hypothesis also predicts a negative relationship between DOC production and DIN uptake; while this relationship was not significant (linear mixed-effects model, df = 21, t = 0.85, P = 0.41 for DIN uptake), there was a negative trend between DOC production and DIN uptake (Fig. 3.5). However, DIN uptake did not explain additional variance in DOC production; inclusion of both tissue percent N and DIN uptake into the mixed-effects

model did not change the likelihood (AIC for percent N only was 149.08 vs. 149.10 with percent N and DIN uptake). Despite much variation, DOC production by *N. luetkeana* blades was highest when blade tissue N content was lowest (Fig. 3.5).

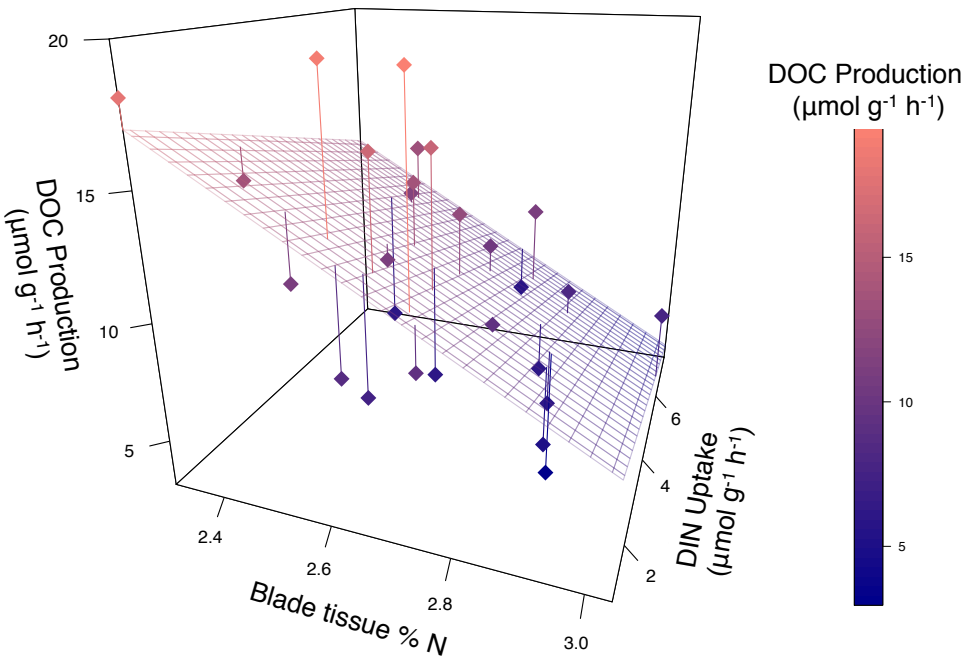

Figure 3.5. Testing the stoichiometric overflow mechanism controlling DOC production using relationships between DOC production (vertical axis and color scale) vs. blade tissue nitrogen content and dissolved inorganic nitrogen (DIN) uptake. Data are pooled across all daytime *N. luetkeana* blades from Tatoosh Island (n = 27). The grid on the 3D plot depicts a best-fit multiple linear regression model plane (DOC production ~ blade % N + DIN uptake); vertical lines show residuals between data points and the model plane surface.

The nitrate addition experiment conducted at Squaxin Island directly tested the stoichiometric overflow hypothesis. At Squaxin Island, the mean seawater DIN concentration was only 8.9 ± 0.22 µmol/L, compared to a mean seawater DIN concentration of 21.58 0.79 µmol/L, with a range of 17.4–28.3 µmol/L, across all experiments conducted at Tatoosh Island. Adding supplemental nitrate to *N. luetkeana* blades from Squaxin Island stimulated DIN uptake compared to the control where nitrate was not added (two-way ANOVA, df = 1, error df = 5, F =

59.15, P < 0.001 for treatment; Table S3.2; Fig. 3.6a), regardless of different light levels during the experiment (df = 1, F = 0.44, P = 0.54 for light). Consistent with the stoichiometric overflow hypothesis, experimental nitrate addition lowered DOC release rates (Fig. 3.6b; two-way ANOVA, df = 1, error df = 5, F = 6.40, P = 0.052 for nitrate addition). While the result was marginal (P = 0.052), each kelp blade that experienced nitrate addition displayed lower DOC production than the controls (Fig. 3.6b). In contrast to total DOC production, the release of recently fixed photosynthate (^{13}DOC) did not differ as a function of nitrate addition when it was measured at 3 or 8 h (df = 1, F = 1.52, P = 0.24 for nitrate addition; df = 1, F = 1.62, P = 0.23 for time point).

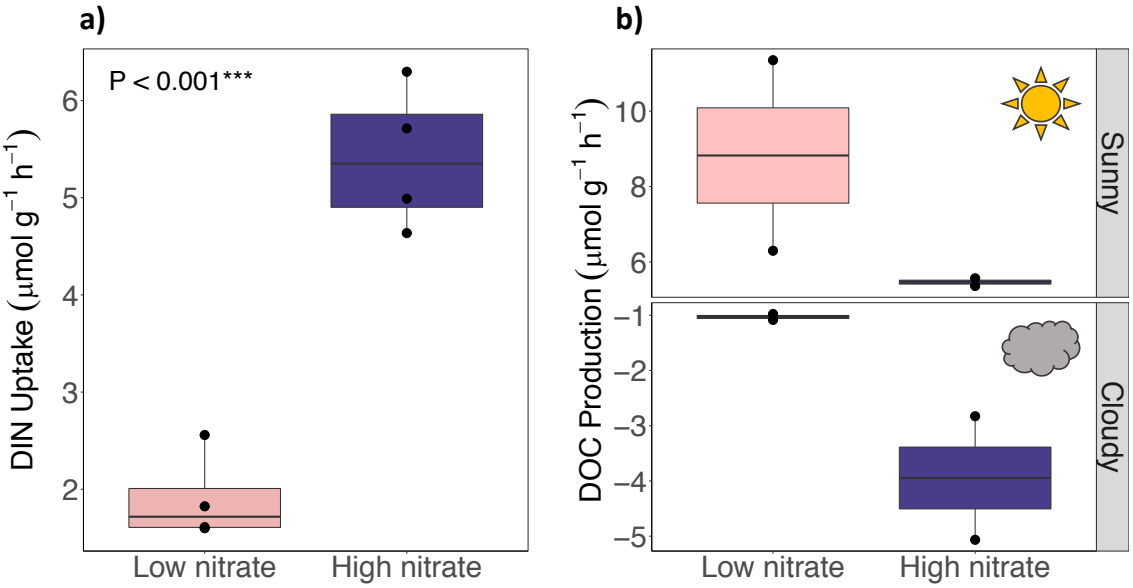

Figure 3.6. Biogeochemical responses of *N. luetkeana* blades from Squaxin Island to nitrate addition. (a) Dissolved inorganic nitrogen (DIN) uptake rates in natural (low nitrate) seawater and with experimental nitrate addition (high nitrate) and (b) DOC production from low and high nitrate treatments under both sunny and cloudy conditions. Light levels (PAR) were 1,438 and 875 µmol m-2 s-1, on the sunny and cloudy day, respectively. Statistically significant differences between treatments are indicated with asterisks and corresponding P values in panel a. In panel b, the effect of light levels on DOC release was significant (P < 0.001***), while nitrate treatment was marginally significant (P = 0.052).

Light levels during the experiment had an even greater effect on DOC release than nitrate addition (two-way ANOVA, df = 1, F = 60.39, P < 0.001 for light), with DOC flux from *N. luetkeana* blades indicating net consumption of DOC on the cloudy day (Fig. 3.6b, Table 3.2). In addition, ^{13}DOC release by *N. luetkeana* blades was marginally higher on the sunny day (ANOVA, df = 1, error df = 12, F = 3.70, P = 0.08; Table 3.2). Finally, compared to measurements with Tatoosh Island kelp, *N. luetkeana* from Squaxin Island displayed lower carbon fixation and DOC release rates, and had significantly lower blade tissue nitrogen content (Table S3.3) despite similar blade mass (Fig. S3.3), although greater replication at Squaxin Island is necessary to confirm this trend.

Comparative carbon and nutrient dynamics of *M. pyrifera* and *N. luetkeana*

The two canopy kelp species differed in key aspects of carbon and nitrogen cycling. When blades of the two canopy-forming kelps were incubated concurrently, *N. luetkeana* displayed significantly higher carbon fixation, DOC release, and DIN uptake rates per unit dry mass than *M. pyrifera*, both during the day and at night (two-way ANOVAs, df = 1, error df = 13, F = 8.21, P = 0.013 for carbon fixation; F = 26.50, P < 0.001 for DOC production; F = 32.52, P < 0.001 for DIN uptake; Fig. 3.7). Blades of *N. luetkeana* (10.9 ± 0.25) had significantly lower C:N ratios compared to *M. pyrifera* (13.74 ± 0.37; ANOVA, df = 1, error df = 14, F = 60.37, P < 0.001; Fig. 3.7d). The average daytime carbon fixation by *N. luetkeana* blades was 60.15 μmol g^{-1} h^{-1}, with a corresponding DIN uptake rate of 4.11 μmol g^{-1} h^{-1} and a DOC production rate of 14.32 μmol g^{-1} h^{-1}. For *M. pyrifera,* mean daytime carbon fixation was 48.36 μmol g^{-1} h^{-1}, DOC release was 8.42 μmol g^{-1} h^{-1}, and DIN uptake was 2.64 μmol g^{-1} h^{-1}. The stoichiometry of these rates indicates that after subtracting the mean amount of carbon lost as DOC from the mean carbon fixation rate, the C:N ratio of assimilated matter was ~11.2 for *N. luetkeana* and ~15.1 for

M. pyrifera. Both ratios are similar to the C:N of blade tissue for each species (Fig. 3.7d), suggesting a possible homeostasis between carbon and nitrogen dynamics.

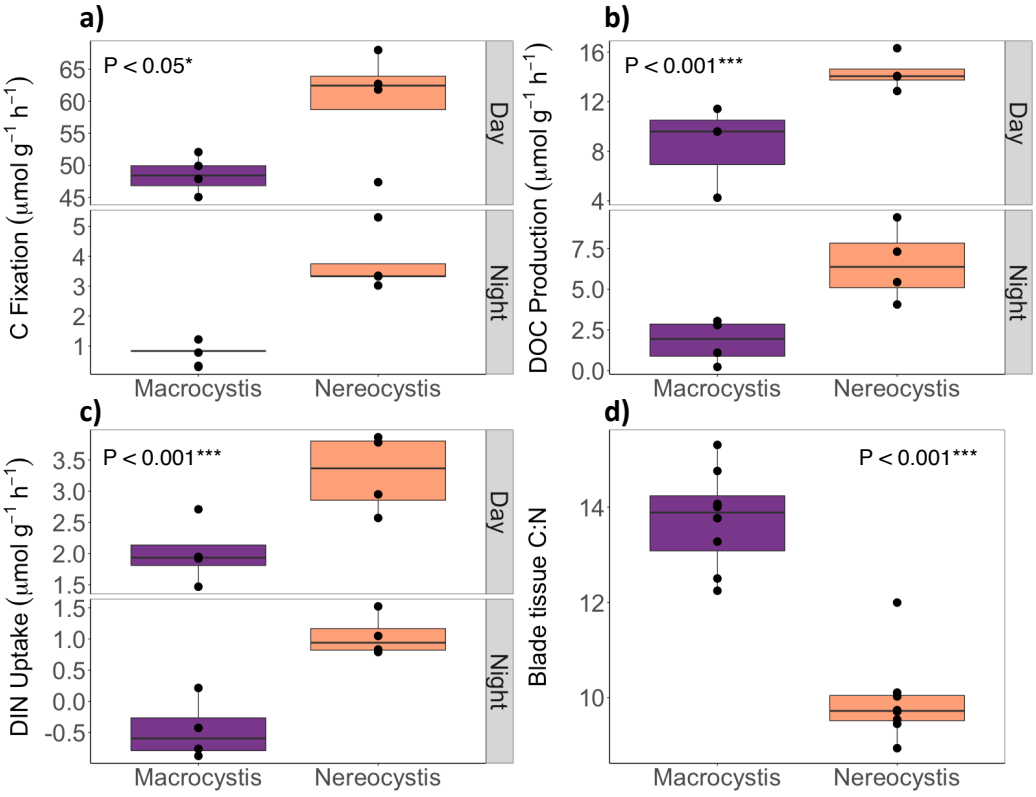

Figure 3.7. Comparisons of biogeochemical rates between *N. luetkeana* and *Macrocystis pyrifera* blades (n = 4 of each species) during the day and at night for (a) carbon fixation, (b) DOC production, (c) dissolved inorganic nitrogen (DIN) uptake rates, and (d) C:N ratios of blade tissue. Statistically significant differences between species are indicated with asterisks and corresponding P values.

Daytime carbon fixation, DOC release, and DIN uptake rates were significantly higher than nighttime rates for both species (two-way ANOVAs, df = 1, error df = 13, $F = 409$, $P < 0.001$ for carbon fixation; $F = 41.13$, $P < 0.001$ for DOC production; $F = 22.26$, $P < 0.001$ for DIN uptake; Fig. 3.7). During the day, *N. luetkeana* blades fixed 20% more carbon (Fig. 3.7a) and produced 41% more DOC than *M. pyrifera* blades (Fig. 3.7b). At night, carbon fixation by *N. luetkeana* was 4.5 times higher than *M. pyrifera* while DOC production was 3.6 times higher,

indicating that *N. luetkeana* is able to perform dark carbon fixation to a greater extent than *M. pyrifera*. The percent of fixed carbon released as DOC was also greater for *N. luetkeana* than *M. pyrifera*, both during the day (24.2% vs. 17.3%, respectively) and at night (10.9 % vs. 3.7%, respectively; Table 3.1). Finally, DIN uptake by *N. luetkeana* was 60% higher than *M. pyrifera* during the day and 195% higher at night (Fig. 3.7c; Table S3.2).

Discussion

Daytime and light-independent carbon fixation by kelp blades

Daytime carbon fixation rates by *N. luetkeana* blades averaged 78 μmol (or 0.94 mg) C g^{-1} dry mass h^{-1}, while blades of *M. pyrifera* assimilated significantly less carbon than *N. luetkeana*, fixing an average of 48 μmol (or 0.58 mg) C g^{-1} dry mass h^{-1}. Our canopy kelp carbon fixation rates are comparable to other measurements of carbon fixation in kelps using the ^{14}C assimilation method, including 0.3 – 3.5 mg C g^{-1} h^{-1} for *M. pyrifera* blades (Towle and Pearse 1973, Arnold and Manley 1985) and 0.3 – 0.7 mg C g^{-1} h^{-1} for *Laminaria spp*. (Küppers and Kremer 1978, Dunton and Jodwalis 1988). One study reported much higher rates for ^{14}C fixation by *N. luetkeana* blades, ranging from 0.6 to 6.5 mg C g^{-1} h^{-1} (Wheeler et al. 1984), but fixation was quantified using small discs of blade tissue in the lab at saturating irradiances. The difference in carbon fixation rates between these two canopy kelp species likely reflects life history differences; *N. luetkeana* is an annual kelp while *M. pyrifera* is perennial that may contain more carbon storage reserves, although individual blades of *M. pyrifera* are rarely older than 6 months (Graham 2002). Willenbrink et al. (1979) found that *N. luetkeana* had a higher photosynthetic efficiency per unit chlorophyll and fixed more carbon than *M. pyrifera*. Further, annual macroalgae have been shown to have higher photosynthetic rates than perennials (King

and Schramm 1976). In addition to fixing more carbon, *N. luetkeana* also assimilated more DIN and released greater quantities of DOC compared to *M. pyrifera*, suggesting that kelp forests comprised of annual kelps may cycle carbon more quickly and produce substantial amounts of DOC during the spring and summer growing season. When scaled up to seasonal kelp forest net primary productivity, we found that *N. luetkeana* can fix 2.35 kg C m^{-2} yr^{-1}, with a range of 1.15 – 4.28 kg C m^{-2} yr^{-1}. Other studies report similar productivity for canopy-forming kelps, including 1.4 kg C m^{-2} yr^{-1} for *N. luetkeana* (Foreman 1984) and 1.3 kg C m^{-2} yr^{-1} for *M. pyrifera* (Wheeler and Druehl 1986).

In both kelp species, carbon fixation was higher at the older, more distal regions of the blade, including the mid-blade and tip for *N. luetkeana* and the mid-blade for *M. pyrifera*. This is consistent with other studies reporting higher photosynthetic rates in older kelp tissues (Towle and Pearse 1973, Kremer 1981), including *N. luetkeana* blades (Willenbrink et al. 1979, Wheeler et al. 1984). One study also reported a higher concentration of Rubisco in older blade tissues (Kueppers and Kremer 1978). Our findings support the consensus that more carbon is assimilated in the older, distal portions of the kelp blade, which is then translocated to the actively growing region at the base of the blade (Schmitz and Lobban 1976, Go,mez et al. 2007).

As in our study, light-independent carbon fixation has been observed in multiple brown macroalgae (Thomas and Wiencke 1991, Go,mez et al. 2007), including *N. luetkeana* and *M. pyrifera* (Willenbrink et al. 1979, Kremer 1981). We quantified light-independent carbon fixation at night by *N. luetkeana* and *M. pyrifera* blades, which averaged ~ 6% and 1.7%, respectively, of daytime carbon fixation. These rates are comparable to other brown algae (Ku€ppers and Kremer 1978, Kremer 1981), though less than the Antarctic brown macroalgae *Ascoseira mirabilis* (13%; Thomas and Wiencke 1991). Carbon assimilation at night did not

differ with blade position, despite studies demonstrating higher light-independent carbon fixation at the base of the blade (Kueppers and Kremer 1978, Willenbrink et al. 1979, Kremer 1981). Most studies of carbon fixation at night do not concurrently quantify DOC production. Interestingly, the rate of light- independent carbon assimilation by *N. luetkeana* blades was approximately equal to the amount of DOC released, indicating a net zero balance of carbon at night, while DOC production by *M. pyrifera* blades exceeded dark carbon fixation.

Extracellular release of fixed carbon as DOC

During the day, the average percentage of fixed carbon released as DOC by *N. luetkeana* and *M. pyrifera* blades, often referred to as percent extracellular release (PER), was 16.2% and 17.3%, respectively. With a mean PER of 16% and estimated net primary productivity of 2.35 kg C m-2 yr-1, *N. luetkeana* may release as much as 376 g C m-2 yr-1 as DOC. Another study found a similar rate; the mean annual PER for *M. pyrifera* blades estimated in situ was 14% (Reed et al. 2015). Reported rates of DOC release by kelps averaged 26–35% of fixed carbon for Laminaria spp. (Sieburth 1969, Hatcher et al. 1977, Abdullah and Fredriksen 2004). The kelp Ecklonia cava has the highest reported DOC release rates, with a mean PER of 43% (Wada et al. 2007). Earlier studies argue that the proportion of fixed carbon released as DOC by macroalgae is much lower, from <1% (Fankboner and Burgh 1977, Søndergaard 1981) up to 6% (Pregnall 1983, Søndergaard 1990). However, these studies quantified the fixation and release of radiolabeled 14DOC, which detects only recently fixed and released photosynthate (Pregnall 1983). In our study, we found that the release of labeled ^{13}DOC made up an average of only 18% of the total DOC released. Because DOC release includes both recently and previously fixed carbon, radiolabeled and stable isotope studies that rely on tracer production alone underestimate

total DOC release. Wada et al. (2007) caution that carbon isotope tracer studies can also underestimate DOC release when the fixed carbon is synthesized into macromolecules such as mucopolysaccharides, as this process dilutes the isotopic signature of the fixed carbon in the bulk DOC that is released. Here, we demonstrated that DOC release by *N. luetkeana* was comprised of <20% recently fixed carbon, thus >80% of DOC released was previously fixed, such as intracellular compounds, or recently synthesized macromolecules that dilute the isotopic signature of recently assimilated and released carbon.

Effects of light availability on DOC release

DOC release by *N. luetkeana* and *M. pyrifera* was 3.5 and 4.7 times higher during the day than at night, respectively. Other studies report that kelps release 1.3–2 times more DOC during the day than at night (Sieburth 1969, Abdullah and Fredriksen 2004, Reed et al. 2015). Beyond diurnal contrasts, we found that carbon fixation by *N. luetkeana* blades increased with irradiance, but DOC production did not, thus the percent extracellular release of fixed carbon (PER) declined with increasing irradiance. Maranon et al. (2004) found a similar relationship between PER and irradiance with phytoplankton. Other studies report that DOC release increases with irradiance (Mueller et al. 2016), although the PER may be highest at low light levels and at extreme irradiances (Fogg et al. 1965, Zlotnik and Dubinsky 1989), where photoinhibition of photosynthesis can occur. During the Squaxin experiment, DOC release was higher on the sunny day compared to the cloudy day, when the DOC flux was negative, and in all experiments DOC release responded to changing light levels, warranting further investigation into the effects of light on DOC release by kelp.

DOC release by kelp blades: diffusion of fixed carbon and stoichiometric overflow

We examined DOC release rates in relation to kelp productivity and nutrient availability to evaluate aspects of the photosynthate diffusion (Bjørnsen 1988; Fig. 3.1a) and stoichiometric overflow (Fogg 1983; Fig. 3.1b) hypotheses. These hypotheses are not mutually exclusive; for example, it is possible that stoichiometric constraints promote DOC release under nutrient-limited conditions, while passive diffusion prevails when nutrients are replete (Livanou et al. 2017). Diffusion of photosynthates as DOC, whether passive or active, has been hypothesized to be dependent on the concentration of intracellular carbon pools (Bjørnsen 1988), and thus may be positively related to the rate of carbon fixation (e.g. Moran and Estrada 2002). In contrast, we found no relationship between DOC production and carbon fixation by *N. luetkeana* blades, despite a large range of productivity quantified at different light levels, suggesting that DOC release is not dependent on the rate of new carbon assimilation. It is important to note that the passive diffusion hypothesis was devised for and has been supported by studies with microalgae, which may differ from macroalgae in many important ways. For example, microalgae have a higher surface area to cell volume ratio, faster biomass-specific growth rates, and more rapid nitrogen acquisition per unit biomass than macroalgae (Hein et al. 1995), thus morphological differences may lead to different physiological constraints on DOC release between microalgae and macroalgae. Previous studies with macroalgae found that DOC release was unrelated to gross primary production (Barron et al. 2014) or net primary production (Abdullah and Fredriksen 2004), although Reed et al. (2015) found a positive relationship between reef-scale net primary production and DOC release. Bjørnsen (1988) suggests that nighttime DOC release is consistent with the passive diffusion hypothesis, as it demonstrates carbon leakage without concurrent photosynthesis. We found substantial DOC release at night by both canopy kelp

species, at a rate equal to or greater than nighttime carbon fixation, likely indicating passive diffusion. Further, we demonstrated that recently fixed carbon (^{13}DOC) comprised a small proportion (< 20%) of the total DOC released, thus the majority of DOC release was not a result of immediate photosynthate spillover. Release of DOC that is not dependent on photosynthesis could be due to myriad other processes, including cell death and lysis, viral cell lysis, or grazing (Nagata 2000). We found that DOC release was not proportional to carbon fixation and the bulk of DOC released was not recently fixed. Rather, DOC release by macroalgae may be a process that integrates internal carbon stores and tissue nitrogen dynamics over longer time scales.

We found multiple lines of support for the stoichiometric overflow hypothesis, which predicts that DOC released by kelp blades should decrease with greater nitrogen availability. For all *N. luetkeana* incubations conducted on Tatoosh Island, DOC release declined as blade tissue nitrogen content increased. While the relationship was marginally significant, the magnitude of DOC release changed drastically over a small gradient in blade tissue nitrogen, ranging from 5 to nearly 20 μmol DOC g-1 h-1 as tissue nitrogen decreased. Moreover, the short-term nitrate addition experiment with kelp from nitrogen-poor Squaxin Island demonstrated that nitrate addition lowered DOC release rates, although light levels exerted a much stronger control on DOC release than experimental nitrate addition. Overall, our results demonstrate that DOC release was not dependent on carbon fixation and the bulk of DOC released was not recently fixed photosynthate, yet DOC release declined with increasing nitrogen availability. Thus, DOC released by kelp may be comprised mostly of stored carbon, with a small amount of recently assimilated carbon, and the bulk release rate may be constrained by nitrogen availability.

The composition of extracellular carbohydrates released by kelp has not been well characterized and it was not determined in this study, yet composition may provide further hints

about the mechanisms and consequences of DOC release. While simple monosaccharides such as rhamnose, fucose, ribose, xylose, galactose, and glucose were among the products exuded by the kelp *Ecklonia cava* (Wada et al. 2007), other intracellular storage carbohydrates, such as mannitol, can also be released by kelp (Newell et al. 1980, Wada et al. 2007). Laminarin, a key polysaccharide storage compound in algae, is released extracellularly and contributes significantly to the global carbon cycle (Becker et al. 2020). Studies using 14C to trace photosynthesis in brown algae over similar time periods to this study (3 h) determined that the storage product mannitol comprised the majority of newly assimilated carbon, while cell wall polysaccharides such as laminarin, alginate, and fucoidan had a slower rate of isotopic carbon incorporation (Yamaguchi et al. 1966, Bidwell 1967). Thus, it is possible that our stable isotope enrichment experiments quantified the assimilation and release of rapidly ^{13}C labeled products such as mannitol. However, the bulk of DOC released by *N. luetkeana* blades was unlabeled, suggesting that it contained other previously fixed intracellular carbohydrates, possibly the result of a significant time lag between assimilation and release of photosynthates as DOC. Future studies combining isotopic labeling and compositional analysis of intracellular and extracellular carbon pools may provide exceptional insight into the time course and the nature of DOC release, revealing whether released compounds are dependent on the availability of intracellular compound concentrations, recent photosynthates, or intracellular nitrogen pools.

Nutrient uptake and production associated with *N. luetkeana* blades

In addition to releasing DOC, *N. luetkeana* blades were associated with strong diurnal fluxes in inorganic nutrient concentrations. Mainly, *N. luetkeana* blades removed NO_3^- at a much higher rate (3.2 μmol g^{-1} h^{-1}) than NH_4^+ (0.53 μmol g^{-1} h^{-1}). The only other study to measure

nutrient uptake by *N. luetkeana* also found that NO_3^- was removed at a higher rate than NH_4^+, where NH_4^+ removal peaked at 10 μM availability but NO_3^- removal increased with availability up to 30 μM (Ahn et al. 1998). However, we emphasize that the mean availability of NH_4^+ (1.98 μM) was ~9 times lower than that of NO_3^- (17.65 μM) at Tatoosh Island, indicating that the mean uptake rate of NH_4^+ relative to its availability was 1.5 times higher than for NO_3^-. This difference in preference vs. availability of these two nitrogen sources may also reflect the high flux of NH_4^+ at this site (Pfister et al. 2014). Uptake of NO_3^- was significantly higher during the day than at night, consistent with Gerard (1982), and may be driven by higher daytime nitrate reductase activity (Young et al. 2007). Interestingly, we found that *N. luetkeana* blades displayed net production of NO_2^- and inorganic silica ($Si(OH)_4$), both during the day and at night. It is possible that production of NO_2^- is a result of microbial activity associated with kelp blades. The most abundant bacterial taxa living on *N. luetkeana* blades collected from Tatoosh Island was *Granulosicoccus sp.* (Weigel and Pfister 2019), and a genome from *Granulosicoccus antarcticus* contained the nitrate reductase gene (Kang et al. 2018), responsible for reducing NO_3^- to NO_2^-. Further experiments are necessary to determine how kelp-associated microbes may contribute to nutrient fluxes in kelp forests.

Coastal implications of DOC release and relation to microbial processes

Neither the stoichiometric overflow nor the diffusion hypothesis explains why *N. luetkeana* and *M. pyrifera* blades release such a high proportion of fixed carbon (16– 17%) into the surrounding seawater. Photosynthate released by canopy-forming kelps can elevate DOC concentrations in seawater by almost 50% inside of kelp forests compared to outside (Pfister et al. 2019). It is likely that photosynthates released by kelp provision heterotrophic microbes living

on the kelp surface (Bengtsson et al. 2011), as well as heterotrophic microbes in the surrounding seawater (Fogg 1983, Pregnall 1983, Carlson and Ducklow 1996). For example, brown algae in the genus *Carpophyllum* predominantly released low molecular weight compounds, which were highly labile and readily decomposed by seawater microbes (Søndergaard 1990). Release of photosynthates may contribute to the productivity of the bacterial biofilm that characterizes many macroalgae, as reported for seagrass, where epiphytic bacterial production was fueled almost entirely by DOC release (Kirchman et al. 1984). Microbes in the seawater (Sieburth 1969, Fankboner and Burgh 1977, Pregnall 1983) and on the kelp surface likely consume some proportion of the DOC before it is detected, so this study and others may be underestimating DOC release rates. For example, we found net consumption of DOC from *N. luetkeana* blades on the cloudy day of the nitrate addition experiment (Fig. 3.6). Microbial consumption of DOC likely fuels growth of the biofilm, while microbial respiration of DOC may provide a means of recycling CO2 back to the kelp for photosynthesis, or it could act as a net source of carbon to the atmosphere. Glucose can stimulate microbial nitrate uptake (Pfister and Altabet 2019), thus DOC release by kelp may also be coupled to local microbial nitrogen cycling. Further, microbial processing of organic matter can influence nutritional content (Dethier et al. 2014), as well as export and subsidies among coastal ecosystems (Sawstrom et al. 2016). Some of the DOC may be exported to the deep sea and thus act as a carbon sink; this proportion is estimated at ~ 30% (Krause-Jensen and Duarte 2016), but empirical validation is necessary to quantify this carbon flux. Changing and variable ocean pH dynamics (Wootton et al. 2008) may interact with DOC cycling in the nearshore, thus the fate of this large DOC pool is likely an essential aspect of the current and future coastal carbon cycle.

Appendix 3.1 Supplemental Equations for Chapter 3

Description of equations for calculating carbon fixation, ^{13}DOC production, DOC production and nutrient uptake rates, and methods for scaling up to the seasonal productivity of *N. luetkeana* on Tatoosh Island.

Section S1) Equation for calculating carbon fixation using ^{13}C-bicarbonate assimilation

Stable isotope data are expressed using the standard δ notation, describing the difference in parts per thousand (‰) of the $^{13}C/^{12}C$ isotope ratio in the sample from the international PDB (Pee Dee Belemnite) isotope standard. The R notation directly expresses the $^{13}C/^{12}C$ isotope ratio in the sample (R_{sample}). To convert from $\delta^{13}C$ to R_{sample}, we used the following equation: $R_{sample} = ((\delta^{13}C_{sample} / 1000) \times R_{standard}) + R_{standard}$, where $R_{standard} = 0.0112372$. The carbon fixation calculations are based on the atom% ^{13}C value, which can be converted from R_{sample} using the following equation: atom% $^{13}C = (R_{sample} / (R_{sample} + 1)) \times 100$. After converting from the $\delta^{13}C$ notation, the following equation was used to calculate carbon fixation, based on equations in Mateo et al. (2001) and Miller and Dunton (2007):

$$\text{Carbon fixation } \left(\text{mg C g}^{-1}\ \text{h}^{-1}\right) = \frac{(\text{at\%}_{K\_T_F} - \text{at\%}_{K\_T_0})}{(\text{at\%}_{DIC\_T_0} - \text{at\%}_{K\_T_0})} \times \frac{C}{M \times T} \quad (S1)$$

where $\text{at\%}_{K\_T_F}$ is the atom% ^{13}C of enriched kelp tissues at the end of the experiment, $\text{at\%}_{K\_T_0}$ is the atom% ^{13}C of natural kelp tissues at the start of the experiment, $\text{at\%}_{DIC\_T_0}$ is the atom% ^{13}C of dissolved inorganic carbon in the seawater within the chambers at the beginning of the experiment after adding the enriched $NaH^{13}CO_3$, M is the dry mass of the kelp blade (g), C is the mass of carbon (mg) in the kelp tissue as determined by elemental analysis of solid samples, and T is time (hrs).

Section S2) Equation for calculating ^{13}DOC production

Using the $\delta^{13}C$ of DOC in seawater samples collected at the start and end of each kelp blade incubation experiment, the following equation was used to calculate ^{13}DOC production:

$$13\text{-DOC production}\left(\mu\text{mol C g}^{-1}\text{ h}^{-1}\right) = \frac{(at\%_{DOC\_T_F} - at\%_{DOC\_T_0})}{(at\%_{DIC\_T_0} - at\%_{DOC\_T_0})} \times \frac{DOC_{T_F} \times V}{M \times T} \qquad (S2)$$

where $at\%_{DOC\_T_F}$ is the atom% ^{13}C of enriched DOC at the end of the experiment, $at\%_{DOC\_T_0}$ is the atom% ^{13}C of natural DOC at the start of the experiment, $at\%_{DIC\_T_0}$ is defined above, DOC_{T_F} is the final concentration of DOC in the chamber (µmol / L), V is the chamber volume (L), M is kelp dry mass, and T is time. Note that by using $(at\%_{DIC\_T_0} - at\%_{DOC\_T_0})$ as the ^{13}C enrichment above the background, this equation assumes that either a) the ^{13}C enrichment of DIC in the chambers was fully incorporated into kelp tissue and available for release as ^{13}DOC, or b) ^{13}DOC production results from carbon that is fixed and immediately released, without ever being assimilated into the kelp tissue.

Section S3) Equation for calculating unlabeled DOC production

DOC concentrations were measured at the beginning and end of chamber incubations. The following equation was used to calculate unlabeled DOC production:

$$\text{DOC production}\left(\mu\text{mol g}^{-1}\text{ h}^{-1}\right) = ((DOC_{KT_F} - DOC_{KT_0}) - \Delta DOC_C) \times \frac{V}{M \times T} \qquad (S3)$$

where DOC_{KT_F} is the final DOC concentration (µmol / L) and DOC_{KT_0} is the initial DOC concentration (µmol / L) in kelp chambers. The average change in DOC concentration in seawater control chambers (ΔDOC_C) was subtracted from production in kelp chambers prior to multiplying by volume (V) and dividing by dry mass (M) and time (T), accounting for DOC production by phytoplankton in the surrounding seawater.

Section S4) Equation for calculating nutrient uptake

Nutrient uptake followed a nonlinear exponential decay function (Appendix S2: Fig. S3.1a). Log-transformed rates were linear between 0 and 3 hours (Appendix S2: Fig. S3.1b), thus nutrient uptake rates were calculated from the slope of log-transformed nutrient concentrations over this interval. The following equation was used to calculate nutrient uptake for all inorganic nutrients:

$$\text{Nutrient uptake}\left(\mu\text{mol nutrient g}^{-1}\ \text{h}^{-1}\right) = (-1 \times \text{B} \times \text{N}_{\text{AVG}}) - \Delta\text{N}_{\text{SC}} \times \frac{\text{V}}{\text{M}} \qquad \text{(S4)}$$

where B is the slope is from the regression between the natural log-transformed nutrient concentration and time for each individual kelp chamber, N_{AVG} is the average nutrient conc. (µmol / L) in each chamber during the incubation, ΔN_{SC} is the average change in nutrient conc. in all seawater control chambers (also determined from the slope of log-transformed nutrient concentration vs. time), V is volume (L), and M is dry mass (g). Note that subtracting ΔN_{SC} accounts for nutrient uptake by phytoplankton in the seawater surrounding the kelp.

Section S5) Description of methods for scaling up to seasonal productivity per m^2

To scale up carbon fixation to units of kg C m^{-2} yr^{-1}, we counted the mean density of *N. luetkeana* individuals per m^2 from n = 20 haphazardly thrown quadrats (0.64 m^2), and the mean number of blades from n = 20 randomly selected individuals on Tatoosh Island. Kelp bed density was quantified in August using *N. luetkeana* exposed within the intertidal zone at low tide (-0.76 m tide). To convert mass-specific to areal rates, we multiplied the mean carbon fixation rate in kg C g DM^{-1} hr^{-1} by the dry mass of individuals per m^2 using the mean number of individuals per m^2 (7.66 ± 0.86), the mean number of blades per individual (41.5 ± 2.95), and the mean dry mass

of *N. luetkeana* blades (4.63 ± 0.15 g). We converted hourly to annual rates by multiplying by the number of daylight hours in a year (2617) for the annual growing season (April – September) using sunrise and sunset data from Seattle, Washington. Finally, we converted our carbon fixation rates, which represent gross primary production (GPP), to net primary production (NPP) by subtracting the proportion of GPP lost as respiration. For the proportion of GPP attributable to respiration, 0.27 (± 0.08), we used the mean from numerous studies with brown algae that measured GPP or NPP and respiration (Littler and Murray 1974, Hatcher et al. 1977, Abdullah and Fredriksen 2004, Tait and Schiel 2013, Blain and Shears 2019). Our mean density measurement (7.66 kelp per m^2) is higher than other published *N. luetkeana* density measurements, including 2.25 (Foreman 1984), 3.7 (Barns and Kalvass 1993), and 4.57 individuals per m^2 (Stekoll et al. 2006); however, roughly half of the sites in Stekoll et al. (2006) had a density of >7 individuals per m^2. We note that our annual productivity calculation assumes that productivity is only contributed by the kelp blades and does not account for carbon fixed by the photosynthetic stipe and the holdfast.

To account for variation in kelp mass, kelp bed density and photosynthetic rates, we quantified the range in annual productivity by using the mean parameter estimate and the minimum and maximum values based on 95% confidence intervals. The mean, minimum and maximum parameters used to scale up carbon fixation rates to seasonal productivity per m^2 are listed below:

Parameter	**Mean (± SE)**	**Min. (lower 95% CI)**	**Max. (upper 95% CI)**
Blade dry mass (g)	4.13 (± 0.27)	3.60	4.66
Number of blades per individual	41.50 (± 2.95)	35.72	47.28
Kelp density (individuals per m2)	7.66 (± 0.86)	5.97	9.35
C fixation (μmol C g-1 h-1)	78.50 (± 6.45)	65.86	91.14

Appendix 3.2: Supplemental Tables and Figures for Chapter 3

Table S3.1. Summary of linear mixed-effects models using pooled data from all daytime measurements with *N. luetkeana* blades (a-b), all experiments where ^{13}DOC was quantified (c-d), and all *N. luetkeana* measurements conducted on Tatoosh Island (e-f).

Response variable	Explanatory Factors	df	t	*P*	Figure
a) DOC release	Carbon fixation (fixed) & experiment (random)	28	0.50	0.62	Fig. 4a
b) Percent fixed carbon released as DOC	PAR light level (fixed) & experiment (random)	28	3.52	0.002	Fig. 4b
c) ^{13}DOC release	Carbon fixation (fixed) & experiment (random)	11	2.13	0.057	Fig. 4c
d) ^{13}DOC release	DOC release (fixed) & experiment (random)	19	3.25	0.004	Fig. 4d
e) DOC release	Blade tissue %N (fixed) & experiment (random)	21	2.03	0.0548	Fig. 5
f) DOC release	DIN uptake (fixed) & experiment (random)	21	0.85	0.41	Fig. 5

Table S3.2. Summary of mean NO3-, NO2-, NH4+, PO4- and Si(OH)4 uptake rates (± std. error) across all experiments.

Experiment	Site	Date	Treatment	Replication	NO_3 uptake (umol /g*hr)	NO_2 uptake (umol /g*hr)	NH_4 uptake (umol /g*hr)	PO_4 uptake (umol /g*hr)	$SiOH_4$ uptake (umol /g*hr)
1) *Nereocystis* blade	Tatoosh	July 2017	Day	n = 4	2.61 (0.13)	0.03 (0.00)	0.72 (0.17)	0.04 (0.02)	0.02 (0.19)
1) *Nereocystis* blade	Tatoosh	July 2017	Night	n = 4	1.62 (0.46)	0.02 (0.00)	0.32 (0.07)	0.02 (0.01)	-0.26 (0.13)
2) *Nereocystis* blade	Tatoosh	Aug 2018	Day	n = 4	3.77 (0.36)	-0.82 (0.06)	0.34 (0.02)	0.08 (0.03)	-0.40 (0.11)
2) *Nereocystis* blade	Tatoosh	Aug 2018	Night	n = 4	1.12 (0.31)	-0.87 (0.16)	0.79 (0.21)	0.08 (0.01)	0.07 (0.03)
3) *Macrocystis* blade	Tatoosh	Aug 2018	Day	n = 4	2.36 (0.27)	-0.63 (0.02)	0.28 (0.02)	0.11 (0.01)	0.08 (0.15)
3) *Macrocystis* blade	Tatoosh	Aug 2018	Night	n = 4	0.38 (0.26)	-1.18 (0.06)	0.34 (0.03)	0.08 (0.01)	0.24 (0.18)
4) *Nereocystis* blade	Tatoosh	Sept 2018	Day	n = 8	1.82 (0.14)	-0.33 (0.03)	0.02 (0.01)	0.01 (0.01)	-0.21 (0.01)
5) *Nereocystis* blade	Tatoosh	June 2019	Day	n = 8	5.62 (0.28)	0.03 (0.01)	0.19 (0.01)	0.15 (0.01)	0.03 (0.01)
6) *Nereocystis* blade	Tatoosh	July 2018	Day	n = 3	3.24 (0.23)	-0.27 (0.04)	0.03 (0.01)	0.07 (0.01)	-0.56 (0.12)
7) *Nereocystis* NO_3 addition	Squaxin	June 2018	Low NO_3	n = 4	1.28 (0.13)	0.32 (0.08)	0.31 (0.03)	0.10 (0.01)	0.41 (0.51)
7) *Nereocystis* NO_3 addition	Squaxin	June 2018	High NO_3	n = 4	5.19 (0.43)	0.03 (0.01)	0.19 (0.07)	0.08 (0.01)	0.21 (0.03)

Table S3.3. Comparison of Tatoosh Island and Squaxin Island blade tissue characteristics and carbon dynamics.

Metric compared	DF, error DF	F value	P value	Tatoosh mean value (± SE)	Squaxin mean value (± SE)
Blade tissue C:N	1, 33	2.85	0.10	9.88 (0.28)	10.77 (0.07)
Blade tissue % C	1, 33	1.06	0.31	26.43 (0.86)	24.79 (0.22)
Blade tissue % N	1, 33	35.97	< 0.001*	2.68 (0.03)	2.30 (0.02)
Carbon fixation	1, 33	4.42	0.043*	78.50 (6.45)	53.08 (3.23)
DOC production	1, 33	19.31	< 0.001*	10.80 (0.87)	2.33 (1.99)

Figure S3.1. Nitrate (NO_3) uptake by Nereocystis blades incubated in chambers during the day a) over the duration of 3- and 8-hour experiments, b) log-transformed nitrate uptake from 0-3 hrs.

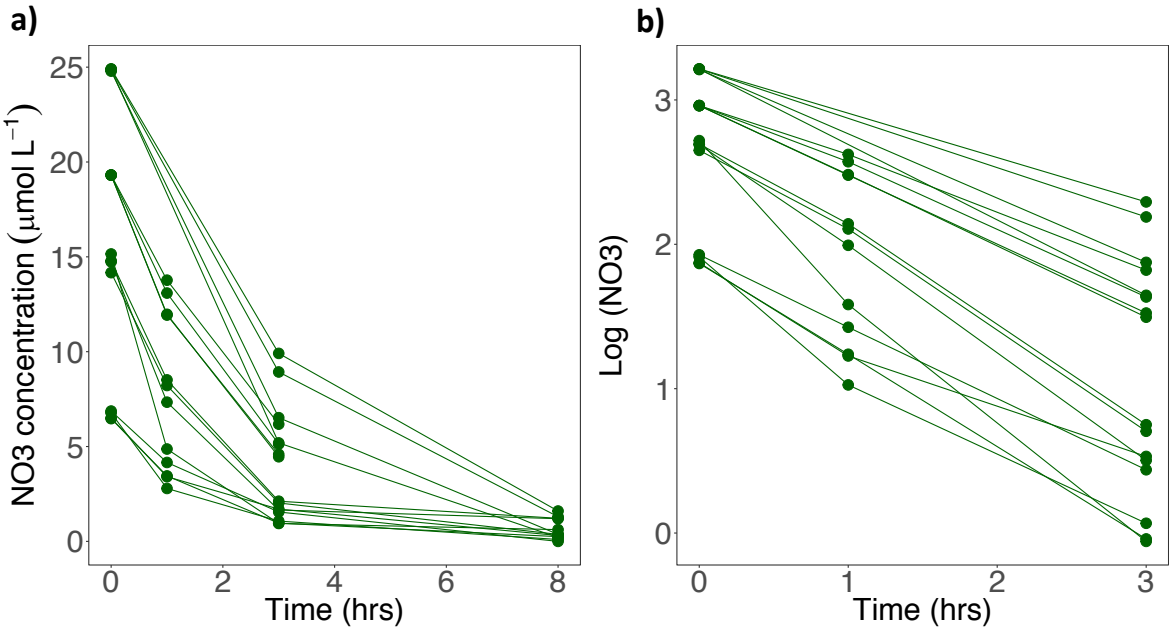

Figure S3.2. Biogeochemical responses in chamber experiments with N. luetkeana blades during the day and at night. a) Uptake rates of inorganic nutrients (NH_4^+, NO_2^-, NO_3^-, PO_4^-, $Si(OH)_4$) by *N. luetkeana* blades, normalized by dry mass. Nutrient uptake by seawater control chambers was subtracted from all kelp chambers. b) Changes in seawater pH over time with the presence of a kelp blade (green) and in seawater control chambers (blue).

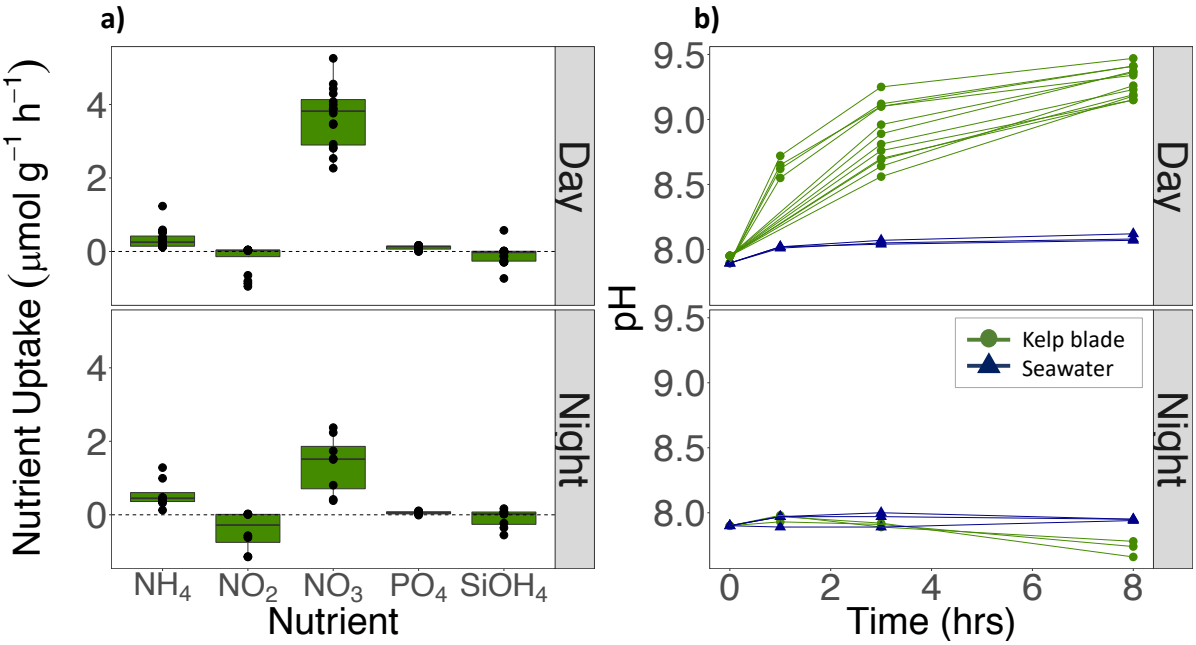

Figure S3.3. Relationships between *N. luetkeana* blade dry mass and a) blade tissue percent nitrogen, b) DOC production. Tatoosh Island kelp are represented by blue circles, while Squaxin Island kelp are represented by pink triangles.

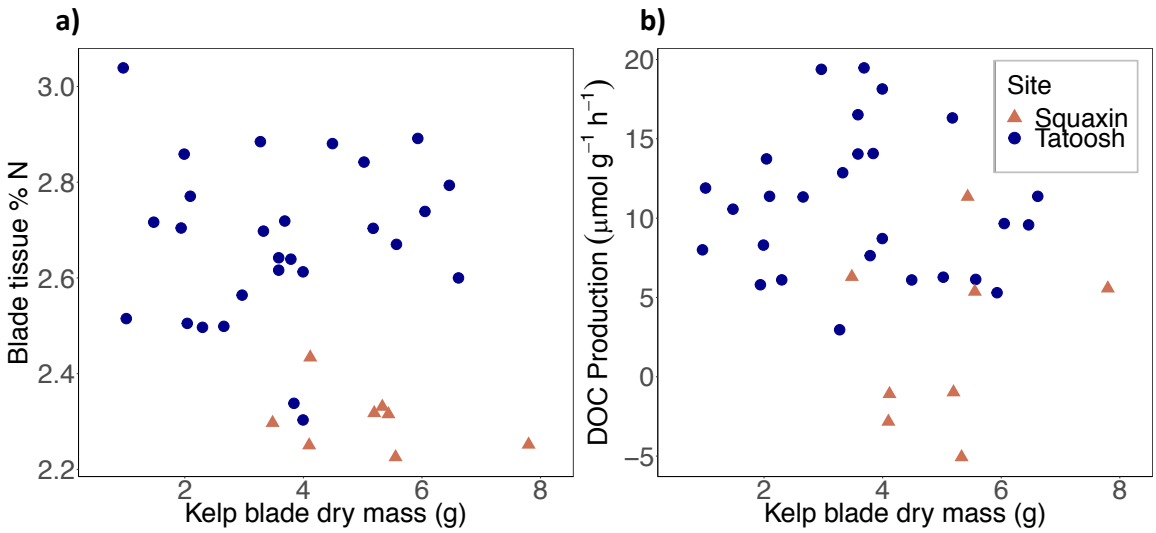

CHAPTER 4: FUNCTIONAL INSIGHTS INTO THE KELP MICROBIOME FROM METAGENOME ASSEMBLED GENOMES

Introduction

Associations between eukaryotic hosts and microbial communities are ubiquitous, yet we are just beginning to discover the functional roles of the microbial partners in many of these associations. It is particularly important to understand the metabolic role of microbes associated with large, habitat-forming organisms, as microbes influence eukaryotic host biology and directly participate in ecosystem-level biogeochemical cycles (Beinart 2019). Kelp, brown macroalgae in the order *Laminariales*, are among the fastest growing and most productive marine algae (Wheeler and Druehl 1986, Graham et al. 2007), fixing up to 2.35 kg of carbon per m^2 annually (Weigel and Pfister 2021a). Canopy-forming kelp species form vast underwater forests, creating structural habitat in temperate and arctic coastal regions worldwide (Steneck et al. 2002). Photosynthetic kelp blades are covered by a dense and diverse microbiome, with up to 10^8-10^9 bacterial cells per cm^2 of kelp tissue (Bengtsson and Øvreås 2010, Ramirez-Puebla et al. 2020). Despite the potential importance of high-density bacterial communities living on kelp hosts, which achieve a tremendous biomass in coastal ecosystems, we know little about the functional role of the kelp microbiome.

It is critical to determine the functional roles of kelp-associated microbial symbionts, as microbial metabolisms can greatly influence the biology of their hosts. For example, bacteria associated with phytoplankton can provide fixed or reduced nitrogen and cofactors such as vitamin B12 to their host algae in exchange for organic carbon (Amin et al. 2015, Seymour et al. 2017). Microbial nitrogen metabolisms such as nitrate and nitrite reduction have been identified in the microbiome of *Macrocystis pyrifera* (Minich et al. 2018), while nitrogen fixation was

quantified from *M. pyrifera* blades (Hamersley et al. 2015). Kelp release ~16% of carbon fixed through photosynthesis into the surrounding seawater as dissolved organic carbon, or DOC (Reed et al. 2015, Weigel and Pfister 2021a), providing a consistent metabolic resource to heterotrophic bacteria. Bacteria in the surrounding seawater consume kelp-derived DOC (Thomas et al. 2021, Gao et al. 2021), and cultured bacterial isolates from the kelp surface degrade polysaccharides such as alginate, fucoidan, laminarin and mannitol (Bengtsson 2011, Lin et al. 2018). To determine their importance for the host kelp, it is important to understand the range of metabolisms present in the kelp microbiome as well as the identity of the uncultured bacterial groups that perform these metabolisms in natural kelp surface biofilms.

Microbial communities associated with macroalgae are often specific to each host species and distinct from microbial communities in the surrounding seawater (Egan et al. 2013, Michelou et al. 2013, Weigel and Pfister 2019), yet many bacterial groups are also shared among diverse host macroalgae (Florez et al. 2017, Lemay et al. 2018). For example, *Granulosicoccus* sp. is among the abundant bacterial genus on the kelps *Nereocystis luetkeana* and *M. pyrifera* (Weigel and Pfister 2019), *Laminaria hyperborea* (Bengtsson et al. 2012), *Laminaria setchellii* (Lemay et al. 2021), *Ecklonia cava* (Jo et al. 2019), and the brown algae *Fucus* spp. (Quigley et al. 2020). *Granulosicoccus* also associates with red, green and brown algal hosts (Singh and Reddy 2014), and its ubiquity on macroalgae suggests it may have an important functional role, but there is currently no genomic information available for kelp-associated *Granulosicoccus*.

Metagenomic sequencing yields fragmented DNA sequences from all species present in a sample, which can be assembled into bacterial genomes (metagenome assembled genomes, or MAGs) to determine the functional genes and metabolic capabilities of each bacterial species. Here, we used a genome-resolved metagenomics approach to determine the functional roles of

bacterial symbionts associated with photosynthetic blades of the canopy-forming bull kelp (*Nereocystis luetkeana*). The bull kelp microbiome is dominated by a few microbial taxa that persist across geographic locations (Weigel and Pfister 2019), colonize new tissues rapidly (Weigel and Pfister 2021b), reach high cell abundances, and display repeatable micron-scale spatial structure (Ramirez-Puebla et al. 2020). We reconstructed 79 metagenome-assembled-genomes (MAGs) from bull kelp blade tissues, spanning 6 bacterial phyla and 18 families. By mapping short sequence reads from kelp blade metagenome samples collected over 3 consecutive years to all bacterial genomes, we tested whether the annual life history of *N. luetkeana* affects the continuity of bacterial taxa present across years. Next, we evaluated whether microbial metabolisms that are likely to interact with host kelp metabolisms or contribute to nutrient cycling in kelp forest ecosystems are present in kelp-associated bacterial genomes by searching for genes related to DOM assimilation, nitrogen metabolisms, and vitamin biosynthesis. We tested the hypothesis that kelp-associated microbes have the capacity to consume dissolved organic matter (DOM) by searching for cell membrane DOM transport proteins in the assembled bacterial genomes, which are used by bacteria to assimilate DOM and provide information about the types of compounds being metabolized by microbes (Poretsky et al. 2010, Bergauer et al. 2018). Finally, we determined the metabolic functions of the most abundant member of the kelp microbiome, *Granulosicoccus* sp. Comparing kelp associated *Granulosicoccus* sp. MAGs to other available genomes, including the full genome of *Granulosicoccus antarcticus* (Kang et al. 2018), facilitated the discovery of novel functions associated with this bacterial genus.

Methods

Sample collection, DNA extraction and metagenomic sequencing

Samples for metagenomic sequencing were obtained from individuals of the kelp *Nereocystis luetkeana* at a well-studied location on Tatoosh Island, Washington, USA (48.39°N, 124.74°W) over three consecutive years. Samples were collected at the north-facing Main Beach site in July 2017, July 2018 and July 2019. In July 2019, additional *N. luetkeana* samples were collected from Squaxin Island in Southern Puget Sound (47.18° N, 122.91° W), the southernmost location in Puget Sound where *N. luetkeana* persists. Previous research with Squaxin Island kelp demonstrated significantly different microbial community composition and reduced cell density compared to kelp from Tatoosh Island (Weigel and Pfister 2019, Ramirez-Puebla et al. 2020). In 2017-2018, whole tissue blade samples from Tatoosh Island were collected by removing 2 x 1 cm^2 of tissue from the middle of the kelp blade with sterile scissors. In 2019, samples from both Tatoosh and Squaxin Island *N. luetkeana* were collected by swabbing the mid to tip of the blade for 20 seconds with a sterile cotton swab. All kelp tissue and swab samples were immediately frozen at -20°C and transferred to -80°C for storage until processing.

DNA was extracted from whole kelp tissues and swabs using the DNeasy Power Soil Kit (Qiagen). To acquire a sufficient quantity of DNA for metagenomic library preparation (>100 ng), DNA extracts from multiple kelp samples were pooled for each individual metagenome, with the number of pooled replicates listed in Table S4.1. In total, 7 metagenome samples were sequenced from *N. luetkeana* blades. DNA extracts were sent to Argonne National Laboratory for library prep and metagenomic sequencing on an Illumina HiSeq 2500 (2x150 bp).

Assembly, annotation and binning of metagenome-assembled-genomes (MAGs)

All analyses, from sequence quality control to binning, were conducted in anvi'o v.7 (Eren et al. 2015, 2021). First, raw sequences from forward and reverse reads were checked for sequence quality using "filter-quality-minoche" (Minoche et al. 2011). For all samples, >92% of sequence reads passed quality control, and the mean number of reads per sample after quality control was 22,339,573 (Table S4.1). Quality sequences were assembled into contigs using IDBA-UD (Peng et al. 2012) with a minimum contig length of 1,000. Metagenome samples collected from the same kelp forest location and same year were co-assembled, resulting in 4 total assemblies (Table S4.1), to ensure that we did not assemble chimeric genomes across multiple years or locations. The command "anvi-gen-contigs-database" was used to generate contigs databases, which computes k-mer frequencies and identifies open reading frames with Prodigal (Hyatt et al. 2010). To determine the occurrence of 22 bacterial single copy genes in each contigs database, hidden Markov models were run using HMMER (Eddy 2011) with "anvi-run-hmms." Genes in each contigs database were annotated with all 3 available databases in anvio: 1) NCBI's Clusters of Orthologous Genes (COGs), 2) EBI's Pfam database, and 3) KEGG (Kyoto Encyclopedia of Genes and Genomes). Metagenomic short reads from all 7 samples were mapped to each of the 4 co-assemblies using Bowtie2 (Langmead and Salzberg 2012), and samtools (Li et al. 2009) was used to produce BAM files.

To perform metagenomic binning of contigs using anvio, profile databases were generated from BAM files and contigs databases using "anvi-profile" with a minimum contig length of 2,500 (to visualize all contigs), and profiles for co-assembled samples were merged. To cluster contigs into MAGs, manual binning and refinement was performed using "anvi-interactive" with both sequence composition (tetranucleotide frequency) and differential coverage across all samples, following previously described approaches to generate high quality

MAGs (Delmont et al. 2018, Shaiber et al. 2020). For co-assemblies derived from whole kelp tissue extracts (Table S4.1), there was one large bin in each assembly consisting of genomic reads from the host kelp, which was clearly differentiated from bacterial bins based on GC content and differential coverage. Further, BLAST revealed that sequences from these bins had a high percent identity match to other brown algae and eukaryotic genomes. To remove host reads from further analyses, the bin containing kelp genomic reads was de-selected from the final bin collection in anvio. While binning, microbial taxonomy was estimated within anvio using "anvi-run-scg-taxonomy," which searches SCGs from each genome against the Genome Taxonomy Database (GTDB). After binning each assembly using "anvi-interactive," bacterial bins were individually inspected using "anvi-refine," where they were checked for contaminating contig clusters with dissimilar GC content and differential coverage. Final bin collections were checked for completeness and contamination (also called redundancy) using "anvi-summarize."

The final MAGs collection was curated using ""anvi-rename-bins," and bins with less than 50% completion or greater than 10% redundancy were removed. Final MAGs were named based on the following scheme: the prefix g1-g4 corresponds to the metagenome assembly from which it was binned (Table S4.1), while the numbers distinguish unique MAGs within each co-assembly (e.g., g1_MAG_00001). A final table of all 79 MAGs assembled from the *Nereocystis luetkeana* kelp blade is available in Table S4.2. In total, we assembled 28 high-quality MAGs (>90% completion, <5% contamination) and 52 medium-quality MAGs (>50% completion and <10% contamination), according to the genomic standards in Bowers et al. (2017).

Taxonomic assignment and curation of a non-redundant MAG dataset

In order to identify highly similar MAGs and pick representative genomes out of the redundant MAGs, the command "anvi-dereplicate-genomes" was used to dereplicate the final MAG collection at 99% average nucleotide identity (ANI) using PyANI (Pritchard et al. 2016). Out of 79 MAGs, 13 were redundant, generating a final dataset of 66 non-redundant MAGs (Table S4.2). Representative MAGs with the highest completion combined with the lowest redundancy were selected. Taxonomy was assigned to each MAG using GTDB-Tk (v1.3.0; Chaumeil et al. 2019), which uses a set of 120 concatenated bacterial gene markers to place MAGs in a reference tree based on the Genome Taxonomy Database (release95, Parks et al. 2020), using both FastANI (Jain et al. 2018) and pplacer (Matsen et al. 2010). To generate contigs.fasta files for GTDB-Tk classification, MAGs were exported from anvio using anvi-summarize. The final maximum-likelihood phylogenetic tree was inferred using the IQ-TREE software (Nguyen et al. 2015) with the alignment of 120 concatenated bacterial gene markers from GTDB-Tk. Using IQ-TREE, ModelFinder (Kalyaanamoorthy et al. 2017) was first implemented to select the best-fit nucleotide substitution model (LG+F+R6), and bootstrap support values were obtained with 1,000 bootstrap replicates. We visualized the abundance and detection of non-redundant MAGs in all metagenome samples using "anvi-interactive" with the minimum detection set to 0.70, indicating that a genome is considered present in a sample if at least 70% of nucleotides in the genome are covered by at least one short read from that sample.

Pangenomic analysis of *Granulosicoccus sp.*

In this study, we generated 8 novel MAGs of *Granulosicoccus* sp., including 6 of high quality (>90% completion; Table S4.2). We generated a pangenome with these 8 MAGs, along with two publicly available *Granulosicoccus* genomes: the complete isolate genome of

Granulosicoccus antarcticus type strain IMCC3135 (Kang et al. 2018), and *Granulosicoccus* sp. 002746645, a MAG assembled from a common bottlenose dolphin's mouth (Dudek et al. 2017). To compare the average nucleotide identity (ANI) among *Granulosicoccus* genomes, we used "anvi-compute-genome-similarity" with PyANI (Pritchard et al. 2016). We used anvi'o to analyze and visualize the pangenome. First, we made a database of all 10 genomes using "anvi-gen-genomes-storage," and generated the pangenome using "anvi-pan-genome" (minbit set to 0.5 and mcl-inflation set to 10), which uses NCBI's BLAST to quantify sequence similarity within and between genomes. To visualize the pangenome, we used "anvi-display-pan." To obtain functional gene annotations and amino acid sequences from all genes within each *Granulosicoccus* genome, we used "anvi-summarize." Finally, to search for KEGG metabolic pathways present in the pangenome and estimate pathway completeness, we used "anvi-estimate-metabolism" with an e-value threshold of 1e-05 and a bitscore fraction of 0.5.

Functional gene presence-absence across all MAGs

We constructed a database of annotated genes (COG, KEGG, Pfam) in each MAG based on anvi'o-generated tables and quantified the number of genes annotated with a given function in each MAG. We searched for genes involved in dissolved organic matter (DOM) transport (list adapted from Poretsky et al. (2010), nitrogen metabolism and transformation (56 genes, including those involved in nitrogen fixation, assimilatory and dissimilatory nitrate reduction, denitrification, nitrification, comammox, and urea hydrolysis), and genes involved in vitamin B12 synthesis (list adapted from Wagner-Döbler et al. 2010 and Lu et al. 2020). E-values are the expected number of false positive hits for a gene annotation, adjusted to the sequence database size. We used e-value cutoffs of 1e-20 for KEGG annotations and 1e-50 for COG annotations.

We visualized the presence-absence of functional genes across MAGs with heatmaps generated using "anvi-interactive," where the phylogeny of MAGs and python-generated functional gene tables were imported as additional layers.

Phylogenetic analysis of photosystem II (*pufLM*) genes

To validate the presence of genes for aerobic anoxygenic phototrophy (AAP) in *Granulosicoccus* sp. MAGs and determine their relationship to other known AAP bacteria, we extracted amino acid sequences for the *pufL* and *pufM* photosystem II reaction center genes from each MAG using "anvi-summarize." We acquired a reference database of 167 *pufL* and *pufM* sequences from Imhoff et al. (2018), including 99 belonging to the *Alphaproteobacteria*, 14 *Betaproteobacteria*, 49 *Gammaproteobacteria*, and 5 from the phylum *Chloroflexi* that were used as an outgroup, as in Tank et al. (2009). Concatenated *pufLM* sequences were aligned using MAFFT v7.309 (Katoh and Standley 2013). A maximum-likelihood phylogeny was inferred using IQ-TREE (Nguyen et al. 2015), with ModelFinder (Kalyaanamoorthy et al. 2017) to select the best-fit nucleotide substitution model, partitioned for *pufL* and *pufM* genes. Model selection resulted in the best-fit model of LG+F+I+G4 across both genes, and bootstrap support values were obtained with 1,000 bootstrap replicates.

Results

Bacterial genomes assembled from kelp blade surface swabs and whole kelp tissues

Shotgun metagenomic sequencing of 7 metagenome samples collected from blades of *N. luetkeana* resulted in 156.4 million high-quality short reads, with an average of 22 million short reads per sample (Table S4.1). From these samples, we reconstructed 79 metagenome assembled

genomes (MAGs) from 6 different bacterial phyla, including 31 *Proteobacteria* (16 *Gammaproteobacteria* and 15 *Alphaproteobacteria*), 22 *Bacteroidetes*, 13 *Verrucomicrobia*, 9 *Bdellovibrionota*, 2 *Planctomycetes*, and 2 *Patescibacteria* (Fig. S4.1, Table S4.2). We successfully assembled bacterial genomes from both whole kelp blade tissue samples and blade surface swabs. The two metagenome assemblies from kelp surface swabs yielded 13 and 38 MAGs, while the two assemblies from whole kelp tissues yielded 4 and 24 MAGs. The metagenome assemblies from whole kelp tissue samples contained 39.0-49.8% kelp host DNA, so despite the mix of kelp host and bacterial genomes, roughly half of our metagenome content was bacterial. Mapping short reads from each metagenome sample to the assembled MAGs revealed that across all samples, an average of 59.1% of all short reads mapped to the bacterial genomes. For metagenome samples from kelp surface swabs, a higher percentage of short reads from mapped to bacterial genomes (88.2% of reads), indicating that the MAGs captured most of the bacterial sequence reads, compared to metagenome samples assembled from whole kelp tissues (37.3% of reads), which contained many short reads from the host kelp.

Detection and abundance of bacterial genomes that persist over multiple years

To test the hypothesis that kelp-associated bacterial taxa can persist across years on the blades of an annual kelp species, we assembled bacterial genomes collected from blades of the annual kelp *N. luetkeana* at Squaxin Island in 2019, and from Tatoosh Island in 2017, 2018 and 2019. Mapping short reads from each metagenome sample to assembled genomes revealed that many bacterial genomes were detected across years, and in both locations (Fig. 4.1). Overall, 31 MAGs (47% of the total number of MAGs) were detected across multiple years, while 15 MAGs (23%) were detected across locations on both Tatoosh and Squaxin Islands. In contrast, 30

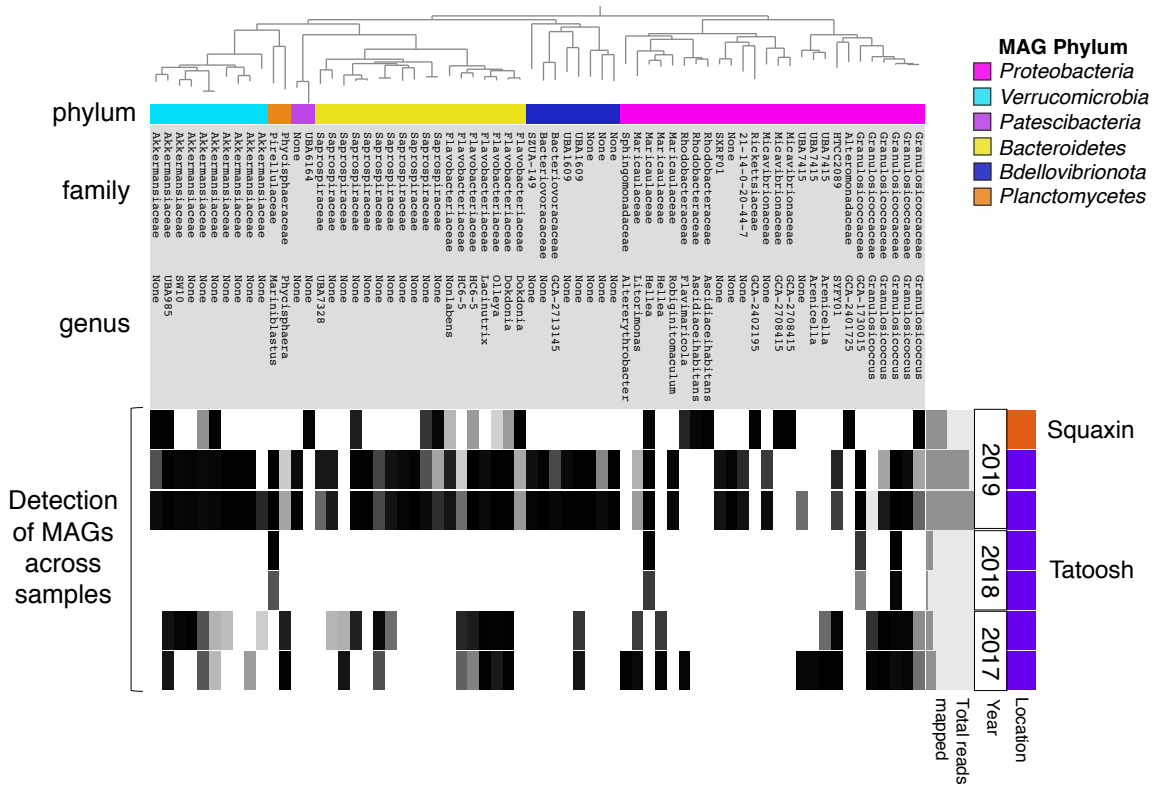

Figure 4.1. A maximum-likelihood phylogenetic tree of kelp-associated metagenome assembled genomes (MAGs) (top), colored by bacterial phylum with the family and genus level taxonomy listed for each MAG, showing the detection of MAGs (with at least 70% of the genome covered by short reads from that sample) across different kelp metagenome samples (below). Black and grey bars indicate MAG presence in a sample, while white bars indicate absence. Samples are grouped by location and year, and the small bar graph to the right shows the total number of short reads mapped to all MAGs in each metagenome sample.

MAGs (45%) were only detected at a single location or year. Only 1 MAG of *Granulosicoccus* sp. was detected across 2017, 2018 and 2019 on Tatoosh Island (Table S4.3). The two metagenome samples from 2018, assembled from whole kelp tissues, had a low detection of bacterial MAGs (Fig. 4.1, Table S4.3). Excluding the 2018 samples, 26 MAGs (39%) were detected across years 2017 and 2019 from Tatoosh (Fig. 4.1, Table S4.3). In addition to persisting across years, 15 MAGs (23%) were detected on both Tatoosh and Squaxin Islands (Table S4.3). MAGs detected across both locations and multiple years on Tatoosh included the

Gammaproteobacteria Granulosicoccus sp., the *Alphaproteobacteria Hellea* sp., *Bacteroidetes* from the families *Saprospiraceae* and *Flavobacteriaceae* (genera *Olleya*, *HC6-5*, and *Dokdonia*), and *Verrucomicrobia* from the family *Akkermansiaceae* (Fig. 4.1, Table S4.3). There were 23 MAGs from diverse families detected only on Tatoosh kelp, while 7 MAGs were detected only at Squaxin; however, differences in sample numbers from each location likely explain this trend.

While detection indicates whether MAGs are present in each sample from the proportion of nucleotides in the genome that are covered by at least one short read, abundance reveals the MAGs that recruited the most reads within a sample, calculated as the mean coverage of short reads per MAG divided by the overall mean coverage within a sample. *Granulosicoccus* sp. were the most abundant genomes assembled from kelp at each location (Fig. S4.2). Different genomes of *Granulosicoccus* sp. were differentially abundant at each location (g1_MAG_00002 at Squaxin and g4_MAG_00004 at Tatoosh (Fig. S4.2, Table S4.4), which are likely to be two separate species based on their ANI of only 82% (Fig. S4.3). Other very abundant genomes from Tatoosh and Squaxin in 2019 included *Hellea* sp. (*Alphaproteobacteria*) and multiple MAGs from the family *Akkermansiaceae* (*Verrucomicrobia*), while *Dokdonia* sp. (*Bacteroidetes*) was the most abundant microbe from Tatoosh in 2017 (Fig. S4.2, Table S4.4). In addition, two members of the phylum *Planctomycetes* were relatively abundant in samples from Tatoosh in 2017 and 2018 – *Phycisphaera* sp. and *Mariniblastus* sp., respectively (Fig. S4.2, Table S4.4).

Widespread occurrence of genes for DOM transport by diverse bacteria

We detected the presence of 72 genes for dissolved organic matter (DOM) transport in our diverse set of 66 unique bacterial genomes assembled from the kelp surface (Fig. 4.2). Genes identified in kelp-associated bacterial genomes transported diverse substrates including amino

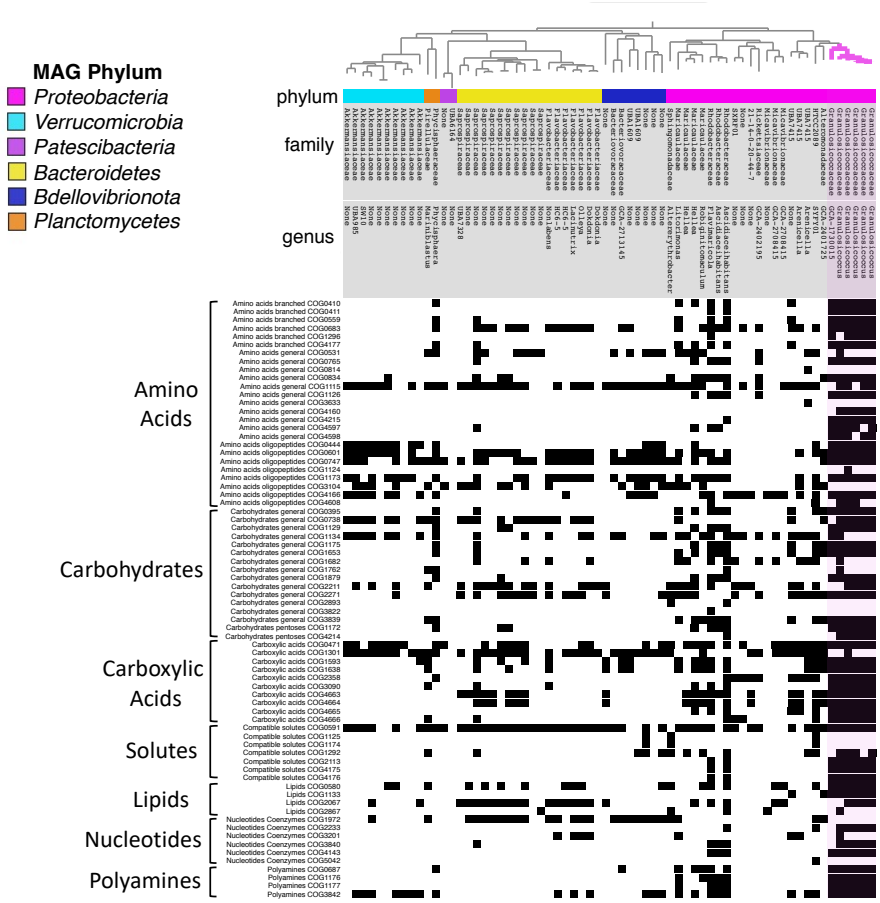

Figure 4.2. A maximum-likelihood phylogenetic tree of kelp-associated MAGs (top), colored by bacterial phylum with the family and genus level taxonomy listed for each MAG, showing the presence (black) and absence (white) of genes involved in dissolved organic matter (DOM) transport across all MAGs. DOM transport genes are grouped by substrate type, with COG annotations listed (list of genes adapted from Poretsky et al. 2010). All gene annotations had e-values of less than 1e-50. The clade of MAGs belonging to the family *Granulosicoccaceae* is highlighted in pink, which contains many DOM transport genes.

acids, oligopeptides, polyamines, lipids (long-chain fatty acids, glycerol), nucleotides, carbohydrate sugars, carboxylic acids, and solutes (Fig. 4.2, Table S4.5). DOM transport proteins were present in members of all bacterial phyla and in every bacterial genome, with the exception of one MAG from the phylum *Patescibacteria* and family UBA6164 (Fig. 4.2), indicating that diverse members of the kelp microbiome have the ability to assimilate DOM. Most bacterial genomes contained multiple genes for DOM transport, with a median of 14 genes per genome.

Gammaproteobacteria in the genus *Granulosicoccus* and *Alphaproteobacteria* in the families *Maricaulaceae* and *Rhodobacteraceae* were particularly enriched in DOM transport genes (Fig. 4.2). *Granulosicoccus* sp. MAGs contained the highest number of DOM transporters, with a range of 53 to 59 distinct transport protein genes per genome (Fig. 4.2). Many of these genes encode ATP-binding cassette (ABC)-type transporters, which are fueled by ATP hydrolysis to actively translocate substrates across the bacterial cell membrane (Rees et al. 2009). ABC-type transporters involved in transporting amino acids and oligopeptides, as well as sugars such as xylose, ribose, arabinose, & galactoside were present in diverse bacteria (Table S4.5). In addition to ABC-type transporters, kelp-associated bacterial genomes contained genes for permeases that facilitate transport across the membrane (e.g., fucose permease), as well as tripartite ATP-independent periplasmic type transporters for mannitol and carboxylic acids (Table S4.5).

Nitrogen metabolisms in the kelp microbiome

Kelp-associated bacterial genomes from the *Proteobacteria*, *Verrucomicrobia*, and *Planctomycetes* contained genes for dissimilatory nitrate and nitrite reduction, as well as urea hydrolysis (Fig. 4.3). MAGs in the family *Akkermansiaceae* (phylum *Verrucomicrobia*) contained genes for dissimilatory nitrite reduction (*nirA*, *nirB* and *nirD*). One *Akkermansiaceae* also had the ability to hydrolyze urea with genes encoding the three urease subunits (*ureABC*). The *Planctomycetes Mariniblastus* sp. contained nitrite reduction (*nirA*), and *Phycisphaera* sp. had *ureAB* and *ureC*. The greatest diversity of nitrogen metabolisms was found within the *Proteobacteria* (Fig. 4.3). Multiple MAGs contained both nitrate and nitrite reduction genes, indicating the potential for reduction from nitrate to ammonium, including *Altererythrobacter* sp., *Ascidiaceihabitans* sp., *Arenicella* sp., and *Granulosicoccus* sp., while *Litorimonas* sp.

contained nitrite reduction genes (Fig. 4.3). *Proteobacteria* with urease genes (*ureABC*) included *Ascidiaceihabitans* sp., *Flavimaricola* sp., *Arenicella* sp., and *Granulosicoccus* sp. (Fig. 4.3). *Granulosicoccus* sp. MAGs contained genes for assimilatory and dissimilatory nitrate reduction (*nasA* and *narI*, respectively), dissimilatory nitrite reduction (*nirBDK*), and urease (Fig. 4.3).

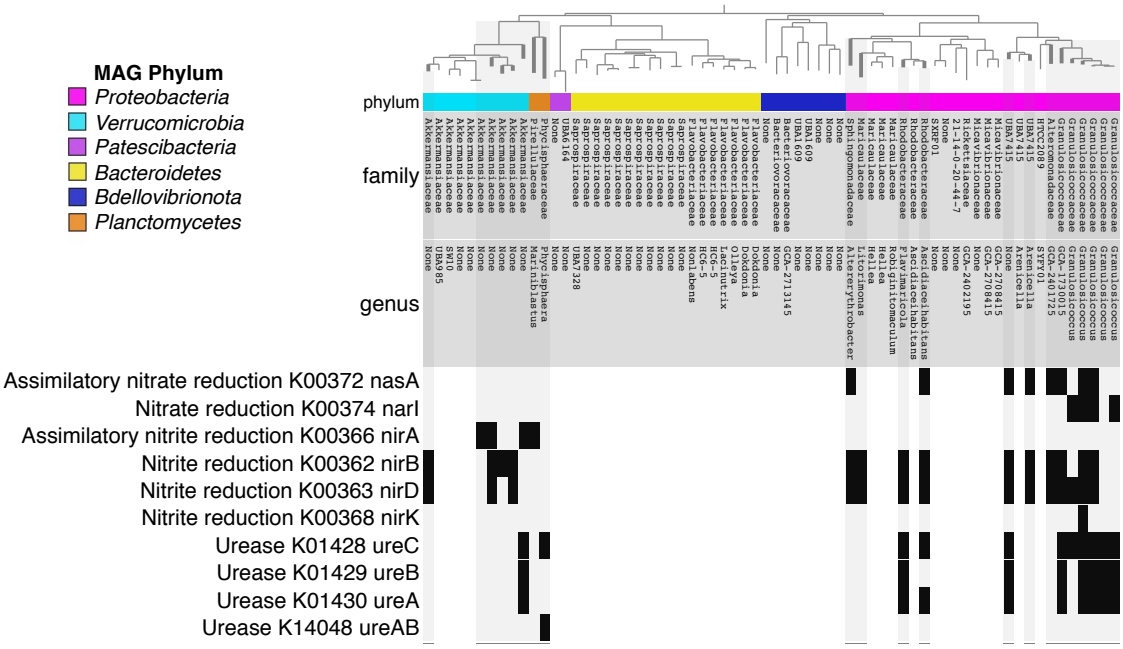

Figure 4.3. A maximum-likelihood phylogenetic tree of kelp-associated MAGs (top), colored by bacterial phylum with the family and genus level taxonomy listed for each MAG, showing the presence (black) and absence (white) of genes involved in nitrogen cycling. KEGG annotations and gene names are listed for each nitrogen metabolism. All gene annotations had e-values of less than 1e-20. MAGs containing nitrogen metabolism genes are highlighted in light grey.

***Granulosicoccus* pangenome reveals high genomic diversity and diverse metabolisms**

We assembled 8 *Granulosicoccus* sp. genomes, with an average genome length of 4,292,108 bp and an average GC content of 49.02%. *Granulosicoccus* sp. MAGs were assembled from samples collected in all 3 years and both locations, with 1 from Squaxin Island in 2019, 2 from Tatoosh Island in 2019, 1 from Tatoosh in 2018, and 4 from Tatoosh in 2017 (Table S4.2). The *Granulosicoccus* sp. MAGs range in completion from 77.5 to 98.6, with 6 MAGs that were >90% complete with <5% contamination (Table S4.2). The demarcation for a bacterial species

using whole-genome average nucleotide identity (ANI) is typically ≥95% (Jain et al. 2018), while ANI values across genera average 73% (Barco et al. 2020). The mean ANI between *Granulosicoccus* sp. MAGs in this study was 81.3%, and the 8 MAGs clustered into 4 distinct clades with ANI > 98% within each clade, likely representing 4 novel species within the genus *Granulosicoccus* (Fig. S4.3). We analyzed the pangenome of the 8 *Granulosicoccus* sp. genomes assembled in this study together with genomes of *Granulosicoccus antarcticus* type strain IMCC3135 (Kang et al. 2018) and *Granulosicoccus* sp. 002746645 (Dudek et al. 2017). The mean ANI between MAGs in this study and the reference genomes was 71.9% for *G. antarcticus* and 70.2% for *Granulosicoccus* sp. 002746645. Two kelp-associated MAGs were more closely related to *G. antarcticus* (>72% ANI) than the others (Fig. S4.3).

The term 'pangenome' describes all of the genes present in all genomes of a given species, which can be subdivided into core genes that are shared by all members of a given species, and accessory genes, present in some but not all genomes of a given species (Brockhurst et al. 2019). The *Granulosicoccus* pangenome contained a core genome of 6,222 genes shared among all 10 genomes (15% of the total number of genes in the pangenome), a large accessory genome of 26,873 genes that were present in at least two but not all genomes (66% of the pangenome), and 7,684 unique genes (19%) that were only present in a single genome (Fig. S4.4). Genes related to amino acid, carbohydrate and lipid transport and metabolism were among the most abundant gene clusters in the core genome (Table S4.6), along with essential cellular functions such as transcription, translation, and cell wall biogenesis. The core genome also contained many gene clusters related to cell motility (Table S4.6).

The *Granulosicoccus* sp. MAGs in this study contained diverse metabolic genes related to DOM transport, nitrogen and sulfur transformation, motility and chemotaxis, aerobic

respiration, and cobalamin (B12) synthesis (Table 4.1, Fig. 4.4). *Granulosicoccus* sp. contained 15 genes for aerobic respiration via the citrate cycle (Fig. 4.4). Surprisingly, *Granulosicoccus* sp. genomes assembled from the kelp surface contained genes for bacteriochlorophyll synthesis and photosystem II reaction center proteins (Table 4.1), making them a novel clade of phototrophic bacteria (detailed below). *Granulosicoccus* sp. has the capacity to harvest light energy with bacteriochlorophyll and photosystem II and generate additional energy with ATP synthase (Fig. 4.4), yet they lack carbon fixation genes, suggesting a photoheterotrophic metabolism. Further, culture studies of *Granulosicoccus* spp. show that they cannot fix carbon and require organic carbon for growth (Lee et al. 2007). *Granulosicoccus* sp. MAGs contained 64 different genes for DOM transport (Fig. 4.2, Fig. 4.4), including proteins that can transport nucleotides, amino acids, oligopeptides, and the sugars xylose, ribose, arabinose, galactoside, fucose and mannitol (Table S4.5). These include ABC-type transporters, indicating active transport. Similar to previously reported motility genes in *G. antarcticus* (Kang et al. 2018), all 8 MAGs contained genes for synthesizing flagella and type IV pili, as well as genes related to chemotaxis (Fig. 4.4, Table 4.1, Table S4.7).

Granulosicoccus sp. MAGs had the capacity to transform both inorganic and organic nitrogen and sulfur. Half of the kelp-associated *Granulosicoccus* sp. genomes contained both assimilatory and dissimilatory nitrate reductases (*nasA*, *narI*), while 6/8 genomes contained dissimilatory nitrite reductases (*nirB*, *nirD*, and *nirK*), indicating the potential for complete dissimilatory nitrate reduction to ammonium (Fig. 4.4, Table 4.1). *G. antarcticus* contained additional nitrate reductases (*narG*, *narY*, *narI*) that were not present in the kelp-associated MAGs (Table S4.7). *G. antarcticus* and kelp-associated *Granulosicoccus* sp. MAGs contained urease genes (*ureABC*), and 6/8 MAGs contained urea transport proteins, indicating the ability to

Table 4.1. Functional categories and metabolisms present in the *Granulosicoccus* pangenome. For the genomes of *G. antarcticus* and *G.* sp. 002746645, presence (+) or absence (-) of each function is indicated. For the kelp-associated *Granulosicoccus* sp. MAGs, X/8 indicates the number of genomes containing genes for each function out of the 8 total genomes.

Functional category	***G. antarcticus***	***G. sp002746645***	***Granulosicoccus* sp. (this study)**
Synthesis of bacteriochlorophyll			
Magnesium chelatase (*bchHI*)	-	-	7/8
Bacteriochlorophyllide reductase (*bchXYZ*)	-	-	7/8
Light-independent protochlorophyllide reductase (*chlLNB*)	-	-	7/8
Photosystem II			
Light-harvesting complex 1 alpha chain (*pufAB*)	-	-	7/8
Photosystem II reaction center (*pufLM*)	-	-	7/8
Photosynthetic reaction center cytochrome c subunit	-	-	7/8
Nitrogen metabolisms			
Nitrate reduction (NO_3 to NO_2)	+	-	4/8
Nitrite reduction (NO_2 to NH_4)	+	-	6/8
Urease (CH_4N_2O to NH_4 and CO_2)	+	-	8/8
Urea transporter	+	-	6/8
Sulfur metabolisms			
Assimilatory sulfate reduction (sulfate to hydrogen sulfide)	+	-	8/8
Thiosulfate oxidation by sox (thiosulfate to sulfate)	+	-	5/8
Sulfide oxidation	+	+	0/8
DMSP transformation	+	-	6/8
Vitamin B12 (cobalamin) biosynthesis			
Corrin ring biosynthesis	+	+	1/8
Cobalt insertion into corrin ring (anaerobic pathway)	-	-	1/8
Cobalt insertion into corrin ring (aerobic pathway)	+	+	8/8
Final B12 biosynthesis & repair	+	+	7/8
Catalyzes B12 into coenzyme form	+	+	8/8
B12 membrane transporter	+	+	7/8
Motility and Chemotaxis			
Motility - Flagella	+	+	8/8
Motility - Type IV pilus	+	+	8/8
Chemotaxis	+	+	8/8

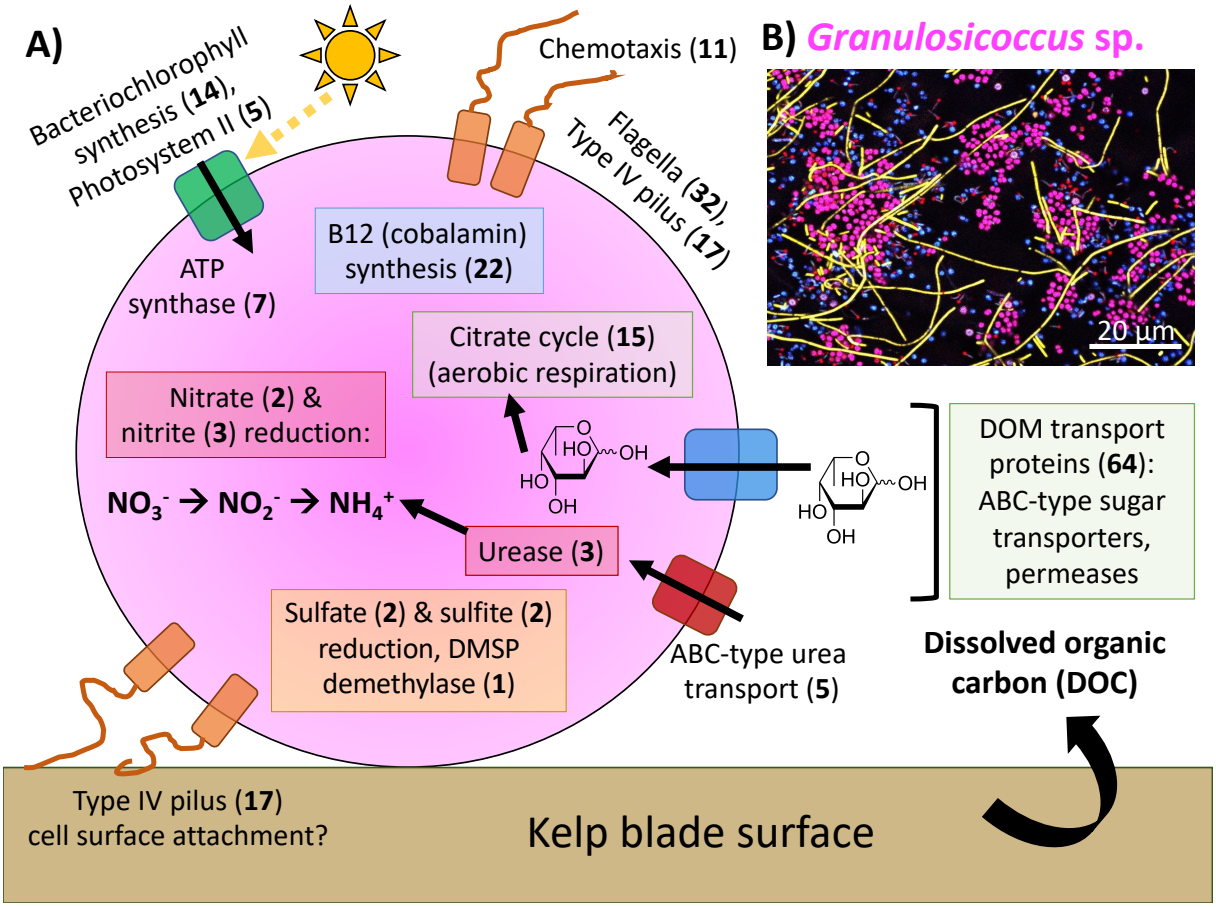

Figure 4.4. A) Conceptual model of the functions and metabolisms of *Granulosicoccus* sp. that are important to its role as a macroalgal symbiont, based on functional gene annotations of 8 MAGs assembled from bull kelp blades. Bold numbers in parentheses indicate the number of unique genes associated with each function. B) Image of the micron-scale spatial structure of the bull kelp surface microbiome depicting clusters of magenta *Granulosicoccus* sp. cells (cocci shaped), adapted with permission from Ramirez-Puebla et al. (2020).

transport urea into the cell and hydrolyze it into ammonium and carbon dioxide (Fig. 4.4, Table 4.1). *G. antarcticus* and all kelp-associated MAGs contained genes for assimilatory sulfate reduction (*cysNC*, *cysH*, *cysI*, *cysJ*), while 5/8 MAGs contained *sox* genes for thiosulfate oxidation to sulfate (Fig. 4.4, Table 4.1, Table S4.7). As reported previously for *G. antarcticus* (Kang et al. 2018), 6/8 MAGs contained dimethylsulfoniopropionate (DMSP) demethylase (*dmdA*), which is the only enzyme known to demethylate DMSP (Fig. 4.4, Table 4.1).

Finally, *Granulosicoccus* sp. MAGs contained many of the genes necessary for cobalamin (vitamin B12) synthesis (Fig. 4.4, Table S4.7). While only one MAG (g3_MAG_00002) contained all 22 genes necessary for complete synthesis of B12, including 11 genes involved in corrin ring synthesis, 7 out of 8 MAGs contained at least 10 genes for B12 biosynthesis (Table 4.1, Table S4.7). Further, all 8 MAGs contained the genes to catalyze B12 into its coenzyme form as well as insert cobalt into the corrin ring through the aerobic pathway (*cobS*, *cobT*), and 7 out of 8 genomes contained the B12 membrane transporter gene *btuB* (Table 4.1, Table S4.7). Interestingly, the MAG with a complete biosynthesis pathway also contained genes for insertion of cobalt into the corrin ring through both aerobic and anerobic pathways (Table S4.7). Other bacterial taxa contained many of the required genes for B12 biosynthesis, with the number of B12 biosynthesis genes indicated in parentheses, including the *Gammaproteobacteria* UBA7415 (16 genes) and *Arenicella* sp. (9 genes) and the *Alphaproteobacteria Ascidiaceihabitans* sp. (11 genes) and *Flavimaricola* sp. (14 genes).

While a full kelp genome would confirm that *N. luetkeana* requires B12, we found genes for the B12-dependent (cobalamin-binding) methylmalonyl-CoA mutase (MCM) in the partial host kelp genomes in both samples extracted from whole kelp tissues. Using nucleotide BLAST, these genes matched with 87% sequence identity to a methylmalonyl-CoA mutase from *Crassostrea virginica*, and another copy matched with 85% sequence identity to a hypothetical protein from *Phytophthora parasitica* (eukaryote in the *Oomycota*, closely related to kelp), indicating that they are eukaryotic MCM genes. If the host kelp has this B12-dependent enzyme, it requires vitamin B12 (Helliwell et al. 2011, Grossman 2016) and may be dependent on associated bacteria for B12 synthesis.

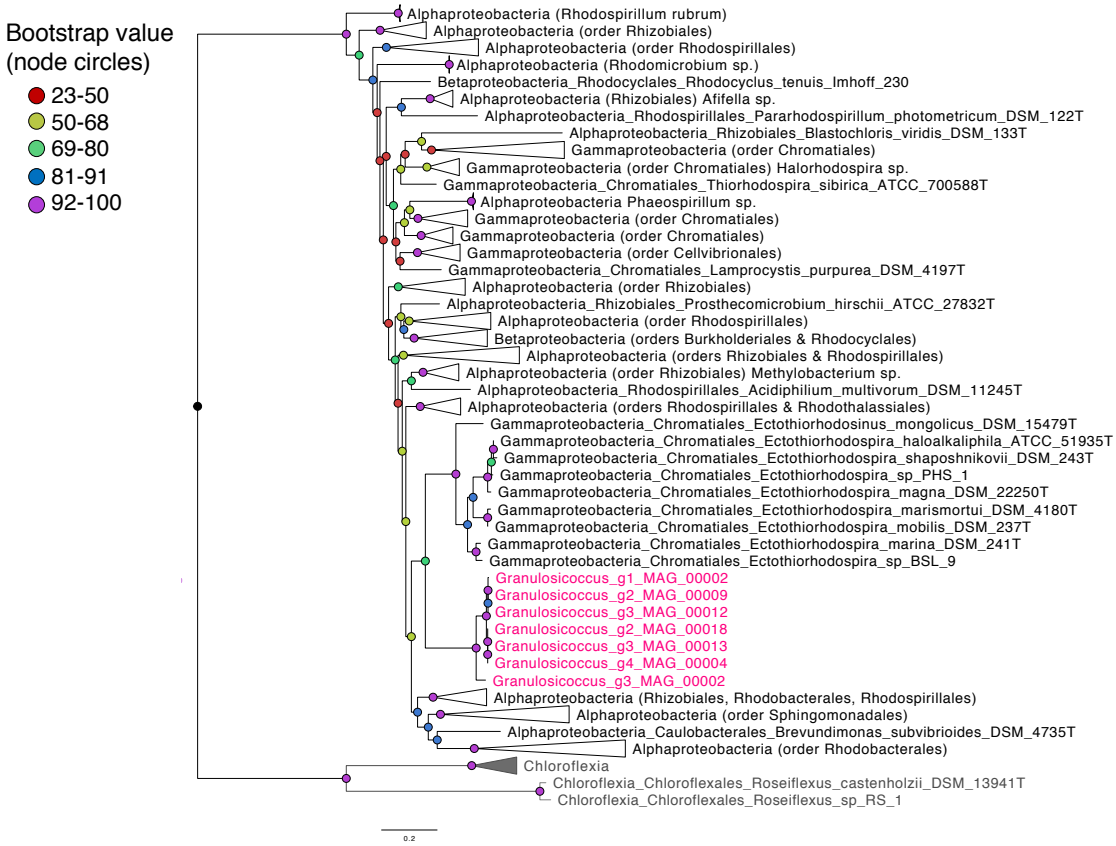

Figure 4.5. A maximum-likelihood phylogenetic tree showing the position of *Granulosicoccus* sp. *pufLM* sequences (indicated in pink) in relation to photosystem II reaction center *pufLM* sequences from other known lineages of aerobic anoxygenic phototrophic bacteria. Bootstrap support values are color-coded at the nodes. The clade containing sequences from *Granulosicoccus* sp. and *Ectothiorhodospira* spp. has a bootstrap support of 76.

***Granulosicoccus* sp. as a new lineage of aerobic anoxygenic phototrophic bacteria**

Seven out of eight of the *Granulosicoccus* sp. MAGs in our study contained a full suite of genes that typify the aerobic anoxygenic phototrophic bacteria (Imhoff et al. 2018), including bacteriochlorophyll synthesis and photosystem II reaction center proteins (Table 4.1). There were 14 genes for bacteriochlorophyll synthesis, including magnesium chelatase (*bchHI*), bacteriochlorophyllide reductase (*bchXYZ*) and protochlorophyllide reductase (*chlLNB*), and 5 genes for harvesting light energy through photosystem II reaction center proteins (*pufAB*, *pufLM*, Table 4.1, Table S4.5). Surprisingly, neither *G. antarcticus* IMCC3135 nor *Granulosicoccus* sp.

002746645 had these genes, with the exception of a single magnesium chelatase gene (*bchI*) in *G. antarcticus*, which lacks the other 18 bacteriochlorophyll synthesis and photosystem II genes.

To confirm that kelp associated *Granulosicoccus* sp. are a novel lineage of aerobic anoxygenic phototrophic bacteria, we inferred a phylogenetic tree with the photosystem II reaction center genes (*pufL* and *pufM*) from each *Granulosicoccus* sp. MAG together with a reference database of 167 *pufL* and *pufM* sequences from Imhoff et al. (2018). Photosystem II protein sequences from *Granulosicoccus* sp. MAGs in this study form a highly supported clade (bootstrap support 76) with *pufM* sequences from *Ectothiorhodospira* spp., which also belongs to the order *Chromatiales* (Fig. 4.5). However, we note that all of the *pufM* protein sequences within the *Proteobacteria* are closely related, and sequences from the *Alpha*-, *Beta*- and *Gammaproteobacteria* are intermixed and do not form monophyletic clades (Fig. 4.5).

Finally, *Granulosicoccus* sp. does not appear to have the enzymes necessary to fix carbon with this light energy. Key enzymes for the reverse tricarboxylic acid cycle (Campbell and Cary 2004) were absent, including ATP citrate lyase (*aclA*, *aclB* genes) and the CO_2-fixing enzyme subunits of pyruvate ferredoxin oxidoreductase (*porABCD*). Further, *Granulosicoccus* sp. lacks genes that code for the CO_2-fixing enzyme of the Calvin cycle, RuBisCo (*cbbLM*, *rbcLS*). Therefore, the kelp-associated *Granulosicoccus* sp. MAGs in this study are most likely photoheterotrophs, harvesting light energy with bacteriochlorophyll and photosystem II as an extra energy source while consuming organic carbon, likely from kelp-derived DOC.

Discussion

Bacterial taxa persist over multiple years and distant geographic locations

N. luetkeana is an annual kelp species that grows from microscopic gametophytes into large sporophytes (5-40 m tall) by mid-summer, and adult sporophytes generally do not survive

through the winter (Foreman 1984, Maxell and Miller 1996). Despite this life history, 31 MAGs (47% of the total) were detected across multiple years on *N. luetkeana* blades from Tatoosh. This remarkable continuity demonstrates that the same bacterial taxa can persist across years on a host that is only seasonally abundant, suggesting the presence of a bacterial reservoir during the months when bull kelp sporophytes are absent. Potential reservoirs include the seawater, where kelp-associated bacteria are found at low abundances (Weigel and Pfister 2019), rocky substrates (Lemay et al. 2021), perennial kelp species (Lemay et al. 2018), or overwintering kelp gametophytes, which deserves further study. The most abundant bacterial genomes on *N. luetkeana* blades included *Granulosicoccus* sp. (*Gammaproteobacteria*), *Hellea* sp. (*Alphaproteobacteria*), *Dokdonia* sp. (*Bacteroidetes*), *Phycisphaera* sp. and *Mariniblastus* sp. (*Planctomycetes*), and the family *Akkermansiaceae* (*Verrucomicrobia*). Because many of the abundant MAGs and those that persisted across years contained genes for nitrogen reduction and B12 biosynthesis, discussed below, thus we hypothesize that these abundant and persistent members of the kelp microbiome may be functionally important to the host kelp.

In addition to persisting across years, 15 MAGs (23% of the total) were detected on bull kelp from both Tatoosh and Squaxin Island populations, which are geographically separated by the length of Puget Sound and the Strait of Juan de Fuca (~300 km). Bull kelp forests in southern Puget Sound have declined 63% over the last century, with continued declines at Squaxin Island (Berry et al. 2021), while kelp forests on the outer coast at Tatoosh Island have been relatively stable over the same historical period (Pfister et al. 2018). We previously found that bull kelp from the declining population at Squaxin Island have lower bacterial cell abundances and a different composition of microbes compared to kelp from Tatoosh Island (Weigel and Pfister 2019, Ramirez-Puebla et al. 2020). While in 2017 16S rRNA gene sequencing revealed that the

Alphaproteobacteria Robiginitomaculum sp. was most abundant on bull kelp from Squaxin Island and *Granulosicoccus* sp. was most abundant at Tatoosh Island (Weigel and Pfister 2019), metagenomic sequencing revealed that *Granulosicoccus* sp. was the most abundant bacteria at both sites in 2019 (Table S4.4). However, two different genomes of *Granulosicoccus* sp. that are likely to be distinct species were differentially abundant at each location, revealing geographic differences in species-level dynamics that are likely to be missed by 16S gene sequencing. However, the functional gene content was nearly identical between these two differentially abundant sequence variants of *Granulosicoccus* sp. (Table S4.7), indicating no loss of function of the dominant bacterial taxa on declining kelp from Squaxin Island.

Diverse bacteria in the kelp microbiome have the capacity to assimilate DOM

Heterotrophic bacteria rely on organic carbon for biomass production. Canopy-forming kelp contribute significantly to the pool of dissolved organic carbon (DOC) in seawater (Pfister et al. 2019) by releasing approximately 15-30% of their total fixed carbon as DOC (Reed et al. 2015, Weigel and Pfister 2021a, Gao et al. 2021). We found that nearly all members of the kelp microbiome contain genes encoding dissolved organic matter (DOM) membrane transport proteins, which are the primary mechanism for DOM uptake by bacteria (Poretsky et al. 2010). Across 66 unique kelp-associated bacterial genomes, we detected the presence of 72 diverse genes for DOM transport, with a median of 14 different DOM transport genes per genome. The most abundant bacteria on *N. luetkeana*, *Granulosicoccus* sp. (Weigel and Pfister 2019) contained the highest diversity of DOM transport genes, with 53-59 per genome. Genes in kelp-associated bacterial genomes facilitate transport of diverse substrates, including amino acids, oligopeptides, polyamines, lipids and fatty acids, nucleotides, carbohydrates and sugars,

carboxylic acids, and other solutes. Many of the genes specific to amino acids and sugars were ATP-binding cassette (ABC)-type transporters, indicating ATP-hydrolysis-fueled active transport into bacterial cells (Rees et al. 2009). The microbiome of the giant kelp *M. pyrifera* was also enriched in transport protein genes relative to metagenomes from the surrounding seawater (Minich et al. 2018), suggesting that DOM assimilation may be a common feature of kelp surface-associated bacteria.

While the chemical composition of the DOM released by *N. luetkeana* is unknown, kelp are known to release monosaccharides including mannitol, fucose, ribose, xylose, and galactose (Newell et al. 1980, Wada et al. 2007), which are all compounds encoded by bacterial DOM transport proteins identified in this study. Kelp-associated bacterial genomes also contained many amino acid transporters. Analogous interactions between phytoplankton and heterotrophic bacteria demonstrate that carbohydrates and amino acids are secreted by phytoplankton, while associated bacteria provide their host with reduced nitrogen and vitamins such as B12 (Luo and Moran 2014, Amin et al. 2015, Seymour et al. 2017). While we cannot infer from genomic content alone that these DOM transport proteins are being expressed, they are good indicators of potential kelp-derived DOM use by members of the kelp microbiome. Further research should use isotope tracer or culture-based studies to demonstrate that biomass production of kelp-associated bacterial taxa is fueled by DOM released by the host kelp.

Kelp-associated bacteria reduce oxidized nitrogen sources to ammonium

The annual kelp *N. luetkeana* grows extraordinarily fast, producing 1-6 cm of new blade tissue per day (Maxell and Miller 1996), and achieve high dissolved inorganic nitrogen uptake rates (Gerard 1982, Ahn et al. 1998, Weigel and Pfister 2021a), indicating a high demand for

inorganic nitrogen to support their rapid biomass production. Bacterial genomes from the *Proteobacteria*, *Verrucomicrobia*, and *Planctomycetes* contained one or more genes for assimilatory nitrate reduction, dissimilatory nitrate and nitrite reduction, and urea hydrolysis, indicating that they reduce oxidized nitrogen compounds to ammonium. Genomes of *Granulosicoccus* sp. contained both dissimilatory nitrate and nitrite reduction genes, indicating complete reduction to ammonium. While it may seem surprising to find dissimilatory nitrate reduction, an anaerobic process, associated with a photosynthetic host, kelp blades generate oxygen-depleted conditions at night through respiration (Noisette and Hurd 2018). Genes for nitrate and nitrite reduction were also enriched in the surface microbiome of the giant kelp *Macrocystis pyrifera* compared to seawater metagenomes (Minich et al. 2018). Ammonium is the most energetically preferable form of dissolved inorganic nitrogen for algae, as it can be directly incorporated into amino acids without expending energy on intracellular nitrate reduction (Solomonson and Barber 1990, Lobban and Harrison 1994). While nitrate concentrations are higher than those of ammonium on the coast of Washington during the summer (Pfister et al. 2007), we found that bull kelp blades assimilate ammonium 1.5 times faster than nitrate relative to its availability (Weigel and Pfister 2021a), indicating a preference for the more reduced form of nitrogen. Finally, surface-associated bacteria also likely compete directly with the host kelp for nitrogen in the seawater (Kirchman 1994), as kelp-associated MAGs also contained assimilatory nitrate reduction genes.

Like dissimilatory nitrate reduction, urea hydrolysis generates ammonium as a reduced nitrogen source that may be favorable to the host kelp. Urea is a nitrogenous waste product excreted by common marine animals, including zooplankton (Cass and Daly 2014). Diverse taxa from the *Proteobacteria* (UBA7415, *Ascidiaceihabitans* sp., *Flavimaricola* sp., and

Granulosicoccus sp.), *Verrucomicrobia* (family *Akkermansiaceae*), and *Planctomycetes* (*Phycisphaera* sp.) contained genes for urease (*ureABC*), which catalyzes the hydrolysis of urea into ammonium and carbon dioxide. Urea can constitute a significant proportion (~20%) of the dissolved nitrogen pool in coastal seawater, and the giant kelp *M. pyrifera* can assimilate urea from the seawater (Smith et al. 2018). However, macroalgae still need to expend energy to hydrolyze urea into ammonium after assimilation (Bekheet and Syrett 1977). Despite the presence of these genes, it is still unknown whether ammonium generated through dissimilatory nitrate reduction or urea hydrolysis is accessible to the host kelp, or whether it remains in bacterial cells. Future studies should test the hypothesis that kelp-associated bacteria provide reduced nitrogen to their host kelp.

Kelp-associated *Granulosicoccus* sp. are motile, photoheterotrophic, nitrogen and sulfur transforming microbes with the potential to synthesize cobalamin (B12)

The genus *Granulosicoccus*, belonging to the order *Chromatiales* within the class *Gammaproteobacteria*, currently contains 4 described species isolated from Antarctic seawater (Lee et al. 2007, Baek et al. 2014), the seagrass *Zostera marina* (Kurilenko et al. 2010), and the kelp *Undaria pinnatifida* (Park et al. 2014). *Granulosicoccus* sp. is the most abundant bacteria associated with *N. luetkeana* (Weigel and Pfister 2019), reaching densities of up to 10^6 cells per cm^2 on kelp blades (Ramirez-Puebla et al. 2020). Bacteria in the genus *Granulosicoccus* associate with diverse kelp species (Bengtsson et al. 2012, Jo et al. 2019, Weigel and Pfister 2019, James et al. 2020, Quigley et al. 2020, Lemay et al. 2021) and other red, green and brown algal hosts (Singh and Reddy 2014). Only a single annotated genome is available for this bacterial genus in the literature, belonging to the free-living *Granulosicoccus antarcticus* type

strain IMCC3135 (Kang et al. 2018). Here, we reconstructed 8 MAGs of *Granulosicoccus* associated with blades of the bull kelp *N. luetkeana* which share, on average, only 71.9% similarity with *G. antarcticus*. The *Granulosicoccus* genomes assembled from the kelp surface likely represent 4 new species belonging to the genus *Granulosicoccus*, as they formed 4 distinct clades with ANI > 98% within each clade (Fig. S4.3). Kelp-associated *Granulosicoccus* sp. had large genomes (~4.3 Mbp), consistent with the large genome of *G. antarcticus* that is also enriched in genes for carbohydrate and amino acid transport and metabolism relative to other bacteria in the order *Chromatiales* (Kang et al. 2018).

Kelp-associated *Granulosicoccus sp.* are motile and likely chemotactic, providing a mechanism for colonizing kelp tissues from the seawater and reaching high abundances on new kelp blade meristem tissues (Bengtsson et al. 2012, Ramirez-Puebla et al. 2020, Weigel and Pfister 2021b, Lemay et al. 2021). *Granulosicoccus* sp. genomes contained 32 flagellar genes and 11 chemotaxis genes, including two-component system chemotaxis proteins and genes for rotation of the flagellar motor (Table S4.7). The motility of *G. antarcticus* is achieved through numerous tufts of flagella (Lee et al. 2007). All *Granulosicoccus* sp. genomes also contained up to 17 type IV pilus assembly protein genes, which are known to be involved in biofilm formation and adhesion to host cells (Ligthart et al. 2020). On the kelp surface, *Granulosicoccus sp.* cells are closely associated with kelp cells at the base of the biofilm (Ramirez-Puebla et al. 2020), possibly mediated by type IV pili.

Granulosicoccus sp. belongs to the order *Chromatiales*, also known as purple sulfur bacteria because they are usually phototrophic and contain carotenoid and bacteriochlorophyll pigments (Tank et al. 2009, Imhoff et al. 2018). While previous isolates of *Granulosicoccus* are obligately chemoheterotrophic (Lee et al. 2007, Kang et al. 2018), we found genomic evidence

that kelp-associated *Granulosicoccus* sp. have the capacity to harvest light energy with bacteriochlorophyll and photosystem II (PSII) reaction center proteins. Genes for CO_2-fixation were absent, suggesting a photoheterotrophic metabolism. PSII reaction center genes (*pufLM*) from *Granulosicoccus* sp. MAGs formed a clade with *pufLM* genes from *Ectothiorhodospira* spp. (Fig. 5), another genus in the order *Chromatiales*. While many purple sulfur bacteria are anaerobic (Imhoff et al. 2018), *Granulosicoccus* sp. MAGs contained genes for aerobic respiration via the citrate cycle, and *G. antarcticus* is obligately aerobic (Lee et al. 2007). Therefore, the *Granulosicoccus* sp. from this study likely represent a novel reported lineage of aerobic anoxygenic phototrophic (AAP) bacteria. As photoheterotrophs, AAP bacteria have the capacity to generate ATP with light energy, providing extra energy for the cell that increases their growth efficiency and gives them a competitive advantage over other heterotrophic bacteria (Koblížek 2015, Ferrera et al. 2017, Piwosz et al. 2020). This energetic advantage may allow them to reach high abundances and form large cell clusters on bull kelp blade surfaces (Ramirez-Puebla et al. 2020). Canopy kelp, which maintain their position in the water column with floats, likely provide ideal habitats for AAP bacteria that benefit from both sunlight exposure and a constant supply of organic carbon resources. AAP bacteria associate with other macroalgae and phytoplankton, including phytoplankton-associated members of the *Roseobacter* clade (Wagner-Döbler et al. 2010, Koblížek 2015), and they likely consume phytoplankton-exuded DOC (Piwosz et al. 2020). While AAP bacteria associated with macroalgae have a constant supply of organic carbon and may not be energy limited, we hypothesize that supplemental energy from photoheterotrophy may also help *Granulosicoccus* sp. during times when it is not host-associated.

The genomes of kelp-associated *Granulosicoccus* sp. encoded carbon assimilation, nutrient transformation and vitamin biosynthesis genes that are hypothesized to play a central role in kelp-microbe interactions. As they require organic carbon for growth, *Granulosicoccus sp.* MAGs contained 50+ different genes for carbohydrate and DOM transport, likely to assimilate kelp-derived dissolved organic carbon resources (Weigel and Pfister 2021a). The most complete (98.6%) *Granulosicoccus* sp. MAG contained 22 genes for complete biosynthesis of vitamin B12 (cobalamin), while 7 out of 8 MAGs contained at least 10 genes for B12 biosynthesis. Bacteria are the only organisms known to synthesize vitamin B12, thus diverse algae rely on associated bacteria to produce vitamin B12 (Croft et al. 2005, Wagner-Döbler et al. 2010), and brown algae are no exception (Dogs et al. 2017). While a full genome of *N. luetkeana* may be necessary to confirm this finding (Helliwell et al. 2011), kelp host genomic content contained the B12-dependent enzyme methylmalonyl-CoA mutase. This enzyme requires B12 as a cofactor to catalyze an essential catabolic reaction in the mitochondria (Helliwell et al. 2011, Grossman 2016), suggesting that *N. luetkeana* requires vitamin B12. However, culture studies are necessary to determine whether B12 is released extracellularly by kelp-associated bacteria. In addition to B12 synthesis, kelp-associated *Granulosicoccus* sp. genomes contained genes for dissimilatory nitrate reduction and urease, which we hypothesize may provide kelp with reduced nitrogen as ammonium. *Granulosicoccus sp.* genomes also contained genes for sulfur metabolisms including assimilatory sulfate reduction, thiosulfate oxidation, and DMSP demethylation. Closely related bacteria in the family *Granulosicoccaceae* are capable of chemolithotrophic growth by oxidizing sulfur compounds (Kojima and Fukui 2016), but the function of these oxidative and reductive sulfur metabolisms in *Granulosicoccus* sp. have yet to be determined (Kang et al. 2018). DMSP demethylase (*dmdA*) is the only enzyme known to

demethylate DMSP (Kang et al. 2018), an organic sulfur compound produced by algae that plays a significant role in the global sulfur cycle (Yoch 2002). Members of the *Roseobacter* clade metabolize phytoplankton-exuded DMSP as a reduced carbon and sulfur source, and they provide phytoplankton with vitamin B12 (Luo and Moran 2014, Seymour et al. 2017), which may be an analogous mutualistic exchange to that between *Granulosicoccus* sp. and kelp.

Conclusions

We reconstructed 79 bacterial metagenome assembled genomes (MAGs) from blades of the bull kelp, *N. luetkeana*, allowing us to match the taxonomic identities of members of the kelp microbiome with their metabolic diversity and functional roles. Bacterial genomes revealed the metabolic potential of the kelp microbiome and illuminated functions that may be important, both for host-microbe interactions as well as nutrient cycling in kelp forest ecosystems. Diverse members of the kelp microbiome, spanning 6 bacterial phyla and 18 families, contained genes for transporting and assimilating DOM, thus the kelp surface microbiome is likely to be a hotspot for organic matter assimilation, and potentially remineralization. Kelp secrete large quantities of fixed carbon into the seawater as DOC, which likely fuels heterotrophic bacteria like *Granulosicoccus* sp., whose genomes contain many DOM transport genes. Bacteria on the kelp surface are positioned at the interface between kelp tissues and the surrounding seawater, and their metabolisms may alter the abundance and forms of inorganic nutrients available to kelp. We found that kelp-associated bacteria reduce oxidized nitrogen sources to ammonium through dissimilatory nitrate reduction and urea hydrolysis, which we hypothesize could provide the kelp with a source of reduced nitrogen. Genomes of the most abundant bacteria on the surface of *N. luetkeana* contained a full suite of genes for synthesizing cobalamin (vitamin B12) while the kelp

host contained a B12-dependent enzyme, suggesting that kelp-associated bacteria have the potential to provide their host kelp with vitamins. Finally, we reconstructed 8 MAGs of the common macroalgal symbiont *Granulosicoccus* sp., demonstrating that they are motile microbes that reduce oxidized forms of nitrogen into ammonium. We also discovered that kelp-associated *Granulosicoccus* sp. are aerobic anoxygenic phototrophic bacteria, making them the first photoheterotrophic representatives of the genus *Granulosicoccus*.

Appendix 4.1: Supplemental Tables and Figures for Chapter 4

*Note: Appendix 4.1 Tables are in included as Supplementary File 1

Table S4.1. List of metagenome samples, co-assembled samples, and sequence reads.

Table S4.2. List of all 79 metagenome assembled genomes (MAGs), length, completion, redundancy, and taxonomy.

Table S4.3. Detection of all MAGs across kelp blade samples.

Table S4.4. Abundance of the top 20 MAGs across kelp blade samples. The top 5 MAGs most abundant MAGs across all samples are bolded.

Table S4.5. List of DOM transporter genes, COG numbers, and descriptions.

Table S4.6. List of core gene clusters and functions in the *Granulosicoccus* pangenome.

Table S4.7. Detailed list of functional genes in the *Granulosicoccus* pangenome and presence (+) or absence (blank) across all 10 *Granulosicoccus* genomes.

Chapter 4 Supplemental Figures:

Figure S4.1. A maximum-likelihood phylogenetic tree showing the 66 non-redundant bacterial MAGs assembled from kelp blades, with branches colored by bacterial phyla. Bootstrap support values are indicated by different colored circles at the nodes.

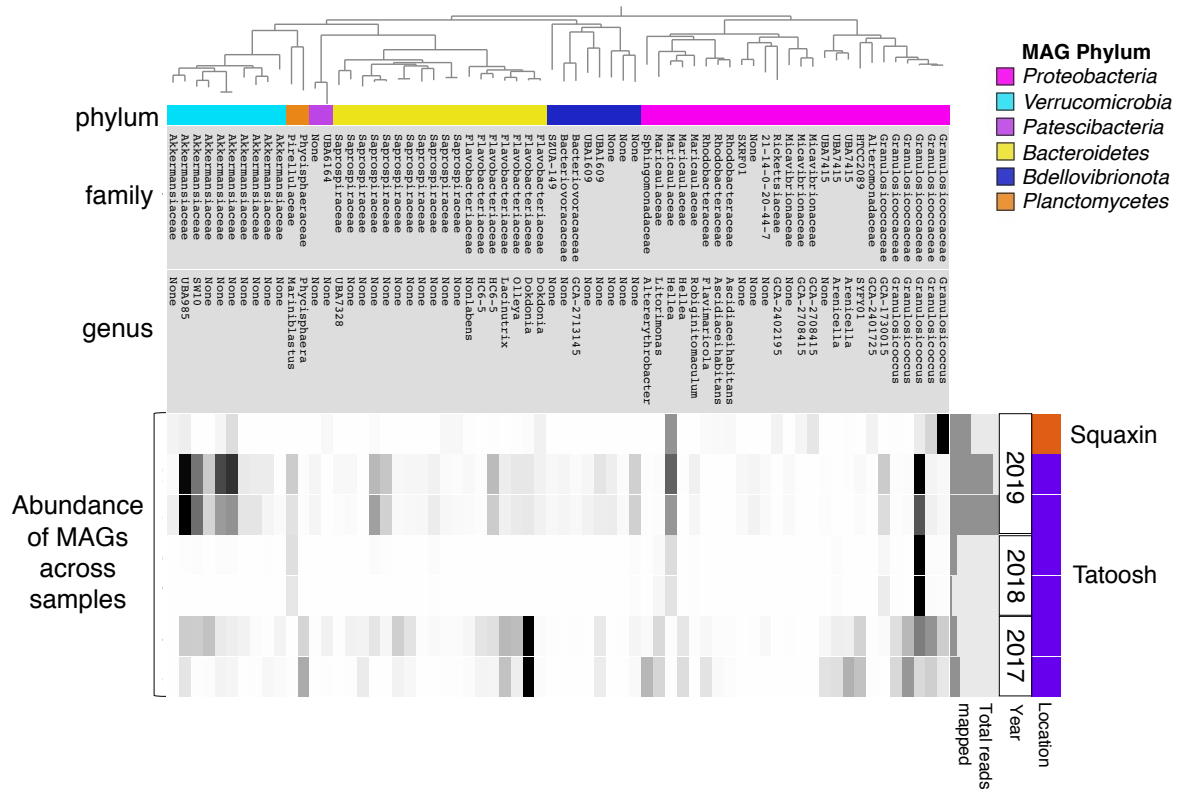

Figure S4.2. A maximum-likelihood phylogenetic tree of kelp-associated MAGs (top), colored by bacterial phylum with the family and genus level taxonomy listed for each MAG, showing the abundance of MAGs across different kelp metagenome samples (below). Dark bars (black and grey) indicate high MAG abundance in a sample, while light grey bars indicate low abundance. Samples are grouped by location and year, and the small bar graph to the right shows the total number of short reads mapped to all MAGs in each metagenome sample.

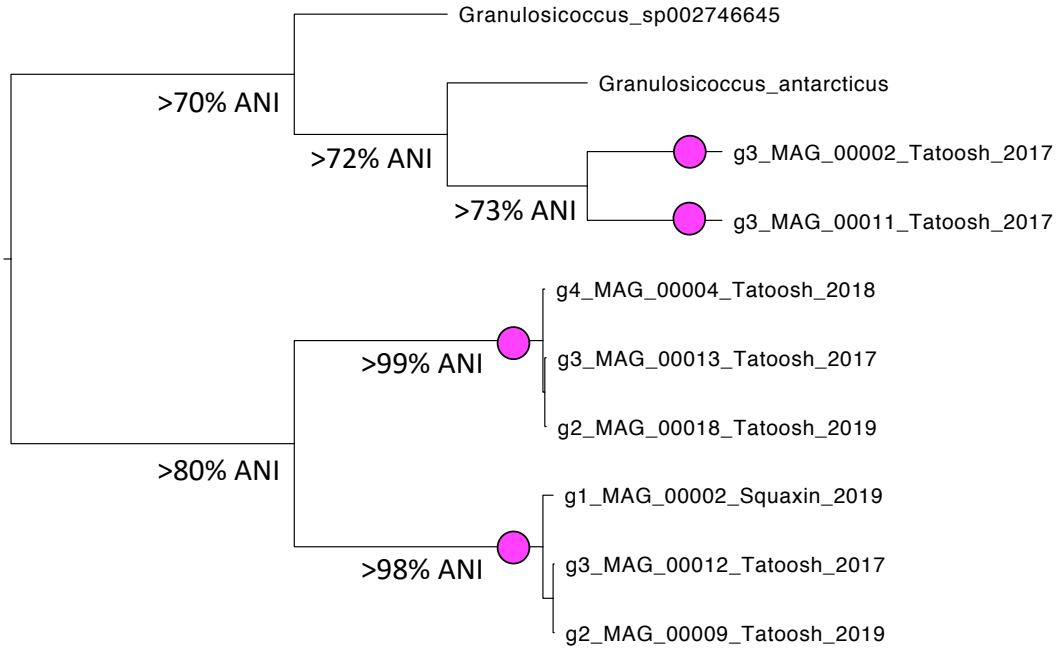

Figure S4.3. Tree of *Granulosicoccus* genomes, including 8 kelp-associated MAGs and two reference genomes, *Granulosicoccus antarcticus* and *Granulosicoccus* sp. 002746645. For each clade, the minimum average nucleotide identity (ANI) among all genomes is listed. The kelp-associated *Granulosicoccus* MAGs from this study fall into four distinct clades with >98% ANI, indicated by pink circles, likely representing four distinct species.

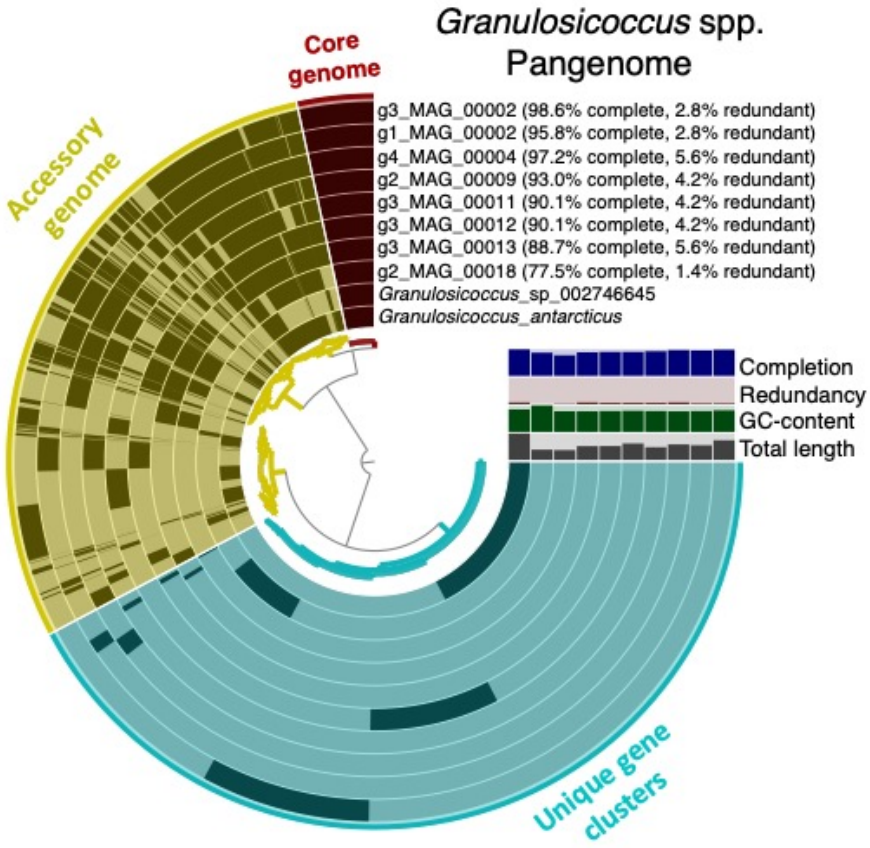

Figure S4.4. Pangenome representing 10 *Granulosicoccus* genomes, including 8 *Nereocystis*-associated MAGs and two reference genomes, *Granulosicoccus antarcticus* type strain IMCC3135 and *Granulosicoccus* sp. 002746645. Each concentric circle represents a bacterial genome, broken down into core gene clusters shared by all 10 genomes, accessory gene clusters present in at least 2 but not all genomes, and unique gene clusters present only in a single genome. Black indicates the presence of a gene cluster in a genome. The inset bar graphs show genome completion in blue, redundancy in red, GC content in green, and genome length in grey.

REFERENCES

Abdullah, M. I., and S. Fredriksen. 2004. Production, respiration and exudation of dissolved organic matter by the kelp *Laminaria hyperborea* along the west coast of Norway. Journal of the Marine Biological Association of the United Kingdom 84:887–894.

Ahn, O., R. J. Petrell, and P. J. Harrison. 1998. Ammonium and nitrate uptake by *Laminaria saccharina* and *Nereocystis luetkeana* originating from a salmon sea cage farm. Journal of Applied Phycology 10:333–340.

Aires, T., Serrão, E. A., and Engelen, A. H. 2016. Host and environmental specificity in bacterial communities associated to two highly invasive marine species (genus *Asparagopsis*). Frontiers in Microbiology 7. doi:10.3389/fmicb.2016.00559.

Aluwihare, L. I., D. J. Repeta, and R. F. Chen. 1997. A major biopolymeric component to dissolved organic carbon in surface sea water. Nature 387:166–169.

Amin, S. A., L. R. Hmelo, H. M. van Tol, B. P. Durham, L. T. Carlson, K. R. Heal, R. L. Morales, C. T. Berthiaume, M. S. Parker, B. Djunaedi, A. E. Ingalls, M. R. Parsek, M. A. Moran, and E. V. Armbrust. 2015. Interaction and signalling between a cosmopolitan phytoplankton and associated bacteria. Nature 522:98–101.

Anderson, M. J., and Willis, T. J. 2003. Canonical analysis of principal coordinates: a useful method of constrained ordination for ecology. *Ecology* 84, 511–525.

Arnold, K., and S. Manley. 1985. Carbon allocation in *Macrocystis pyrifera* (*Phaeophyta*): intrinsic variability in photosynthesis and respiration. Journal of Phycology 21:154–167.

Baek, K., A. Choi, I. Kang, M. Im, and J.C. Cho. 2014. *Granulosicoccus marinus* sp. nov., isolated from Antarctic seawater, and emended description of the genus *Granulosicoccus*. International Journal of Systematic and Evolutionary Microbiology 64:4103–4108.

Baines, S. B., and M. L. Pace. 1991. The production of dissolved organic matter by phytoplankton and its importance to bacteria: Patterns across marine and freshwater systems. Limnology and Oceanography 36:1078–1090.

Barco, R. A., G. M. Garrity, J. J. Scott, J. P. Amend, K. H. Nealson, and D. Emerson. 2020. A genus definition for Bacteria and Archaea based on a standard genome relatedness index. mBio 11:e02475-19, /mbio/11/1/mBio.02475-19.atom.

Barns, A., and P. Kalvass. 1993. Bull kelp, *Nereocystis luetkeana*, abundance in Van Damme Bay, Mendocino County, California. State of California Dept. of Fish and Game Administrative Report No. 93-6:15.

Barrón, C., E. T. Apostolaki, and C. M. Duarte. 2014. Dissolved organic carbon fluxes by seagrass meadows and macroalgal beds. Frontiers in Marine Science 1:1-11.

Becker, S., J. Tebben, S. Coffinet, K. Wiltshire, M. H. Iversen, T. Harder, K.-U. Hinrichs, and J.-H. Hehemann. 2020. Laminarin is a major molecule in the marine carbon cycle. Proceedings of the National Academy of Sciences 117:6599–6607.

Beinart, R. A. 2019. The significance of microbial symbionts in ecosystem processes. mSystems 4:e00127-19, /msystems/4/3/msys.00127-19.atom.

Bekheet, I. A., and P. J. Syrett. 1977. Urea-degrading enzymes in algae. British Phycological Journal 12:137–143.

Bengtsson, M. M., and L. Øvreås. 2010. *Planctomycetes* dominate biofilms on surfaces of the kelp *Laminaria hyperborea*. BMC Microbiology 10:261.

Bengtsson, M. M., K. Sjøtun, A. Lanzén, and L. Øvreås. 2012. Bacterial diversity in relation to secondary production and succession on surfaces of the kelp *Laminaria hyperborea*. The ISME journal 6:2188.

Bengtsson, M., K. Sjøtun, J. Storesund, and J. Øvreås. 2011. Utilization of kelp-derived carbon sources by kelp surface-associated bacteria. Aquatic Microbial Ecology 62:191–199.

Bengtsson, M., Sjøtun, K., and Øvreås, L. 2010. Seasonal dynamics of bacterial biofilms on the kelp *Laminaria hyperborea*. Aquatic Microbial Ecology 60: 71–83.

Bergauer, K., A. Fernandez-Guerra, J. A. L. Garcia, R. R. Sprenger, R. Stepanauskas, M. G. Pachiadaki, O. N. Jensen, and G. J. Herndl. 2018. Organic matter processing by microbial communities throughout the Atlantic water column as revealed by metaproteomics. Proceedings of the National Academy of Sciences 115:E400–E408.

Berman, T. 1976. Release of dissolved organic matter by photosynthesizing algae in Lake Kinneret, Israel. Freshwater Biology 6:13–18.

Berry, H. D., T. F. Mumford, B. Christiaen, P. Dowty, M. Calloway, L. Ferrier, E. E. Grossman, and N. R. VanArendonk. 2020. Long-term changes in kelp forests in an inner basin of the Salish Sea. bioRxiv. 10.1101/2020.02.13.947309

Berry, H. D., T. F. Mumford, B. Christiaen, P. Dowty, M. Calloway, L. Ferrier, E. E. Grossman, and N. R. VanArendonk. 2021. Long-term changes in kelp forests in an inner basin of the Salish Sea. PLOS ONE 16:e0229703.

Bidwell, R. G. S. 1967. Photosynthesis and metabolism in marine algae: VII. Products of photosynthesis in fronds of *Fucus vesiculosus* and their use in respiration. Canadian Journal of Botany 45:1557–1565.

Bjørnsen, P. K. 1988. Phytoplankton exudation of organic matter: Why do healthy cells do it? Limnology and Oceanography 33:151–154.

Blain, C. O., and N. T. Shears. 2019. Seasonal and spatial variation in photosynthetic response of the kelp *Ecklonia radiata* across a turbidity gradient. Photosynthesis Research 140:21-38.

Bondoso, J., Balagué, V., Gasol, J. M., and Lage, O. M. 2014. Community composition of the *Planctomycetes* associated with different macroalgae. FEMS Microbiology Ecology 88, 445–456. doi:10.1111/1574-6941.12258.

Bowers, R. M., N. C. Kyrpides, R. Stepanauskas, M. Harmon-Smith, D. Doud, T. B. K. Reddy, et al. 2017. Minimum information about a single amplified genome (MISAG) and a metagenome-assembled genome (MIMAG) of bacteria and archaea. Nature Biotechnology 35:725–731.

Bowman, J.P. 2014. The Family *Colwelliaceae*. In *The Prokaryotes*. Rosenberg, E., DeLong, E.F., Lory, S., Stackebrandt, E., and Thompson, F. (eds). Springer, pp. 179–195.

Brockhurst, M. A., E. Harrison, J. P. J. Hall, T. Richards, A. McNally, and C. MacLean. 2019. The ecology and evolution of pangenomes. Current Biology 29:R1094–R1103.

Brown, M. T., Nyman, M. A., Keogh, J. A., and Chin, N. K. M. 1997. Seasonal growth of the giant kelp *Macrocystis pyrifera* in New Zealand. Marine Biology 129, 417–424.

Bryantseva, I., Gorlenko, V.M., Kompantseva, E.I., Imhoff, J.F., Süling, J., et al. 1999. *Thiorhodospira sibirica* gen. nov., sp. nov., a new alkaliphilic purple sulfur bacterium from a Siberian soda lake. International Journal of Systematic and Evolutionary Microbiology 49: 697–703.

Burke, C., Steinberg, P., Rusch, D., Kjelleberg, S., and Thomas, T. 2011. Bacterial community assembly based on functional genes rather than species. Proceedings of the National Academy of Sciences 108, 14288–14293. doi:10.1073/pnas.1101591108.

Callahan, B. J., McMurdie, P. J., Rosen, M. J., Han, A. W., Johnson, A. J. A., and Holmes, S. P. 2016. DADA2: High-resolution sample inference from Illumina amplicon data. Nature Methods 13, 581–583. doi:10.1038/nmeth.3869.

Campbell, B. J., and S. C. Cary. 2004. Abundance of reverse tricarboxylic acid cycle genes in free-living microorganisms at deep-sea hydrothermal vents. Applied and Environmental Microbiology 70:6282–6289.

Caporaso, J. G., Lauber, C. L., Walters, W. A., Berg-Lyons, D., Huntley, J., Fierer, N., et al. 2012. Ultra-high-throughput microbial community analysis on the Illumina HiSeq and MiSeq platforms. The ISME Journal 6, 1621–1624. doi:10.1038/ismej.2012.8.

Caporaso, J. G., Lauber, C. L., Walters, W. A., Berg-Lyons, D., Lozupone, C. A., Turnbaugh, P. J., et al. 2011. Global patterns of 16S rRNA diversity at a depth of millions of sequences

per sample. Proceedings of the National Academy of Sciences 108, 4516–4522. doi:10.1073/pnas.1000080107.

Carlson, C. A., and H. W. Ducklow. 1996. Growth of bacterioplankton and consumption of dissolved organic carbon in the Sargasso Sea. Aquatic Microbial Ecology 10:69–85.

Cass, C. J., and K. L. Daly. 2014. Eucalanoid copepod metabolic rates in the oxygen minimum zone of the eastern tropical north Pacific: Effects of oxygen and temperature. Deep Sea Research Part I: Oceanographic Research Papers 94:137–149.

Chaumeil, P.-A., A. J. Mussig, P. Hugenholtz, and D. H. Parks. 2019. GTDB-Tk: a toolkit to classify genomes with the Genome Taxonomy Database. Bioinformatics:btz848.

Chen, M. Y., and Parfrey, L. W. 2018. Incubation with macroalgae induces large shifts in water column microbiota, but minor changes to the epibiota of co-occurring macroalgae. Molecular Ecology 27, 1966–1979. doi:10.1111/mec.14548.

Correa, A. M. S., and Baker, A. C. 2011. Disaster taxa in microbially mediated metazoans: how endosymbionts and environmental catastrophes influence the adaptive capacity of reef corals. *Global Change Biology* 17, 68–75. doi:10.1111/j.1365-2486.2010.02242.x.

Croft, M. T., A. D. Lawrence, E. Raux-Deery, M. J. Warren, and A. G. Smith. 2005. Algae acquire vitamin B12 through a symbiotic relationship with bacteria. Nature 438:90–93.

Cunning, R., Silverstein, R. N., and Baker, A. C. 2015. Investigating the causes and consequences of symbiont shuffling in a multi-partner reef coral symbiosis under environmental change. Proceedings of the Royal Society B 282, 20141725. doi:10.1098/rspb.2014.1725.

Delmont, T. O., C. Quince, A. Shaiber, Ö. C. Esen, S. T. Lee, M. S. Rappé, S. L. McLellan, S. Lücker, and A. M. Eren. 2018. Nitrogen-fixing populations of Planctomycetes and Proteobacteria are abundant in surface ocean metagenomes. Nature Microbiology 3:804–813.

Dethier, M. N., A. S. Brown, S. Burgess, M. E. Eisenlord, A. W. E. Galloway, J. Kimber, A. T. Lowe, C. M. O'Neil, W. W. Raymond, E. A. Sosik, and D. O. Duggins. 2014. Degrading detritus: Changes in food quality of aging kelp tissue varies with species. Journal of Experimental Marine Biology and Ecology 460:72–79.

Dogs, M., B. Wemheuer, L. Wolter, N. Bergen, R. Daniel, M. Simon, and T. Brinkhoff. 2017. Rhodobacteraceae on the marine brown alga Fucus spiralis are abundant and show physiological adaptation to an epiphytic lifestyle. Systematic and Applied Microbiology 40:370–382.

Dudek, N. K., C. L. Sun, D. Burstein, R. S. Kantor, D. S. Aliaga Goltsman, E. M. Bik, B. C. Thomas, J. F. Banfield, and D. A. Relman. 2017. Novel microbial diversity and

functional potential in the marine mammal oral microbiome. Current Biology 27:3752-3762.e6.

Dunton, K. H., and C. M. Jodwalis. 1988. Photosynthetic performance of *Laminaria solidungula* measured *in situ* in the Alaskan High Arctic. Marine Biology 98:277–285.

Eddy, S. R. 2011. Accelerated Profile HMM Searches. PLoS Computational Biology 7:e1002195.

Edwards, M. S., and K. Y. Kim. 2010. Diurnal variation in relative photosynthetic performance in giant kelp *Macrocystis pyrifera* (*Phaeophyceae*, *Laminariales*) at different depths as estimated using PAM fluorometry. Aquatic Botany 92:119–128.

Egan, S., T. Harder, C. Burke, P. Steinberg, S. Kjelleberg, and T. Thomas. 2013. The seaweed holobiont: understanding seaweed–bacteria interactions. FEMS Microbiology Reviews 37:462–476.

Eren, A. M., E. Kiefl, A. Shaiber, I. Veseli, S. E. Miller, M. S. Schechter, I. Fink, J. N. Pan, et al. 2021. Community-led, integrated, reproducible multi-omics with anvi'o. Nature Microbiology 6:3–6.

Eren, A. M., Ö. C. Esen, C. Quince, J. H. Vineis, H. G. Morrison, M. L. Sogin, and T. O. Delmont. 2015. Anvi'o: an advanced analysis and visualization platform for 'omics data. PeerJ 3:e1319.

Espeland, E.M., Francoeur, S.N., and Wetzel, R.G. 2001. Influence of algal photosynthesis on biofilm bacterial production and associated glucosidase and xylosidase activities. *Microbial Ecology* 42: 524–530.

Fahimipour, A. K., Kardish, M. R., Lang, J. M., Green, J. L., Eisen, J. A., and Stachowicz, J. J. 2017. Global-scale structure of the eelgrass microbiome. *Applied and Environmental Microbiology* 83, e03391-16. doi:10.1128/AEM.03391-16.

Fankboner, P., and M. de Burgh. 1977. Diurnal exudation of 14-C labelled compounds by the large kelp *Macrocystis integrifolia* Bory. Journal of Experimental Marine Biology and Ecology 28:151–162.

Fenchel, T. 2001. Eppur si muove: many water column bacteria are motile. *Aquatic Microbial Ecology* 24, 197–201. doi:10.3354/ame024197.

Ferrera, I., O. Sánchez, E. Kolářová, M. Koblížek, and J. M. Gasol. 2017. Light enhances the growth rates of natural populations of aerobic anoxygenic phototrophic bacteria. The ISME Journal 11:2391–2393.

Fischer, M., Friedrichs, G., and Lachnit, T. 2014. Fluorescence-based quasicontinuous and *in situ* monitoring of biofilm formation dynamics in natural marine environments. *Applied and Environmental Microbiology* 80: 3721–3728.

Florez, J. Z., Camus, C., Hengst, M. B., and Buschmann, A. H. 2017. A functional perspective analysis of macroalgae and epiphytic bacterial community interaction. Frontiers in Microbiology 8. doi:10.3389/fmicb.2017.02561.

Fogg, G. E. 1963. The role of algae in organic production in aquatic environments. British Phycological Bulletin 2:195–205.

Fogg, G. E., Czeslawa Nalewajko, and W. D. Watt. 1965. Extracellular products of phytoplankton photosynthesis. Proceedings of the Royal Society of London. Series B, Biological Sciences 162:517–534.

Foreman, R. E. 1984. Studies on *Nereocystis* growth in British Columbia, Canada. Hydrobiologia 116:325–332.

Gao, Y., Y. Zhang, M. Du, F. Lin, W. Jiang, W. Li, F. Li, X. Lv, J. Fang, and Z. Jiang. 2021. Dissolved organic carbon from cultured kelp *Saccharina japonica*: production, bioavailability, and bacterial degradation rates. Aquaculture Environment Interactions 13:101–110.

Gerard, V. A. 1982. In situ rates of nitrate uptake by giant kelp, *Macrocystis pyrifera* (L.) C. Agardh: tissue differences, environmental effects, and predictions of nitrogen-limited growth. Journal of Experimental Marine Biology and Ecology 62:211–224.

Goecke, F., Labes, A., Wiese, J., and Imhoff, J. 2010. Chemical interactions between marine macroalgae and bacteria. Marine Ecology Progress Series 409: 267–299.

Gómez, I., M. Orostegui, and P. Huovinen. 2007. Morpho-functional patterns of photosynthesis in the south Pacific kelp *Lessonia nigrescens*: effects of UV radiation on 14C fixation and primary photochemical reactions. Journal of Phycology 43:55–64.

Graham, M. H. 2002. Prolonged reproductive consequences of short-term biomass loss in seaweeds. Marine Biology 140:901–911.

Graham, M. H., J. A. Vasquez, and A. H. Buschmann. 2007. Global ecology of the giant kelp Macrocystis: from ecotypes to ecosystems:51.

Grossman, A. 2016. Nutrient Acquisition: The Generation of Bioactive Vitamin B12 by Microalgae. Current Biology 26:R319–R321.

Hamersley, M. R., J. A. Sohm, J. A. Burns, and D. G. Capone. 2015. Nitrogen fixation associated with the decomposition of the giant kelp *Macrocystis pyrifera*. Aquatic Botany 125:57–63.

Hanson, C. A., Fuhrman, J. A., Horner-Devine, M. C., and Martiny, J. B. H. 2012. Beyond biogeographic patterns: processes shaping the microbial landscape. Nature Reviews Microbiology 10, 497–506. doi:10.1038/nrmicro2795.

Hatcher, B. G., A. R. O. Chapman, and K. H. Mann. 1977. An annual carbon budget for the kelp *Laminaria longicruris*. Marine Biology 44:85–96.

Hein, M., M. Pedersen, and K. Sand-Jensen. 1995. Size-dependent nitrogen uptake in micro- and macroalgae. Marine Ecology Progress Series 118:247–253.

Helliwell, K. E., G. L. Wheeler, K. C. Leptos, R. E. Goldstein, and A. G. Smith. 2011. Insights into the evolution of vitamin B12 auxotrophy from sequenced algal genomes. Molecular Biology and Evolution 28:2921–2933.

Hill, R., A. Bellgrove, P. I. Macreadie, K. Petrou, J. Beardall, A. Steven, and P. J. Ralph. 2015. Can macroalgae contribute to blue carbon? An Australian perspective. Limnology and Oceanography 60:1689–1706.

Hyatt, D., G.-L. Chen, P. F. LoCascio, M. L. Land, F. W. Larimer, and L. J. Hauser. 2010. Prodigal: prokaryotic gene recognition and translation initiation site identification. BMC Bioinformatics 11:119.

Imhoff, J. F., T. Rahn, S. Künzel, and S. C. Neulinger. 2018. Photosynthesis is widely distributed among Proteobacteria as demonstrated by the phylogeny of pufLM reaction center proteins. Frontiers in Microbiology 8:2679.

Intergovernmental Oceanography Commission. 1994. Protocols for the joint global ocean flux study (JGOFS) core measurements, IOC Manuals and Guides 29, UNESCO, Paris.

Irwin, S. and Davenport, J. 2002. Hyperoxic boundary layers inhabited by the epiphytic meiofauna of *Fucus serratus*. *Mar Ecol Prog Ser* 244: 73–79.

Jackrel, S. L., Owens, S. M., Gilbert, J. A., and Pfister, C. A. 2017. Identifying the plant-associated microbiome across aquatic and terrestrial environments: the effects of amplification method on taxa discovery. Molecular Ecology Resources. doi:10.1111/1755-0998.12645.

Jain, A., Krishnan, K.P., Begum, N., Singh, A., Thomas, F.A., and Gopinath, A. 2020. Response of bacterial communities from Kongsfjorden (Svalbard, Arctic Ocean) to macroalgal polysaccharide amendments. Marine Environmental Research 155: 104874.

Jain, C., L. M. Rodriguez-R, A. M. Phillippy, K. T. Konstantinidis, and S. Aluru. 2018. High throughput ANI analysis of 90K prokaryotic genomes reveals clear species boundaries. Nature Communications 9:5114.

James, A. K., C. J. English, N. J. Nidzieko, C. A. Carlson, and E. G. Wilbanks. 2020. Giant kelp microbiome altered in the presence of epiphytes. Limnology and Oceanography Letters:lol2.10157.

Jo, Y., Oh, Y.S., Woo, S. et al. 2019. Metagenomic analysis of bacterial communities associated with four *Ecklonia cava* populations, including Dokdo Island population. Toxicol. Environ. Health Sci. 11, 11–18. https://doi.org/10.1007/s13530-019-0383-7

Kalyaanamoorthy, S., B. Q. Minh, T. K. F. Wong, A. von Haeseler, and L. S. Jermiin. 2017. ModelFinder: fast model selection for accurate phylogenetic estimates. Nature Methods 14:587–589.

Kang, I., Y. Lim, and J.-C. Cho. 2018. Complete genome sequence of *Granulosicoccus antarcticus* type strain IMCC3135T, a marine gammaproteobacterium with a putative dimethylsulfoniopropionate demethylase gene. Marine Genomics 37:176–181.

Katoh, K., and D. M. Standley. 2013. MAFFT multiple sequence alignment software version 7: Improvements in performance and usability. Molecular Biology and Evolution 30:772–780.

Kembel, S. W., Cowan, P. D., Helmus, M. R., Cornwell, W. K., Morlon, H., Ackerly, D. D., et al. 2010. Picante: R tools for integrating phylogenies and ecology. Bioinformatics 26, 1463–1464. doi:10.1093/bioinformatics/btq166.

King, R. J., and W. Schramm. 1976. Photosynthetic rates of benthic marine algae in relation to light intensity and seasonal variations. Marine Biology 37:215–222.

Kirchman, D. L. 1994. The uptake of inorganic nutrients by heterotrophic bacteria. Microbial Ecology 28:255–271.

Kirchman, D., L. Mazzella, R. Alberte, and R. Mitchell. 1984. Epiphytic bacterial production on *Zostera marina*. Marine Ecology Progress Series 15:117–123.

Koblížek, M. 2015. Ecology of aerobic anoxygenic phototrophs in aquatic environments. FEMS Microbiology Reviews 39:854–870.

Koehl, M.A.R., Silk, W.K., Liang, H., and Mahadevan, L. 2008. How kelp produce blade shapes suited to different flow regimes: A new wrinkle. Integrative and Comparative Biology 48: 834–851.

Kojima, H., and M. Fukui. 2016. *Sulfuriflexus mobilis* gen. nov., sp. nov., a sulfur-oxidizing bacterium isolated from a brackish lake sediment. International Journal of Systematic and Evolutionary Microbiology 66:3515–3518.

Krause-Jensen, D., and C. M. Duarte. 2016. Substantial role of macroalgae in marine carbon sequestration. Nature Geoscience 9:737–742.

Kremer, B. P. 1981. C4-metabolism in marine brown macrophytic algae. Zeitschrift für Naturforschung C 36:840–847.

Krumhansl, K. A., Okamoto, D. K., Rassweiler, A., Novak, M., Bolton, J. J., Cavanaugh, K. C., et al. 2016. Global patterns of kelp forest change over the past half-century. Proceedings of the National Academy of Sciences 113, 13785–13790. doi:10.1073/pnas.1606102113.

Küppers, U., and B. P. Kremer. 1978. Longitudinal profiles of carbon dioxide fixation capacities in marine macroalgae. Plant Physiology 62:49–53.

Kurilenko, V. V., Christen, R., Zhukova, N. V., Kalinovskaya, N. I., Mikhailov, V. V., Crawford, R. J., et al. 2010. *Granulosicoccus coccoides* sp. nov., isolated from leaves of seagrass (*Zostera marina*). International Journal of Systematic and Evolutionary Microbiology 60, 972–976. doi:10.1099/ijs.0.013516-0.

Laycock, R. A. 1974. The detrital food chain based on seaweeds. I. Bacteria associated with the surface of *Laminaria* fronds. Marine Biology 25, 223–231.

Lachnit, T., Blümel, M., Imhoff, J., and Wahl, M. 2009. Specific epibacterial communities on macroalgae: phylogeny matters more than habitat. Aquatic Biology 5, 181–186. doi:10.3354/ab00149.

Lachnit, T., Fischer, M., Künzel, S., Baines, J. F., and Harder, T. 2013. Compounds associated with algal surfaces mediate epiphytic colonization of the marine macroalga *Fucus vesiculosus*. FEMS Microbiology Ecology 84, 411–420. doi:10.1111/1574-6941.12071.

Lachnit, T., Wahl, M., and Harder, T. 2010. Isolated thallus-associated compounds from the macroalga *Fucus vesiculosus* mediate bacterial surface colonization in the field similar to that on the natural alga. *Biofouling* 26: 247–255.

Lalonde, K., P. Middlestead, and Y. Gélinas. 2014. Automation of $^{13}C/^{12}C$ ratio measurement for freshwater and seawater DOC using high temperature combustion. Limnology and Oceanography: Methods 12:816–829.

Langmead, B., and S. L. Salzberg. 2012. Fast gapped-read alignment with Bowtie 2. Nature Methods 9:357–359.

Lee, H. K., T.-H. Choi, K.-M. Kim, and J.-C. Cho. 2007. *Granulosicoccaceae* fam. nov., to include *Granulosicoccus antarcticus* gen. nov., sp. nov., a non-phototrophic, obligately aerobic chemoheterotroph in the order *Chromatiales*, isolated from Antarctic seawater. J Microbiol Biotechnol 17:1483–90.

Lee, K., Lee, H. K., Choi, T.-H., and Cho, J.-C. 2007. *Robiginitomaculum antarcticum* gen. nov., sp. nov., a member of the family *Hyphomonadaceae*, from Antarctic seawater. International Journal of Systematic and Evolutionary Microbiology 57, 2595–2599.

Lemay, M. A., K. M. Davis, P. T. Martone, and L. W. Parfrey. 2021. Kelp-associated microbiota are structured by host anatomy. Journal of Phycology:jpy.13169.

Lemay, M. A., Martone, P. T., Keeling, P. J., Burt, J. M., Krumhansl, K. A., Sanders, R. D., et al. 2018. Sympatric kelp species share a large portion of their surface bacterial communities. Environmental Microbiology 20, 658–670. doi:10.1111/1462-2920.13993.

Li, H., B. Handsaker, A. Wysoker, T. Fennell, J. Ruan, N. Homer, G. Marth, G. Abecasis, R. Durbin, and 1000 Genome Project Data Processing Subgroup. 2009. The sequence alignment/map format and SAMtools. Bioinformatics 25:2078–2079.

Ligthart, K., C. Belzer, W. M. de Vos, and H. L. P. Tytgat. 2020. Bridging bacteria and the gut: functional aspects of type IV pili. Trends in Microbiology 28:340–348.

Lin, J. D., M. A. Lemay, and L. W. Parfrey. 2018. Diverse bacteria utilize alginate within the microbiome of the giant kelp *Macrocystis pyrifera*. Frontiers in Microbiology 9:1914.

Littler, M. M., and S. N. Murray. 1974. The primary productivity of marine macrophytes from a rocky intertidal community. Marine Biology 27:131–135.

Livanou, E., A. Lagaria, S. Psarra, and K. Lika. 2017. Dissolved organic matter release by phytoplankton in the context of the Dynamic Energy Budget theory. Biogeosciences Discussions:1–33.

Lobban, C. S., and P. J. Harrison. 1994. Seaweed Ecology and Physiology. Pages 163–209. Cambridge University Press, Cambridge, London.

Lu, X., K. R. Heal, A. E. Ingalls, A. C. Doxey, and J. D. Neufeld. 2020. Metagenomic and chemical characterization of soil cobalamin production. The ISME Journal 14:53–66.

Luo, H., and M. A. Moran. 2014. Evolutionary ecology of the marine Roseobacter clade. Microbiology and Molecular Biology Reviews 78:573–587.

Mancuso, F. P., D'Hondt, S., Willems, A., Airoldi, L., and De Clerck, O. 2016. Diversity and temporal dynamics of the epiphytic bacterial communities associated with the canopy-forming seaweed *Cystoseira compressa* (Esper) Gerloff and Nizamuddin. Frontiers in Microbiology 7. doi:10.3389/fmicb.2016.00476.

Mandal, S., Van Treuren, W., White, R. A., Eggesbø, M., Knight, R., and Peddada, S. D. 2015. Analysis of composition of microbiomes: a novel method for studying microbial composition. *Microbial Ecology in Health & Disease* 26. doi:10.3402/mehd.v26.27663.

Marañón, E., P. Cermeño, E. Fernández, J. Rodríguez, and L. Zabala. 2004. Significance and mechanisms of photosynthetic production of dissolved organic carbon in a coastal eutrophic ecosystem. Limnology and Oceanography 49:1652–1666.

Martin, M., Barbeyron, T., Martin, R., Portetelle, D., Michel, G., and Vandenbol, M. 2015. The cultivable surface microbiota of the brown alga *Ascophyllum nodosum* is enriched in macroalgal-polysaccharide-degrading bacteria. *Frontiers in Microbiology* 6. doi:10.3389/fmicb.2015.01487.

Marzinelli, E. M., Campbell, A. H., Zozaya Valdes, E., Vergés, A., Nielsen, S., Wernberg, T., et al. 2015. Continental-scale variation in seaweed host-associated bacterial communities is a function of host condition, not geography. *Environmental Microbiology* 17, 4078–4088. doi:10.1111/1462-2920.12972.

Marzinelli, E. M., Qiu, Z., Dafforn, K. A., Johnston, E. L., Steinberg, P. D., and Mayer-Pinto, M. 2018. Coastal urbanisation affects microbial communities on a dominant marine holobiont. *npj Biofilms and Microbiomes* 4. doi:10.1038/s41522-017-0044-z.

Mateo, M., P. Renom, M. Hemminga, and J. Peene. 2001. Measurement of seagrass production using the ^{13}C stable isotope compared with classical O_2 and ^{14}C methods. Marine Ecology Progress Series 223:157–165.

Matsen, F. A., R. B. Kodner, and E. V. Armbrust. 2010. pplacer: linear time maximum-likelihood and Bayesian phylogenetic placement of sequences onto a fixed reference tree. BMC Bioinformatics 11:538.

Maxell, B. A., and K. A. Miller. 1996. Demographic studies of the annual kelps *Nereocystis luetkeana* and *Costaria costata* (*Laminariales*, *Phaeophyta*) in Puget Sound, Washington. Botanica Marina 39.

Mazure, H.G.F. and Field, J.G. 1980. Density and ecological importance of bacteria on kelp fronds in an upwelling region. Journal of Experimental Marine Biology and Ecology 43: 173–182.

McIlroy, S. J., and Nielsen, P. H. 2014. "The family *Saprospiraceae*," in The Prokaryotes: Other Major Lineages of Bacteria and the Archaea, 4th Edn, Vol. 11, eds E. Rosenberg, E. F. Delong, S. Lory, E. Stackebrandt, and F. Thompson (Heidelberg: Springer Science and Business Media), 863–889.

McMurdie, P. J., and Holmes, S. 2013. phyloseq: An R package for reproducible interactive analysis and graphics of microbiome census data. *PLoS ONE* 8, e61217.

Michelou, V. K., Caporaso, J. G., Knight, R., and Palumbi, S. R. 2013. The ecology of microbial communities associated with *Macrocystis pyrifera*. PLoS ONE 8, e67480. doi:10.1371/journal.pone.0067480.

Miller, H., and K. Dunton. 2007. Stable isotope (^{13}C) and O_2 micro-optode alternatives for measuring photosynthesis in seaweeds. Marine Ecology Progress Series 329:85–97.

Minich, J. J., M. M. Morris, M. Brown, M. Doane, M. S. Edwards, T. P. Michael, and E. A. Dinsdale. 2018. Elevated temperature drives kelp microbiome dysbiosis, while elevated carbon dioxide induces water microbiome disruption. PLoS ONE 13:e0192772.

Minoche, A. E., J. C. Dohm, and H. Himmelbauer. 2011. Evaluation of genomic high-throughput sequencing data generated on Illumina HiSeq and Genome Analyzer systems. Genome Biology 12:R112.

Miranda, L. N., Hutchison, K., Grossman, A. R., and Brawley, S. H. 2013. Diversity and abundance of the bacterial community of the red macroalga *Porphyra umbilicalis*: did bacterial farmers produce macroalgae? PLoS ONE 8, e58269.

Morán, X. A. G., and M. Estrada. 2002. Phytoplanktonic DOC and POC production in the Bransfield and Gerlache Straits as derived from kinetic experiments of ^{14}C incorporation. Deep Sea Research Part II: Topical Studies in Oceanography 49:769–786.

Morris, R.L. and Schmidt, T.M. 2013. Shallow breathing: bacterial life at low O_2. Nat Rev Microbiol 11: 205–212.

Mueller, B., J. den Haan, P. M. Visser, M. J. A. Vermeij, and F. C. van Duyl. 2016. Effect of light and nutrient availability on the release of dissolved organic carbon (DOC) by Caribbean turf algae. Scientific Reports 6.

Myklestad, S. M. 1995. Release of extracellular products by phytoplankton with special emphasis on polysaccharides. Science of The Total Environment 165:155–164.

Nagata, T. 2000. Production mechanisms of dissolved organic matter. Pages 121–153 *in* D. L. Kirchman, editor. Microbial ecology of the oceans. First edition. Wiley-Liss, New York.

Newell, R. C., M. I. Lucas, B. Velimirov, and L. J. Seiderer. 1980. Quantitative significance of dissolved organic losses following fragmentation of kelp (*Ecklonia maxima* and *Laminaria pallida*). Marine Ecology Progress Series:45–59.

Nguyen, L.-T., H. A. Schmidt, A. von Haeseler, and B. Q. Minh. 2015. IQ-TREE: A fast and effective stochastic algorithm for estimating maximum-likelihood phylogenies. Molecular Biology and Evolution 32:268–274.

Nichols, C. M. 2005. *Olleya marilimosa* gen. nov., sp. nov., an exopolysaccharide-producing marine bacterium from the family *Flavobacteriaceae*, isolated from the Southern Ocean. International Journal of Systematic and Evolutionary Microbiology 55, 1557–1561. doi:10.1099/ijs.0.63642-0.

Noisette, F. and Hurd, C. 2018. Abiotic and biotic interactions in the diffusive boundary layer of kelp blades create a potential refuge from ocean acidification. *Funct Ecol* 32: 1329–1342.

Oksanen, J., Blanchet, F. J., Kindt, R., Minchin, P. R., O'Hara, R. B., Simpson, G. L., et al. 2014. vegan: community ecology package. R package version 2.0-10. Available at: http://CRAN.R-project.org/package=vegan.

Parada, A. E., Needham, D. M., and Fuhrman, J. A. 2016. Every base matters: assessing small subunit rRNA primers for marine microbiomes with mock communities, time series and global field samples. *Environmental Microbiology* 18, 1403–1414. doi:10.1111/1462-2920.13023.

Park, S., Jung, Y.-T., Won, S.-M., Park, J.-M., and Yoon, J.-H. 2014. *Granulosicoccus undariae* sp. nov., a member of the family *Granulosicoccaceae* isolated from a brown algae reservoir and emended description of the genus *Granulosicoccus*. Antonie van Leeuwenhoek 106, 845–852. doi:10.1007/s10482-014-0254-9.

Parks, D. H., M. Chuvochina, P.-A. Chaumeil, C. Rinke, A. J. Mussig, and P. Hugenholtz. 2020. A complete domain-to-species taxonomy for Bacteria and Archaea. Nature Biotechnology 38:1079–1086.

Peng, Y., H. C. M. Leung, S. M. Yiu, and F. Y. L. Chin. 2012. IDBA-UD: a de novo assembler for single-cell and metagenomic sequencing data with highly uneven depth. Bioinformatics 28:1420–1428.

Pessarrodona, A., P. J. Moore, M. D. J. Sayer, and D. A. Smale. 2018. Carbon assimilation and transfer through kelp forests in the NE Atlantic is diminished under a warmer ocean climate. Global Change Biology 24:4386–4398.

Pfister, C. A., and M. A. Altabet. 2019. Enhanced microbial nitrogen transformations in association with macrobiota from the rocky intertidal. Biogeosciences 16:193–206.

Pfister, C. A., Berry, H. D., and Mumford, T. 2018. The dynamics of kelp forests in the Northeast Pacific Ocean and the relationship with environmental drivers. Journal of Ecology. doi:10.1111/1365-2745.12908.

Pfister, C. A., J. T. Wootton, and C. J. Neufeld. 2007. Relative roles of coastal and oceanic processes in determining physical and chemical characteristics of an intensively sampled nearshore system. Limnology and Oceanography 52:1767–1775.

Pfister, C. A., M. A. Altabet, and B. L. Weigel. 2019. Kelp beds and their local effects on seawater chemistry, productivity, and microbial communities. Ecology 100:ecy2798.

Pfister, C. A., M. A. Altabet, and D. Post. 2014. Animal regeneration and microbial retention of nitrogen along coastal rocky shores. Ecology 95:2803–2814.

Philippot, L., Raaijmakers, J. M., Lemanceau, P., and van der Putten, W. H. 2013. Going back to the roots: the microbial ecology of the rhizosphere. Nature Reviews Microbiology 11, 789–799. doi:10.1038/nrmicro3109.

Pita, L., Turon, X., López-Legentil, S., and Erwin, P. M. 2013. Host rules: spatial stability of bacterial communities associated with marine sponges (*Ircinia spp.*) in the Western Mediterranean Sea. *FEMS Microbiology Ecology* 86, 268–276.

Piwosz, K., A. Vrdoljak, T. Frenken, J. M. González-Olalla, D. Šantić, R. M. McKay, K. Spilling, L. Guttman, P. Znachor, I. Mujakić, L. K. Fecskeová, L. Zoccarato, M. Hanusová, A. Pessina, T. Reich, H.-P. Grossart, and M. Koblížek. 2020. Light and primary production shape bacterial activity and community composition of aerobic anoxygenic phototrophic bacteria in a microcosm experiment. mSphere 5:e00354-20.

Pontarp, M., Canbäck, B., Tunlid, A., and Lundberg, P. 2012. Phylogenetic analysis suggests that habitat filtering is structuring marine bacterial communities across the globe. *Microbial Ecology* 64, 8–17. doi:10.1007/s00248-011-0005-7.

Poretsky, R. S., S. Sun, X. Mou, and M. A. Moran. 2010. Transporter genes expressed by coastal bacterioplankton in response to dissolved organic carbon. Environmental Microbiology 12:616–627.

Pregnall, A. M. 1983. Release of dissolved organic carbon from the estuarine intertidal macroalga *Enteromorpha prolifera*. Marine Biology 73:37–42.

Price, M. N., Dehal, P. S., and Arkin, A. P. 2010. FastTree 2 – Approximately maximum-likelihood trees for large alignments. PLoS ONE 5, e9490.

Pritchard, L., R. H. Glover, S. Humphris, J. G. Elphinstone, and I. K. Toth. 2016. Genomics and taxonomy in diagnostics for food security: soft-rotting enterobacterial plant pathogens. Analytical Methods 8:12–24.

Quigley, C. T. C., K. A. Capistrant-Fossa, H. G. Morrison, L. E. Johnson, A. Morozov, V. S. Hertzberg, and S. H. Brawley. 2020. Bacterial communities show algal host (*Fucus* spp.)/ zone differentiation across the stress gradient of the intertidal zone. Frontiers in Microbiology 11:563118.

Ramirez-Puebla, S. T., B. L. Weigel, L. Jack, C. Schlundt, C. A. Pfister, and J. L. Mark Welch. 2020. Spatial organization of the kelp microbiome at micron scales. preprint, Microbiology. bioRxiv: https://doi.org/10.1101/2020.03.01.972083.

Reed, D. C., Carlson, C. A., Halewood, E. R., Nelson, J. C., Harrer, S. L., Rassweiler, A., et al. 2015. Patterns and controls of reef-scale production of dissolved organic carbon by giant kelp *Macrocystis pyrifera*. Limnology and Oceanography 60, 1996–2008.

Rees, D. C., E. Johnson, and O. Lewinson. 2009. ABC transporters: the power to change. Nature Reviews Molecular Cell Biology 10:218–27.

Rivett, D. W., Scheuerl, T., Culbert, C. T., Mombrikotb, S. B., Johnstone, E., Barraclough, T. G., et al. 2016. Resource-dependent attenuation of species interactions during bacterial succession. The ISME Journal 10, 2259–2268. doi:10.1038/ismej.2016.11.

Rosenberg, E., DeLong, E.F., Lory, S., Stackebrandt, E., and Thompson, F. 2014. The prokaryotes: Other major lineages of bacteria and the archaea, 4th ed. Springer.

Rubol, S., Freixa, A., Sanchez-Vila, X., and Romaní, A.M. 2018. Linking biofilm spatial structure to real-time microscopic oxygen decay imaging. Biofouling 34: 200–211.

Saha, M. and Weinberger, F. 2019. Microbial "gardening" by a seaweed holobiont: Surface metabolites attract protective and deter pathogenic epibacterial settlement. Journal of Ecology 1365-2745.13193.

Säwström, C., G. A. Hyndes, B. D. Eyre, M. J. Huggett, M. W. Fraser, P. S. Lavery, P. G. Thomson, F. Tarquinio, P. D. Steinberg, and B. Laverock. 2016. Coastal connectivity and spatial subsidy from a microbial perspective. Ecology and Evolution 6:6662–6671.

Schmitz, K., and C. S. Lobban. 1976. A survey of translocation in *Laminariales* (*Phaeophyceae*). Marine Biology 36:207–216.

Seymour, J. R., Amin, S. A., Raina, J.-B., and Stocker, R. 2017. Zooming in on the phycosphere: the ecological interface for phytoplankton–bacteria relationships. *Nature Microbiology* 2, 17065. doi:10.1038/nmicrobiol.2017.65.

Seymour, J., Ahmed, T., Durham, W., and Stocker, R. 2010. Chemotactic response of marine bacteria to the extracellular products of *Synechococcus* and *Prochlorococcus*. Aquatic Microbial Ecology 59: 161–168.

Shaiber, A., A. D. Willis, T. O. Delmont, S. Roux, L.-X. Chen, A. C. Schmid, M. Yousef, A. R. Watson, K. Lolans, Ö. C. Esen, S. T. M. Lee, N. Downey, H. G. Morrison, F. E. Dewhirst, J. L. Mark Welch, and A. M. Eren. 2020. Functional and genetic markers of niche partitioning among enigmatic members of the human oral microbiome. Genome Biology 21:292.

Sieburth, J. McN. 1969. Studies on algal substances in the sea. III. The production of extracellular organic matter by littoral marine algae. Journal of Experimental Marine Biology and Ecology 3:290–309.

Singh, R. P., and C. R. K. Reddy. 2014. Seaweed-microbial interactions: key functions of seaweed-associated bacteria. FEMS Microbiology Ecology 88:213–230.

Smith, J. M., M. A. Brzezinski, J. M. Melack, R. J. Miller, and D. C. Reed. 2018. Urea as a source of nitrogen to giant kelp (*Macrocystis pyrifera*). Limnology and Oceanography Letters.

Solomonson, L. P., and M. J. Barber. 1990. Assimilatory nitrate reductase: functional properties and regulation. Annu. Rev. Plant. Physiol. Plant. Mol. Biol.:29.

Søndergaard, M. 1981. Kinetics of extracellular release of ^{14}C-labelled organic carbon by submerged macrophytes. Oikos 36:331.

Søndergaard, M. 1988. Comparison of $^{14}CO_2$ and $^{12}CO_2$ uptake in marine macroalgae. Botanica Marina 31:417–422.

Søndergaard, M. 1990. Extracellular organic carbon (EOC) in the genus *Carpophyllum* (*Phaeophyceae*): diel release patterns and EOC lability. Marine Biology 104:143–151.

Staufenberger, T., Thiel, V., Wiese, J., and Imhoff, J. F. 2008. Phylogenetic analysis of bacteria associated with *Laminaria saccharina*. FEMS Microbiology Ecology 64, 65–77.

Stekoll, M. S., L. E. Deysher, and M. Hess. 2006. A remote sensing approach to estimating harvestable kelp biomass. Journal of Applied Phycology 18:323–334.

Steneck, R. S., M. H. Graham, B. J. Bourque, D. Corbett, J. M. Erlandson, J. A. Estes, and M. J. Tegner. 2002. Kelp forest ecosystems: biodiversity, stability, resilience and future. Environmental Conservation 29:436–459.

Stratil, S.B., Neulinger, S.C., Knecht, H., Friedrichs, A.K., and Wahl, M. 2013. Temperature-driven shifts in the epibiotic bacterial community composition of the brown macroalga *Fucus vesiculosus*. Microbiology Open 2: 338–349.

Tait, L. W., and D. R. Schiel. 2013. Impacts of temperature on primary productivity and respiration in naturally structured macroalgal assemblages. PLoS ONE 8:e74413.

Tank, M., V. Thiel, and J. F. Imhoff. 2009. Phylogenetic relationship of phototrophic purple sulfur bacteria according to pufL and pufM genes. International Microbiology:175–185.

Thar, R. and Fenchel, T. 2001. True chemotaxis in oxygen gradients of the sulfur-oxidizing bacterium *Thiovulum majus*. *Appl Environ Microbiol* 67: 3299–3303.

Thomas, F., N. Le Duff, T.-D. Wu, A. Cébron, S. Uroz, P. Riera, C. Leroux, G. Tanguy, E. Legeay, and J.-L. Guerquin-Kern. 2021. Isotopic tracing reveals single-cell assimilation of a macroalgal polysaccharide by a few marine *Flavobacteria* and *Gammaproteobacteria*. The ISME Journal.

Thomas, D. N., and C. Wiencke. 1991. Photosynthesis, dark respiration and light independent carbon fixation of endemic Antarctic macroalgae. Polar Biology 11.

Thompson, L.R., Sanders, J.G., McDonald, D., Amir, A., Ladau, J., Locey, K.J., et al. 2017. A communal catalogue reveals Earth's multiscale microbial diversity. *Nature* 551: 457-463.

Thornton, D. C. O. 2014. Dissolved organic matter (DOM) release by phytoplankton in the contemporary and future ocean. European Journal of Phycology 49:20–46.

Tolbert, N., and L. Zill. 1956. Excretion of glycolic acid by algae during photosynthesis. The Journal of Biological Chemistry:895–906.

Towle, D. W., and J. S. Pearse. 1973. Production of the giant kelp, *Macrocystis*, estimated by *in situ* incorporation of ^{14}C in polyethylene bags. Limnology and Oceanography 18:155–159.

Wada, S., M. N. Aoki, Y. Tsuchiya, T. Sato, H. Shinagawa, and T. Hama. 2007. Quantitative and qualitative analyses of dissolved organic matter released from *Ecklonia cava* Kjellman, in Oura Bay, Shimoda, Izu Peninsula, Japan. Journal of Experimental Marine Biology and Ecology 349:344–358.

Wagner-Döbler, I., B. Ballhausen, M. Berger, T. Brinkhoff, I. Buchholz, B. Bunk, H. Cypionka, et al. 2010. The complete genome sequence of the algal symbiont *Dinoroseobacter shibae*: a hitchhiker's guide to life in the sea. The ISME Journal 4:61–77.

Walters, W., Hyde, E. R., Berg-Lyons, D., Ackermann, G., Humphrey, G., Parada, A., et al. 2016. Improved bacterial 16S rRNA gene (V4 and V4-5) and fungal internal transcribed spacer marker gene primers for microbial community surveys. mSystems 1, e00009–15.

Weigel, B. L., and C. A. Pfister. 2019. Successional dynamics and seascape-level patterns of microbial communities on the canopy-forming kelps *Nereocystis luetkeana* and *Macrocystis pyrifera*. Frontiers in Microbiology 10:346.

Weigel, B. L., and C. A. Pfister. 2021a. The dynamics and stoichiometry of dissolved organic carbon release by kelp. Ecology 102: e03221.

Weigel, B. L., and C. A. Pfister. 2021b. Oxygen metabolism shapes microbial settlement on photosynthetic kelp blades compared to artificial kelp substrates. Environmental Microbiology Reports 13:176–184.

Wheeler, W. N., and L. D. Druehl. 1986. Seasonal growth and productivity of *Macrocystis integrifolia* in British Columbia, Canada. Marine Biology 90:181–186.

Wheeler, W. N., R. G. Smith, and L. M. Srivastava. 1984. Seasonal photosynthetic performance of *Nereocystis luetkeana*. Canadian Journal of Botany 62:664–670.

Wilkins, L.G.E., Leray, M., O'Dea, A., Yuen, B., Peixoto, R.S., Pereira, T.J., et al. 2019. Host-associated microbiomes drive structure and function of marine ecosystems. *PLoS Biol* 17: e3000533.

Willenbrink, J., B. P. Kremer, K. Schmitz, and L. M. Srivastava. 1979. Photosynthetic and light-independent carbon fixation in *Macrocystis*, *Nereocystis*, and some selected Pacific Laminariales. Canadian Journal of Botany 57:890–897.

Wilmers, C. C., J. A. Estes, M. Edwards, K. L. Laidre, and B. Konar. 2012. Do trophic cascades affect the storage and flux of atmospheric carbon? An analysis of sea otters and kelp forests. Frontiers in Ecology and the Environment 10:409–415.

Wootton, J. T., and C. A. Pfister. 2012. Carbon system measurements and potential climatic drivers at a site of rapidly declining ocean pH. PLoS ONE 7:e53396.

Wootton, J. T., C. A. Pfister, and J. D. Forester. 2008. Dynamic patterns and ecological impacts of declining ocean pH in a high-resolution multi-year dataset. Proceedings of the National Academy of Sciences 105:18848–18853.

Yamaguchi, T., T. Ikawa, and K. Nisizawa. 1966. Incorporation of radioactive carbon from $H^{14}C0_3$ into sugar constituents by a brown alga, *Eisenia bicyclis*, during photosynthesis and its fate in the dark. Plant and Cell Physiology 7:217–229.

Yoch, D. C. 2002. Dimethylsulfoniopropionate: its sources, role in the marine food web, and biological degradation to dimethylsulfide. Applied and Environmental Microbiology 68:5804–5815.

Young, E. B., M. J. Dring, and J. A. Berges. 2007. Distinct patterns of nitrate reductase activity in brown algae: light and ammonium sensitivity in *Laminaria digitata* is absent in *Fucus* species. Journal of Phycology 43:1200–1208.

Zlotnik, I., and Z. Dubinsky. 1989. The effect of light and temperature on DOC excretion by phytoplankton. Limnology and Oceanography 34:831–839.